

Gaute Hånsnar
Benedicte Gjersdal
Trygve Mikal Viga Skretting

Design and Implementation of a Minitature Rig for Autonomous and Directional Drilling

Contribution to the Drillbotics Competition 2021

Master's thesis in Petroleum Geoscience and Engineering
Supervisor: Alexey Pavlov, Tor Berge Gjersvik, Sigbjørn Sangesland,
Sigve Hovda
June 2021

Gaute Hånsnar
Benedicte Gjersdal
Trygve Mikal Viga Skretting

Design and Implementation of a Minitature Rig for Autonomous and Directional Drilling

Contribution to the Drillbotics Competition 2021

Master's thesis in Petroleum Geoscience and Engineering
Supervisor: Alexey Pavlov, Tor Berge Gjersvik, Sigbjørn Sangesland,
Sigve Hovda
June 2021

Norwegian University of Science and Technology
Faculty of Engineering
Department of Geoscience and Petroleum

Abstract

This thesis presents the project work done by three petroleum engineering students and one cybernetics student representing Norwegian University of Science and Technology (NTNU) in the international drilling competition “Drillbotics” arranged by DSATS. The petroleum students wrote this thesis as their final assignment in completing a Master’s Degree in Petroleum Engineering at NTNU. It is written at the Department of Geoscience and Petroleum (IGP) in the period from January to June 2021. Autonomous drilling is highly relevant today because oil and gas operators have a desire to reduce drilling costs. Automating drilling operations can be a step towards that goal.

The audience is advised to read the preliminary project report “Design Report NTNU - Drillbotics 2021 Phase I” written by Benedicte Gjersdal, Gaute Hånsnar, Trygve Mikal Viga Skretting and Magnus Steinstø from August to December 2020 [9]. The report covers the planning and preliminary work related to the competition’s first phase. The report was the specialization project in the student’s ninth semester and as the “Phase 1 Design Report” submitted to the Drillbotics committee in December 2020 [9]. The “Phase 1 Design Report” covers the background and purpose of the Drillbotics competition, the structure of the project team, safety and potential hazards, theoretical background for directional drilling, controllers, and filters in addition to design parameters limits, and uncertainties. It also presents the proposed rig design in detail with its new drilling concept leaving the Positive Displacement Motor (PDM) for a rod transmitting torque from a top drive motor through the drillpipe to rotate the drilling bit.

Entering the second phase of the competition, the miniature rig was built based on its proposed design from Phase I. Implementing the design introduced challenges related to vibrations, torsion and material strength. High torque readings and torque spikes proved the top drive Revolutions Per Minute (RPM) too low when increasing Weight On Bit (WOB). Greater RPM proved to drill with less vibration, enabling higher WOB and thus increasing Rate of Penetration (ROP), without twisting the rod. Titanium rod withstood the forces present and performed successfully on the competition day.

The control system was implemented in MATLAB and Simulink with a high and low-level system. Drilling parameters such as WOB and azimuth rotational velocity were controlled by a PID-controlled and filtered with extended Kalman filters. The model is based on non-linear Model Predictive Controller (MPC). The predicted well trajectory was based on the Bezier Curve method to create a smooth well path intersecting the desired targets in the rock.

The team has successfully designed, built, and implemented a functional miniature rig to autonom-

ously drill deviated wells through a rock sample with preset targets. The rig can drill straight, with varying azimuth and varying inclination, and all these different operations can run both manually and autonomously. All that is required prior to drilling is to enter the targets into the control system. 53 deviated wells have been successfully drilled during the project for testing and tuning the rig systems to meet the objectives and requirements in the final competition run. On the day of the competition, the rig drilled successfully to targets in 23 minutes. The maximum potential of the rig was demonstrated to the Drillbotics committee in an extra run, drilling through the 60 cm x 30 cm x 60 cm (24 inches x 12 inches x 24 inches) rock in six minutes with an inclination of 37 degrees.

Sammendrag

Denne avhandlingen presenterer arbeidet gjort av tre petroleumsstudenter og en kybernetikkstudent for å representere Norges Teknisk Naturvitenskapelig Universitet (NTNU) i den internasjonale borekonkurransen "Drillbotics". Petroleumsstudentene skrev denne avhandlingen som sin avsluttende masteroppgave for en mastergrad i Petroleumsteknologi ved NTNU. Den ble skrevet ved Institutt for Geovitenskap og Petroleum i perioden Januar til Juni 2021. Autonom boring er høyst relevant i dag fordi olje- og gassoperatører har et ønske om å redusere kostnader. Automatisering av boreoperasjoner kan derfor være et steg i riktig retning.

Leseren er anbefalt å lese den innledende prosjektrapporten "Design Report NTNU - Drillbotics 2021 Phase I" skrevet av Benedicte Gjersdal, Gaute Hånsnar, Trygve Mikal Viga Skretting og Magnus Steinstø fra August til Desember 2020 [9]. Rapporten beskriver planleggingen og innledende arbeid relatert til første fase av konkurransen. Fase 1 rapporten var et spesialiseringssprosjekt i studentenes niende semester, og ble levert som "Phase I Design Report" til Drillbotics kommiteen i Desember 2020.

"Phase I Design Report" tar for seg bakgrunn og formålet med Drillbotics konkurransen, prosjektstrukturen innad i laget, sikkerhet og potensielle farer, teoretisk bakgrunn for retningsbestemt boring, kontrollere og filter i tillegg til begrensende parametere og usikkerheter. Den presenterer også det foreslåtte riggdesignet i detalj med det nye konseptet som erstatter nedihulls slammotor med en roterende aksling som overfører moment og rotasjon fra tårnboremaskinen til borekrona. Designet fra fase I av prosjektet ble implementert i den andre fasen av konkurransen. Denne fasen bydde på utfordringer relatert til vibrasjoner, torsjon og materialstyrke. Høye målinger og plutselige økninger i dreiemoment viste at rotasjonen fra tårnboremaskinen var for lav når vekten på borekrona økte. Høyere rotasjonsverdier reduserte vibrasjoner og la til grunn for høyere vekt på borekrona, som førte til høyere borerate uten å vri i stykker akslingen.

Kontrollsystemet ble utviklet i MATLAB og Simulink med to separate systemer; lavnivå- og høynivåsystem. Boreparametere som vekt på borekrona og azimuth-rotasjonshastighet ble kontrollert av PID-kontrollere og filtrert med Kalman-filtre. Styringsmodellen er basert på en ikke-lineær Modell Prediktiv Kontroller. Den kalkulerte brønnbanen er basert på Bezier-kurvemetoden for å lage en jevn og kontinuerlig brønnbane som treffer de ønskede punktene i steinen.

Laget har vært vellykket i å designe, bygge og implementere en funksjonell miniatyr borerigg for å bore retningsbeste brønner autonomt gjennom en steinprøve med forhåndsbestemte mål.

Boreriggen kan bore rett frem eller med varierende inklinasjon og azimut. Begge boremetodene kan gjennomføres manuelt eller autonomt. 53 vellykkede avviksbrønner ble boret i løpet av prosjektet for å teste og stille inn riggsystemet for å møte kravene i konkurransen. På konkurransedagen boret riggen vellykket gjennom steinen på 23 minutter. Det maksimale potensialet til riggen ble demonstrert for Drillbotics kommiteen i en ekstra gjennomgang, der steinprøven med målene 60cm x 30 cm x 60 cm ble boret gjennom på seks minutter med en inklinasjon på 37 grader.

Acknowledgements

We would like to express our thanks to our primary supervisors Professor Alexey Pavlov, Professor Tor Berge Gjersvik, Professor Sigve Hovda and Professor Sigbjørn Sangesland, for guidance throughout the Drillbotics project August 2020 to June 2021. Regular meetings and continuous feedback have motivated us throughout the project and helped us improve the design. Thank you for your support, availability, and for believing in us and the project.

We also want to show our appreciation to the supporting engineer team. They have put down many hours to make the drilling rig functional, for which we are very grateful. The close collaboration has been a great learning experience giving the us a practical and technical understanding we will bring with us in the future. Noralf Vedvik has been our primary supervisor concerning the construction of the drilling rig. He saved us a lot of time with his clever ideas and elegant solutions when we encountered challenges along the way. Terje Bjerkan and Håkon Myhren in the workshop have been of critical assistance for the Drillbotics competition and the master thesis project. Their solid competence and skills for fabricating and repairing our components have made the modifications of the rig a smoother process than first anticipated. The project would not have been possible without you.

Lyng Drilling sponsored and manufactured of our self-designed drill bits for the team to use in the Drillbotics Competition. Are Funderud, thank you for inviting us to Lyng Drilling in Vanvikan to show us the bit manufacturing process in full scale.

We want to acknowledge Drilling System Automation Technical Section (DSATS) and Society of Petroleum Engineers (SPE) for arranging the Drillbotics competition, which addresses an important topic such as autonomous drilling. The acquired knowledge during this project will unquestionably benefit us when starting our careers within the oil and gas industry.

We also want to thank the Department of Geoscience and Petroleum (IGP) at Norwegian University of Science and Technology (NTNU) for allowing us to conduct our thesis on such a comprehensive, practical, and multidisciplinary project. The department has funded the project together with the BRU21-program and Equinor. John-Morten Godhavn played an essential role in promoting our project and have been involved in the Drillbotics project at NTNU since the very beginning.

Lastly, we wish to express our gratitude to our families, friends, and significant others for their love, support, and motivation during this project.

(This page is intentionally left blank)

Contents

Abstract	ii
Sammendrag	iv
Acknowledgements	v
Abbreviations	xix
List of Tables	xxii
List of Figures	xxx
1 Introduction	1
2 Organization	3
2.1 Drillbotics Team 2021	3
2.2 Roles	5
2.3 Project Management	6
2.4 Time Management	6

3	Safety	9
3.1	Safety in the Oil and Gas Industry	9
3.2	COVID-19	11
3.3	Potential Safety Hazards	12
3.4	Safety Measures for Handling Potential Hazards	14
3.4.1	Safety Measures During Rig Construction	14
3.4.2	Safety Measures During Rig Operation	15
 4	 Theoretical Background	 19
4.1	Directional Drilling	19
4.1.1	Application of Directional Drilling	19
4.1.2	Well Path	20
4.1.3	Survey Calculation Methods	21
4.2	Bottom Hole Assembly (BHA)	25
4.2.1	Directional Steering	25
4.2.2	Dogleg Severity Based on BHA Configuration	25
4.2.3	Bent Sub	26
4.2.4	Transmission Section	27
4.2.5	Bearing Section	28
4.2.6	Rotary Steerable System (RSS)	29
4.3	Drill String Mechanics	30
4.3.1	Buckling	30
4.3.2	Burst	33
4.3.3	Pipe Twist-Off	33
4.3.4	Pipe Bending	34
4.3.5	Stresses in Rod	35

CONTENTS

4.3.6	Fatigue	35
4.3.7	Natural Frequency	36
4.4	Drill Bits	37
4.4.1	Bit Profile and Cone Angle	39
4.4.2	Cutter Design	41
4.4.3	Bit Balling	43
4.5	Drilling Hydraulics	43
4.5.1	Hole Cleaning	44
4.5.2	Pressure Losses	45
5	Design Limits	49
5.1	Well Path	51
5.2	Buckling	52
5.3	Burst	54
5.4	Twist-Off	54
5.5	Pipe Bending	55
5.6	Rod Stresses	58
5.7	Fatigue	59
5.8	Drilling Requirements	59
5.8.1	Drilling Rate	59
5.8.2	Bit Tilt	60
5.9	Drilling Hydraulics	61
5.9.1	Hole Cleaning	61
5.9.2	Pressure Losses	61
5.10	Natural Frequency	63
5.10.1	Drillpipe	63

5.10.2	Rod	64
6	Mechanical Rig Design	67
6.1	Drillbotics Rigs 2016-2020	68
6.2	Drillbotics 2021 Rig	68
6.3	Rig Component Overview	70
6.4	Rig Framework	71
6.5	Hoisting System	73
6.5.1	Hoisting Motor	73
6.5.2	Carriage Mount	74
6.5.3	Load Cell	74
6.5.4	Safety Stop Buttons	76
6.6	Drilling System	78
6.6.1	Top Drive Motor no. 1	78
6.6.2	Top Drive Motor no. 2	79
6.6.3	Drill Chuck and Top Drive Connection	79
6.6.4	Rod	80
6.6.5	Drillpipe	81
6.6.6	Stabilizers	81
6.7	Azimuth Control System	84
6.7.1	Hollow Gearbox with Rotary Table	84
6.7.2	Azimuth Servo Motor and Gearboxes	85
6.7.3	T-shaft	87
6.7.4	Torque Sensor	88
6.8	Circulation System	91
6.8.1	Swivel House	91

CONTENTS

6.8.2	Hollow Swivel Shaft	92
6.8.3	Roller Bearings	95
6.8.4	Drillpipe Connection	97
6.9	BHA Design	99
6.9.1	Initial Design	99
6.9.2	Pilot Hole Drilling	101
6.10	Drill Bit Design	102
6.10.1	Design Considerations	102
6.11	3D Bit Modeling	104
6.11.1	2D Sketch	105
6.11.2	2D sketch to 3D model	107
6.11.3	Design Alternative	109
6.11.4	Drill Bit Overview	110
6.12	Electrical System	112
6.12.1	Downhole Sensor	112
6.12.2	DAQ	113
7	Risk Analysis and Risk Mitigation for Rig Components	115
7.1	Top Drive Motor and Hoisting Motor	116
7.2	Drill Chuck and Drill Chuck Connection	117
7.3	Rotating Rod	117
7.4	Azimuth Motor and Gearboxes	117
7.5	Azimuth Torque Sensor	117
7.6	T-shaft	118
7.7	Hydraulic Swivel	118
7.8	Drillpipe Connections	118

7.9	Drillpipe	118
7.10	Drillfloor Stabilizer	119
7.11	USB-cable and Connections	119
7.12	Upper Stabilizer and Sensor Housing	119
7.13	Sensor Card	120
7.14	Bent Sub	120
7.15	Rod Connection in BHA	121
7.16	Lower stabilizer, Packer and Bit Sub	121
7.17	Drill Bit	121
7.18	Computers	121
8	Power Consumption	123
8.1	Top Drive Motor	123
8.2	Hoisting Motor	124
8.3	Azimuth System	125
8.4	Torque Sensor	125
8.5	Computer	125
8.6	Total Power Consumption	126
9	Control System Design	127
9.1	Background Theory	127
9.1.1	PID Controller	127
9.1.2	PID Tuning	130
9.1.3	Kalman Filter	131
9.1.4	Extended Kalman Filter	132
9.1.5	Model Predictive Controller (MPC)	133

9.1.6	Position Estimate	137
9.2	Implementation in Control System	140
9.2.1	PID Controller	140
9.2.2	Kalman Filter	142
9.2.3	Graphical User Interface (GUI)	143
9.2.4	Directional Model Predictive Controller (MPC) Model	145
10	API	147
10.1	OPC UA	147
10.1.1	Information Model	148
10.1.2	Server Implementation	148
10.1.3	Server Nodes	149
10.1.4	Rig Request	150
10.1.5	Events	151
10.1.6	Rig Data	152
10.1.7	Third Party Tools	152
10.2	Connection to Rig Control System	154
10.2.1	Request Handling	154
10.2.2	Events	155
10.2.3	Sending and Receiving Rig Parameters	155
11	Testing and Qualification	157
11.1	Factory Acceptance Test For Equipment	157
11.1.1	FAT Plan	157
11.1.2	Azimuth Rotation Test	158
11.1.3	Top Drive Rotation Test	159

11.2 Pipe and Rod Limit Tests	160
11.2.1 Buckling	161
11.2.2 Test Setup and Procedure	161
11.2.3 Results	161
11.2.4 Errors and discussion	163
11.2.5 Bending	164
11.3 Twist-off	167
11.4 Rock Sample Cement Testing	170
11.4.1 Mixing and Test Procedure	172
11.4.2 Errors and Discussion	173
11.5 Vertical Section	173
11.6 Variation of DLS	176
11.6.1 WOB approach	176
11.6.2 Full Azimuth Rotation Approach	176
11.6.3 Little Azimuth Rotation Approach	177
11.7 Drill Bit	177
11.7.1 Rate of Penetration (ROP)	178
11.7.2 Torque	179
11.7.3 Vibrations and Hole Quality	180
11.7.4 Overall Performance	181
11.8 Sensor Card Tests	182
11.9 Competition	183
11.9.1 Pilot Hole	183
11.9.2 Competition Run	183
11.9.3 Extra Run	187

12 Budget and Accounting	191
12.1 In-house Contributions	191
12.2 Labor	192
12.3 Funding	193
12.4 Expenses and accounting	193
13 Challenges and Lessons Learned	195
13.1 Project Management and Norwegian Holidays	195
13.2 Corona Virus	195
13.3 Locating A Torque Sensor	196
13.4 Rig System Alignment	196
13.4.1 Hydraulic System	196
13.4.2 Azimuth System	199
13.4.3 Top Drive Motor	200
13.4.4 Rig Frame	201
13.5 Inclination	202
13.6 Challenges Related to Stuck Drillstring	204
13.7 BHA Integration of Sensor Card	206
13.7.1 Epoxy	207
13.7.2 Cabled Implementation	208
13.8 Bottom Hole Assembly (BHA)	212
13.8.1 First Testing Stage	212
13.8.2 Second Iteration	214
13.8.3 Third Iteration	216
13.8.4 Fourth Iteration	216
13.8.5 Fifth Iteration	217

14 Conclusions	221
15 Future Work	223
15.1 Easier Protective Glass	223
15.2 Adjustable Bent Sub	223
15.3 Whipstock	224
15.4 Hydraulic System	224
15.4.1 Swivel Design	226
15.5 Computer Space	226
15.6 Rock Sample Space	227
15.7 Electromagnet	227
15.8 Sensor Card	228
15.9 Kick-Off Point (KOP)	228
References	231
Appendices	236
A Drillbotics Guidelines 2021	237
B Labview/Simulink Control system	279
C Framework and Cabinet	281
D Hoisting Motor Specifications	285
E Top Drive Motor Specifications	287
F Drill Chuck Specifications	289

CONTENTS

G T-shaft Specifications	291
H Hypoid Hollow Shaft Gearbox	293
I Azimuth Servo Motor	297
J Azimuth Right-Angle Gearbox	299
K Adaptor Plates	301
L Torque Sensor Specifications	307
M Hydraulic Swivel Specifications	309
N Riser Design	313
O Bottom Hole Assembly (BHA) Specifications	317
P DSATS Drill bit	327
Q Bit Design	329
R Cuttings Transportation Derivation	333

(This page is intentionally left blank)

Abbreviations

API American Petroleum Institute.

API Application Programming Interface.

BHA Bottom Hole Assembly.

CL Course Length.

CRS Critical Rotary Speed.

DAQ Data Acquisition.

DLS Dogleg Severity.

DOC Depth of Cut.

DSATS Drilling System Automation Technical Section.

FAT Factory Acceptance Test.

GUI Graphical User Interface.

HSE Health, Safety, and Environment.

IGP Department of Geoscience and Petroleum.

ITK Department of Engineering Cybernetics.

KOP Kick-Off Point.

LPM Liters per Minute.

MPC Model Predictive Controller.

MWD Measurement While Drilling.

NCS Norwegian Continental Shelf.

NIOSH The National Institute for Occupational Safety and Health.

NPT Non-Productive Time.

NTNU Norwegian University of Science and Technology.

OD Outer Diameter.

PDC Polycrystalline Diamond Compact.

PDM Postive Displacement Motor.

PID Proportional Integral Derivative.

POI Point of Interest.

PPE Personal Protective Equipment.

PTS Petroleum Technical Center.

RC Radius of Curvature.

RKB Rotary Kelly Bushing.

ROP Rate of Penetration.

RPM Revolutions Per Minute.

RSS Rotary Steerable System.

SDK Software Development Kit.

SPE Society of Petroleum Engineers.

UCS Uniaxial Compressive Strength.

TSP Thermally Stable Polycrystalline Diamond.

URL Uniform Resource Locator.

TVD True Vertical Depth.

WOB Weight On Bit.

UA Unified Architecture.

XML Extensible Markup Language.

List of Tables

4.1	Effective length factor, K , for different end conditions [29]	32
5.1	Design parameters.	50
5.2	Buckling calculations for drillpipe.	53
5.3	Buckling calculations with BHA length of 16.2 cm (6.38 inches).	53
5.4	Twist-off limits for aluminum 7075-T6 drillpipe for different horizontal displacements.	55
5.5	Twist-off limits for different rod materials.	55
5.6	Results from hole cleaning calculations.	61
5.7	Pressure drop across drilling components for different flow rates.	62
6.1	Specifications for different bits.	111
6.2	Arduino Nano 33 BLE Sense sensors.	112
7.1	Risk matrix for rig components before risk mitigation.	116
7.2	Risk matrix for rig components after risk mitigation.	116
8.1	Estimates of the hoisting motors power consumption at different RPM values.	124

8.2 Overview of the expected and maximum power consumption for each component on the rig.	126
11.1 Top drive rotation test results.	160
11.2 Results from buckling tests on aluminium 7075 drillpipe.	161
11.3 Bending test results showing all the materials passed.	166
11.4 Results from testing of cement with different water to concrete ratio.	173
12.1 Overview of the labor expenses related to the theses project with an exchange rate of 1 USD = 8.3 NOK as of 05.05.2021.	192
12.2 Total cost throughout the project with an exchange rate of 1 USD = 8.26 NOK as of 08.06.2021.	194

List of Figures

2.1	2021 NTNU Drillbotics Team.	4
2.2	Team system for the 2021 NTNU Drillbotics Team.	4
2.3	Student team organization chart.	5
2.4	Kanban-structure.	6
2.5	Time management in Microsoft Teams written in Norwegian for convenience. . .	7
3.1	NIOSH’s hierarchy triangle of controls. It highlights different measures efficiency with respect to avoiding hazards [32].	10
3.2	Direction of moving components on the miniature drilling rig.	13
3.3	Team member with correct PPE under construction of the rig.	14
3.4	The rotary system seen behind the protective glass.	15
3.5	Safety cabinet beneath drill floor for placement of rock sample.	16
3.6	Emergency stop button.	17
4.1	Types of well paths. [10].	20
4.2	Relevant parameters for the minimum curvature method [8].	23
4.3	Relevant parameters for development of a well path [8].	24

4.4 Dogleg Severity parameters based on BHA configurations [8].	26
4.5 Fixed bent sub.	26
4.6 Adjustable bent sub [31].	27
4.7 Transmission joints; universal joint and flexible joint respectively [8].	28
4.8 Bearing section showing flow paths in red [11].	29
4.9 The two methods of RSS [8].	30
4.10 Illustration of first and second stage of buckling respectively [68].	31
4.11 drillpipe stresses as a result of pressure, WOB and torque [52].	34
4.12 Overview of PDC drill bit components [69].	38
4.13 Energy needed to fail two different formations for different stress types [69].	39
4.14 Varying bit profiles and belonging properties [35].	40
4.15 Deep($\approx 90^\circ$), medium($\approx 120^\circ - 140^\circ$) and shallow($\approx 150^\circ$) cone angles [35].	40
4.16 Increasing cutter density towards outer rows along bit profile [34].	41
4.17 Two types of drill bit cutter layout [67].	42
4.18 Varying back rake angles [69].	42
4.19 Side-rake angle viewed from behind the drill bit [69].	43
4.20 Relationship between Re and f for settling particles in Newtonian fluids [7].	45
5.1 Theoretical possible well path inside given rock dimensions, 12in x 24in x 24in.	51
5.2 Critical buckling limit calculations for aluminium drillpipe.	52
5.3 Twist-off torques on drillpipe for different bending cases and WOB.	54
5.4 Axial stresses on pipe for different values of RC , P , and WOB	56
5.5 Contribution of axial stress from bending illustrated for different values of RC compared with material yield strength.	56
5.6 Performance of aluminum 7075-T6 drillpipe.	57

5.7	Comparative stress from bending and twisting for different values of RC compared with material yield strength.	58
5.8	Comparative stress for grade 5 titanium.	59
6.1	Proposed design of the miniature drilling rig 2021.	69
6.2	Framework of the miniature drilling rig without drilling components.	71
6.3	Folded rig structure	72
6.4	Hoisting servo motor.	73
6.5	Hoisting system components.	74
6.6	Load cell mounted on the ball screw	75
6.7	Load cell: TC4-AMP transducer by APE Transducer [4].	75
6.8	Stop button on hoisting system.	76
6.9	Picture of the BHA seen below the derrick floor. Arrow points at upper stabilizer.	77
6.10	Complete rotary system. From top: top drive motor, drill chuck fastener, drill chuck, "T-shaft", azimuth motor, torque sensor, stabilizing plates and hydraulic swivel.	78
6.11	Drill chuck components.	80
6.12	Rods.	81
6.13	Upper and lower stabilizer on the rig.	82
6.14	Manual hoisting mechanism of the riser.	83
6.15	Azimuth control system with servo motor, gearbox system, torque sensor, and T-shaft.	84
6.16	Hollow shaft Hypoid gearbox with rotary table [38].	85
6.17	Azimuth servo motor components.	86
6.18	Gigager gearbox.	86
6.19	T-shaft design.	87
6.20	Torque sensor.	88

6.21	Alignment and mounting plates.	89
6.22	Alignment plates implemented on the rig.	90
6.23	Picture of the complete swivel.	91
6.24	Swivel house design.	92
6.25	Swivel house holder.	92
6.26	Hydraulic swivel shaft design.	93
6.27	O-rings illustrated in red.	94
6.28	Connection between T-shaft and hollow shaft in swivel.	95
6.29	Illustration of the roller bearing used in the swivel.	96
6.30	Cross-section of hydraulic swivel. Top and bottom roller bearings shown in red.	96
6.31	Drillpipe connected below the swivel.	97
6.32	From the top: Nipple, spring collet with o-ring, collet nut and drillpipe.	98
6.33	Initial design of bottom hole assembly.	99
6.34	Sensor housing design.	100
6.35	Lower stabilizer and packer design.	100
6.36	Design of first produced and tested BHA.	101
6.37	Design of straight sub.	102
6.38	Overview of bit and were bit profile, active and passive gauge are placed [60].	103
6.39	Traditional cutter layout to the left and new layout to the right [67].	104
6.40	2D base sketch with cutters profile.	105
6.41	Geometry of cutters.	106
6.42	Cutter back rake angle seen from side view.	107
6.43	Cutter side angle seen from top view.	107
6.44	From 2D sketch to bit body and then with blades.	108
6.45	Top to the left and side view to the right of the bit with cylinders.	108

LIST OF FIGURES

6.46 Four nozzles extruded from bit face. 109

6.47 Final bit ready for 3D printing. 109

6.48 Alternative design seen from the top to the left and from the side to the right in the figure. 110

6.49 From left to right: Alibaba pilothole bit, NTNU bit 1, NTNU bit 2, Alibaba bit 1, Alibaba bit 2 and DSATS bit. 111

6.50 Arduino Nano 33 BLE Sense [77]. 112

6.51 USB-6212 by National Instruments used for topside sensors [48]. 113

9.1 Illustration of the proportional error the process variable and the set point [42]. . . 128

9.2 Illustration of the integral error [42]. 129

9.3 Illustration of the derivative error [42]. 129

9.4 Response types for a PID controller system [78]. 131

9.5 2nd order bezier curves [51]. 134

9.6 PID block in Simulink with tuned parameters. 140

9.7 WOB PID Controller in Simulink. 141

9.8 Azimuth controller system in Simulink. 142

9.9 Extended Kalman filter block in Simulink with input y_1 and state estimate output \hat{x} . 142

9.10 The ROP estimation with kalman filtering. 143

9.11 Azimuth rotation velocity estimation with kalman filtering. 143

9.12 Graphical User Interface (GUI) for manual operation. 144

9.13 Graphical User Interface (GUI) for autonomous operation. 145

10.1 Free OPC UA Modeler main window. This specific screenshot highlights object RigRequest_Hoist with child method component "eRapExecute" and reference event "eRapProgressChange". 153

10.2 UaExpert main window. This screenshot shows a connection to the OPC UA server in python in the upper left corner. The available objects in the address space is shown in the bottom left corner. Data access is located in the middle, and the attributes of the chosen node is shown in the upper right corner. The prompt in this screenshot shows the input parameters for the ROPSetpoint request. . . . 154

10.3 Event related to ROPSetpoint request call. Progress, Status, and RequestID are written to console. 155

11.1 Azimuth rotation test setup. 158

11.2 Resulting direction after running 180/deg for a minute. 159

11.3 Top drive rotation test setup. 160

11.4 Buckling test of aluminium 7075 pipe. 162

11.5 Drillpipe buckled. 163

11.6 Setup of simple bending test. 164

11.7 Bending test resembling fixed-free scenario. 165

11.8 "Rolling test" to check the results of the bending test. 166

11.9 Twisted rod. 167

11.10 WOB, RPM and torque plots from the run where twist-off occurred. 169

11.11 Cement test cylinder 171

11.12 Mixing of cement 172

11.13 Poor hole quality with spiral pattern. 174

11.14 Second attempt with improved hole quality. 175

11.15 Smooth vertical borehole with a clear kick-off point and direction. 176

11.16 ROP measurements for Alibaba bit 2. 179

11.17 Torque measurements for Alibaba bit 2. 180

11.18 Accelerometer data noise for Alibaba bit 2. 181

11.19 Accelerometer data noise for NTNU bit 2. 181

LIST OF FIGURES

11.20 Plotted well path from the sensor card estimates of position. 182

11.21 Pilot hole procedure. 183

11.22 WOB, torque and ROP plots from the Equinor-demo run. 185

11.23 Measured azimuth rotational velocity during Equinor-demo run. 186

11.24 WOB, torque and ROP plots from the extra run during competition. 188

11.25 Measured displacement of 17 cm. 189

13.1 Hydraulic swivel alignment. 197

13.2 T-shaft and swivel shaft connection with O-ring and Teflon disk. 198

13.3 Alignment of azimuth system. 199

13.4 Azimuth system mount adapter. 200

13.5 Top drive adaptor block. 201

13.6 Aligning of rig frame. 201

13.7 Practical and theoretical path of maximum inclination build with a bend angle of
5.28 degrees. 202

13.8 Measured angle of bent sub equal to approximately 5 degrees. 203

13.9 Verification of new bent sub equal angle. 203

13.10 Drilling parameters during the stuck pipe run. 205

13.11 Measured azimuth rotation with gradually increasing set-point. 206

13.12 Location of downhole sensor card in the BHA. 207

13.13 3M Scotch-Weld Epoxy Adhesive DP110. 207

13.14 Bottom hole assembly with sensor card submerged in water. 209

13.15 Bottom hole assembly with sensor card submerged in water during drilling. 210

13.16 The Plasti Dip used to seal the downhole sensor card. 211

13.17 Drive shaft and packer modifications. 212

13.18 Connection between rod and joint made up of two set screws and a steel sleeve. 213

13.19 Bronze disc in lower stabilizer to minimize friction between joint and inside of stabilizer.	213
13.20 Set screw inserted through the packer and into the lower stabilizer to prevent packer from unscrewing.	214
13.21 Set screws to prevent threads from unscrewing in the joints between components.	214
13.22 Melted steel joint because of friction between the steel disc and the joint.	215
13.23 Drive shaft and packer modifications.	216
13.24 Snapped shaft in the universal joint because of too high rotational velocity.	216
13.25 Universal joint and drive shaft welded together.	217
13.26 Spot welded cap to prevent it from popping out.	218
13.27 Packer made of PEEK with flat head screws to prevent it from unscrewing.	219
15.1 Dirty acrylic glass from cuttings squirting when flushed out of rock.	225
15.2 Semi-closed loop mud system from 2018 where the interface between rock and riser is sealed to guide flushing up through the rubber hose directly to the drain [52].	225
15.3 Picture showing limited space on the rig when working with two computers.	226
15.4 Setup of magnetic field with an electromagnet (black) [42].	228
J.1 Right-angled gearbox from Gigager.	300
P.1 DSATS drill bit.	328
R.1 Relationship between Re and f for settling particles in Newtonian fluids [7].	334

Introduction

A large amount of the drilling operations on the Norwegian Continental Shelf (NCS) are time-consuming and costly with big energy consumption. In the past couple of years, the focus has been directed to the economic measures of the industry. The most recent oil price drop forced companies to develop more efficient administrative and operational processes in order to save costs. The 2020 Russia–Saudi Arabia oil price war and the Coronavirus pandemic has put additional pressure on the oil and gas industry worldwide in 2020 [62].

In Norway, drilling activity is said to continue for the next 50 years. Thus research and development of new technology are still important to ensure improved efficiency and reduction of operational costs related to drilling [62]. Despite the challenges mentioned above, the petroleum industry should continue to invest in new technology and extended research related to drilling and well technology.

Oil companies are usually the most significant contributors to research with the intention of reducing costs and Non-Productive Time (NPT) in drilling operations. There are multiple challenges in the drilling operations that lead to reduced drilling speed, and downtime related to human errors is one. Therefore, automating drilling operations have been a goal in the oil and gas industry for over a decade. A benefit of automated drilling operations is minimizing the potential hazards on personnel and equipment while improving the overall efficiency. Autonomous drilling is a multidisciplinary field linking together people with different competencies. Although the level of automation varies on drilling rigs today, companies are constantly trying to develop and improve technology using intelligent planning and execution of drilling operations [79].

The industry is working to increase efficiency with fully automated processes such as tripping of drillpipes with continuous circulation and back-pressure control. Downhole sensors, control systems, and technology such as wired pipe enable continuous feedback control and can optimize the drilling operations based on real-time drilling parameters [42]. A motivation for autonomous drilling is to reduce and possibly eliminate hazards related to drilling operations. The safety of drilling personnel is a considerable driving mechanism to fully automate offshore operations because the risk of pipe handling, heavy lifting, and unforeseen accidents can decrease significantly by replacing rig personnel with automated machines. A reduced headcount will further reduce the operating cost significantly because of high wages on the NCS [42].

A group of Society of Petroleum Engineers (SPE) members founded the Drilling System Automation Technical Section (DSATS) in 2008 to "help accelerate the uptake of automation in the drilling industry". In 2014, the section organized the Drillbotics competition for young engineering talents from universities worldwide to further explore new solutions within the field of drilling technology and automation.

The Norwegian University of Science and Technology (NTNU) first participated in the Drillbotics competition in 2016 and placed second before landing the first place the year after with excellent results. In the consequent years, the teams have been among the top three finalists. In 2019 and 2020, the teams were hindered from competing because of customs issues and restrictions related to the Corona pandemic.

The main challenge in the competition of 2021 is to drill a deviated well autonomously. The team must drill a vertical pilot hole before kicking off to reach multiple pre-defined targets in a provided sandstone rock sample. The rig must drill with a closed-loop control system.

This thesis presents the students' work before the Drillbotics competition in June 2021. The team investigated autonomous solutions and performed multiple tests and modifications of the system during the project's design phase. Many changes were made to the proposed design presented in the "Phase 1 report"[9]. Proper project management was essential to ensure that the necessary tasks were completed and goals were achieved on time without compromising the safety of personnel and equipment involved. The management also had to include contingency plans should something unexpected occur during the project.

Chapter 2

Organization

A project of this magnitude requires collaboration and teamwork across disciplines to be executed effectively. The Drillbotics committee advises the universities to gather students from different disciplines to solve engineering challenges related to the competition requirements. To achieve this, and because of the project's complexity, a well-structured and organized team with good planning and scheduling will be crucial. Splitting tasks and distributing duties is important to cover all the tasks needed within the time constraint. This section will introduce the team members from Norwegian University of Science and Technology (NTNU) participating in the 2021 Drillbotics competition, presenting delegation of responsibility and roles, as well as the project management approach and strategy.

2.1 Drillbotics Team 2021

A maximum of five students can form a team, according to the Drillbotics guidelines (Appendix A). The 2021 NTNU Drillbotics team consist of four members, three from Department of Geoscience and Petroleum (IGP) and one from Department of Engineering Cybernetics (ITK), all depicted in Figure 2.1. In addition, the team is supported by four supervisors; three from IGP and one from ITK. Furthermore, two lab engineers are available for technical support with practical challenges that may occur. The full team structure is visualized in Figure 2.2.



Figure 2.1: 2021 NTNU Drillbotics Team.

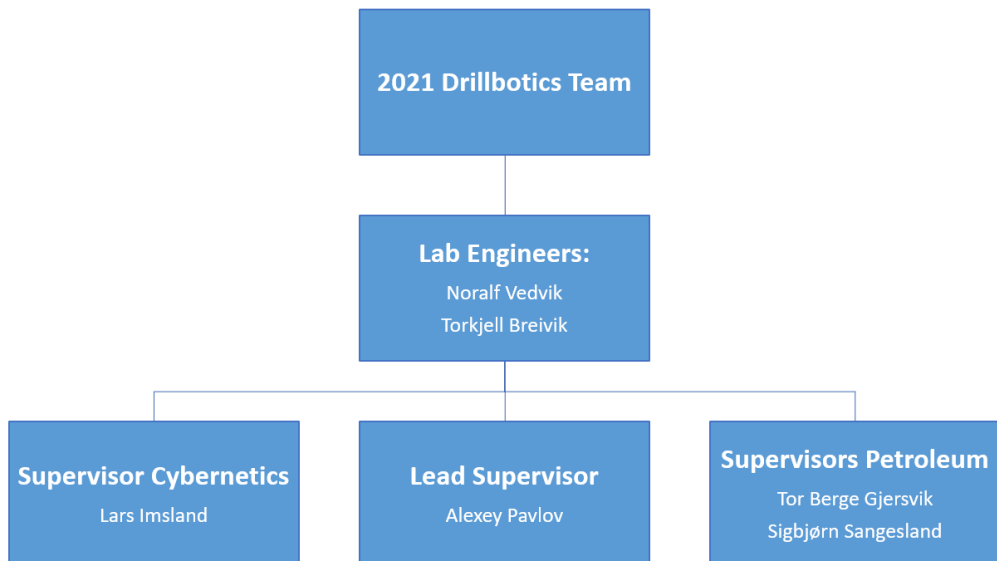


Figure 2.2: Team system for the 2021 NTNU Drillbotics Team.

2.2 Roles

Specific roles and areas of responsibility were assigned to the team members to ensure an efficient workflow throughout the project. It is essential to map out the team members' abilities, knowledge, experience, and interests to ensure a sustainable, healthy and efficient work environment. This was done at an early stage of the project to have the best possible pre-requisites to assign tasks and areas of responsibility. Specific roles and responsibilities were assigned to each member, but most problems were discussed in the plenary and solved with close collaboration between the team members and the supportive members. Figure 2.3 presents the assigned team roles and responsibilities.

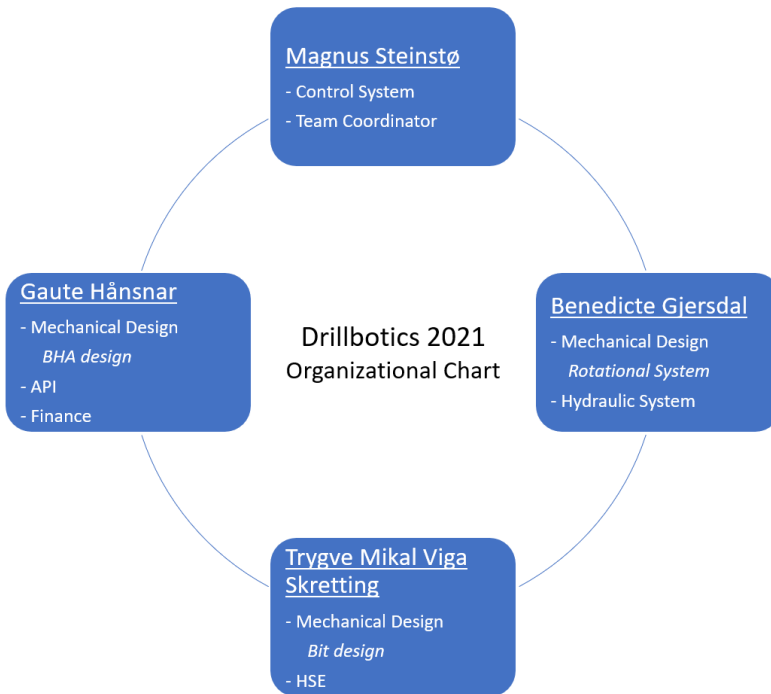


Figure 2.3: Student team organization chart.

The supervisory team will be responsible for guidance and feedback during the project. Scheduled meetings every two weeks with everyone involved in the project ensured continuous information flow and close collaboration. The lab engineers were located in the same building as the team members and served as their closest discussion partners.

2.3 Project Management

To work according to a planned schedule, a clear project management strategy was established. The student team presented ground rules and expectations in Drillbotics "kick-off" with their supervisors in September 2020. The intention was to avoid misunderstandings and unnecessary discussions at a later stage. A Kanban structure provided each member with planned tasks, tasks under execution, and completed tasks as illustrated in Figure 2.4. The student team members held weekly meetings within the team on Mondays and Fridays to present completed tasks and plans. The Kanban after each meeting.

A shared office close to the lab engineers and supervisors opened up for low-threshold day-to-day discussions within the team and support team. Because of restrictions related to the coronavirus pandemic, a second office was acquired to comply with the regulations.

Based on experience with project management in other projects, Microsoft Teams seemed like a sufficient platform for storing all the documents related to the project. The Kanban structure, budget sheet, Moments of Meetings, codes and scripts, Solidworks-files, and calculations were stored on the platform. To ensure efficient and thorough writing of the project report and thesis, Overleaf allowed everyone to work on the document simultaneously.

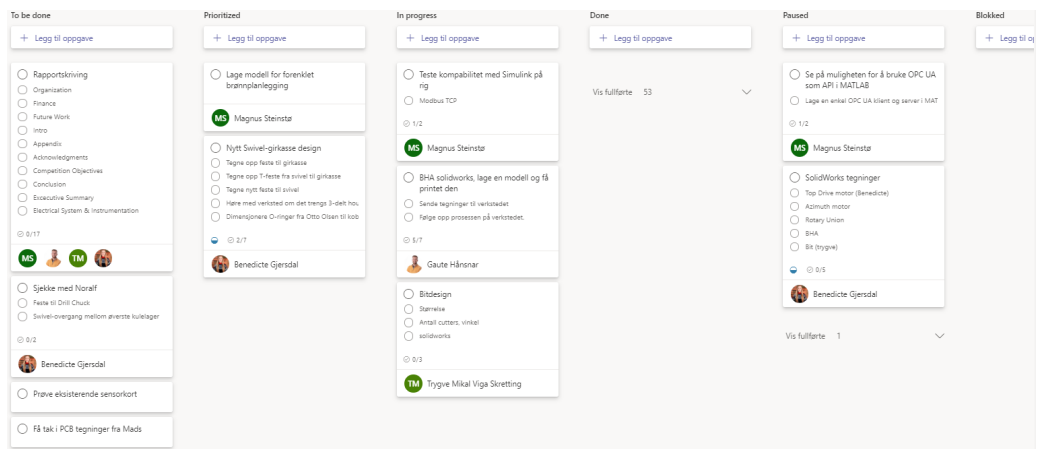


Figure 2.4: Kanban-structure.

2.4 Time Management

Good time management is of utmost importance to have control and overview of associated tasks in a project. The Drillbotics project is complex, with numerous small tasks. It is also a highly

practical project where many tasks depend on each other, amplifying the need for time management. A time planner was set up in Microsoft Teams as shown in Figure 2.5, such that every team member could both edit and inspect the tasks and their respective deadlines.

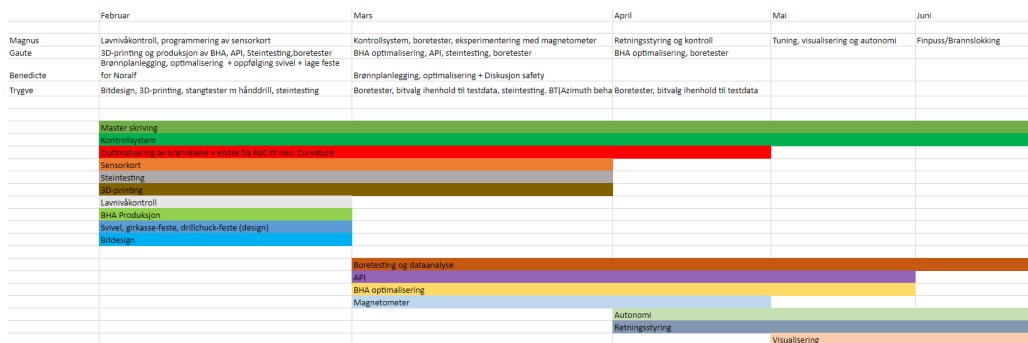


Figure 2.5: Time management in Microsoft Teams written in Norwegian for convenience.

Phase II of the project offered challenges due to numerous tests that resulted in the discarding of concepts and changes related to the components present on the rig. This led to delays and downtime on the rig that was not accounted for beforehand. The team held meetings to assign new tasks to members waiting for parts to be manufactured, repaired, or in transit to save time.

(This page is intentionally left blank)

Chapter 3

Safety

Hazards are present in any engineering project, and safety was the most important priority and concern in the thesis project. Not identifying the possible hazards could lead to severe damage to the people involved, the rig components, and the surrounding environment. The developed safety routines of this thesis project aim to meet the Health, Safety, and Environment (HSE) regulations at the Petroleum Technical Center (PTS).

This chapter discusses all safety aspects related to the project and how they can be related to the oil and gas industry. It continues to discuss how the authors have handled the situation with COVID-19. Furthermore, the chapter present and discuss present hazards during construction work of the rig. This section will be somewhat brief because most of the construction work such as the framework, drill floor and hoisting system have been recycled from the past years project. Finally, a discussion of hazards while operating the rig will be presented. Many of the safety regulations from the Phase I report [9] are still relevant and may be already familiar to the reader.

3.1 Safety in the Oil and Gas Industry

The authors involved in this project have constructed and operated a miniature drilling rig. Therefore, the authors have investigated safety procedures in the oil and gas industry to locate potentially similar hazards. However, the miniature drilling rig is scaled down by a factor of nearly 1:115 compared to industry size. Scaling down, some hazards remain unchanged while others can be dismissed. Safety regulations as per industry standard are still suitable for the project, but some hazards and safety aspects was examined by using other standards.

In the oil and gas industry many potential hazards may cause severe damage if not properly controlled. The use of flammable and toxic chemicals is a common potential hazard if not handled correctly. Same holds for high pressures and use of heavy equipment. As a consequence, the industry is known for its comprehensive safety standards. However, in the US, the fatality rate is seven times higher in the oil and gas industry compared to other industries [70]. The article from *EHSToday*, state that the most imminent hazards an oil rig worker is exposed to are caused by human error, worker culture, recklessness, negligence, lack of proper PPE, miscommunication and misuse of equipment.

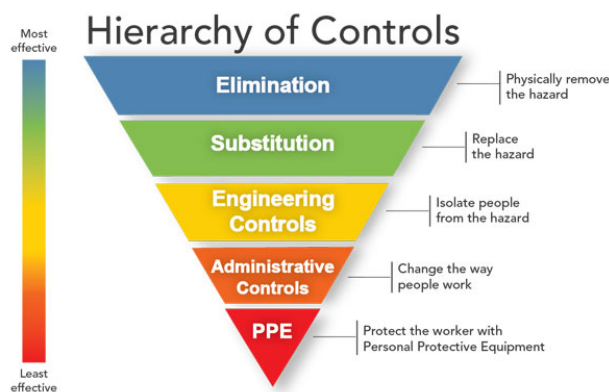


Figure 3.1: NIOSH's hierarchy triangle of controls. It highlights different measures efficiency with respect to avoiding hazards [32].

Although, implementing autonomous processes and digitizing data and communication methods can reduce these factors, in order to build a fully autonomous drilling rig, manual labor is still necessary. The work must be performed with respect to safety. Figure 3.1 illustrates a hierarchy triangle highlighting the most effective methods when handling hazards. The most effective solution is, obviously, to eliminate the hazards all together. Unfortunately this is not always possible. Therefore other approaches to handle the hazards must be done.

In this thesis project, it was important to ensure that all personnel involved in the project, including the team members, were familiar with the regulations. Everyone present was responsible that the regulations were followed correctly at all times. The correct use of PPE is often very effective but easy to forget. All personnel have completed a mandatory safety course at NTNU. The course emphasize the importance of correct use of PPE. In addition, other possible hazards related to laboratory work was investigated. Relevant measures to handle the hazardous situations were discussed. This could be to eliminate the hazard, replace the hazard, isolate the hazard, change

the way of working or use PPE. A safety walk-through in the workshop was performed with trained personnel. Fire extinguishers and emergency exits were shown. Other safety issues like the crane in the ceiling and toxic chemicals in the workshop were highlighted.

3.2 COVID-19

A new hazard to the thesis project this year compared to previously, was the corona virus and the risk of becoming ill with COVID-19. As a consequence, an infection control was established with inspiration from the national online health services in Norway, Helsenorge.no. This was the official information page about the corona virus in Norway. The most important and relevant instructions are listed below[28]:

- If you are ill, stay at home.
- Avoid coughing or sneezing directly onto others.
- Keep a distance of at least one metre to others.
- Cough / sneeze into a paper tissue that you then dispose of. You should then wash your hands.
- Cough / sneeze into the crook of your elbow if you do not have tissues available to avoid spreading droplets into the air.
- Wash hands frequently and thoroughly with soap and luke-warm water, especially when you have been in contact with other people.
- You can also use an alcohol-based disinfectant if soap and water is not available.
- Find alternatives to shaking hands and hugging.

These guidelines must be followed at all times to decrease the chances of catching the virus. All personnel were assigned personal PPE equipment and were placed on separate offices. This was done to reduce the risk of spreading the virus should someone get infected. The 1-meter instruction was possible to achieve when the team members sat on three separate offices. However, staying home in case of any symptoms was the most important measure to minimize the risk of infection. There was a low threshold for working from home and all persons involved in the project corrected each other if the recommended social distance was not complied with.

3.3 Potential Safety Hazards

To maintain a good safety standard during the course of the thesis project, it was important to be aware of, and be reminded of, the potential hazards present during construction and operations. All possible hazards was identified prior to any new task or operation. In the following section, these hazards are presented.

Hazardous energy generated by electrical components can be present during operation mode or when modifying the electrical system. The most typical electrical hazards are short circuits and electrical shock. This can damage equipment and personnel. Safe and proper installation of the equipment minimize the exposure of uncontrolled hazardous energies to the operating personnel. Cutting and other types of lacerations can also occur if operating procedures are not followed and maintained. Insufficient attention to electrical hazards may also damage the other components on the rig. Because the rig operated without a hydraulic pump, hazards related to hydraulic power were not present.

Chemical hazards from drilling fluid are not present in this project because the drilling fluid is clean water. However, there was a potential health risk related to the use of cement when making rock samples for test drilling. The cement cuttings are flushed out of the drilled hole. Insufficient cleaning after each drilling session could lead to cuttings remaining on the floor. When dried, people walking near this area, could kick up and inhale the cement dust. The risk of inhaling cement dust was also present when mixing the cement slurry. The process of making the rock sample depended on the rate of test drilling sessions but was approximately done every two weeks. This resulted in a potentially increased risk for future lung diseases if not correct PPE were used.

Ergonomic hazards are related to activities that may cause injuries such as back pain, muscle strains and shoulder injuries. Activities related to this project such as pushing, pulling and heavy lifting of equipment and the rock sample are examples that may causes mentioned injuries. If done in a non-ideal body positions or if the same task is done repetitively, the risk for permanent damage increases.

Mechanical hazards are related to the moving parts on the drilling rig and can endanger the involved personnel if not handled. The potential mechanical hazards are pinching, cutting, crushing, and injuries related to heavy lifting. Moving parts on the rig are: the drill bit, drillstring and the top assembly. The motions are illustrated in Figure 3.2.

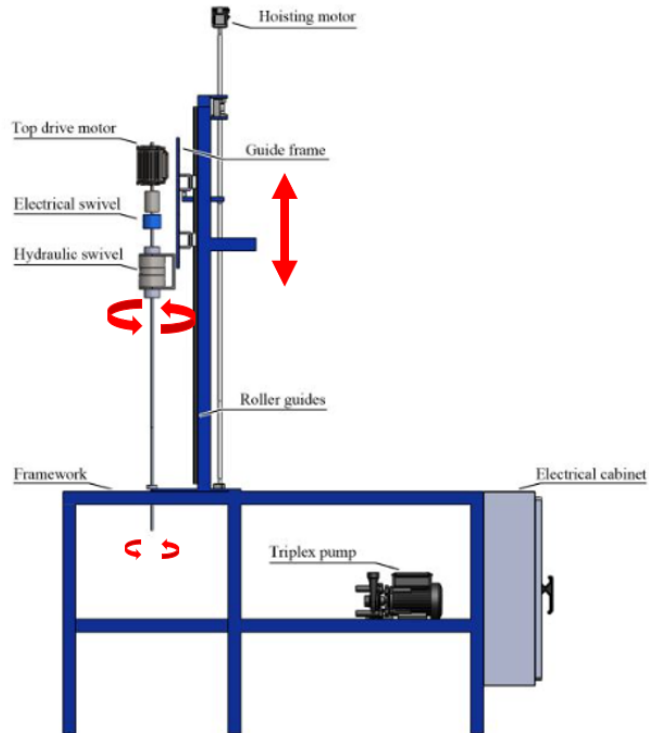


Figure 3.2: Direction of moving components on the miniature drilling rig.

Other mechanical hazards are related to modifications done on the rotary system and hydraulic system. This includes the top drive motor with the rotating rod as well as the hydraulic swivel which were all changed, modified or mounted with new components. Vibrations and pipe stresses is also present during drilling operations, posing a potential threat.

3.4 Safety Measures for Handling Potential Hazards

To provide the reader with an overview of the safety measures related to this project, they have been divided into two categories: safety measures during construction of the rig, and measures to consider during operation.

3.4.1 Safety Measures During Rig Construction

A large part of the construction work was done during the previous years of the Drillbotics project. The hazards related to construction work are therefore fewer than before. When dealing with the potential hazardous energies, NTNU safety regulations states that work that involves high voltage can only be done by authorized and properly skilled personnel. Measures related to the electrical system were to separate water from electrical wires and sources. In addition, the rig power system was shut off when working with the electrical system.

To avoid hazards when modifying the the rotary system and hydraulic system, these activities were always performed with guidance from skilled workshop personnel. Suitable PPE such as overalls, safety glasses, helmet, gloves, hearing protection and protective footwear was used during construction work. Figure 3.3 shows team member with correct use of PPE.



Figure 3.3: Team member with correct PPE under construction of the rig.

All personnel involved must ensure that there are no loose clothes or hair when working on the rig. When dealing with chemical hazards such as cementing, the people involved must wear a dust mask for the intended use.

3.4.2 Safety Measures During Rig Operation

After the construction work was done, the team started operating the rig for drilling. In this phase, the electrical, hydraulic, mechanical, and ergonomic hazards are present. The team therefore established several protective measures on the rig when in operation. The measure implemented to avoid mechanical hazards from moving parts is the protective cabinet. This is to be used at all times during operation. Figure 3.4 is a picture of the rotary system seen behind the protective acrylic cabinet.



Figure 3.4: The rotary system seen behind the protective glass.

Figure 3.5 shows the protective walls on all sides beneath the drill floor where the rock sample was placed. One of the four sides had hinges such that the rock sample easily could be placed underneath the drill floor. A lock was placed on it to prevent it from opening if moving parts such as the drillstring and drill bits got out of control. These measures ensured that none of the team members were exposed to moving parts, rock cuttings and drilling fluid when the rig was in operational mode.

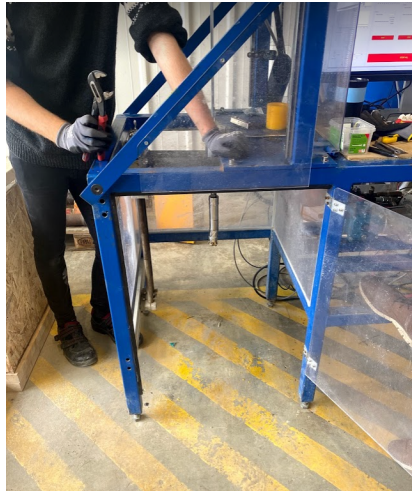


Figure 3.5: Safety cabinet beneath drill floor for placement of rock sample.

The measure done to avoid electrical circuits was to separate the electrical system from the hydraulic system. The protective walls were sealed using a sealant between the glass and the beams on the framework, as can be seen in Figure 3.5. Another measure was to have one person standing close to the water hose valve and drilling system to observe for any leakage in the hydraulic system. This ensured that the water supply was stopped quickly to avoid any water on the electrical components.

Limiting Operational Forces

Vibrations and pipe stresses in the system were another aspect of drilling safety that was considered. Setting operational limits for the rig such that the pressure inside the drill pipe was kept below the burst pressure reduced the risk of complications while drilling. The mechanical forces involved were kept at a level to which there is minimal risk of twist-off or buckling of the aluminum drill pipe and titanium rod. Weight On Bit (WOB) provided by the hoisting system was the biggest mechanical force that posed hazard to the people and equipment involved. WOB propagates through the drillstring down to the rock sample. Excessive WOB could lead to buckling of the drillpipe. This represented a risk of injury if a component were to loosen or break and hit a person at high speed. To reduce the risk of buckling, limit tests were done and a safety factor was added to the test limit. This value is then set as the maximum WOB value in the control script for the system.

Fire Safety Measures

The rig consist of a complex electrical equipment system in which can be considered as a po-

tential fire hazard during operation. Protective measures to mitigate this hazard were to know the location of fire extinguishers and fire hoses. The team did also have an understanding of the different type of fire extinguishers and how to act if a fire should arise. Because the electrical equipment is quite complex, modifications was only done by qualified personnel.

Ergonomic Measures

The authors considered ergonomic hazards when handling heavy rock samples. The risk was reduced by using a jack trolley when moving the samples. It was necessary to perform some tuning when placing the rock sample on the floor to ensure that the rock is horizontally with respect to the rig, not the floor. Operations performed with the rock sample also involved a risk of pinching hands and feet. It was necessary to use appropriate PPE such as proper gloves and footwear. Lastly, to avoid any hazards related to cement cuttings on the floor, the area was washed thoroughly and assured that there were minimum cuttings remaining around the rig.

Stop button and Stop work authority

There is an emergency button to stop an unwanted situation during operations. The button from Figure 3.6 will break the electrical circuit to all rig components and the operation will cease immediately.



Figure 3.6: Emergency stop button.

The team ensured that there were always one person close to the button while operating the rig. In addition to the stop button every team member had a stop work authority. Meaning all team members had a authority such that if a team member encountered an unsafe situation, the work could and should be stopped. The work did not continue before the hazard was handled.

(This page is intentionally left blank)

Chapter 4

Theoretical Background

Disclaimer: The contents of this section are a slight modification of the contents in the project report [9]. Control system theory can be found in chapter 9.

This chapter provides the reader with theoretical background knowledge to understand the justifications for choosing the specific components when designing the miniature drilling rig. The rig system account for factors related to directional drilling, BHA design, drillstring mechanics, drilling hydraulics and bit theory.

4.1 Directional Drilling

The essential aspect of directional drilling in this project was building and adjusting inclination while steering azimuth. This section presents the background theory on and research related to supporting the choice of the directional drilling system.

4.1.1 Application of Directional Drilling

The application of directional drilling varies with access and restrictions to the location of a reservoir in a field. Desired well paths and depletion patterns may also affect the choice of the drilling system. Some areas of application are [8]:

- Geo-steering.
- Drilling multiple wells from a single location.
- Drilling multiple wells from the same wellbore, often referred to as multi-lateral wells.

- Bypassing challenging formations and geological structures, e.g. salt domes and faults.
- Accessing reservoirs below urban areas or lakes.
- Correcting unwanted deviations in the well path.
- Increase depletion area, because vertical permeability and drainage area often increase with horizontal patterns vs. vertical.

4.1.2 Well Path

The trajectory of wells can be designed in many different ways depending on the formation and field geometry. Figure 4.1 shows a simplified illustration of three different types of well path design [10]. The proposed design in this project is built on a model which aims at drilling a type III well. However, in the Drillbotics competition, the targets provided may call for another type, and thus the system must be capable of drilling all three types.

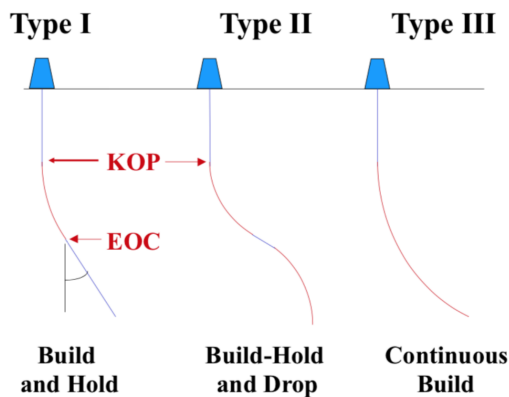


Figure 4.1: Types of well paths. [10].

A set of $\{X,Y,Z\}$ coordinates will be given on the day of the competition. The objective is to reach these targets as accurately as possible. The team will be given a total scoring based on evaluation criteria such as drilling efficiency and accuracy. Achieving a well path that meets the scoring criteria requires a control system that can understand and control changes in azimuth and inclination. The definitions of inclination and azimuth are given below.

- Inclination is irrespective of the compass direction and is the deviation from the vertical at a certain point. More specifically it is the angle between a vertical line and a tangent to the well path.

- Azimuth is the compass direction of a directional survey, more specifically the angle between the well path and North axis measured clockwise from North in the plane view.[8]

Each coordinate on the well path is measured with reference to a known fixed point, normally the Rotary Kelly Bushing (RKB) on the drill floor. The coordinates at this point will be $\{X,Y,Z\} = \{0,0,0\}$, which in field terminology corresponds to $\{0^\circ\text{North}, 0^\circ\text{East}, 0 \text{ m TVD}\}$. The well path design is developed from this point to the desired target(s). Petroleum wells start off with a vertical section until reaching a formation strong enough to handle the extra strain from building inclination. The point in the well where inclination begins to build, is referred to as the Kick-Off Point (KOP). It is illustrated in Figure 4.1.

The rate at which the gradient of the borehole direction change in compass direction with respect to North, is called the turn rate. It is expressed in deg/m or deg/ft. The designed well path is plotted in 3D, and the curve corresponding to the well path cannot be composed into inclination and azimuth separately because of turning and building. To present an accurate well path with accurate coordinates, it is given in dogleg angle (θ) or Dogleg Severity (DLS). The DLS [$^\circ/\text{m}$] is estimated using the following equation:

$$DLS = \frac{\phi}{CL} \quad (4.1)$$

Where $\phi[^\circ]$ is the dogleg angle and $CL[m]$ is the curve length. The dogleg angle is obtained using survey calculation methods presented in the next section.

4.1.3 Survey Calculation Methods

The wellbore position with respect to the surface is calculated with survey calculation methods [8]. Accepted methods are:

- Tangential method
- Balanced tangential
- Average Angle
- Minimum curvature
- Radius of curvature

Minimum Curvature Method

The Drillbotics guidelines require that the minimum curvature method is implemented in this project (Appendix A). This method is a further improvement of the balanced tangential method. The balanced tangential method assumes the well path to be approximated by two straight lines. With the minimum curvature method, these lines are replaced with a circular arc. A ratio factor, F , corrects the two lines based on the amount of bending between two survey points. This bend is referred to as the dogleg angle, ϕ [°], and is illustrated in Figure 4.2 along with other parameters mentioned in the equations below. The ratio factor is given by Equation 4.2:

$$F = \frac{AB + BC}{arcAC} \quad (4.2)$$

AB and BC in this equation are the two tangents between point A and C and can be expressed by Equation 4.3:

$$AB = BC = R \tan\left(\frac{\phi}{2}\right) \quad (4.3)$$

Where R is the radius of the bend and ϕ is the dogleg angle. The circular arc, AC , between the two survey points is calculated with Equation 4.4:

$$\frac{AC}{2\pi R} = \frac{\phi}{360} \rightarrow AC = \frac{\pi R \phi}{180} \quad (4.4)$$

By inserting Equation 4.3 and 4.4 in Equation 4.2, the ratio factor can be fully expressed as:

$$F = \frac{2}{\phi} \left(\frac{180}{\pi}\right) \tan\left(\frac{\phi}{2}\right) \quad (4.5)$$

where the dogleg angle, ϕ , is calculated using Equation 4.6:

$$\phi = \cos^{-1}[\cos\alpha_1 \cos\alpha_2 + \sin\alpha_1 \sin\alpha_2 \cos(\beta_2 - \beta_1)] \quad (4.6)$$

The change in North, East and Vertical is calculated with the following equations:

$$\Delta V = \frac{F \cdot L}{2} (\cos\alpha_1 + \cos\alpha_2) \quad (4.7)$$

$$\Delta N = \frac{F \cdot L}{2} (\sin\alpha_1 \cos\beta_1 + \sin\alpha_2 \cos\beta_2) \quad (4.8)$$

$$\Delta E = \frac{F \cdot L}{2} (\sin\alpha_1 \sin\beta_1 + \sin\alpha_2 \sin\beta_2) \quad (4.9)$$

Where L is the measured depth, α is the inclination and β is the azimuth.

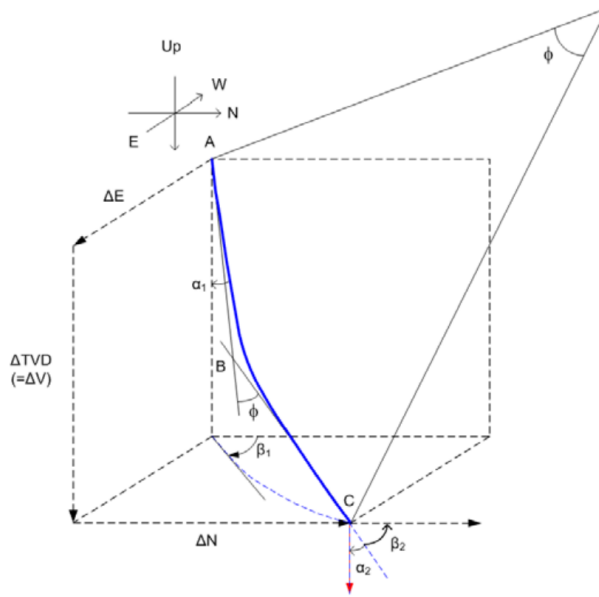


Figure 4.2: Relevant parameters for the minimum curvature method [8].

Radius of Curvature Method

For simplicity, the radius of curvature method has been used in this thesis. This method assumes that the curve between two points is estimated by the curve of a cylinder [8]. The radius of the cylinder can then be expressed as:

$$\frac{I_2 - I_1}{360} = \frac{CL}{2\pi RC} \quad (4.10)$$

$$RC = \frac{180CL}{\pi(I_2 - I_1)}$$

Where I_2 and I_1 are the angles at two survey points. An equation for CL can be found from Equation 4.10.

$$CL = \frac{RC\pi(I_2 - I_1)}{180} \quad (4.11)$$

Radius of Curvature (RC) [m] is calculated separately for azimuth and inclination angle.

$$RC_A = \frac{(180)(30)}{\pi B},$$

$$RC_I = \frac{(180)(30)}{\pi T}$$
(4.12)

Where B is build-up rate and T is turn rate. Relevant parameters for creating a well path, such as inclination, azimuth, and dogleg angle (ϕ), are illustrated in Figure 4.3.

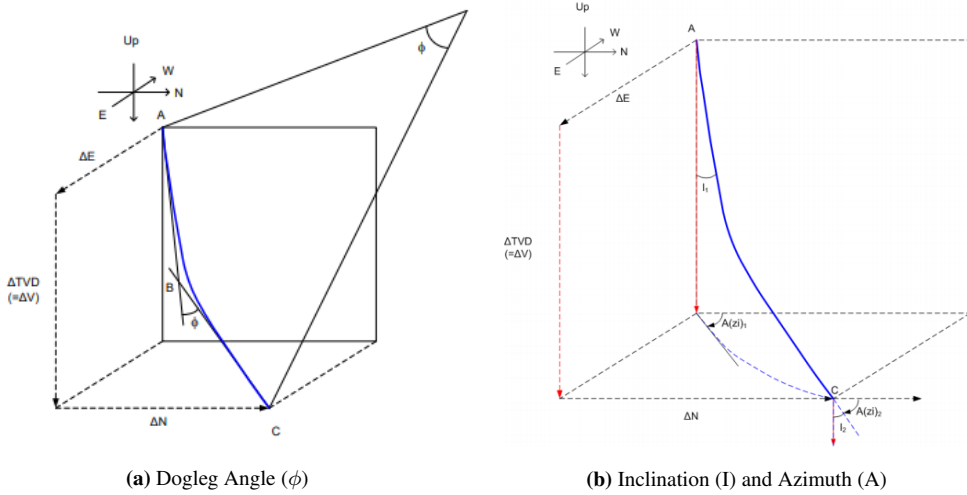


Figure 4.3: Relevant parameters for development of a well path [8].

4.2 Bottom Hole Assembly (BHA)

Bottom Hole Assembly (BHA) design is decisive to whether the drilling rig will be mechanically sustainable and capable of building well paths as expected or not. The basics of BHA design will be covered in this section to justify the design used on the rig.

4.2.1 Directional Steering

The BHA has to be designed to drill well paths and build an angle that matches the planned trajectory. Three common BHA design alternatives for directional control are [8]:

- Traditional assemblies
- Steerable motor assemblies
- Rotary Steerable System (RSS)

Traditional assemblies use a bent sub and a straight motor. Because this inhibits drill string rotation, it is not often seen in the industry today. The traditional assemblies are therefore dependent on a mud motor for bit rotation [8].

Direction control changed significantly with steerable motor assemblies. They consisted of a mud motor with a bent sub or bent housing. In comparison to a traditional assembly, the steerable motor assemblies are more versatile and sustainable. They can kick off and build angle, drill tangential sections, which provide directional control. This technology is often implemented to improve the drilling performance in challenging formations.

Rotary Steerable System (RSS) is often the preferred solution to directional control. A RSS is capable of rotating and steering the drill bit simultaneously. Although it is the superior directional control system, it is complex and often not economically viable. Two main concepts make up the RSS; push the bit and point the bit, discussed in further detail in subsection 4.2.6.

4.2.2 Dogleg Severity Based on BHA Configuration

DLS can be calculated in two ways. Equation 4.1 can be used to calculate dogleg severity based on well trajectory parameters. To design a BHA capable to build the required well path inclination, the DLS can be calculated based on BHA configurations [8]:

$$DLS = \frac{2\theta}{L_1 + L_2} \quad (4.13)$$

Where $\theta[^\circ]$ is the bit tilt, $L_1[m]$ is the distance from the upper stabilizer to the bend, and $L_2[m]$ is

the distance from the bend to the bit. These parameters are illustrated in Figure 4.4.

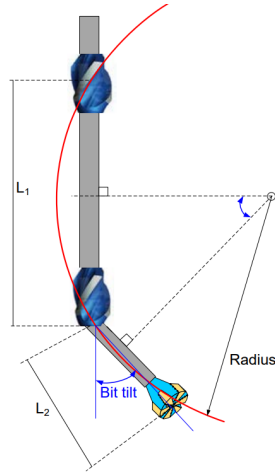


Figure 4.4: Dogleg Severity parameters based on BHA configurations [8].

4.2.3 Bent Sub

To achieve a BHA tilt as illustrated in Figure 4.4, a bent sub is used. Bent subs can have a fixed angle or adjustable angle. Figure 4.5 shows a fixed angle bent sub manufactured in steel.

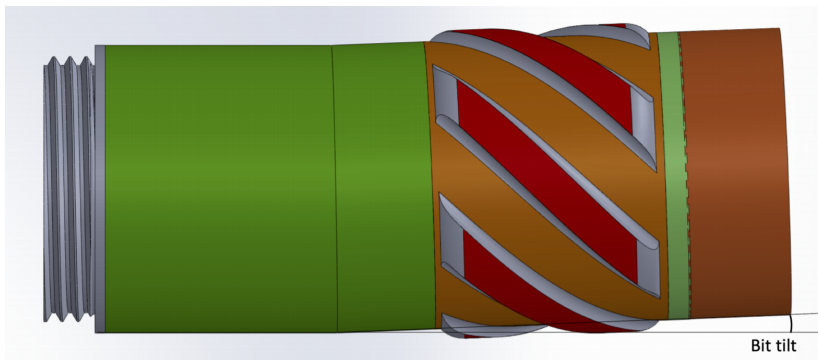


Figure 4.5: Fixed bent sub.

A surface adjustable bent sub consists of a double pin, lock housing, adjusting sleeve and offset housing. The sequence of adjusting the angle is shown in Figure 4.6 and is performed in the following manner:

1. Unscrew the lock housing and disengage the sleeve from its gear teeth.
2. Adjust the preferred angel.
3. Tighten the lock housing to detain the desired angle.

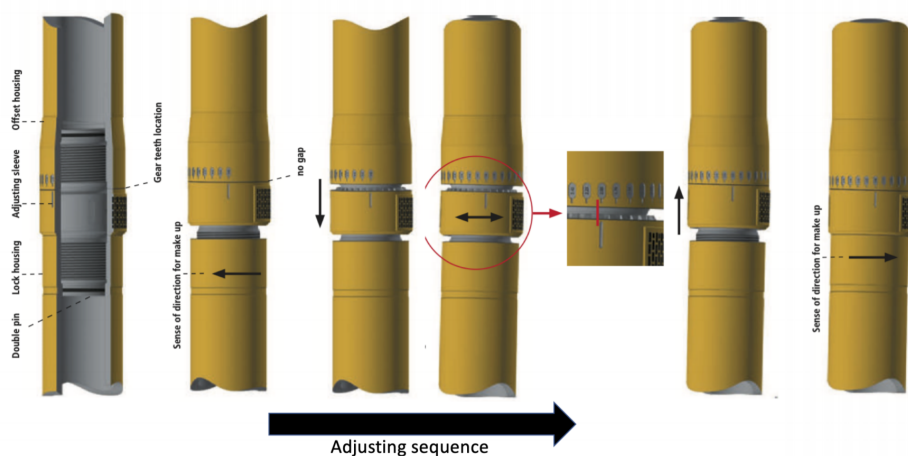


Figure 4.6: Adjustable bent sub [31].

4.2.4 Transmission Section

If a bend is present in the BHA, the rotation provided by the power section will be eccentric with respect to the bit. A transmission section is therefore necessary to generate concentric rotation from the eccentric rotation. The torque and RPM are transmitted from the power section to the bearing section. Flexible rod and universal joints are two frequently used methods for transmitting rotation [8].

Because flexible rods does not require lubrication and have low maintenance costs, they are usually preferred in the industry. However, they are different from universal joints which allow for much greater lateral bending. Both equipment types are illustrated in Figure 4.7.

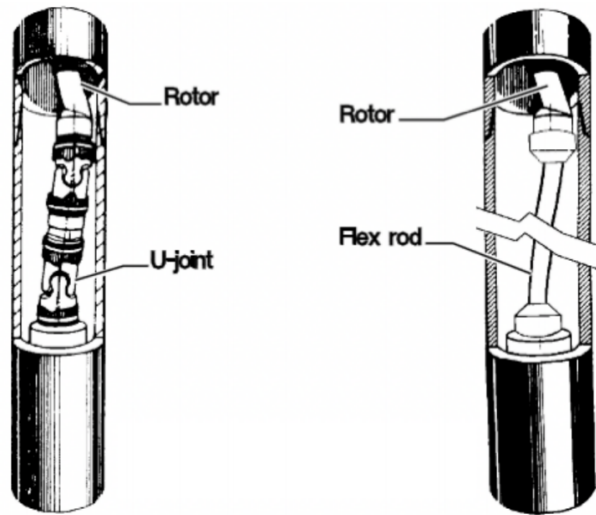


Figure 4.7: Transmission joints; universal joint and flexible joint respectively [8].

4.2.5 Bearing Section

The bearing section in the BHA transmits concentric torque and RPM from the transmission shaft through a drive shaft to the drill bit. In addition to this, the bearing section acts as radial and axial support. The system that supports on and off bottom load and hydraulic thrust consists of three sets of bearing, two radial, and one axial bearing.

The drilling fluid can flow through the drive shaft as illustrated in Figure 4.8. The bearings are cooled and lubricated by the diverted fluid that flows through them. This diverted flow generates downwards hydraulic thrust that must be balanced by the upward thrust from the WOB to increase bearing lifetime.

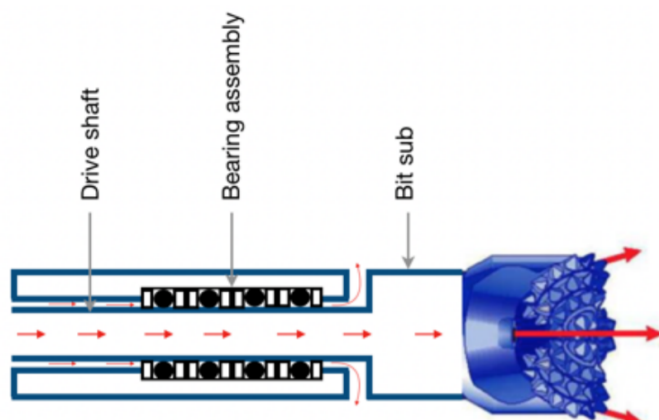


Figure 4.8: Bearing section showing flow paths in red [11].

4.2.6 Rotary Steerable System (RSS)

Rotary Steerable System (RSS) can improve directional drilling significantly by solving challenges related to conventional rotary assemblies and steerable motors. RSS allows for continuous drill string rotation while steering the bit. This feature increases the ROP which then again improves the overall drilling performance. RSS will lower the torque and drag forces and also improve hole cleaning and hole quality. Directional control is attained using the three-point contact principle. The points are; the drill bit, a near-bit stabilizer, and an upper stabilizer [8]. As mentioned, there are two types of RSS:

- **Push the bit.** Motorized pads are mounted on the outer part of the middle geometric contact point. The pads are activated by drilling fluid and pushed against the borehole wall to build direction.
- **Point the bit.** Motorized mechanism point the bit in the desired direction. This is different from a mud motor which has to orient the drill string manually. . The general concept is the same; the bit will have an offset from its center axis.

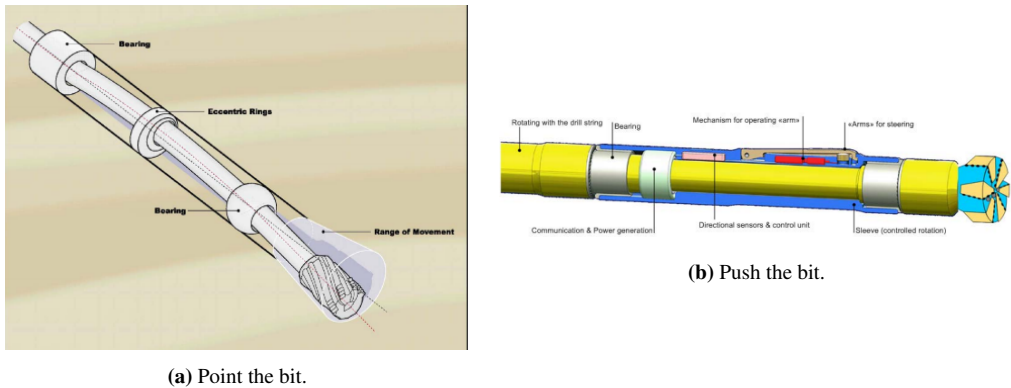


Figure 4.9: The two methods of RSS [8].

RSSs provide constant drilling parameters which result in more efficient management and control of the weight transfers and vibrations in the system [8]. The well profile tends to be smoother because of decreased tortuosity. Although the advantages are many, use is limited to complex operations such as extended reach drilling or complex well profiles. The technology is complex and expensive, both mechanically and electronically.

4.3 Drill String Mechanics

Understanding the mechanical limits present during drilling is crucial to prevent drill string failures. This section presents challenges that may be encountered during drilling operations and the formulas associated with them.

4.3.1 Buckling

One of the main parameters that are monitored and adjusted to optimize the drilling is the WOB. On a full-scale drilling rig, the WOB is applied to the BHA using drill collars and heavyweight drillpipes. The miniature rig presented in this project applies WOB using a hoisting system, later described in section 6.5. The applied WOB propagates to the BHA through the drillpipe. This motion introduces the risk of buckling effects on the pipe.

Drill string buckling can appear in two stages; sinusoidal and helical [18]. Increasing the compressive load in the system, i.e., the WOB, will generate sinusoidal buckling, and the drill string will resemble a two-dimensional waveform or a sinus wave. As a result, the drill string will wind back and forth against the wellbore. If additional compressive load is applied, the deformation generates helical buckling. In this stage, the drillpipe will deform into a helical shape moving along the wellbore—this increases the contact area between the drill string and wellbore, which

further increases the drag force. Maintaining a constant WOB will thus require more axial load. Figure 4.10 illustrates the two stages of drill string buckling.

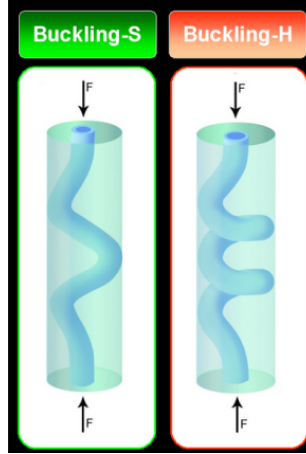


Figure 4.10: Illustration of first and second stage of buckling respectively [68].

Drill string buckling occurs when the axial compressive force exceeds the drill strings' critical limit. This limit can be estimated using Euler's formula assuming the drillpipe as a long slender column [29]:

$$\sigma_{cr} = \frac{F_{cr}}{A} = \frac{\pi^2 E}{\left(K \frac{L}{r_g}\right)^2} \quad (4.14)$$

Where $\sigma_{cr}[Pa]$ is the critical buckling load, $E[Pa]$ is the modulus of elasticity, $L[m]$ is the unsupported drillpipe length and $r_g[m]$ is the radius of gyration. K is the effective length factor determined by end condition of the column, seen in Table 4.1.





The radius of gyration, $r_g[m]$, represents the distance from a centroid at which all the area could be concentrated, without affecting the moment of inertia [30]. It is calculated using Equation 4.15:

$$r_g = \sqrt{\frac{I}{A}} \quad (4.15)$$

$$I = \frac{\pi}{64}(OD^4 - ID^4) \quad (4.16)$$

Where $I[m^4]$ is the second moment of area for a pipe, $A[m^2]$ is the cross-sectional area of the pipe, and $OD[m]$ and $ID[m]$ is the outer and inner diameter of the pipe, respectively.

Table 4.1: Effective length factor, K , for different end conditions [29]

End condition	Pinned-pinned	Fixed-fixed	Fixed-pinned	Fixed-free
Illustrations				
Theoretical K	1	0.5	$1/\sqrt{2}$	2
Recommended K	1	0.9	0.9	2.1

The relation L/r_g in Equation 4.14 is often referred to as the slenderness ratio, R_s [29]:

$$R_s = \frac{L}{r_g} \tag{4.17}$$

The ratio increase with the column length such that longer columns are more susceptible to buckling. Because Equation 4.14 is only valid for long and slender columns, the critical limit for intermediate columns are calculated with the Johnson formula, where $\sigma_{ys}[Pa]$ is the yield strength of the pipe material [29]:

$$\sigma_{cr} = \sigma_{ys} - \left(\frac{\sigma_{ys}KL}{2\pi r}\right)^2 \left(\frac{1}{E}\right), \quad \frac{L}{r_g} \leq \left(\frac{L}{r_g}\right)_{cr} \tag{4.18}$$

Whether or not the Euler's or Johnson's formula can be used to predict the buckling limit for a given column with certain end conditions depends on the critical slenderness ratio estimated with Equation 4.19.

$$\left(\frac{L}{r_g}\right)_{cr} = \sqrt{\frac{2\pi^2 E}{K^2 \sigma_{ys}}} \tag{4.19}$$

The maximum WOB can be estimated using Equation 4.20, when the critical compression load have been estimated with either Euler's or Johnson's formula.

$$F_{max\ WOB} = \sigma_{cr} A \quad (4.20)$$

4.3.2 Burst

Burst is a phenomenon that occurs when the internal pressure of the drillpipe exceeds the internal yield strength of the pipe. Barlow's formula was for a long time used for burst calculations. However, it has been proven too conservative for thick-walled pipes [6]. To account for the uncertainties concerning wall thickness, the American Petroleum Institute (API) added a reduction factor of 0.875. This has been inserted in Equation 4.21 [7].

$$P_{burst} = 2 \frac{0.875 \sigma_{ys} t}{OD\ SF} \quad (4.21)$$

Where $t[m]$ is the pipe wall thickness and SF is a safety factor. The safety factor is 3 for drilling and 2 for tripping.

4.3.3 Pipe Twist-Off

Drillpipe twist-off occurs when the induced shear stress exceeds the shear strength of the pipe. The shear stress is caused by applied torque, thus being a limiting factor for torque allowance. Under the assumption of thin wall thickness, constant $\tau(r)$ and a mean radius, the maximum allowable torque is defined by Equation 4.22 [68]:

$$T_{max} = \tau_{max} \frac{\pi}{16} (OD^2 - ID^2) (OD + ID) \quad (4.22)$$

τ_{max} is calculated using the Von-Mises criterion that assume $\sigma_{23} = \sigma_{31} = 0$ and $\sigma_{12} = \tau_{max}$:

$$\tau_{max} = \sqrt{\frac{2\sigma_{ys}^2 - [(\sigma_z - \sigma_\theta)^2 + (\sigma_\theta - \sigma_r)^2 + (\sigma_r - \sigma_z)^2]}{6}} \quad (4.23)$$

The radial, angular and axial stresses occur as a result of pipe bending, pressure, and WOB as shown in Figure 4.11. The radial and angular stresses are calculated using Equation 4.24 and 4.25 [49]. The only parameter not related to the dimensions of the drillpipe, is internal pressure and indicates that pressure is the only cause for radial and angular stresses. The total axial stress on the drillpipe is a sum of the axial stresses from pressure, WOB and bending, and is predicted using Equation 4.26, 4.27 and 4.28.

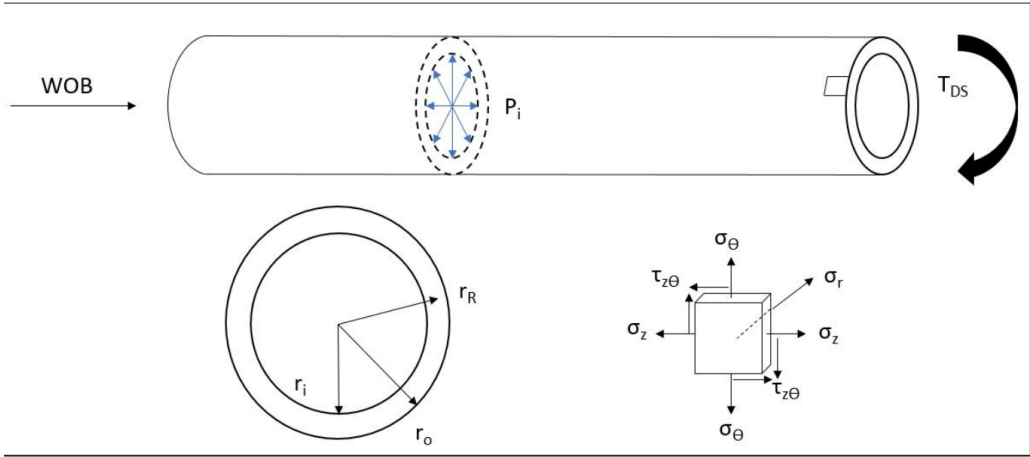


Figure 4.11: drillpipe stresses as a result of pressure, WOB and torque [52].

$$\sigma_r = \frac{\left(\frac{ID}{OD}\right)^2 - \left(\frac{ID}{2r}\right)^2}{1 - \left(\frac{ID}{OD}\right)^2} p \quad (4.24)$$

$$\sigma_\theta = \frac{\left(\frac{ID}{OD}\right)^2 + \left(\frac{ID}{2r}\right)^2}{1 - \left(\frac{ID}{OD}\right)^2} p \quad (4.25)$$

$$\sigma_z^p = \frac{\left(\frac{ID}{OD}\right)^2}{1 - \left(\frac{ID}{OD}\right)^2} p \quad (4.26)$$

Where $r[m]$ is the distance from center of pipe to Point of Interest (POI).

$$\sigma_z^{WOB} = \frac{WOB}{A_{cs}} \quad (4.27)$$

4.3.4 Pipe Bending

Axial stress generated by the drillpipe is referred to as bending stress. Bending stress for a beam is estimated using Equation 4.28. This equation assumes a constant cross-section perpendicular to the neutral axis of the beam [49]. In a bending situation, the pipe wall will become thicker where compressed and thinner where it is stretched [16].

$$\sigma_z^b = \frac{E}{RC} r \quad (4.28)$$

4.3.5 Stresses in Rod

Torque allowance on the rotation rod will be limited by induced shear stress. The shear stress for a rotating, solid, cylindrical shaft is defined by Equation 4.29 [50]:

$$\tau_s = \frac{M_s}{W_p}; \quad W_p = \frac{\pi}{16}d^3 \quad (4.29)$$

Where M_s is the applied torque, W_p is the polar moment of inertia and d is the rod diameter.

Bending stress for a solid, cylindrical shaft is given by Equation 4.30 [50]:

$$\sigma_b = \frac{M_b}{W_x}; \quad W_x = \frac{\pi}{32}d^3 \quad (4.30)$$

Where M_b is the applied torque, and W_x is the second area moment of inertia.

The overall limiting factor for the rod will be comparative stress, σ_c , that occur when the rod experience axial stress and shear stress simultaneously [50]. This effective stress is defined by Equation 4.31:

$$\sigma_c = \sqrt{\sigma_b^2 + 3\tau_s^2} \quad (4.31)$$

Where σ_c is the comparative stress, σ_b is the bending stress, and τ_s is the shear stress.

4.3.6 Fatigue

A familiar drill string failure is fatigue. Fatigue is a result of repeatedly applied stress to the drill string. It can create micro-cracks in the string that may develop into macro-cracks over time. The expected lifetime will be significantly shortened because of this cyclic stress in combination with corrosion.

The drill string is more susceptible to fatigue when the drill string rotates while being bent. The curved drillpipes will experience one stress cycle per revolution [18]. The amplitude of stress is proportional to the degree of curvature. Thus the cyclic stress will be related to the bending stress from this curvature. The cyclic stress is therefore represented by the bending stress calculated with Equation 4.28. This equation indicates that the bending stress increases with increasing outer diameter. Smaller outer diameters are preferred to reduce fatigue damage where Dogleg Severity (DLS) is expected.

The fatigue limit for different materials is indicated by its correlating S-N (Stress-cycle) curve. This limit is where bending stress equals endurance stress limit in the fatigue (S-N) curve. The reason is that the drill string is not limited to a number of rotations. Hence the bending stress should not exceed the endurance stress limit. If the material enters its plastic regime due to applying too much stress, fewer stress cycles are needed to break the material.

4.3.7 Natural Frequency

Reaching the natural frequency of the system may lead to resonance. The natural frequency is defined as the frequency where the system oscillates without any driving force or damping force. If a system oscillates at this frequency, it causes free vibrations in the body, also referred to as natural vibrations. If a forced vibration equals the free vibrations, the amplitude of the vibrations increases significantly as a result of resonance.

Drilling through a formation will cause vibrations to propagate from the drill bit, through the BHA and to the drillpipes. If the vibrations reach the same frequency as the natural frequency of the drilling equipment, resonance will occur and may wear the equipment. When the forced vibrations begin at the drill bit, it is essential to locate the RPMs at which the natural frequencies are created. The goal is to avoid the specific RPMs with a set margin to increase the lifetime of the drilling equipment.

Vibrations in the system occur in the lateral and longitudinal directions. To simplify the calculations, it is assumed that the drillpipe behaves like a uniform beam. The natural frequencies in lateral direction can be estimated by using Equation 4.32 [57]:

$$\omega_n^2 = \left(\frac{n\pi}{l}\right)^2 \frac{T}{A\rho} + \left(\frac{n\pi}{l}\right)^4 \frac{EI}{A\rho} \quad (4.32)$$

Where ω_n is the frequency at given mode n , l is the drillpipe length, T is the tension in the drillpipe, A is the cross-sectional area, ρ is the density of the material, E is Young's modulus of the material and I is the second moment of inertia.

The natural frequencies in longitudinal direction can be estimated with Equation 4.33 [57]:

$$\omega_n = \frac{\alpha_n c}{l} \quad (4.33)$$

Where α_n is estimated with Equation 4.34, c is the sonic sound in the material and l is the drillpipe length.

$$\alpha_n \tan(\alpha_n) = \beta \quad (4.34)$$

Where β is estimated with Equation 4.35:

$$\beta = \frac{m}{M} \quad (4.35)$$

Where m is the weight of the drillpipe and M is the weight of the BHA.

To verify the results obtained by Equation 4.32, the lateral natural frequency can be estimated with Equation 4.36 [8]. This equation estimates the first vibrations occurring on the pipes between each tool joints. The accuracy of Equation 4.36 is $\pm 15\%$, and frequencies within that range should be avoided.

$$CRS = \sqrt{D^2 - d^2} \frac{4760000}{l^2} \quad (4.36)$$

Where D is the outer diameter of the drillpipe, d is the inner diameter of the drillpipe, and l is the length of one joint.

Natural frequencies are also present in the BHA. The Critical Rotary Speed (CRS) with respect to a BHA which does not contain a shock sub can be estimated with Equation 4.37:

$$CRS = k \frac{84240}{l_b} \quad (4.37)$$

Where k is the mode($\{1,3,5,7,\dots\}$) and l_b is the length of the BHA.

4.4 Drill Bits

This section will cover drill bit theory that will be beneficial for the justification of the designed drill bits in this project. A custom drill bit design will be advantageous to increase the probability of efficient drilling and accurate steerability. Many parameters affect bit properties. This section covers the most relevant of these parameters.

The two main types of drill bits frequently used in the drilling industry are classified into two categories: roller cone bits and fixed cutter bits. A roller cone bit consists of one to three cones. The cones could either have milled teeth or insert bits. The fixed-cutter bits use blades with cutters integrated into the bit body to cut the rock formation. The bit body, also referred to as matrix body, is normally made in stainless steel or infiltrated tungsten carbide. The latter is a

chemical compound containing tungsten and carbon atoms [81]. The cutters consist of either a bonded layer of poly-crystalline or tungsten carbide and placed on the bit matrix's inner and outer rows. The inner rows cover two-thirds of the bit radius from the bit center. The remaining area is the outer rows. Cone, nose, shoulder, gauge, and nozzles are the other main elements of a drill bit. There are three sub-categories for fixed-cutter bits: Polycrystalline Diamond Compact (PDC), natural diamond, and fishtail bits. On the NCS, the most frequently used drill bit is the PDC [69]. Figure 4.12 shows an illustration of the main features on a PDC drill bit.

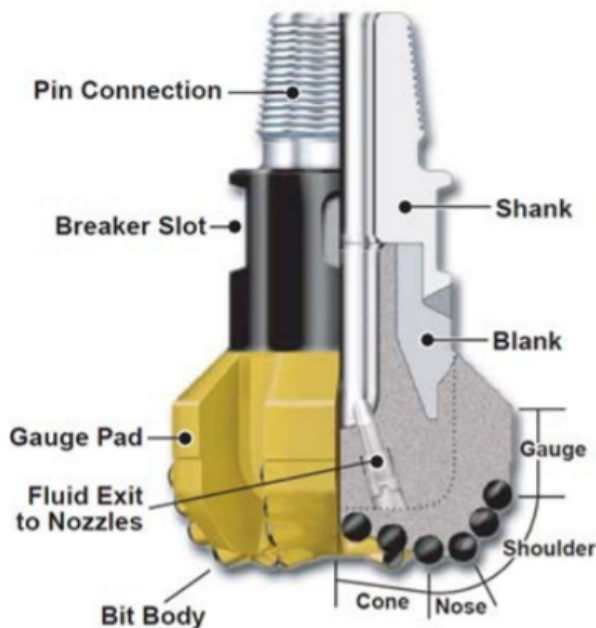


Figure 4.12: Overview of PDC drill bit components [69].

The PDC drill bits cut through rock formation by inducing shear stress failure. This is different from roller cone bits, which apply compressive stress. Figure 4.13 illustrate the energy required to cut two different types of shale. The plot shows that much less energy is needed to fail the shales with shear stress. This means that PDC bits require less WOB than roller cone bits. Lower WOB is positive with respect to buckling and twist-off issues.

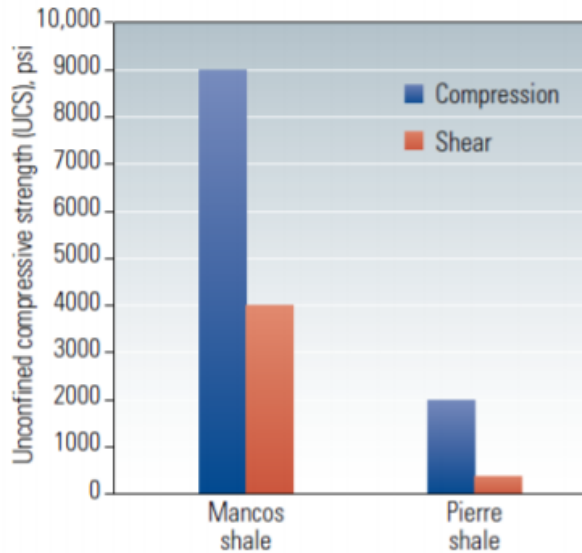


Figure 4.13: Energy needed to fail two different formations for different stress types [69].

4.4.1 Bit Profile and Cone Angle

Bit profile and cone angle have an essential impact on bit properties. Bit profiles are usually divided into the following bit types: long, medium, short and flat. Figure 4.14 illustrates the bit profiles and their suitability with respect to the hardness of rock drilled, steerability needed, and abrasiveness. A flat profile is beneficial for steering when drilling hard formations. However, it is less resistant to abrasive formations. Resistance to abrasive formations increases with the degree of parabolic bit profile but subsequently reduces steerability and, thus less suitable for hard formations. There is no standard bit profile that suits all drilling operations. Choosing the most fitting bit profile depends on the rock formation and the well type the drilling operation involves. The final result is, therefore, often to choose something between long parabolic and flat profile as a compromise between those properties [35].

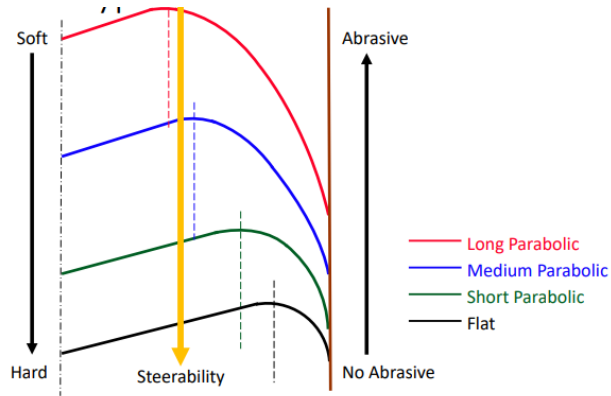


Figure 4.14: Varying bit profiles and belonging properties [35].

When selecting the bit cone angle, a similar principle as for bit profile holds. There is not a standard angle best for all drilling operations. Figure 4.15 illustrates a side view of deep ($\approx 90^\circ$), medium ($\approx 120^\circ - 140^\circ$) and shallow ($\approx 150^\circ$) cone angles. A deep cone angle stimulates high bit stability because the cuttings from the inner rows will form a cylindrical cone that contributes to a centering effect. A shallow cone angle improves steerability, bit cleaning and increases bit aggressiveness. Directional wells drilled from offshore rigs require a high amount of bit steerability. In that case, a shallow cone angle with a short parabolic to flat profile is a natural selection [35].

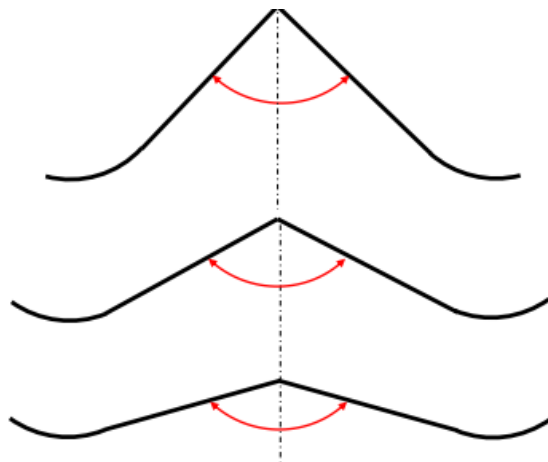


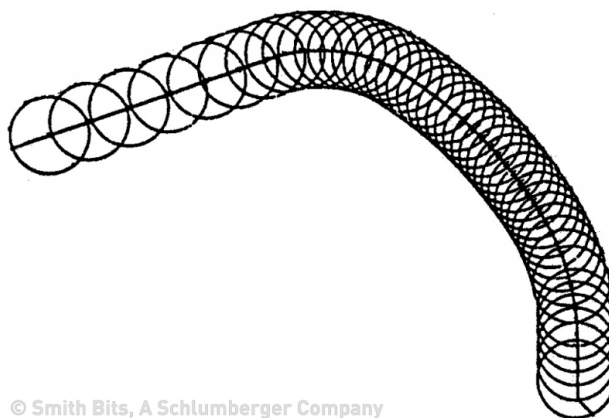
Figure 4.15: Deep ($\approx 90^\circ$), medium ($\approx 120^\circ - 140^\circ$) and shallow ($\approx 150^\circ$) cone angles [35].

4.4.2 Cutter Design

Cutter layout

The cutters are important for how the bit drills through the rock formation. The size and number of cutters influence the Depth of Cut (DOC) and Rate of Penetration (ROP). A larger number of cutters will decrease the DOC and subsequently decrease the ROP. Increasing the number of cutters will result in more cutters to cut the same volume, reducing torque and wear on each cutter. However, many cutters will also reduce the cleaning efficiency because a smaller junk slot area between the blades makes less space for cuttings to flow. The size of each cutter affects the DOC. Larger cutters increase DOC and subsequently increase the ROP. However, increased size means larger rock volume removed per cutter, possibly generating higher torque readings and bit vibrations which reduce the ROP. A lower amount of big cutters can therefore have a contradictory effect.

When choosing the layout of the cutters, the goal is to leave no formation uncut. When the bit drills, the angular velocity from the bit center towards the gauge increases, and the cutters will remove more cuttings. Therefore, to avoid wear and tear, it is preferable to increase the cutter density towards the outer rows of the bit [34]. Figure 4.16 shows a typical cutter density profile.



© Smith Bits, A Schlumberger Company

Figure 4.16: Increasing cutter density towards outer rows along bit profile [34].

The cutters can overlap in different ways. Figure 4.17 illustrate the two main cutter layouts; single-set layout and track-set layout. In a single-set layout, the cutters do not share the same longitudinal and radial position, enabling equal distribution of the loads each cutter experiences. In a track-set layout, the cutters overlap each other, enabling less evenly distributed cutting between the cutters.

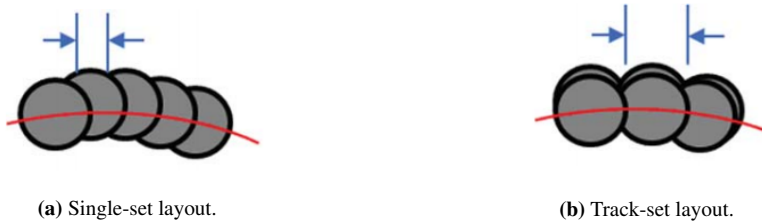


Figure 4.17: Two types of drill bit cutter layout [67].

According to Besson et al. (2000), laboratory and field tests show improved drilling efficiency using a PDC bit with single-set cutters drills when compared with track-set cutters [21].

Cutter orientation

Cutter orientation is important for bit properties. Designing a suitable cutter orientation involves choosing an appropriate back-rake and side-rake angle. The back-rake angle often called the attack angle, is measured from the cutter face perpendicular to the drilling direction. Figure 4.18 illustrates that a zero degree back-rake angle result in the highest DOC. Therefore, smaller back-rake angles result in more aggressive drill bits. Typical back-rake angles range from 20° to 25° for the inner rows and from 10° to 15° for the outer rows. Bit damage and changes in torque are typical limitations for choosing a back-rake angle of zero.

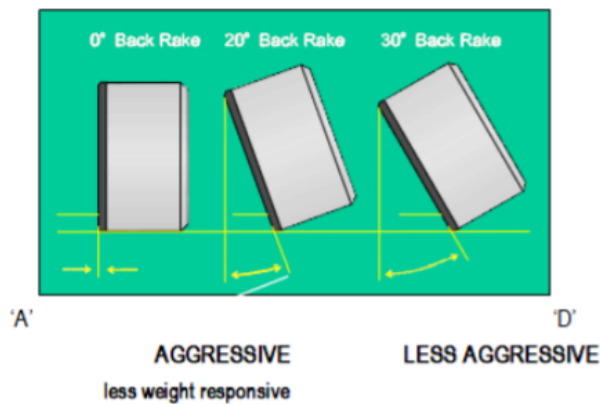


Figure 4.18: Varying back rake angles [69].

Figure 4.19 shows an illustration of the side-rake angle viewed from behind the bit. The side rake angle is the angle perpendicular to the direction of bit rotation. A frequently used side-rake angle is 10° . A positive valued side-rake angle contributes to improved hole cleaning by leading the cuttings towards the outer region of the drill bit. It provides a shearing effect to the cutting

activity.

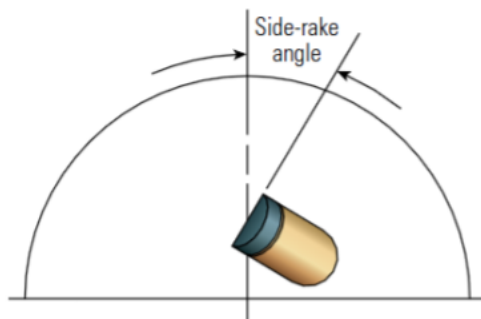


Figure 4.19: Side-rake angle viewed from behind the drill bit [69].

4.4.3 Bit Balling

Bit balling is a drilling condition where shale cuttings accumulate at the bit surface. This phenomenon may occur when drilling through clay formations or water-reactive shale. The main mechanisms which contribute to bit balling are mechanical and electro-chemical sticking. Poor hole cleaning and static mud in the well generate electrostatic forces that cause cuttings to stick to the bit surface. the accumulated cuttings lead to balling of the drill bit.

An indication of bit balling is the sudden reduction in ROP without significant change in other drilling variables [36]. Torque readings may be lower than expected because of cuttings covering the cutters. Accumulation of cuttings may result in increased standpipe pressure because of a reduction in the annular flow area. Bit balling is best mitigated by reducing the WOB and increase the fluid flow rate, which will most likely wash out the cuttings stuck on the bit and drill string.

4.5 Drilling Hydraulics

Achieving sufficient drilling performance is highly dependent on the hydraulic system. The most critical drilling parameter related to the hydraulics system is the ROP, which is significantly affected by the hole cleaning. This section cover theory behind hole cleaning and pressure losses relevant for the rig design in this project.

The drilling fluid, or mud, has several properties which contribute to improved drilling performance, such as [8]:

- Transport rock cuttings from bottom of the well to surface.

- Maintaining wellbore stability, keep the system overbalanced.
- Cooling and lubrication of bit and drill string components.
- Produce mud cake, to prevent fluid loss to natural or induced cracks.
- Information transferring by mud pulse telemetry.

4.5.1 Hole Cleaning

ROP can be directly related to the time scope of a drilling process. It is desirable to optimize the ROP to reduce time and expenses. Sufficient hole cleaning is therefore important to achieve the desired ROP.

Hole cleaning varies from one flow regime to another and is generally divided into three different situations:

- Vertical section - $[0^\circ - 30^\circ]$
- Tangent section - $[30^\circ - 65^\circ]$
- Horizontal section - $[65^\circ - 90^\circ]$

Because this year's Drillbotics competition is limited to an inclination of 30° , the trajectory is considered as a vertical section. Appendix P present the derivation of the equations in this section. Slip velocity is the velocity by which a spherical particle travels through laminar flow regime and is given by:

$$v_{sl} = \frac{d_s^2 g (\rho_s - r \rho_f)}{18 \mu_f} \quad (4.38)$$

Where $d_s [m]$ is diameter of the cuttings particle, $\rho_s [kg/m^3]$ is the density of the cuttings particle, $\rho_f [kg/m^3]$ is fluid density and $\mu_f [Pas]$ is the fluid viscosity.

Some parts of the hydraulic system cannot be described by laminar regime. Equation 4.39 describe slip velocity for a particle in any given flow regime:

$$v_{sl} = \sqrt{\frac{4(\rho_s - \rho_f) g d_s^2}{3 f \rho_f}} \quad (4.39)$$

where f is a friction factor extracted from Figure 4.20.

The final slip velocity is calculated in the following way:

First, v_{sl} is estimated using Equation 4.38, then the Reynolds number is calculated with Equation R.7 and friction factor is extracted from Figure 4.20. Lastly, v_{sl} is calculated using Equation 4.39.

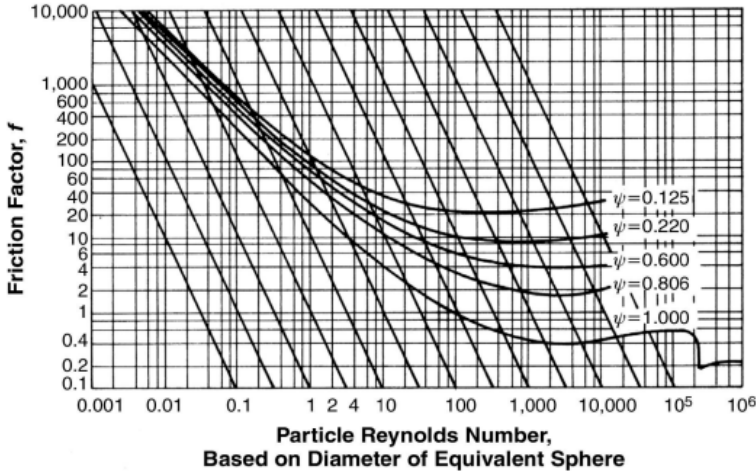


Figure 4.20: Relationship between Re and f for settling particles in Newtonian fluids [7].

When the final slip velocity is derived, the required flow rate for sufficient hole cleaning can be estimated using Equation 4.40:

$$q = A_{cs} \frac{v_{sl}}{1 - R_t} \quad (4.40)$$

4.5.2 Pressure Losses

Pressurized mud is transported through several components on the rig before entering or re-entering the wellbore, which generates a continuous pressure loss throughout the hydraulic system. The required pressure to overcome the pressure loss is expressed by decomposing the pressure loss into losses over the components in the system. In this project, the components are the water hose, hydraulic swivel, drillpipe, BHA, drill bit, and annulus. Because the return fluid exits the system from the top of the well, the annulus is considered the cross-sectional area of the wellbore minus the cross-sectional area of the drillpipe. Equation 4.41 can be used to estimate the

required pressure to overcome the pressure losses in this system.

$$P_{required} = \Delta P_{Waterhose} + \Delta P_{Swivel} + \Delta P_{Drillpipe} + \Delta P_{BHA} + \Delta P_{bit, nozzles} + \Delta P_{annulus} \quad (4.41)$$

Minor pressure losses are neglected in Equation 4.41. A safety factor is usually added to the required pressure to compensate for this.

Pipe Pressure Losses

Pressure losses have to be estimated for both the flow inside the drillpipe and the annular flow outside the drillpipe. Pressure losses in both situations can be estimated with Equation 4.42[68]:

$$\Delta P_i = f_i \frac{L_i}{d_{h,i}} \frac{\rho_f v_i^2}{2} \quad (4.42)$$

Where ΔP_i is the pressure loss, L_i is the length of the part where the pressure loss occurs, ρ_f is the fluid density, and v_i is the velocity of the fluid.

For pressure loss inside the drillpipe, $d_{h,i}$ is the inner diameter of the drillpipe. For the annular pressure loss, $d_{h,i}$ is equal to $OD_{borehole} - OD_{drillpipe}$. Equation 4.42 can also be used to calculate the pressure loss in the BHA. $d_{h,i}$ is then the inner diameter of the BHA.

f_i is a friction factor that varies depending on the flow regime. The type of flow regime depends on the Reynolds number calculated with Equation R.7. The flow regime is laminar for Reynolds numbers less than 2 300 and turbulent for Reynolds numbers greater than 2 300. For turbulent flow, the friction factor is estimated with Equation 4.43 and 4.44 [26]. The friction factor will then be the average of the two results.

$$\frac{1}{\sqrt{f}} = -1.8 \log \left[\left(\frac{\epsilon/D}{3.7} \right)^{1.11} + \frac{6.9}{Re} \right] \quad (4.43)$$

$$f = \frac{0.25}{\left[\log \left(\frac{\epsilon/D}{3.7} + \frac{5.74}{Re^{0.9}} \right) \right]^2} \quad (4.44)$$

If the flow is laminar, then the friction factor can be calculated with Equation 4.45.

$$f = \frac{64}{Re} \quad (4.45)$$

Bit Pressure Losses

Sufficient fluid velocity in front of the bit is essential to remove cuttings and prevent accumulation on the bottom of the well. The fluid enters the wellbore through nozzles in the drill bit. Velocity is inversely proportional to cross-sectional area. Thus high velocity is achieved by reducing the cross-sectional nozzle area. As a result, the nozzles introduce a pressure drop over the bit. The velocity of drilling fluid through the nozzles, v_n , can be estimated with Equation 4.46:

$$v_n = C_d \sqrt{\frac{2\Delta P_{bit,nozzle}}{\rho_f}} \quad (4.46)$$

Where C_d is a discharge coefficient, $\Delta P_{bit,nozzle}$ is the pressure drop over the nozzles and ρ_f is the fluid density.

The discharge coefficient is introduced because of experimental measurements showing that v_n is overestimated with Equation 4.46. From these experiments, it is suggested that a discharge coefficient of 0.95 is appropriate. By expressing v_n as flow rate over area, and rearranging Equation 4.46, the pressure loss over the bit can be calculated by:

$$\Delta P_{bit,nozzle} = \frac{\rho_f q^2}{2A_n^2 C_d^2} \quad (4.47)$$

Where q is the flow rate and A_n is the total flow area of the nozzles.

(This page is intentionally left blank)

Chapter 5

Design Limits

Several limits and constraints introduce restrictions on the mechanical rig design and its coherent control system. Some design limits originate from the Drillbotics guidelines (Appendix A), and others are associated with the chosen rig components. This chapter will present the foreseen design limits and constraints associated with the drilling rig design to justify the implementation of each rig component. The Table 5.1 presents all design parameters on the following page.

Table 5.1: Design parameters.

Variable	Symbol	Value	Unit
OD DP	OD_{DP}	9.53	mm
Wall Thickness	t_{DP}	1.24	mm
Length DP	L_{DP}	91.44	cm
Diameter Rod	d	4	mm
Length Rod	L_{rod}	1.42	m
Density Aluminum 7075-T6[13]	ρ_a	2810	kg/m ³
Density Grade 5 Titanium[80]	ρ_t	4429	kg/m ³
Sound speed Aluminum[71]	c	3100	m/s
Sound speed Titanium[71]	c	3125	m/s
Elasticity Modulus (Stainless Steel, AISI316) [5]	E	200	GPa
Elasticity Modulus (Aluminium 6061-T6) [12]	E	68.90	GPa
Elasticity Modulus (Aluminium 7075-T6) [13]	E	71.70	GPa
Elasticity Modulus (Beryllium Copper UNS C17200) [20]	E	125	GPa
Elasticity Modulus (Grade 5 Titanium) [19]	E	114	GPa
Material Yield Strength(Stainless Steel, AISI316)[5]	σ_{ys}	196	MPa
Material Yield Strength(Aluminium 6061-T6)[12]	σ_{ys}	276	MPa
Material Yield Strength(Aluminium 7075-T6)[13]	σ_{ys}	503	MPa
Material Yield Strength(Beryllium Copper UNS C17200)[20]	σ_{ys}	965	MPa
Material Yield Strength(Grade 5 Titanium)[19]	σ_{ys}	1100	MPa
Fatigue Strength (Aluminum 7075-T6) [13]	σ_{ys}	159	MPa
Fatigue Strength (Grade 5 Titanium) [19]	σ_{ys}	700	MPa
Shear Strength (Stainless Steel, AISI316)	τ_s	344	MPa
Shear Strength (Aluminum 7075-T6)[13]	τ_s	331	MPa
Shear Strength (Grade 5 Titanium)[19]	τ_s	760	MPa
OD BHA	OD_{BHA}	36.07	mm
ID BHA	ID_{BHA}	26.42	mm
Length BHA	L_{BHA}	120.14	mm
ID Swivel + Hose	$ID_{Swivel+Hose}$	11.94	mm
Length Swivel + Hose	$L_{Swivel+Hose}$	2.50	m
Aluminium Pipe Roughness[27]	ϵ_{dp}	$1.30 \cdot 10^{-6}$	m
Steel Pipe Roughness[27]	ϵ_{rod}	$1.50 \cdot 10^{-5}$	m
Fluid Density	ρ_f	1000	kg/m ³
Solid Density	ρ_s	2650	kg/m ³
Fluid Viscosity	μ_f	1	cP

5.1 Well Path

The requirements from the Drillbotics guidelines have been carefully considered to find limitations for designing and building the most efficient well path possible. The well path requirements in the Drillbotics competition are as follows (Appendix A):

- *Hit one or more targets at one or more vertical depth(s) and X/Y coordinates.*
- *For the Group B competition, the starting directional plan to hit the targets will not require wellbore inclinations larger than 30° from vertical, 15° change in azimuth, or 10 inches displacement (departure from the vertical axis at well center). The max displacement/inclination/azimuth are total/accumulated from the start to the end of the well path.*

The authors have interpreted the guideline objectives such that either a maximum of 30° inclination or 25.40 cm (10 inches) displacement from the vertical axis is required. To determine the limiting factor of the two, further examination was conducted. First and foremost, this geometrical requirement takes place in a rock sample with the following dimensions: 30 x 60 x 60 cm (12 x 24 x 24 inches). Before reaching the Kick-Off Point (KOP), a vertical pilot hole not shorter than 10.16 cm (4 inches) is required. With these requirements and limitations, the possible well path is illustrated in Figure 5.1.

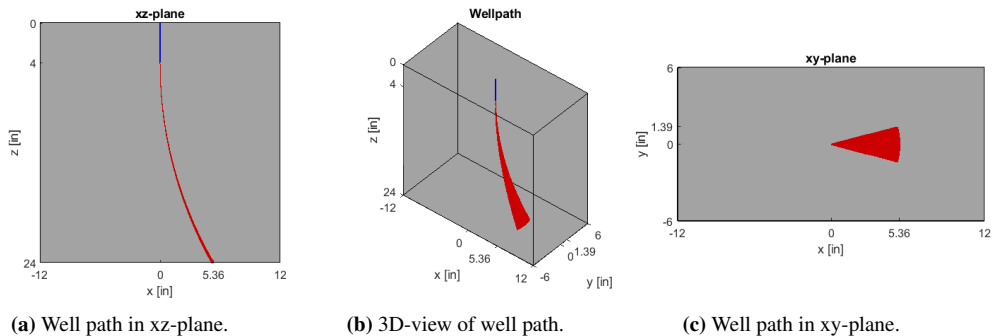


Figure 5.1: Theoretical possible well path inside given rock dimensions, 12in x 24in x 24in.

Constructing the well path illustrated in Figure 5.1, a constant build rate is assumed. Figure 5.1(a) illustrates that an inclination of 30° will result in a displacement from the vertical axis of 13.61 cm (5.36 inches). This will thus be the limitation because it is below the other suggested requirement of 10 inches. The requirement of 15° azimuth will result in a displacement of 3.53 cm (1.39 inches) as illustrated in Figure 5.1(c).

5.2 Buckling

The estimation for the critical buckling limit of the drillpipe is made using Equation 4.14 and 4.18. Because WOB propagates through the drillpipe only, the rod will not experience buckling effects. The drillpipe dimensions are chosen with respect to the Drillbotics requirements. It has an outer diameter of 9.53 mm (3/8 inches) and a wall thickness of 1.24 mm (0.049 inches) (Appendix A). The critical buckling limit is calculated with representative end conditions and effective length factors (K) presented in Table 4.1. For simplicity, the drillpipe have been divided into three sections from top to bottom; The length above drill floor, the length between drill floor and riser and length between riser and top of the BHA. Figure 5.2 shows the critical WOB versus the unsupported length for different K -values.

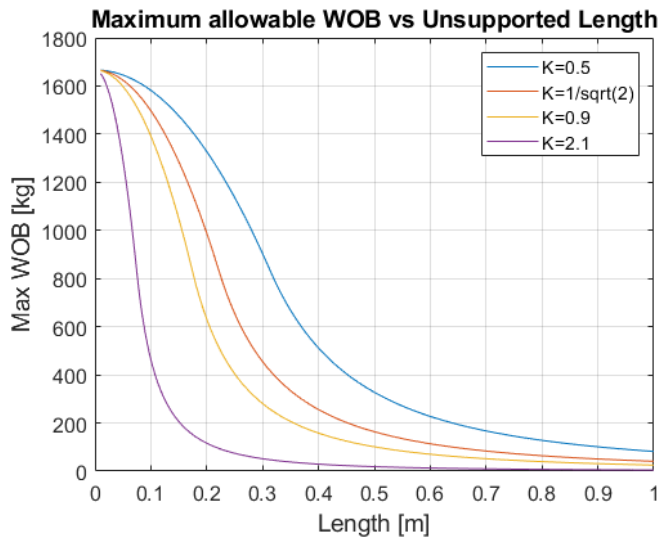


Figure 5.2: Critical buckling limit calculations for aluminium drillpipe.

The two uppermost sections of the drillpipe are fixed against radial movement and resemble fixed-fixed scenarios. The top section is fixed at the hydraulic swivel connection and the drill floor stabilizer. The middle section is fixed between the upper stabilizer on the drill floor and the lower stabilizer in the riser element. The third and lower sections can be represented by a scenario between fixed-free and fixed-pinned end conditions. The borehole wall provides some support to the drillpipe when drilling deviated. Hence it will be a conservative scenario when estimating the buckling limit at fixed-free end conditions. The pipe will be pinned to the BHA because the stabilizer's outer diameter is similar to the bit diameter and thus the borehole diameter. It is,

therefore, reasonable to estimate the buckling limit at a fixed-pinned scenario for the lower-most section.

The results from calculations are presented in Table 5.2, showing the maximum WOB for the intended unsupported pipe lengths. An entirely unsupported drillpipe is not desirable because it will limit the maximum WOB to 5.6 kg (12.32 lbs). This emphasizes the necessity of stabilizers to limit the unsupported pipe lengths. The results in the far-right column in Table 5.2 represent a fixed-free scenario but will, as mentioned, not be representative for the pipe system.

Table 5.2: Buckling calculations for drillpipe.

		Fixed-Fixed		Fixed-Pinned		Fixed-Free
	K	0.5	0.9	$\frac{1}{\sqrt{2}} = 0.71$	0.9	2.1
	L [m]	Maximum WOB [kg]				
Drillpipe length	0.91	97.90	30.20	49	30.20	5.60
Rock height	0.610	220.30	68	110.2	68	12.50
Curved section	0.51	317.30	97.90	158.60	97.90	18
Length of pipe	0.30	878.70	272	440.70	272	50

The BHA will occupy a significant length of the well, thus further reducing the unsupported drillpipe length. Table 5.3 shows that the maximum WOB increases when a BHA length of 16.20 cm (6.38 inches) is taken into account.

Table 5.3: Buckling calculations with BHA length of 16.2 cm (6.38 inches).

		Fixed-Fixed		Fixed-Pinned		Fixed-Free
	K	0.5	0.9	$\frac{1}{\sqrt{2}} = 0.71$	0.9	2.1
	L [m]	Maximum WOB [kg]				
Well length - BHA	0.45	404.30	124.80	202.20	124.80	22.90
Curved section - BHA	0.35	668.40	206.30	334.20	206.30	37.90

The conservative fixed-free scenario limits the WOB to approximately 38 kg (83.80 lbs) at the end of the drilling operation. The actual limit will be somewhere between the limits of fixed-free and fixed-pinned. The conservative fixed-free limit will however give sufficient WOB.

5.3 Burst

The burst pressure of the drillpipe is calculated using Equation 4.21 under the assumption of a thin-walled pipe. Pipe properties presented in Table 5.1 are inserted into Equation 4.21 under an assumption of a drilling scenario. The reason for presenting the drilling scenario is that it gives the most conservative approach, with a safety factor of 3.

$$P_{burst} = 2 \frac{0.875 \cdot 503 \text{MPa} \cdot 1.24 \text{mm}}{9.53 \text{mm} \cdot 3} = 383 \cdot 10^5 \text{Pa} \tag{5.1}$$

The calculated burst pressure of $385 \cdot 10^5 \text{ Pa}$ will not be a problem for this rig system because the hydraulic pump will not be implemented this year.

5.4 Twist-Off

The applied torque limits on drillpipe and rod during drilling are determined by twist-off calculations. The drillpipe twist-off values are calculated using Equation 4.22 and 4.23. The inputs to these equations are calculated with the following equations: σ_r (Equation 4.24), σ_θ (Equation 4.25) and σ_z (sum of Equation 4.26, 4.27 and 4.28).

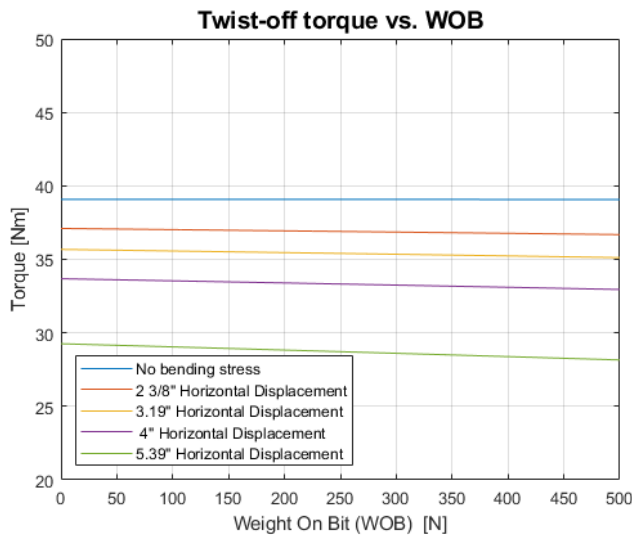


Figure 5.3: Twist-off torques on drillpipe for different bending cases and WOB.

Figure 5.3 presents the result of five twist-off calculations for five different bends. The maximum bend is equal to the bend of the maximum horizontal displacement shown in Figure 5.1. All

stresses are calculated outside the pipe wall. As shown in Table 5.4, the internal pressure of the drillpipe has a negligible effect on torque. This table presents the twist-off limits extracted from Figure 5.3.

Table 5.4: Twist-off limits for aluminum 7075-T6 drillpipe for different horizontal displacements.

Pressure	Horizontal Displacement				
	0"	2 3/8"	3.19"	4"	5.39"
10 bar	39.10-39.10 Nm	36.70-37.10 Nm	35.10-35.70 Nm	33-33.70 Nm	28.20-29.30 Nm
100 bar	39.10-39.10 Nm	36.70-37.10 Nm	35.10-35.70 Nm	33-33.70 Nm	28.20-29.30 Nm
Twist-off limit	39.10 Nm	36.70 Nm	35.10 Nm	33 Nm	28.20 Nm

Table 5.4 shows that the drillpipe twist-off limit for the maximum horizontal displacement is 28.20 Nm (20.80 ft-lbs). This is sufficient according to the torque values during drilling shown in subsection 11.7.2. Twist-off calculations for the rod are simple because the angular and radial stresses are equal to zero because of no internal pressure. The axial stress will not have contribution from pressure of the same reason, and zero contribution from WOB because the WOB propagates through the drillpipe. Hence, the rod torque limit can be calculated directly using Equation 4.29 where τ_s is the shear strength of the material. Table 5.5 shows the resulting twist-off limits for the three available materials.

Table 5.5: Twist-off limits for different rod materials.

Material	Twist-off limit [Nm]
Stainless Steel 316	4.33
Aluminum 7075-T6	4.17
Grade 5 Titanium	9.58

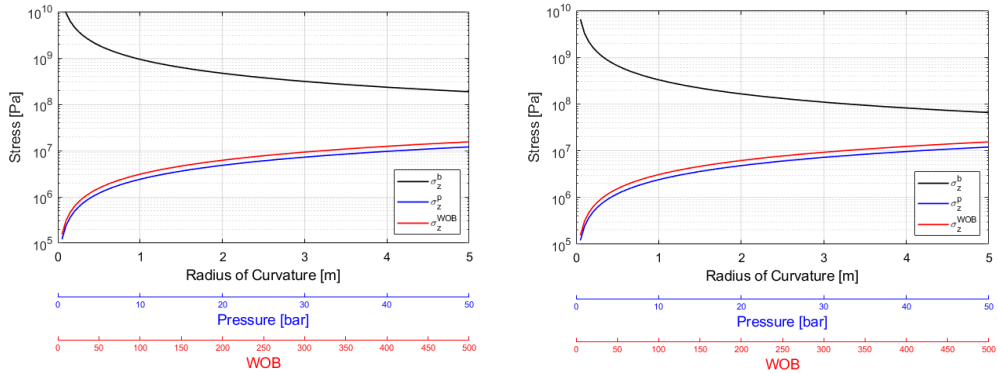
The titanium rod is superior to the other materials with respect to twist-off, and is more than sufficient according to the torque during drilling in subsection 11.7.2.

5.5 Pipe Bending

Constructing a well trajectory through multiple targets at different coordinates in the {X,Y,Z} plan depends on the drillpipe operating within its elastic limits. Pipe bending results from axial stresses and the point of transition between plastic and the elastic regime where the total axial stresses equal the yield strength of the material. Therefore, it is critical to keep the total axial stresses notably lower than the yield strength of the material.

The Drillbotics guidelines allow the use of two possible materials; stainless steel and aluminum.

It is necessary to examine their differences to select the superior material for this purpose. Previous years from NTNU have compared the two materials suggested in the guidelines. Figure 5.4 and 5.5 illustrate the differences. The stresses are calculated using Equation 4.26, 4.27 and 4.28, with inputs from Table 5.1.

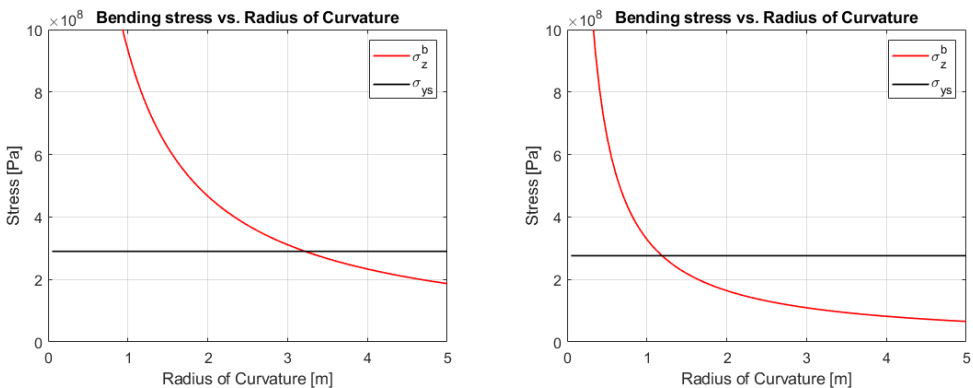


(a) Stainless steel, grade 316.

(b) Aluminum 6061-T6.

Figure 5.4: Axial stresses on pipe for different values of RC , P , and WOB .

As illustrated in Figure 5.4, the bending contributes to significantly more axial stress than pressure and WOB for both materials. By comparing the axial stress contribution from bending to the material yield strength, it is possible to attain the minimum allowable Radius of Curvature (RC) to keep the drillpipe within its elastic limits.



(a) Stainless steel, grade 316.

(b) Aluminum 6061-T6.

Figure 5.5: Contribution of axial stress from bending illustrated for different values of RC compared with material yield strength.

Figure 5.5(a) shows that the minimum allowable RC for the stainless steel pipe to stay within the elastic regime is 3.32m (1.06 ft). This value results in a horizontal displacement of 3.99 cm (1.57 inches). However, Figure 5.5(b) illustrates that an aluminum pipe gives room for a RC of 1.19 m (3.90 ft). This value means it is possible to achieve a displacement of 11.38 cm (4.48 inches). Because of this, stainless steel pipe is not an option.

The results obtained in section 5.1 require a displacement of 13.61 cm (5.36 inches), which implies that the performance of the aluminum 6061-T6 drillpipe is insufficient. For that reason, another aluminum alloy was considered, and the axial stresses and performance of aluminum 7075-T6 are illustrated in Figure 5.6.

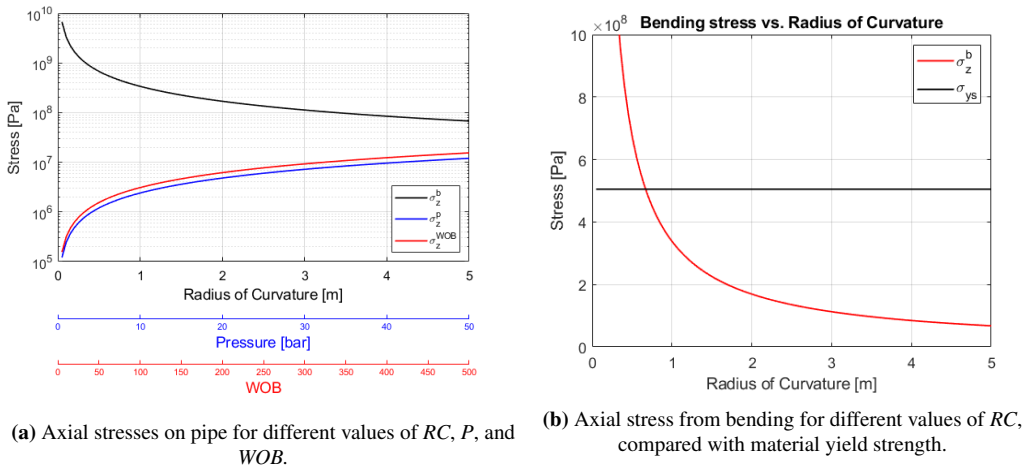


Figure 5.6: Performance of aluminum 7075-T6 drillpipe.

Axial stress contribution from WOB and pressure is still negligible for aluminum 7075-T6 compared to the contribution from bending, seen in Figure 5.6(a). The minimum allowable RC is 0.76 m (2.69 ft), illustrated in Figure 5.6(b). This RC results in a horizontal displacement of 23.14 cm (9.11 inches), which is almost twice the requirement of 13.61 cm (5.36 inches).

The required displacement of 13.61 cm (5.36 inches) is related to a RC of 1.02 m (3.35 ft). At this RC, the axial stress contribution from bending is equal to 334 MPa (48.44 ksi). For the yield strength of 505 MPa (73.24 ksi), this yields a safety factor of $\frac{505}{505-344} = 3.14$. Based on these examinations, the drillpipe material will be an aluminum 7075-T6 alloy.

5.6 Rod Stresses

There are two stress factors related to the rod; axial stress and shear stress, because WOB will be subjected onto the drill bit through the drillpipe and the BHA. These stresses are estimated with Equation 4.29 and 4.30 with inputs from Table 5.1. These limiting factors are better illustrated for three different materials by a comparative stress calculated with Equation 4.31 in Figure 5.7.

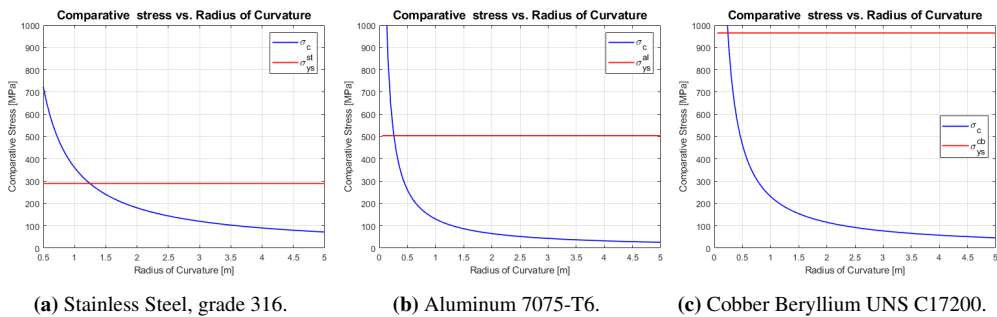


Figure 5.7: Comparative stress from bending and twisting for different values of RC compared with material yield strength.

The three considered rod materials during phase I were; stainless steel 316, aluminum 7075-T6, and copper-beryllium alloy [9]. Figure 5.7 show the comparative stresses for all three. The original drillpipe material, stainless steel 316, would not be sufficient in this scenario either. The two other materials can meet the requirements, but the copper-beryllium alloy proved expensive and difficult to acquire. Therefore, it was decided to go for the same alloy as the drillpipe for the rod, which is aluminum 7075-T6.

After substantial testing, the 7075-T6 aluminum rods were proven insufficient, and titanium rods were acquired. Figure 5.8 shows the calculated comparative stress for a grade 5 titanium rod. With more than twice the yield strength of aluminum 7075-T6, grade 5 titanium rods should be a significant upgrade. Testing also confirmed this in section 11.3.

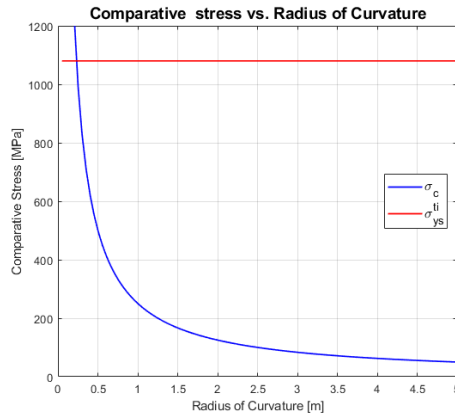


Figure 5.8: Comparative stress for grade 5 titanium.

5.7 Fatigue

Previous Drillbotics teams from NTNU have met challenges related to fatigue. The 2018 team experienced drillpipe twist-off at lower torques than expected from tests and calculations. To drill a well with maximum inclination of 30 degrees and maximum azimuth of 15 degrees, the drillpipe and rod will be subject to significant bending stresses. The bending stress of 334 MPa (48.44 ksi) calculated in section 5.5 is more than twice the fatigue strength of the pipe. In addition to the bending, the pipe will be subject to wear because of friction between the pipe and the borehole wall. There will be minimal wear between the pipe and rod because the two components are made of the same material. According to Figure 5.8, the comparative stress for titanium at the requirements is equal to 248 MPa (36 ksi). This value is less than the fatigue strength, which is equal to 700 MPa of the chosen titanium [19].

5.8 Drilling Requirements

Component and equipment selection best suited for the performance of the rig depends on the drilling requirements.

5.8.1 Drilling Rate

The minimum required drilling rate is obtained under the assumption of the least efficient well path, which in section 5.1 is found to be a horizontal displacement of 13.61 cm (5.36 inches). With this displacement, the RC is equal to 1.02 m (3.35 ft) and will exit the rock with an angle of 30 degrees.

Setting the radius curve, RC equal to 1.02 m, $I_1=0^\circ$ and $I_2=30^\circ$ in Equation 4.11 gives a CL of 53.20 cm (20.94 inches). The time limit in the competition is 3 hours. Aiming for 2 hours should yield a sufficient safety factor when determining the required ROP. With these assumptions, an average ROP of 0.44 cm/min (0.17 inches/min) is required to complete the task within the time constraint.

5.8.2 Bit Tilt

To reach the inclination of 30 degrees, a sufficient bit tilt angle must be implemented. This is achieved by having a fixed bent sub in the BHA. Dogleg Severity (DLS) is calculated using Equation 5.2 from subsection 4.2.2:

$$DLS = \frac{2\theta}{L_1 + L_2} \quad (5.2)$$

Where ϕ is the desired inclination of 30° . Calculated in subsection 5.8.1, we have that the required course length, CL , is 53.20 cm. The result is a DLS of $56.40^\circ/\text{m}$ ($17.20^\circ/\text{ft}$) and is put into Equation 5.3 to calculate the bit tilt, θ .

With estimated BHA lengths, $L_1 = 8.70\text{cm}$ (3.43 inches) and $L_2 = 10\text{cm}$ (3.94 inches) as illustrated in Figure 4.4, the bit tilt angle required is:

$$\theta = \frac{DLS(L_1 + L_2)}{2} = 5.28^\circ \quad (5.3)$$

5.9 Drilling Hydraulics

A functioning hydraulic system is critical in preventing the accumulation of cuttings in the well, and calculations related to hydraulics are essential to enable the best possible drilling performance.

5.9.1 Hole Cleaning

Drilling fluid is provided directly from the on-site water tap, which means that calculations for hole cleaning will be done with water as drilling fluid. The calculations also assume that the cuttings are spherical. The cutting particle diameter is assumed to be $d_s = 2.40$ mm (0.095 inches), which is an increase of 0.40 mm from what was assumed by the 2018 NTNU team. This is caused by an increase in size [42]. The rock sample to be drilled is a homogeneous sandstone. Cutting density assumed to be 2250kg/m^3 . Parameters related to hole cleaning calculations are listed in Table 5.6.

Table 5.6: Results from hole cleaning calculations.

Parameters	Equations	BHA	DP
$v_{sl} [m/s^2]$	Equation 4.38	5.18	5.18
Re	Equation R.7	10 525 (Turbulent)	148 000 (Turbulent)
f	Figure 4.20	0.44	0.55
$v_{sl} [m/s^2]$	Equation 4.39	0.017	0.015
q [lpm]	Equation 4.40	0.24	1.93

The final result indicates that a flow rate of 1.93 LPM is necessary to achieve sufficient hole cleaning while drilling. A safety margin on top of that gives a required flow rate of 3 LPM.

5.9.2 Pressure Losses

In section subsection 4.5.2, Equation 4.41 was introduced to estimate the required pressure to overcome the pressure losses in this system. The flow rate required to clean the hole was calculated to be 3 LPM, and the pressure output from the water tap is 7 bar. The pressure losses in the system must therefore not exceed 7 bar with a flow rate of 3 LPM. Equation 4.42 and 4.47 are used to calculate the pressure losses for drillpipe and bit, respectively. The inputs for these equations are found in Table 5.1.

When drilling, a rod with 4 mm diameter is rotating inside the drillpipe. Water flowing inside

the drillpipe will therefore interact with two different pipe roughness factors. In this project, the rod material is primarily titanium, but a stainless steel rod of the same dimensions will be used as a redundant solution should the titanium rod fail. Because steel has the highest pipe roughness factor, ϵ , this factor is considered the worst-case scenario regarding pressure losses. The pipe roughness factor for a steel rod and a aluminium drillpipe are: $\epsilon_{rod} = 1.50 \cdot e^{-5}$ and $\epsilon_{dp} = 1.30 \cdot e^{-6}$ [27].

An examination of the flow area percentage with respect to the surface area of the rod and inside the drillpipe has been conducted to estimate a final pipe roughness factor. Hydraulic flow area inside the drillpipe is given by:

$$A_{flow} = 2\pi r h \tag{5.4}$$

Where h is the length of which the water flows inside the drillpipe.

Because the length of drillpipe and rod through which water flows are approximately the same, each part h is neglected from Equation 5.4. Equation 5.4 simplifies to the equation for the circumference of a circle. Thus, the equation calculates the fraction of flow to be 63% around the drillpipe and 37% around the rod. Multiplying these fractions with the rod and drillpipe roughness factors provides a final pipe roughness value of $\epsilon_{total} = 6.37 \cdot e^{-6}$. This factor will be used for calculating pressure loss inside the drillpipe.

Table 5.7 present the pressure losses. It shows that the main pressure loss occurs inside the drillstring mainly because of the small flow area. With a flow rate of 3 LPM, the pressure loss will become 2.23 bar, which is less than the requirement of a maximum 7 bar. However, according to calculations, pressure loss exceeds this limit with a flow rate of 6 LPM. Thus, the design is limited to provide hole cleaning with a flow rate of a maximum 6 LPM.

Table 5.7: Pressure drop across drilling components for different flow rates .

Q[lpm]	$\Delta P_{dp,inside}$	$\Delta P_{bha,i}$	$\Delta P_{dp,ann}$	$\Delta P_{bha,ann}$	$\Delta P_{swivel+hose}$	$\Delta P_{bit,nozzle}$	ΔP_{tot}
1.50	0.60	3.43e-6	8.38e-6	0.0014	0.0024	0.022	0.63
2	1.08	4.58e-6	1.12e-5	0.0019	0.0039	0.039	1.12
2.50	1.53	1.02e-5	1.39e-5	0.0023	0.0057	0.061	1.59
3	2.14	1.38e-5	1.68e-5	0.0028	0.0078	0.088	2.23
3.50	2.84	1.79e-5	1.96e-5	0.0032	0.010	0.12	2.96
4	3.65	2.25e-5	2.24e-5	0.0037	0.013	0.16	3.83
4.50	4.55	2.74e-5	2.51e-5	0.0042	0.015	0.20	4.75
5	5.54	3.28e-5	2.79e-5	0.0046	0.019	0.24	5.82

5.10 Natural Frequency

This section provides calculations made to avoid operating at natural frequencies of the components in the system. By avoiding these frequencies, extensive vibrations can be avoided.

5.10.1 Drillpipe

Lateral vibrations

The drillpipe is assumed to behave like a uniform beam. Its properties are listed in Table 5.1. The lateral natural vibrations is estimated with Equation 4.32. The tension force is assumed to be equal to zero because compression forces neutralizes it. Calculations are made on the first mode, because it is the first frequency expected to be encountered.

$$\omega_1 = \sqrt{\left(\left(\frac{\pi}{0.914}\right)^4 \frac{71.70 \cdot 10^9 \cdot 1.74 \cdot 10^{-10}}{1.74 \cdot 10^{-5} \cdot 2810}\right)} = 188 \text{ rad/s} = 1795 \text{ RPM} \quad (5.5)$$

A natural frequency of 1 795 RPM is considerably greater than the operational values and will not be a problem for the system. To verify whether the result is reliable, Equation 4.36 for Critical Rotary Speed (CRS) can be used.

$$CRS = \sqrt{0.38^2 + 0.33^2} \frac{4\,760\,000}{36^2} = 1825 \text{ RPM} \quad (5.6)$$

The system should avoid RPM values in the range of $\pm 15\%$ to 1 825 RPM. Operations between 1 551 and 2 099 RPM should be avoided.

Longitudinal vibrations

Longitudinal natural vibrations are estimated with Equation 4.33, 4.34 and 4.35:

$$\begin{aligned} \beta &= \frac{0.060}{1.50} = 0.040 \\ \alpha_1 \tan(\alpha_1) &= 0.040 \rightarrow \alpha_1 = 0.20 \\ \omega_1 &= \frac{0.20 \cdot 4928}{0.914} = 1067 \text{ rad/s} = 10189 \text{ RPM} \end{aligned} \quad (5.7)$$

A operation with an RPM of 10 189 cannot be achieved and will therefore not be an issue. An estimation of natural frequencies in the BHA is conducted with Equation 4.37:

$$CRS = \frac{84240}{0.53} = 158\,644 \text{ RPM} \quad (5.8)$$

The RPM of 158 644 is not achievable and far outside the operating window planned for this rig

design.

5.10.2 Rod

To calculate for which frequencies natural lateral and longitudinal vibrations occur, the assumptions for the drillpipe were also made for the rod. The frequency regimes for stainless steel 316 and titanium grade 5 will be calculated and presented in this section. The values used in the equations are listed in Table 5.1. The length of the rod is 1.42 m, but some part of it is attached in the drill chuck and BHA. The free length of the rod is therefore 1.40 m.

Lateral Vibrations

The natural frequency for lateral vibrations for steel is calculated:

$$\omega_1 = \sqrt{\left(\frac{1 \cdot \pi}{1.4}\right)^4 \frac{190 \cdot 10^9 \cdot 1.26 \cdot 10^{-11}}{1.26 \cdot 10^{-5} \cdot 8000}} = 24.54 \text{ rad/s} = 234.34 \text{ RPM}. \quad (5.9)$$

To avoid this natural frequency with a safety margin of $\pm 15\%$, RPM values between 200 and 270 should be avoided. The successive natural frequency occurs at 2 109.06 RPM which is greater than the maximum RPM the top drive motor can deliver.

$$\omega_1 = \sqrt{\left(\frac{1 \cdot \pi}{1.4}\right)^4 \frac{110 \cdot 10^9 \cdot 1.26 \cdot 10^{-11}}{1.26 \cdot 10^{-5} \cdot 4420}} = 25.12 \text{ rad/s} = 239.88 \text{ RPM}. \quad (5.10)$$

With titanium rod, the first natural frequency occurs at 239.88 RPM which gives a window from 204 to 276 RPM in when the drilling system should not be operated. The following natural frequency occurs at 2 158.90 RPM and which is also greater than the maximum RPM the top drive motor can deliver.

Longitudinal Vibrations

Longitudinal natural vibrations for the rod are estimated with the same equations used for the drillpipe. The natural frequency for the steel rod is calculated as follows:

$$\begin{aligned} \beta &= \frac{0.14}{1.50} = \frac{7}{75} \\ \alpha_1 \tan(\alpha_1) &= \frac{7}{75} \rightarrow \alpha_1 = 0.30 \\ \omega_1 &= \frac{0.30 \cdot 3272}{1.40} = 701.14 \text{ rad/s} = 6695.39 \text{ RPM} \end{aligned} \quad (5.11)$$

The first natural frequency with respect to longitudinal vibrations occurs at 6 695.39 RPM. Operating with RPM values at this level is not applicable for this system. Equation 4.34 has multiple

solutions.

$$\beta = \frac{0.078}{1.5} = 0.052$$
$$\alpha_1 \tan(\alpha_1) = 0.052 \rightarrow \alpha_1 = 0.23 \quad (5.12)$$
$$\omega_1 = \frac{0.23 \cdot 3125}{1.4} = 513.39 \text{ rad/s} = 4902.51 \text{ RPM}$$

Equation 5.12 shows that the first natural frequency for titanium with respect to longitudinal vibrations occurs at 4 902.51 RPM. This is not a problem because these RPM values are greater than what the rig operates. Calculations are therefore not made to express the RPM at greater modes.

(This page is intentionally left blank)

Chapter 6

Mechanical Rig Design

The miniature drilling rig in this thesis project is used to drill deviated wells autonomously to meet the standards and requirements set in the annual Drillbotics competition of 2021. Each year, the requirements change, and the drilling rig must be modified accordingly. This chapter is based on the design proposal from Phase I of the Drillbotics competition and explains the mechanical rig design with all hardware components used for autonomous directional drilling [9].

The first section introduces the previous rig designs in the Drillbotics competition. The following sections each present the system on today's rig one by one. The hoisting system provides the vertical movement of the drilling components. The rotary system provides rotational torque to the drill bit using a rod inside the drillpipe. The azimuth systems steer the drill string and Bottom Hole Assembly (BHA) in the desired direction. The circulation system provides fluid flow to transfer rock cuttings out of the well and cool and lubricate the bit. After that, the section presents the drillstring design with the stabilizing elements on the drill floor for reducing drill string vibrations. The two following sections describe the BHA and drill bit design in detail. The last section presents the electrical hardware for downhole measurements and system control.

To enhance the total drilling performance, the authors aimed at constructing a rig with a robust mechanical design. Many components are reused and already available in the university workshop to make the project cost-efficient because of budget limitations [63]. The main challenge was to design a rig able to withstand the physical stresses and motions inflicted by each component.

6.1 Drillbotics Rigs 2016-2020

The 2021 drilling rig recycles many components from previous years' designs at NTNU. This section will therefore provide a brief description of the previous designs. The NTNU team in 2017 constructed the rig used each year since. The objective was then to "design a fully automated drilling rig that could autonomously drill a vertical well as quickly as possible while maintaining rig and drill string integrity". Their design had a hoisting system using a motor and balls crew. The drilling concept was a top drive motor providing rotation to the drill bit by means of rotating the drillpipe. A hydraulic and electrical swivel connects to the computer. The team placed 2nd in the Drillbotics competition with this design [63].

The 2018 team implemented a protective acrylic glass, a semi-closed circulation system to direct the return flow, and a new ball screw to improve control responsiveness and decrease drillstring vibrations. A universal coupling absorbed some of the axial vibrations. The team placed 1st in the Drillbotics competition using this design [52].

In 2019, the competition focus was directed towards autonomous directional drilling and down-hole measurements. A new motor was implemented in the BHA with a fixed bent sub to enable deviated drilling. The team was unable to compete in the competition because of restrictions in the custom. The 2020 competition was canceled due to the corona pandemic. Each year, the rig has been recycled, enabling the teams to spend money on improving the rig components instead of fundamental parts such as framework, computes, motors, etc.

6.2 Drillbotics 2021 Rig

The NTNU team of 2021 decided to abandon the PDM and focused on designing an improved rig using a long rod to drive the drill bit instead. The new drilling concept allowed the authors to recycle the following parts: rig framework, castor wheels, hoisting system, electrical components, safety cabinets and panels, hydraulic swivel, and riser set up. The goal was to create a robust mechanical design that could enhance the overall drilling efficiency and steering precision.

The 2021 rig was designed to meet the requirements set by the Drillbotics Committee for the competition. It had to resemble an actual full-scale drilling rig from the oil and gas industry. Previous students focused on the mobility and functionality of the drilling when constructing the rig framework. In the design, versatility, safety, and high precision drilling performance were also important for the authors. The latter was an essential focal point this year to drill deviated wells. The authors have improved workplace safety by carefully investigating all present work hazards, described in section 3.3. Figure 6.1 illustrates the miniature drilling rig to be used in 2021.

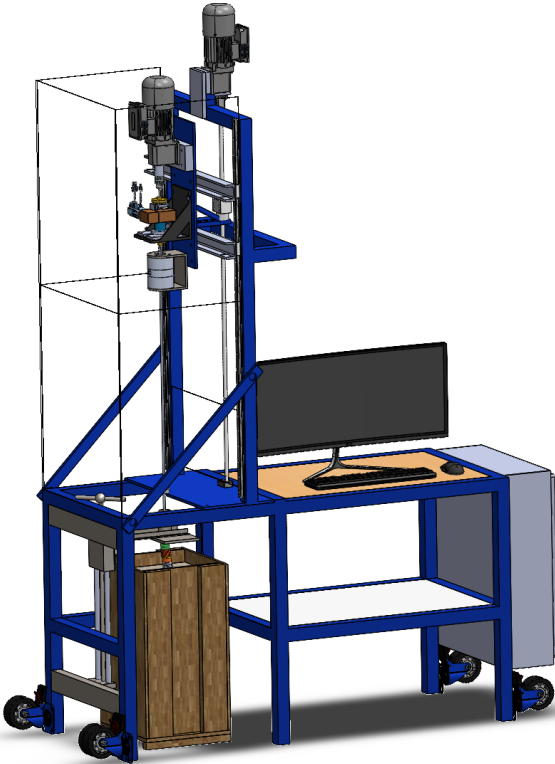


Figure 6.1: Proposed design of the miniature drilling rig 2021.

6.3 Rig Component Overview

The miniature drilling rig is a setup of components working together to execute the drilling operation. Each designed component was built and tested by the authors, and the communication between them constitutes the complete drilling concept. The components are divided into smaller systems based on their functions. The purpose of a detailed description of each component is to provide the reader with a complete technical understanding of how the miniature drilling rig works. The following sections present the reader with the complete design used in the Drillbotics competition. Chapter 13 gives a presentation of the decisions, challenges, and iterations made to the components and the design. Given below is an overview of the rig systems:

- **Section 6.4: Rig framework**

Rig structure, rock sample house, computer table, acrylic protection glass, and castor wheels.

- **Section 6.5: Hoisting system**

Hoisting motor, ball screw, carriage mount, WOB load cell, roller guides, and safety stop buttons.

- **Section 6.6: Drilling system**

Top drive motor (old and new), drill chuck and top drive connection, titanium rod, drillpipe, stabilizers, and parts for alignment.

- **Section 6.7: Azimuth system**

Hollow gearbox, azimuth servo motor and gearboxes, T-shaft, and torque sensor.

- **Section 6.8: Circulation system**

Swivel house, hollow swivel shaft, roller bearings, and drillpipe connection.

- **Section 6.12: Electrical system**

Downhole sensor, pressure transmitter, and Data Acquisition (DAQ)

6.4 Rig Framework

The framework of the drilling rig was designed and constructed in 2017 when NTNU first attended the competition. The framework consists of the derrick, drill floor, rock sample house, and computer table. It holds all drilling components and electrical components which are separated on the rig. Separating the two reduces the risk of damaging the electrical components. Hollow steel beams have been welded together and mounted with bolts and nuts for extra support. It can effortlessly and safely hold and protect the drilling components. The total height of the rig is 285 cm (9.35 ft) to fit a rock sample of height 60 cm. Figure 6.2 shows an illustration of the framework without its drilling components.

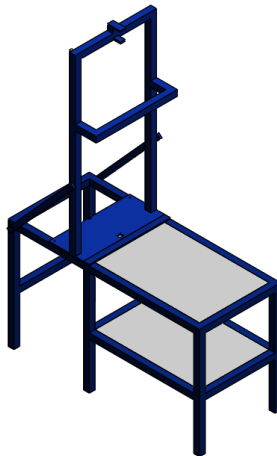


Figure 6.2: Framework of the miniature drilling rig without drilling components.

The rig structure is 165 cm (13.75 ft) long and 70 cm (2.3 ft) wide. Its total weight is approximately 170 kg (370 lbs). Castor wheels (not showed in Figure 6.2) ensures the mobility of the rig. Figure 6.3 illustrates a fold-down feature of the derrick, which allows for more manageable transportation. If necessary, a gantry crane can lift and position the rig in the workshop safely.

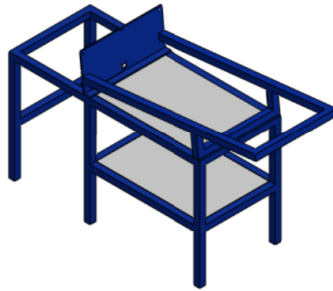


Figure 6.3: Folded rig structure

All sides of the derrick are covered with acrylic glass to protect personnel and surroundings against hazards related to the drilling operations. Section 3.3 describe hazards related to moving objects. The protection glass on the backside of the derrick, facing the computer table, is bolted to the framework. A liftable cabinet surrounding the derrick can slide up and down on a heavy-duty telescopic expansion slide. This feature allows for easy access when operation ceases. Pins keep the cabinet in place when lifted to the top. Versatility was essential when the rig was built in 2017. Future students avoid building a new rig structure if the competition changes the rock sample dimensions. The rig allows for a formation rock with a total height of 85 cm (33.5 inches) and an area of 60x60cm (23.6 inches).

6.5 Hoisting System

A motor that rotates a ball screw combined with a linear roller guide system hoists the rig's drilling equipment. The system converts rotational motion to vertical motion by a nut and bracket moving up and down on the ball screw. All drilling components are attached to a carriage mount linked to the ball screw. The following sections describe each component in detail.

6.5.1 Hoisting Motor

The motor is a Lenze motor with a helical gearbox recycled from previous years. It hoists the system up and down to move the drilling system in and out of the well. This vertical motion provides WOB when drilling. The hoisting motor is a GST 03-2M VBR 063C42 model by Lenze controlled by an E84AVTCE7512SX0 inverter. This inverter has a maximum power output of 0.75 kW. The maximum rotational motor speed is 3400 RPM and a maximum torque of 45 Nm [55]. As the motor provides the rotational force, it has to be converted into linear motion by a ball screw. The gear ratio between this ball screw and the motor RPM is 1:8.935. Figure 6.4 shows the hoisting motor connected to the ball screw using a standard Oldham coupling from Huco.



Figure 6.4: Hoisting servo motor.

The drive used for motor control is a Lenze drive of model 8400 Topline C. Torque and RPM measurements are gathered from sensors integrated in the motor. The drive is a frequency converter and controls frequencies and current to operate at the desired torque and speed. The hoisting motor output signals are first converted into a voltage range of 0-10 volts and then converted into torque and RPM signals. The drill string position is adjusted by the motor rotation and is estimated by a combination of the incremental encoder output of the motor and the load cell lead. The communication between the computer and the motor is set up through a Modbus protocol with

its drive. An Ethernet/IP module from the drive to the computer establishes the communication. Appendix D provides more detailed motor specifications.

6.5.2 Carriage Mount

A nut and bracket can move in the vertical direction along the ball screw. The bracket connects to a steel plate referred to as the carriage mount. The carriage mount holds all necessary drilling equipment in place. The picture in Figure 6.5(a) shows the carriage mount from behind. It is welded onto two vertical channel struts moving up and down along the derrick on roller guides shown in Figure 6.5(b).



(a) The carriage mount from behind



(b) A slider on one of the roller guides

Figure 6.5: Hoisting system components.

The channel struts can slide up and down using roller guides shown in Figure 6.5(b). These allow for support and guiding of the drilling system [63]. This hoisting system with all components attached to the carriage mount weighs approximately 50 kg (110 lbs). Its weight (and additional weight if desired) is transferred from the ball screw to the drilling components via the carriage mount. However, the ball screw enables the system to not put any of its weight on the bit by using a load cell to control the WOB.

6.5.3 Load Cell

A cylindrical load cell placed on top of the ball screw nut controls the amount of WOB. Figure 6.6 shows a picture of the load cell on the carriage mount. It is connected to the carriage mount using a 45 degree support beam and registers the weight applied by the hoisting system. The load cell resets the weight of the drilling system (similar to when taring a kitchen weight) such that when

the bit is lifted off-bottom, WOB is zero.

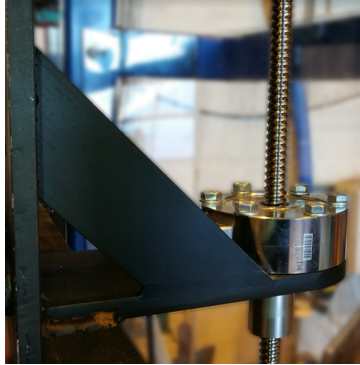


Figure 6.6: Load cell mounted on the ball screw

The load cell is a TC4-AMP made by AEP Transducer. This force transducer converts the force created by the vertical motion of the hoisting system into a voltage signal. The voltage signal is then interpolated into WOB readings. A built-in amplifier in the load cell has options for voltage output in the range ± 5 V and ± 10 V, and current output of 4-20 mA [4]. The load sensor can measure force in a range of ± 5 kN



Figure 6.7: Load cell: TC4-AMP transducer by APE Transducer [4].

A NI USB-6212 Multifunction I/O connects the load cell shown in Figure 6.7 to the computer. This force transducer converts the output force to an electrical signal. Applied WOB deforms a strain gauge inside the load cell. This deformation is measured as a change in electrical signal and interpolated into the weight measurement. This linear interpolation can be described by

Equation 6.1:

$$WOB = -509.7 \text{ kg} + \frac{V_{in} + 10 \text{ V}}{20 \text{ V}} 1019.4 \text{ kg} \quad (6.1)$$

The hoisting system is an efficient method of applying weight to the system with high precision and step resolution while making easy adjustments. Without the load cell, excessive weight on the system can compress the drillpipe and lead to buckling and failure.

6.5.4 Safety Stop Buttons

Two safety stop buttons are installed on the rig to break the circuit to the hoisting motor when the carriage mount is moved too high or low. The two buttons are placed on the roller guide rails on the derrick. One stop button is placed at the top of the derrick, which prevents the system from hoisting the carriage mount off the rails. Such a stop button is depicted in Figure 6.8.



Figure 6.8: Stop button on hoisting system.

The upper stop button is also placed at a point such that when raising the drilling system, the top of the BHA does not reach the derrick floor. The roller bearing on the derrick floor that stabilizes the drillpipe pointed out in Figure 6.9 has an inner diameter smaller than the outer diameter of the BHA. Without the stopping mechanism, hoisting the drilling system with the BHA attached could do severe damage to the system. The button is placed at 85 cm above the derrick floor to ensure that the BHA will be kept below the upper stabilizer at all times.



Figure 6.9: Picture of the BHA seen below the derrick floor. Arrow points at upper stabilizer.

The lower stop button is located near the drill floor to prevent the drilling system from reaching the stabilizer on deck.

6.6 Drilling System

The components in the rotary system are providing rotation and stabilization to the drill bit during drilling. It consists of rotational torque transmission from a top drive motor to a titanium rod located inside the drilling system. The drillpipe will only rotate when the azimuth is changed. This technique can remind of the drilling method “slide drilling” in the industry. Figure 6.10 shows a picture of the complete rotary system.



Figure 6.10: Complete rotary system. From top: top drive motor, drill chuck fastener, drill chuck, "T-shaft", azimuth motor, torque sensor, stabilizing plates and hydraulic swivel.

6.6.1 Top Drive Motor no. 1

The top drive motor that drives the rod is located on the top of the drilling system. The purpose of the top drive motor in this system is to rotate the rod going through the entire rig down to the drill bit. The rod rotates freely inside the drillpipe and transfers torque and RPM directly to the bit.

At first, the top drive motor from 2020 was replaced by a motor equivalent to the hoisting motor, GST 03-2M VBR 063C42 model by Lenze. The reason was that the previous motor was difficult

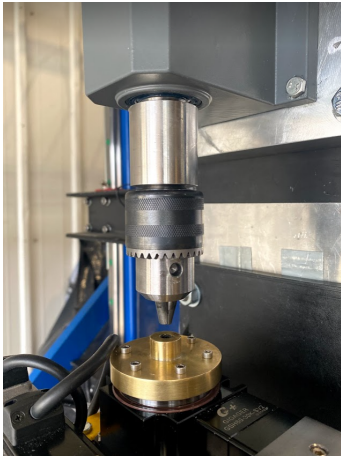
to control and to read data from in the chosen control system. In addition, the motor limited the maximum update frequency in the system. However, the hoisting motor has been used for many years and has proven reliable and easy to handle. Because the only required component for the motor to work was a communication model of type E84AYCEO and because it uses the same drive and communication protocol as the hoisting motor, it seemed reasonable to use it as a top drive as well. This Lenze *motor* can provide a speed of 3400 RPM. However, the gear ratio of 1:8,935 reduces the speed capacity to approximately 380 RPM in actual output. After test drilling, the authors noticed that the drilling system needed a much greater RPM to drill efficiently. A decision was made to replace the motor with a new one.

6.6.2 Top Drive Motor no. 2

The new motor is a Lenze motor and gearbox of model G500-H45 MF 063-42. With a gear ratio of 1:2,597, the motor and gearbox provide the system with an output speed of 1309,2 Revolutions Per Minute (RPM), and an output torque of 5 Nm. The motor is mounted to the carriage mount using an adapter plate design by the authors. It can be seen behind the top drive motor in Figure 6.10. The adapter is designed in SolidWorks and produced in steel by professional workers at the worksite. The adapter spares the carriage mount for additional holes such that future teams can modify the drilling system without changing large parts on the rig. More detailed motor specifications are found in Appendix E.

6.6.3 Drill Chuck and Top Drive Connection

A special-made fastener in stainless steel connects a drill chuck to the shaft on the top drive motor. The drill chuck is similar to those found on hand-held drills and transfer the torque from the top drive motor to the titanium rod. Figure 6.11(a) shows a picture of the adaptor and drill chuck mounted on the top drive shaft. The drill chuck has three jaws that lock the rod in place using a special key shown in Figure 6.11(b). This technique is a cheap, simple, and efficient method to keep the rod stable during rotation while enabling quick and safe replacement. Although the rotary system rotates in a clockwise direction, vibrations in the system can lead to the dismantling of threaded components. The screw is, therefore, important because it locks the chuck in place.



(a) Rotary system (from top): End of top drive motor, drill chuck fastener, drill chuck with three jaws.



(b) (from left): Drill chuck key, drill chuck and screw

Figure 6.11: Drill chuck components.

6.6.4 Rod

The thin, cylindrical rod has an outer diameter of 4 mm (0.16 inches). The material used is titanium. The rod extends from the drill chuck jaws and down to the drill bit, which corresponds to 1.42 m (56 inches). The drillpipe has an outer diameter of 9.53 mm (3/8 inches) and an inner diameter of 7.04 mm (0.28 inches). These dimensions correspond to an annular area of 3.04 mm (0.12 inches) for drilling fluid to travel down to the drill bit using a 4 mm titanium rod inside. Calculations on twist-off and bending were done in the design phase of the project and showed that there was a risk of twisting the rod [9]. The team, therefore, ordered a large quantity in different diameters, as depicted in Figure 6.12 . Chapter 5 describes the justifications for choosing to drill with a titanium rod of 4 mm.



Figure 6.12: Rods.

6.6.5 Drillpipe

Because the competition does not require making or breaking of drillpipe connections, the length of the drillpipe was customized to drill through the rock sample without stopping, approximately 90 cm (35 inches). In the competition guidelines, only stainless steel and aluminum are allowed. The materials' ability to withstand plastic deformation when subjected to bending is the most significant difference. Chapter 5 presents the calculations made when examining the performance of stainless steel and aluminum pipe. The calculation showed that stainless steel quickly enters plastic regime when subjected to bending stress. The aluminum alloy named "7075-T6" is the superior material and is therefore used in this design.

6.6.6 Stabilizers

The drilling system has two stabilizers mounted to improve performance and workload limits, both depicted in Figure 6.13. The drilling system uses an upper and lower stabilizer for shortening the effective length of the drilling system to reduce the risk of pipe buckling. Both stabilizers also reduce the lateral vibrations in the system.

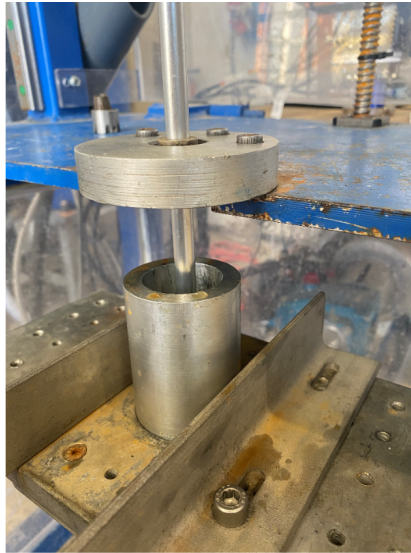


Figure 6.13: Upper and lower stabilizer on the rig.

The upper stabilizer is a 10 cm wide disc fastened to the drill floor with three socket screws. A roller bearing is placed in the middle with an inner diameter equal to the outer diameter of the drillpipe, 9.525 mm (3/8 in). The stabilizer simulates the bushing used on the drill floor in full-scale drilling operations. The roller bearing reduces the rotational resistance while stabilizing the pipe.

The lower stabilizer, also referred to as the riser, is placed beneath the drill floor and consists of an aluminum cylinder screwed onto an aluminum plate. The riser, which has an adjustable height, guides and stabilizes the BHA on top of the rock sample drilling starts. The hoisting mechanism is based on a ball screw concept and uses a manual lever depicted in Figure 6.14 to regulate the height.



Figure 6.14: Manual hoisting mechanism of the riser.

By separating the two stabilizers at a certain distance, the drillpipe is divided into parts with a smaller unsupported length to raise the buckling limit as much as possible. Previous years have used a hollow cylinder with a bell nipple on the bottom for diverting the return fluid. Because this years' design uses much lower drilling pressures, the return fluid runs freely out onto the floor and into a drain.

6.7 Azimuth Control System

The steering concept required an accurate system to orient the drillpipe and BHA. The system had to be used in a closed-loop control based on its current position estimate. Initially, the plan was to use a hollow shaft servo motor, but one that fit our requirements proved to be rare and expensive. An alternative became to use a hollow shaft gearbox with a servo or stepper motor. Using a gearbox reduces orientation accuracy and makes torque estimates from a servo motor less accurate. Because the differences in accuracy were in the ratio of a few arc-min, this was an acceptable trade-off. The primary purpose of measuring torque is to avoid mechanical damage during rotation rather than making accurate measurements during drilling.

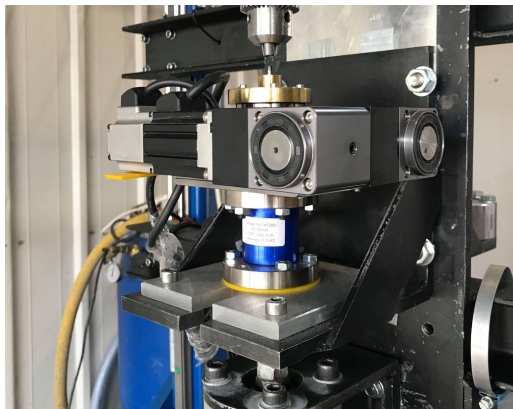


Figure 6.15: Azimuth control system with servo motor, gearbox system, torque sensor, and T-shaft.

Figure 6.15 shows a picture of the Azimuth system. On the left is the servo motor, and to the right are two right-angled gearboxes. The hollow shaft gearbox with rotary table (not seen) is in the middle, located below the brass shaft seen under the drill chuck.

6.7.1 Hollow Gearbox with Rotary Table

The rotary table allows for changes in orientation without interfering with the rotating rod. The maximum torque is 30 Nm, and rotational output speed is 2 500 RPM with a gear ratio of 1:30. The gearbox runs smoothly with little noise or vibration while still providing the system with a high transfer of torque [38]. The hollow shaft gearbox, depicted in Figure 6.16 is a Hypoid GSH 60-30K-SV1. Detailed specifications can be found in Appendix G.

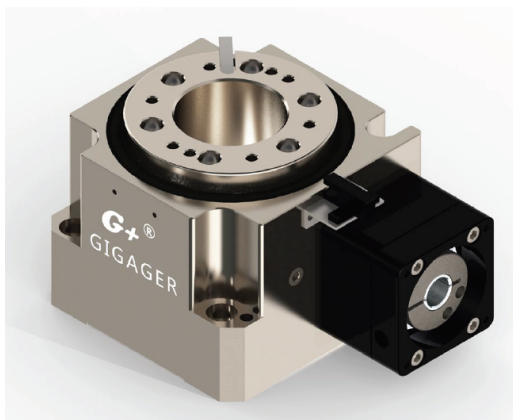


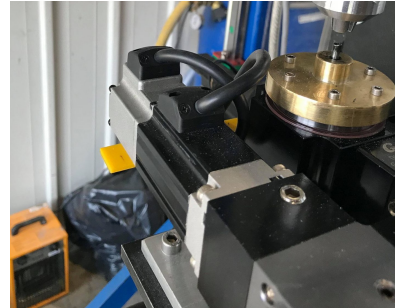
Figure 6.16: Hollow shaft Hypoid gearbox with rotary table [38].

6.7.2 Azimuth Servo Motor and Gearboxes

Moons' Industries make the azimuth servo motor, depicted in Figure 6.17(b) connected to the hollow shaft gearbox providing torque to the azimuth system. The motor model is SM0402AE4-KCD-NNV with a corresponding drive of type M2DV-1D82IP, depicted in Figure 6.17(a). The maximum output power of the motor is 0.1 kW, and rotational output speed is 3000 RPM. It has a maximum rated torque of 0.32 Nm and a peak torque of 0.93 Nm. Early testing proved the minimum rotational motor speed to exceed the necessary speed for accurate velocity control of the drillpipe when rotating against the wellbore wall. Two additional gearboxes of ratio 3:1 reduce the speed and increase the accuracy of the azimuth system.



(a) Moons' Industries Azimuth drive (left) and servo motor (right) [47].



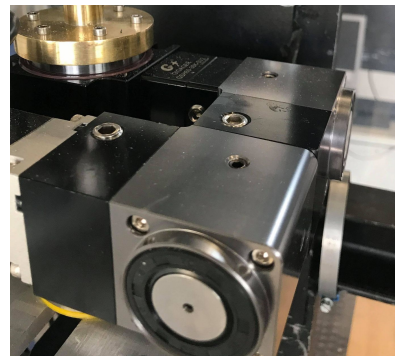
(b) Installed azimuth servo motor.

Figure 6.17: Azimuth servo motor components.

The gearbox model is a GSZ042-03K-SV from Gigager shown in Figure 6.18. In the hollow shaft gearbox, a gear ratio of 1:270 is obtained, thus allowing accurate azimuth control. The gearboxes connect to the hollow shaft gearbox and the servo motor. The permissible input speed of the gearboxes is 2 500 RPM, and permissible torque is 12 Nm. Each gearbox has a backlash of less than 0.5 arc-min. Equipment from Moons' Industries supports both Ethernet/IP and Modbus communication. Because the control system only supports Modbus TCP, this communication protocol was chosen over Ethernet/IP [40].



(a) Gigager right-angled gearbox [39].



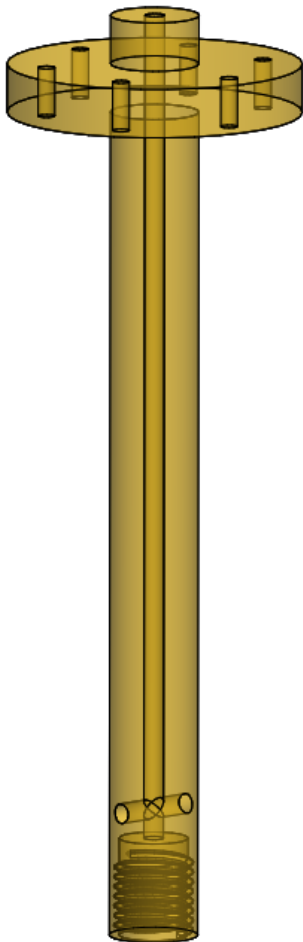
(b) Installed azimuth gearboxes

Figure 6.18: Gigager gearbox.

Detailed specifications for the Moons' azimuth servo motor and Gigager right-angle gearboxes are found in Appendix H and I, respectively.

6.7.3 T-shaft

Because the rotating rod must pass through the azimuth components, a long hollow "T-shaft" in brass is mounted on the rotary table of the hollow shaft gearbox to transmit torque to the system below. A passage inside the shaft of 4 mm enables rotation of the rod while minimizing water migration from the hydraulic swivel below. The brass shaft also has a safety outlet illustrated in Figure 6.19(a). Figure 6.19(b) shows the final component.



(a) T-shaft SolidWorks design.



(b) T-shaft final product.

Figure 6.19: T-shaft design.

A hollow, cylindrical torque sensor is installed below the rotary table. The brass shaft passes through the gearbox and torque sensor and screws onto a new hollow shaft located inside the swivel. Appendix K show detailed drawings with all dimensions.

6.7.4 Torque Sensor

Because of the increased gear ratio, torque estimates from the motor were not accurate enough for a closed-loop control when driving the bit against the wellbore wall. The solution was to implement an external torque sensor. The sensor measures torque differences between a mechanical reference on the rig and the torque provided by the azimuth servo motor and its gearboxes.

Torque estimates on the drillpipe were initially supposed to be gathered from the azimuth motor to control the angular velocity. In this relation, the steel shelf under the sensor serves as the static mechanical reference rigidly connected to the carriage mount. The torque force exceeded on the drillpipe is the static part of the hollow shaft gearbox. The torque sensor in Figure 6.20 is a TAT200 made by GT Sensor Technology and has a torque range of ± 30 Nm.

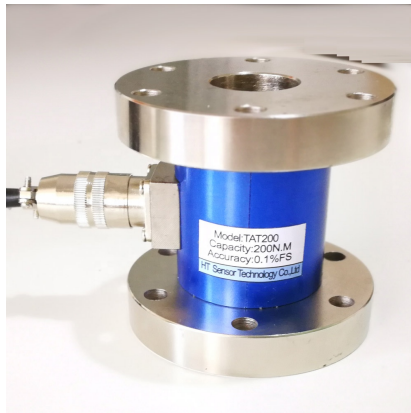
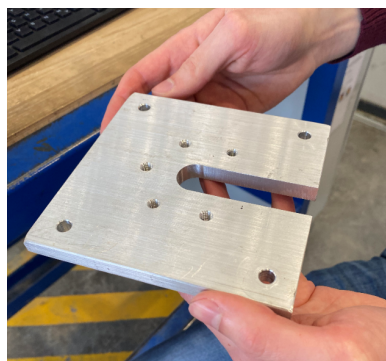


Figure 6.20: Torque sensor.

In contrast to the load cell, the torque sensor has no built-in amplifier. An external amplifier is used to get measurable signals from the sensor to the DAQ (see subsection 6.12.2). The amplifier is made by HT Sensor Technology and is a model of type SIC-A5. The amplifier amplifies the slight difference of a few mV into a range measurable by the Data Acquisition (DAQ).



(a) Aluminum plates to mount azimuth gearbox and torque sensor together.



(b) Aluminum plate to mount torque sensor to carriage mount shelf.

Figure 6.21: Alignment and mounting plates.

The two aluminum plates in Figure 6.21 allowed for mounting the hollow gearbox directly on top of the torque sensor. Figure 6.21(b) shows a picture of an aluminum plate used to fix the torque sensor to the carriage mount in addition to aligning its height. Figure 6.22 show the plates installed on the rig. An additional yellow 3D-printed disc has been installed to improve the alignment in the system further.

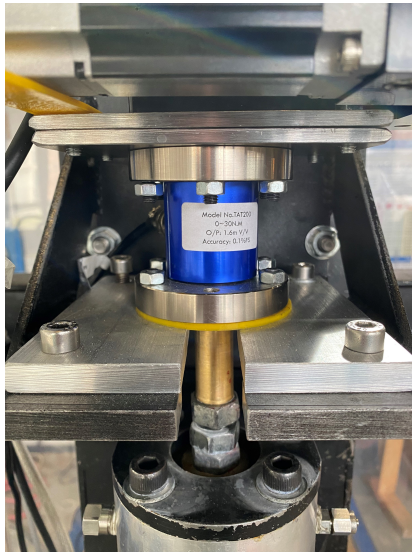


Figure 6.22: Alignment plates implemented on the rig.

6.8 Circulation System

The hydraulic system consists of a water supply through a water hose connected to a hydraulic swivel. The swivel illustrated in Figure 6.23, is located beneath the gearbox and torque sensor. The swivel is the element that connects the hoisting system to the rotary system and the circulation system.

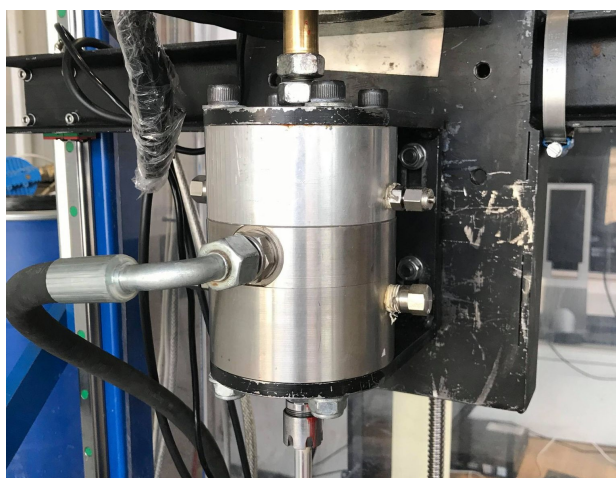
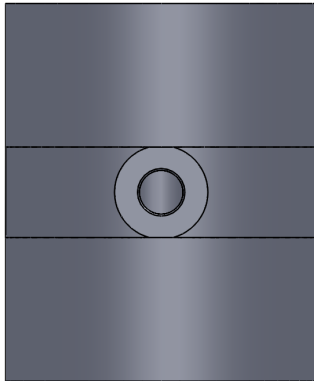


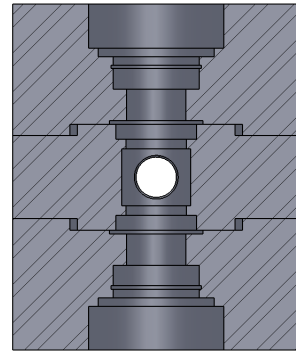
Figure 6.23: Picture of the complete swivel.

6.8.1 Swivel House

The primary function of the swivel is to supply the drilling operation with enough water to transport cuttings out of the well. The hydraulic system cools and lubricates the drill bit during operation. The original swivel house design was made in 2017. The authors have recycled it and made improvements to prevent leakage and enabling both clockwise and counter-clockwise rotation of the shaft inside. Figure 6.24(a) shows the swivel house from the front with the water inlet in front. Figure 6.24(b) shows a cross-section of the swivel house. It has varying inner diameters to fit roller bearings, O-rings, and gaskets.



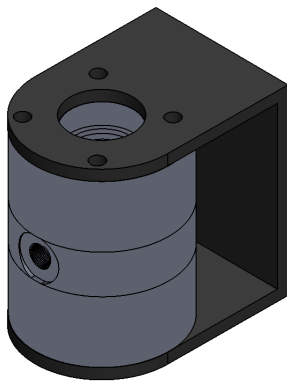
(a) Hydraulic swivel house design seen from the front.



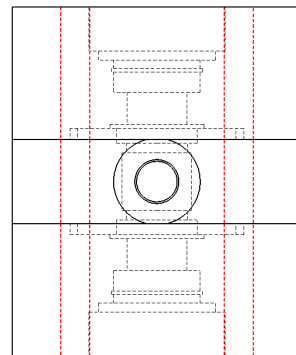
(b) Section of hydraulic swivel house, seen from the front.

Figure 6.24: Swivel house design.

The swivel house consists of three parts; top, middle, and bottom. The parts are made of stainless steel and are pressed together and locked inside an iron cast swivel holder, illustrated in Figure 6.25(a). Four iron bolts go through the holes in the swivel illustrated (in red) in Figure 6.25(b). They lock the parts together with stainless steel nylon-insert lock nuts on the top and bottom of the holder.



(a) Hydraulic swivel design with holder in iron.



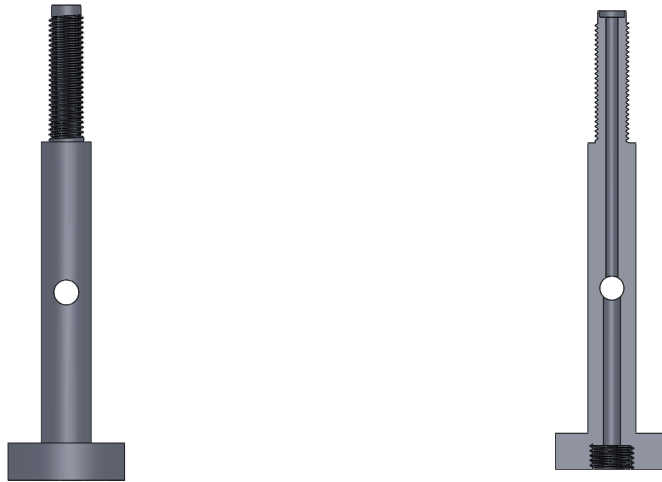
(b) Illustration of holes (in red) going through the full length of the hydraulic swivel.

Figure 6.25: Swivel house holder.

6.8.2 Hollow Swivel Shaft

Inside the swivel house is a hollow shaft that can rotate both clockwise and counter-clockwise while the rod rotates inside. The shaft design is illustrated in Figure 6.26(a) with a cross-section

in Figure 6.26(b) showing the hollow passage and internal thread at the bottom.



(a) Hydraulic swivel shaft design, seen from the front in Solid-Works.

(b) Section of hydraulic swivel, seen from the front in Solid-Works.

Figure 6.26: Hydraulic swivel shaft design.

Water enters the middle part of the swivel via a hose and further into the hollow shaft through a 10 mm opening. The water travels down the hollow shaft and into the drillpipe connected below the swivel. To prevent too much water from migrating up the hollow shaft, the inner diameter above the opening is 5 mm, and the inner diameter below is 7 mm.

The hollow shaft also allows the rod to rotate freely while providing the system with water. The outer diameter of the shaft is equal to the inner diameter in the top and bottom parts of the swivel housing. Because of the new concept of using a rotating hollow swivel shaft, the middle part was milled to fit additional sealing O-rings to prevent leakage. The grooves with O-rings (in red) are illustrated in Figure 6.27.

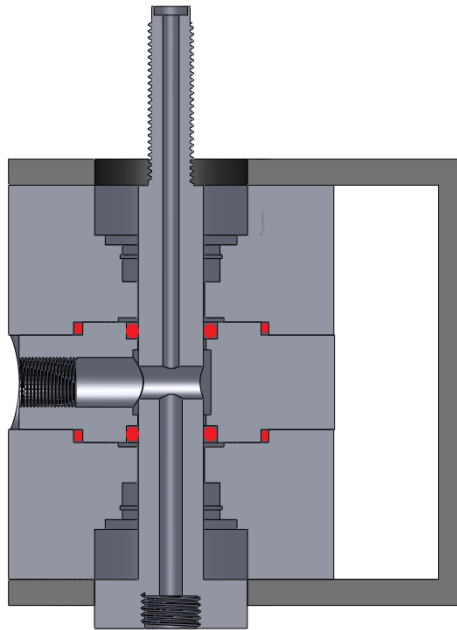


Figure 6.27: O-rings illustrated in red.

The shaft is connected to the brass T-shaft above the swivel house using threads. The two shafts will thus rotate together when the azimuth changes. A nut prevents the threads from unscrewing when the system rotates counter clock-wise. The connection is illustrated in Figure 6.28. The two lower nuts lock roller bearings in place.

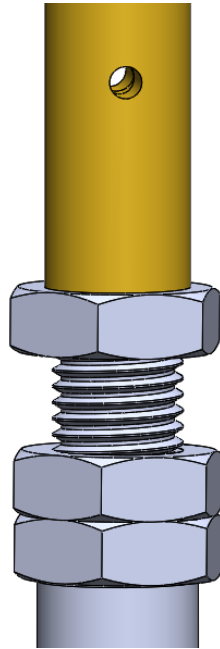


Figure 6.28: Connection between T-shaft and hollow shaft in swivel.

The top and bottom each have a sealing element and roller bearings to enable smooth rotation of the hollow shaft going through the housing.

6.8.3 Roller Bearings

The top and bottom parts of the swivel house are symmetrical and have a cavity containing a roller bearing. While they can withstand higher loads than conventional ball bearings, their functions are generally limited to low-speed operations. Because the hollow shaft rotates with the azimuth steering, which will not exceed 1 RPM, roller bearings seem to be a reasonable choice. An illustration of the roller bearing is seen in Figure 6.29.

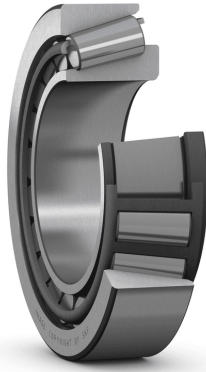


Figure 6.29: Illustration of the roller bearing used in the swivel.

Figure 6.30 shows a cross-section of the swivel house, holder, and hollow shaft. The roller bearings are illustrated in red, inside the swivel. The bearings minimize the friction from the rotating hollow shaft while sustaining the heavy load inflicted by the hoisting system.

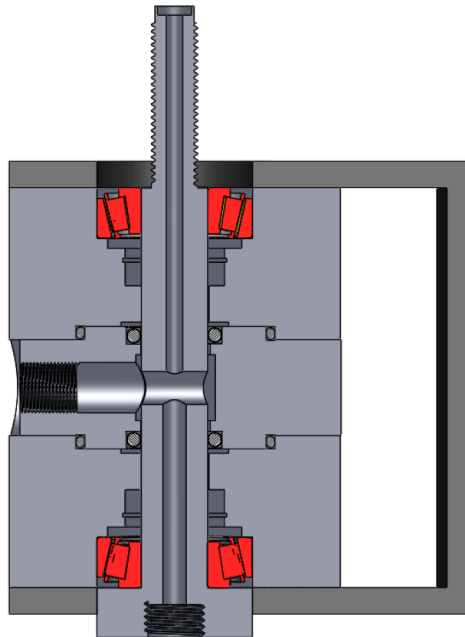


Figure 6.30: Cross-section of hydraulic swivel. Top and bottom roller bearings shown in red.

The hollow swivel shaft with two nuts fixes and secures both bearings. This design keeps the

bearings in place at all times. The nuts are fastened before each run.

6.8.4 Drillpipe Connection

The team implemented the drillpipe connection in 2018 to limit the swivel's need for a threaded drillpipe. The connection tolerates 17 Nm torque. The maximum torque applied by the azimuth system and onto the drillpipe is 15 Nm when azimuth changes during drilling. Drilling tests have shown that rotating the azimuth system 360 degrees/min with a ROP of 1cm/min, the torque is approximately 4.5 Nm which means that the risk of the connection unscrewing is small. Figure 6.31 shows the connection beneath the swivel house.



Figure 6.31: Drillpipe connected below the swivel.

Figure 6.32 shows the components making up the hydraulic connection beneath the swivel to transfer rotational motion to the drillpipe. A spring collet and cap screwed onto a specially made nipple is screwed into the bottom of the hollow shaft as depicted in Figure 6.31. The nipple is hollow and thus allows water to enter the drillpipe. The connection uses an o-ring to provide hydraulic integrity and mechanically locks the pipe to the nipple. The risk for damaging the pipe is low, and the connection can be made up quickly with a special tightening chuck spanner

wrench.



Figure 6.32: From the top: Nipple, spring collet with o-ring, collet nut and drillpipe.

6.9 BHA Design

The Bottom Hole Assembly (BHA) is one of the components the system dependent the most on to be able to build angle and steer in the $\{X, Y, Z\}$ plane. It is a collective name for all the drill string components located below the drillpipe. The rig performance can be greatly improved by designing the BHA to fit the requirements and design of the rig. This section contains the initial design and iterations of the design to fix problems encountered during testing.

6.9.1 Initial Design

The initial BHA design from Phase I of the project was based on work done by previous NTNU teams. The Phase I report describing the initial design is shown in Figure 6.33 [9].

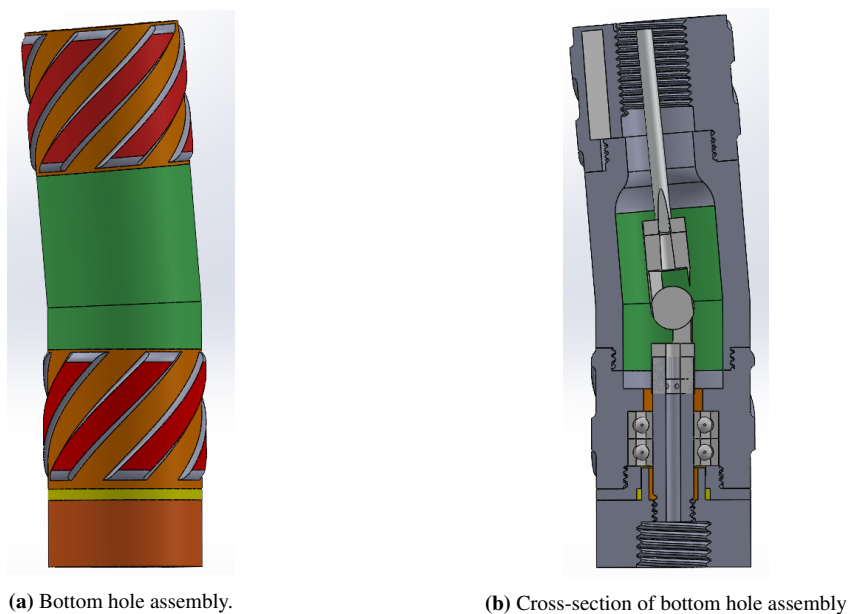


Figure 6.33: Initial design of bottom hole assembly.

The initial plan was to use the same sensor card as the previous and house it in the upper stabilizer. Because the firmware in the old sensor card was outdated, a new sensor card was purchased. Because the new sensor card had larger dimensions than before, the BHA had to be re-designed. The plan was then to place it in the upper stabilizer. Still, there was limited space because of the drillpipe connector, and it had to be placed in a separate component as shown in figure Figure 6.34.

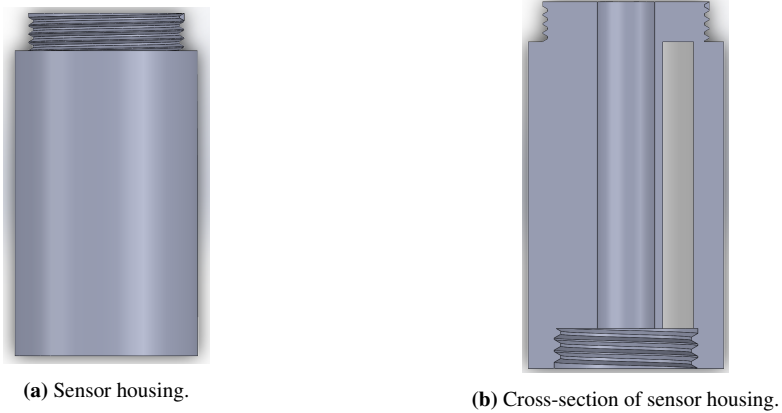


Figure 6.34: Sensor housing design.

Discussions with the lab engineers concluded that the bearing assembly did not perform as expected because of sand production and accumulation. A packer replaced the bearings using two o-rings to seal against the fluid flow as shown in Figure 6.35. This component was made in Teflon to minimize friction between the bit sub and the lower stabilizer.

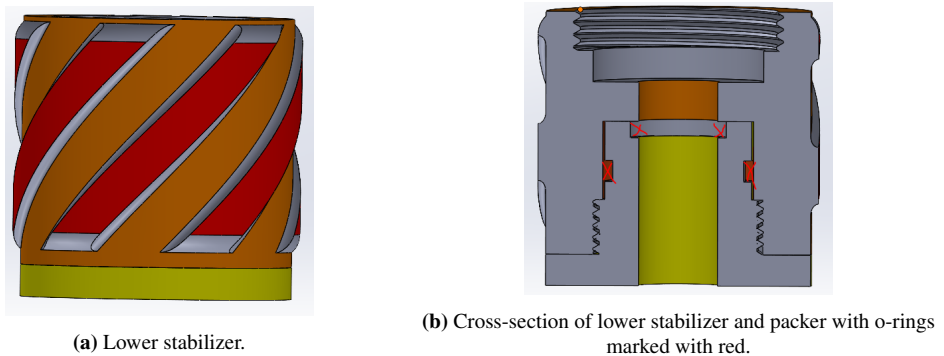


Figure 6.35: Lower stabilizer and packer design.

After implementing the changes, the first BHA was produced and ready for testing. The full first BHA design is shown in Figure 6.36.

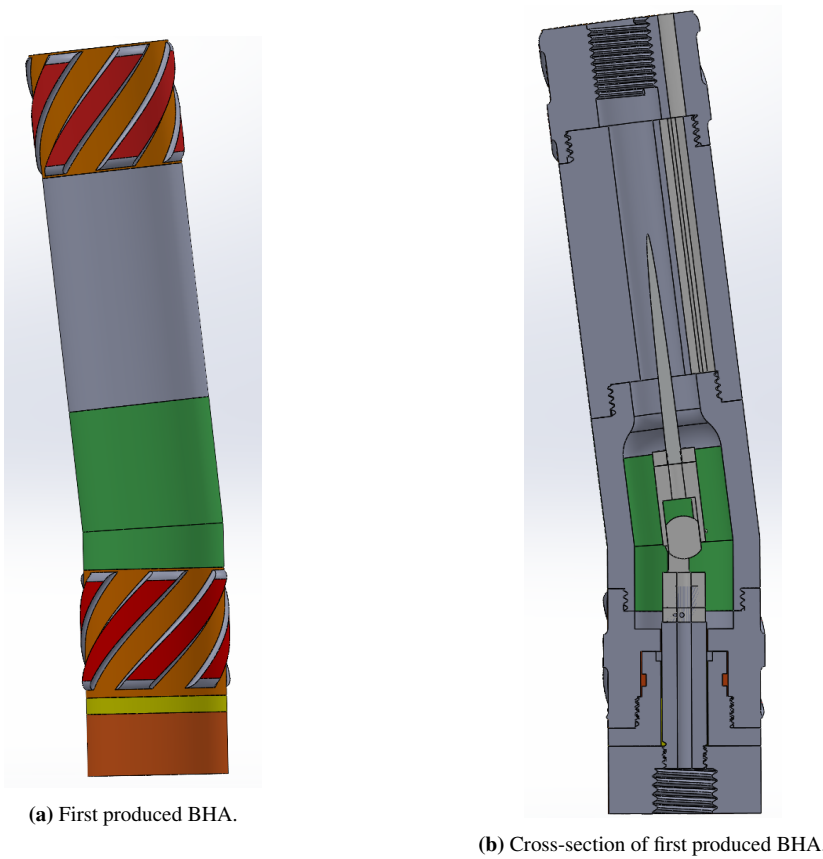


Figure 6.36: Design of first produced and tested BHA.

6.9.2 Pilot Hole Drilling

The Drillbotics competition required manually pre-drilling a pilot hole of 2.54 cm (1 inch) before starting the autonomous drilling. The pilot hole should be as straight as possible to provide stability for further drilling with the bent sub. A straight sub, shown in Figure 6.37, was therefore designed to replace the bent sub for drilling of this section. Together with the 5.08 cm (2 inches) diameter drill bit, it drills a suitable pilot hole to initiate the autonomous drilling operation.

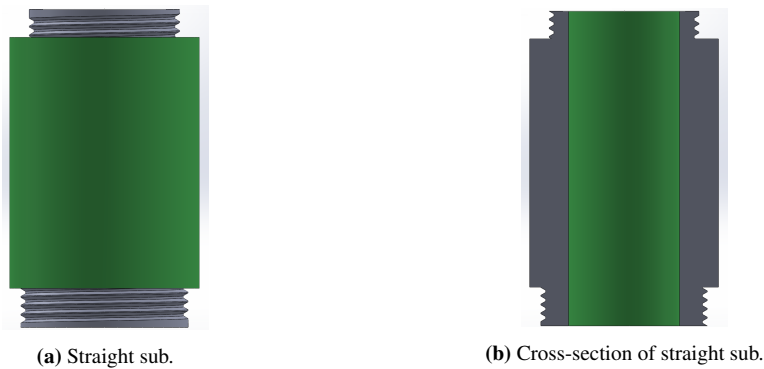


Figure 6.37: Design of straight sub.

6.10 Drill Bit Design

A crucial component of the drilling system is the drill bit. It is a small part of the rig, but it is essential for improving the drilling performance. Several different drill bits acquired from Alibaba have been tested to pinpoint the best bit for our drilling operation. DSATS, which arrange the Drillbotics competition, provided each team with a drill bit made by Baker Hughes.

Two drill bits were designed by the authors themselves and produced by Lyng Drilling, a Schlumberger company located near Trondheim. The collaboration with Lyng Drilling was initiated by earlier NTNU teams and was also a success in this rig design. The NTNU bit design was designed in SolidWorks and then proposed to Lyng Drilling for feedback before production. The final bit design is based on the theory from section 4.4 and the design considerations presented in this section. A completely new drill bit design enabled optimization of a bit best suited for the BHA and well to be drilled. Knowing the type of well and rock formation allows for optimizing the bit with respect to lifetime and performance. When the type of well and formation rock is known, considerations concerning drilling performance, such as improved borehole quality and ROP can be made. This section presents the design considerations and progress for making the NTNU bit. Lastly, all drill bits available for the rig, together with its specifications, are presented.

6.10.1 Design Considerations

The bit design considerations were affected by the competition requirements for the well to be drilled with the rig. Increasing ROP was not the most crucial aspect when designing the bit because of the generous time limit of 3 hours. The primary focus was to design a steerable drill bit with a high degree of stability while avoiding bit vibrations and minimizing bit torque.

Steering and Stability

The steerability of the bit can be quantified using Equation 6.2:

$$B_s = \frac{D_{lat}}{D_{ax}} \tag{6.2}$$

Where D_{ax} and D_{lat} are the axial and lateral drillability, respectively. These parameters are defined as the displacement per bit revolution in axial or lateral direction. For PDC bits, the steerability, B_s , is generally in the range between 0.001 to 0.1. An increased steerability could result from increased lateral drillability or reduced axial drillability. The gauge aggressiveness affects the lateral drillability. Increased aggressiveness is achieved when choosing lower back rake angles for the cutters on the gauge. Increasing the Depth of Cut (DOC) for the gauge cutters could also increase the lateral drillability. The problem with these measures is that they could potentially lead to increased vibrations and drilling issues. The bit profile and gauge, both the passive and active viewed in Figure 6.38 are essential for the steering properties of the bit [60].

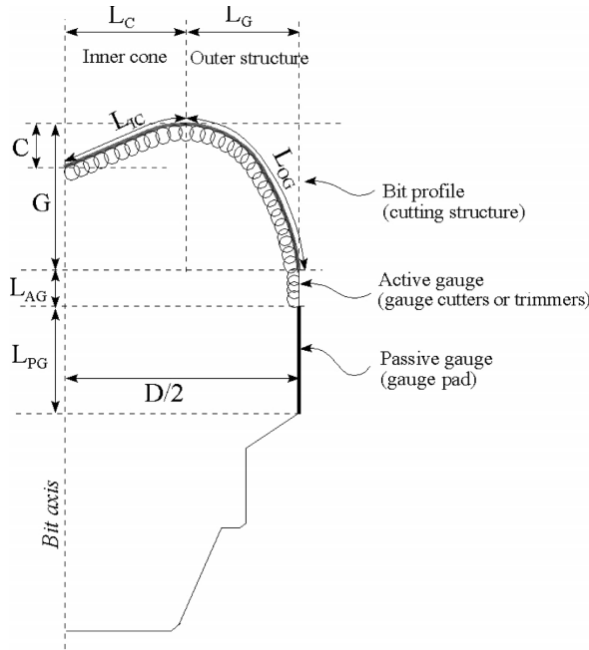


Figure 6.38: Overview of bit and where bit profile, active and passive gauge are placed [60].

A limitation on bit steerability is that the bit should be effective at drilling laterally, but it must also be stable because unstable bits experience more vibrations. Bit stick-slip and whirl will be typical

issues related to the bit. Less aggressive bit by decreasing DOC and reduced WOB and increased RPM will help with respect to stick-slip. To avoid whirl, it is important to minimize imbalance in force. Often it is a trade-off between steerability and stability. For example, reducing the length of the gauge to improve steerability reduces stability. For this very reason, two drill bits with different gauge lengths have designed.

Force-balanced Design

A relatively new concept called force-balanced design advance the cutters outwards to minimize the imbalance forces. The goal of this design concept is to minimize the forces that often offset the bit [67]. This design has been applied for earlier bit designs at NTNU and proved to be a success. Instead of advancing the cutters with gradually increased distance from bit center as seen to the left in Figure 6.39, they advance with the system as seen to the right. The strategy is to distribute the amount of rock removed per cutter more evenly. The first cutter will remove significantly less rock volume in the inner ring than the second cutter when applying the traditional design. Cutter one and two will remove approximately the same amount of rock by changing the position of the cutter angularly as in the illustration to the right in Figure 6.39. Applying this principle for all the cutters working at the formation will make the cutters cut more even and promote better performance.

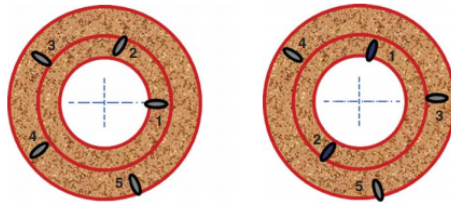


Figure 6.39: Traditional cutter layout to the left and new layout to the right [67].

6.11 3D Bit Modeling

In collaboration with Lyng Drilling, two different drill bits were designed and produced. When the designs made by the NTNU team was approved, the bits were 3D-printed before Lyng Drilling inserted the cutters, inserts and created the threads. The bits were different in terms of the number of cutters, cone angles, and blade layout. There is no apparent bit design which seemed superior with respect to the rigs drilling operation, and therefore two different designs were made.

This section presents the process of modeling the drill bits in SolidWorks. The designs are based on the theory and design considerations presented earlier. The modeling process started with a

2D sketch that was the foundation for the 3D model. Because the modeling processes of the bits are somewhat similar, only one of the designs are explained.

6.11.1 2D Sketch

The 2D sketch was the foundation for the final bit design. It defined the bit and blade geometry. From Figure 6.40 it is evident that the bit diameter is determined by defining the distance from bit center to the gauge pad. Bit profile, cone angle, and cutter distribution are also in the sketch. For this design, a short gauge pad with a short parabolic profile was chosen, and the cone angle was shallow. The primary focus was to increase the steerability of the bit.

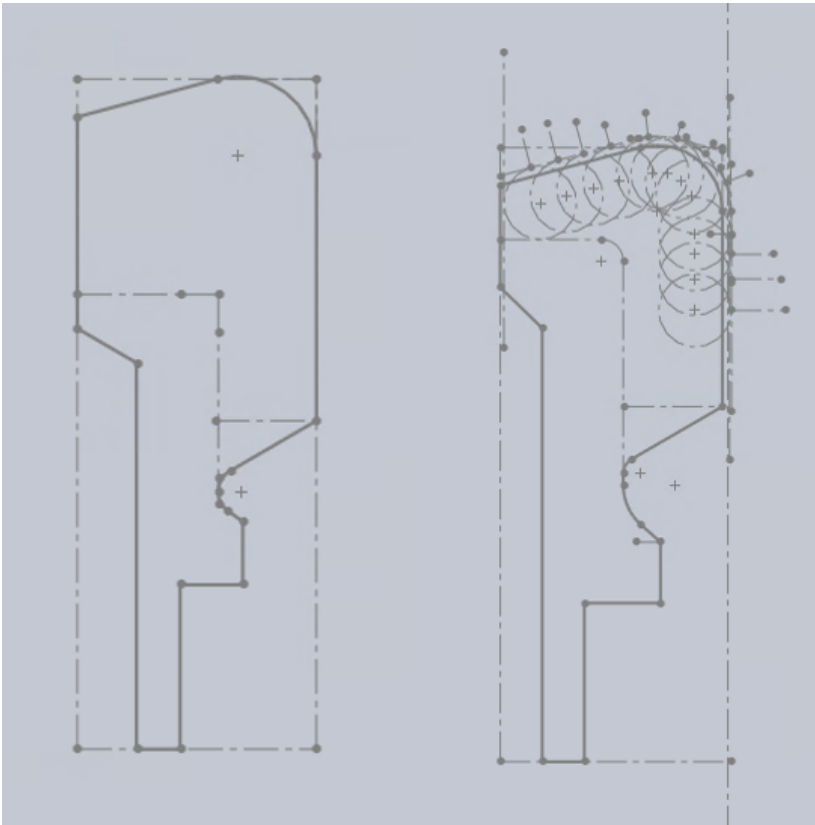


Figure 6.40: 2D base sketch with cutters profile.

When the drill bit diameter increased from 1.25 inches to 1.5 inches, the number of cutters was increased from 12 to 16 for this design. The DOC was limited to 0.75 mm for the bit face and 0.1 mm for the gauge cutters. A short DOC, in combination with a single set layout, is advantageous because it lessens the risk for cutter failure and decreases vibrations. Increasing the number of

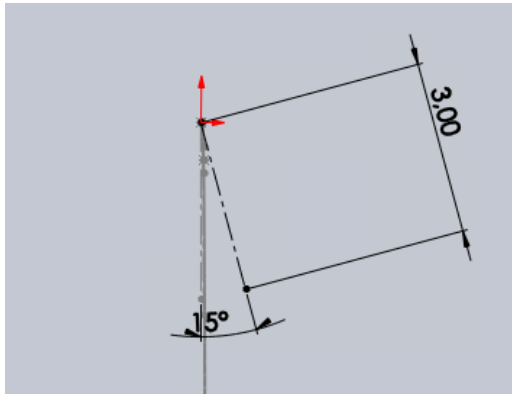


Figure 6.42: Cutter back rake angle seen from side view.

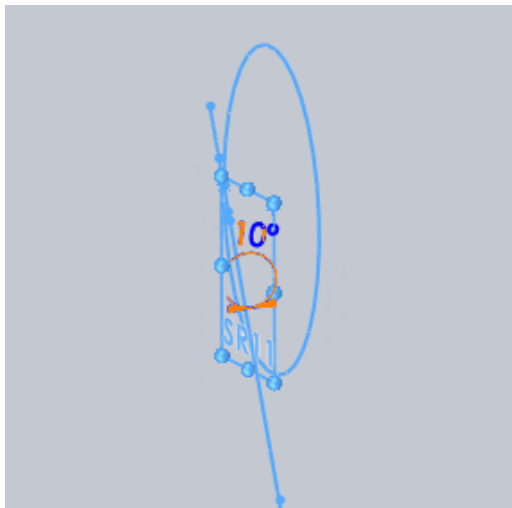


Figure 6.43: Cutter side angle seen from top view.

6.11.2 2D sketch to 3D model

After the 2D sketch was complete, the 3D model was the next step. The first step was to use the 2D sketch and use the revolved boss/base application in SolidWorks. Figure 6.44 shows how 2D sketches have been used to make the 3D model bit body. Next, the bit blades were put in place. The bit blades have an asymmetrical layout to avoid amplified vibration.

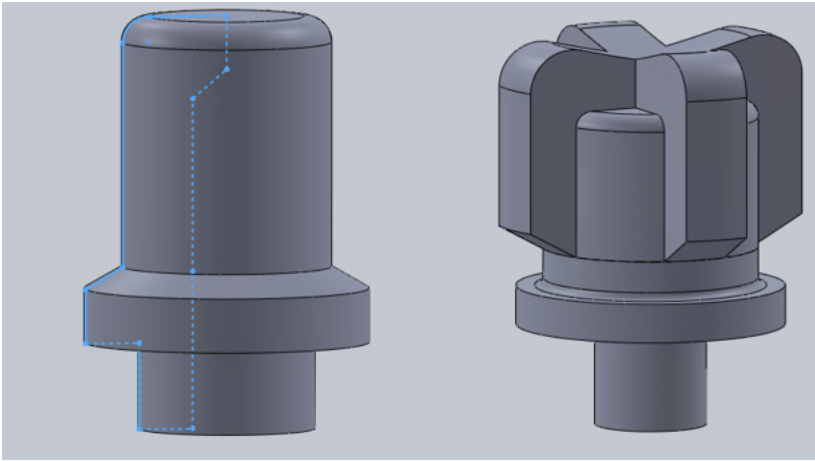


Figure 6.44: From 2D sketch to bit body and then with blades.

The next step was to create cutter sockets. They were made by cylinders simulating PDC cutters. Firstly, cylinders with orientation from the back and side rake angle from the 2D sketch were created. The dimensions of the cylinders were the same as for the cutters. They are illustrated in Figure 6.45. The same principle was used for the Thermally Stable Polycrystalline Diamond (TSP) inserts. Eight TSP inserts, with two for each gauge, was implemented to generate low friction surfaces and increase lateral stability. Nozzles were made by extruding a nozzle and using a linear pattern to make four similar nozzles across the bit face, as illustrated in Figure 6.46.

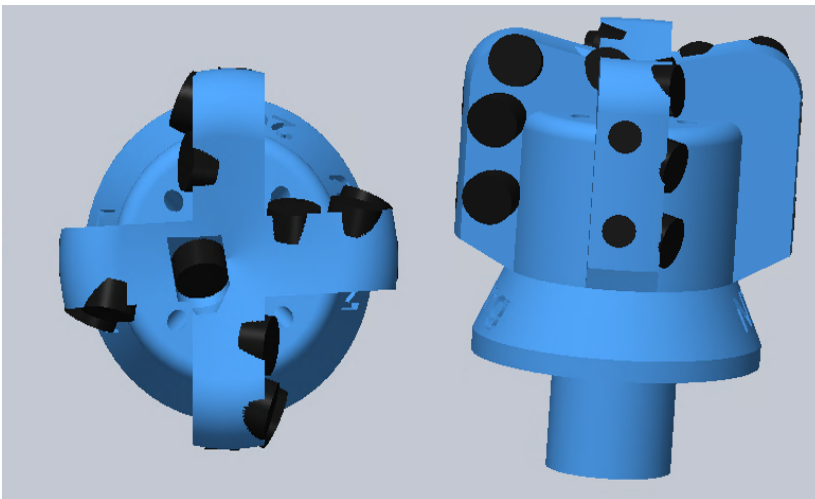


Figure 6.45: Top to the left and side view to the right of the bit with cylinders.

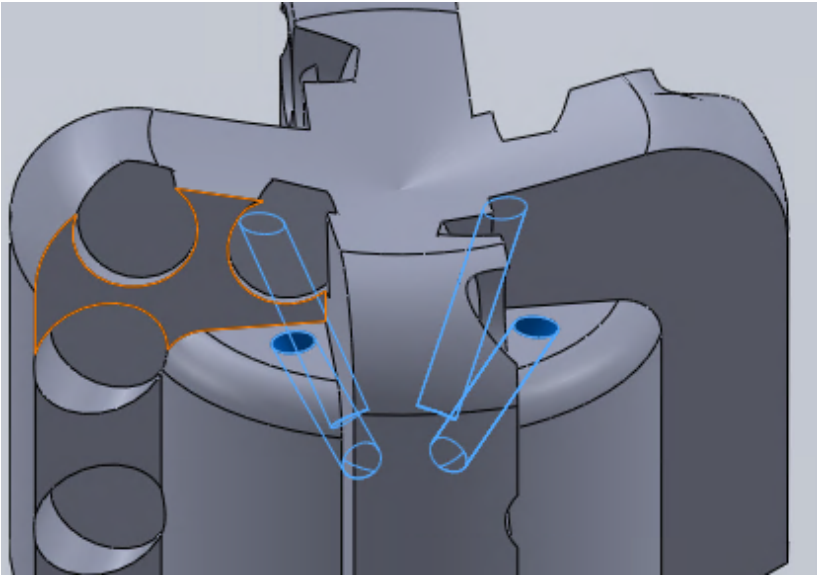


Figure 6.46: Four nozzles extruded from bit face.

After removing the cylinders, the bit was ready for 3D printing as illustrated in Figure 6.48. The last step was to place the cutters and inserts on the bit body, which Lyng Drilling did.

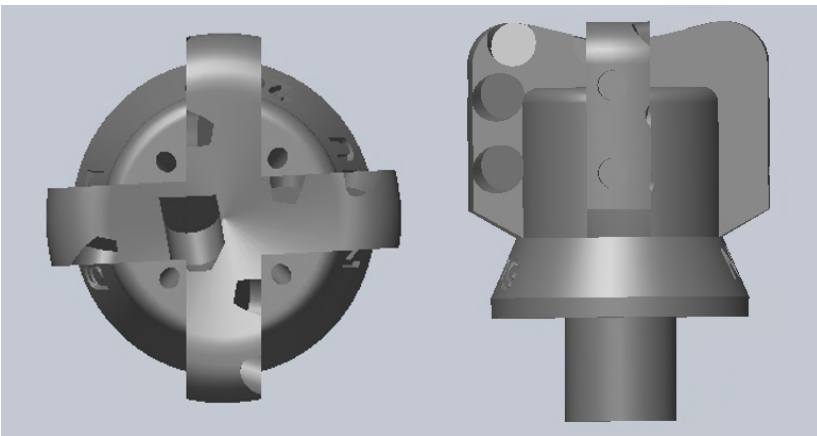


Figure 6.47: Final bit ready for 3D printing.

6.11.3 Design Alternative

Four significant changes were made to the second drill bit design. The gauge pad length was increased to test if this improves bit stability, and the design only used 12 cutters with only

one cutter located at the gauge. This will further limit the side aggressiveness and limit lateral vibrations. A medium cone angle was used to achieve better stability. The blades were also formed spiraling, which will reduce gauge stresses, minimize vibrations, and promote bit stability. Compared with the first design, this was a more time-consuming design and with a more complex manufacturing process. Therefore, the design was applied for only one of the bit designs to test its impact on lateral vibrations and stability.

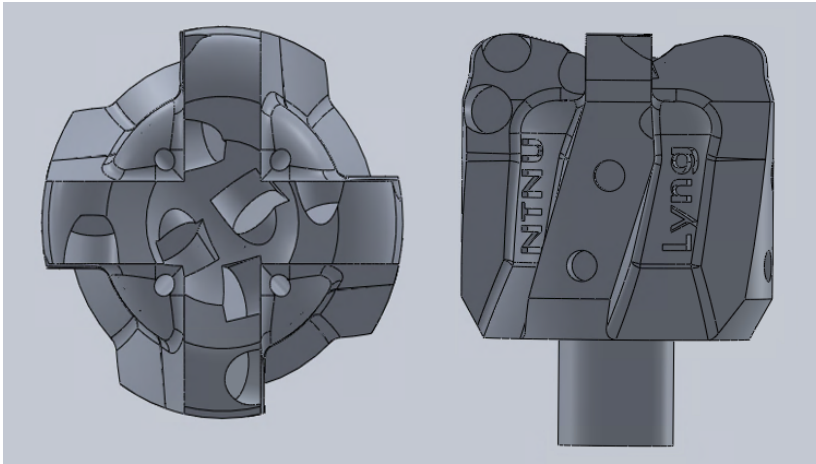


Figure 6.48: Alternative design seen from the top to the left and from the side to the right in the figure.

6.11.4 Drill Bit Overview

In total, there are 15 drill bits available for use in this thesis project and competition. DSATS provide two bits, five bits of "type 1" and three of "type 2" are from Alibaba, and lastly, the two self-designed drill bits produced by Lyng Drilling. In addition, three pilot hole drill bits were purchased from Alibaba. All bits have an OD of 1.5 inch except for the pilot hole bit, which has an OD of 2 inches. The bit provided by DSATS is a generic directional PDC micro-bit from Baker Hughes. The main difference between the Alibaba bits is that "type 1" has one pdc cutter on each blade, and "type 2" has 1.5 PDC cutters on each blade. Appendix O provides additional details of the Lyng-NTNU bits. The drill bit specifications are found in Table 6.1 and the different types are depicted in Figure 6.49.

Table 6.1: Specifications for different bits.

heightBit type	DSATS bit	NTNU bit 1	NTNU bit 2	Alibaba bit 1	Alibaba bit 2	Pilothole bit
Bit diameter	1.5"	1.5"	1.5"	1.5"	1.5"	2"
Length	1.34"	1.8"	1.8"	2"	1.93"	2.1"
Blade number	4	4	4	2	2	2
Cutter number	4	16	12	2	1.5x2	4
Cutter diameter	0.323"	0.236"	0.236"	0.532"	0.532"	0.532"
TSP inserts	0	8	8	0	0	0
TS inserts	5	0	0	0	0	0
Nozzles	4	4	4	3	1	1



Figure 6.49: From left to right: Alibaba pilothole bit, NTNU bit 1, NTNU bit 2, Alibaba bit 1, Alibaba bit 2 and DSATS bit.

6.12 Electrical System

6.12.1 Downhole Sensor

Implementing a method for downhole measurements in a closed-loop control has been a requirement since the Drillbotics competition in 2019. Sufficient downhole measurements are more important than before because accurate downhole readings are necessary to build the desired well path. Therefore, this design uses a downhole sensor card with gyroscope, triaxial accelerometer, magnetometer, and pressure and temperature sensors. Readings from the accelerometer combined with the magnetometer provide inclination and azimuth measurements for the position of the BHA. A larger and more complex sensor card replaced the one previously used. The new BHA design has an increased sensor housing to contain and seal the sensor card. Figure 6.34(a) illustrates the new solution. This years sensor card is a card of type Arduino Nano 33 BLE Sense, illustrated in Figure 6.50.



Figure 6.50: Arduino Nano 33 BLE Sense [77].

Table 6.2: Arduino Nano 33 BLE Sense sensors.

Name	Type	Sample Rate [Max]	Unit	Range
LSM9DS1	Accelerometer	119Hz[76]	g	$\pm 2 / \pm 4 / \pm 8 / \pm 16$
LSM9DS1	Magnetometer	119Hz[76]	gauss	$\pm 4 / \pm 8 / \pm 12 / \pm 16$
LSM9DS1	Gyroscope	119Hz[76]	dps	$\pm 245 / \pm 500 / \pm 2000$
MP34DT05	Microphone	62.5kHz[2]	-	0/1
APDS9960	Gesture, light, proximity	-	-	-
LPS22HB	Barometric pressure	75Hz[75]	hPa	260-1260
HTS221	Temperature	12.5Hz[74]	$^{\circ}\text{C}$	-40-120
HTS221	Humidity	12.5Hz[74]	rH	0-100

6.12.2 DAQ

All the topside sensors are communicated via the USB-6212 made by National Instruments shown in Figure 6.51. This DAQ samples the signal from connected components at a constant rate such that the computer is able to read them. It has a maximum resolution of 16-bit with a maximum sampling rate of 400 kS/s [48].



Figure 6.51: USB-6212 by National Instruments used for topside sensors [48].

(This page is intentionally left blank)

Risk Analysis and Risk Mitigation for Rig Components

This chapter examines the risks related to the thesis project and Drillbotics competition. Equation 7.1 defines risk as a function of probability and consequence. In this project, a suitable definition for risk can be; plans failing or other negative events affecting the project. For example, the probability related to drillpipe failure can be high because of prolonged wear. The consequence, however, is not too severe because there are several drillpipes to spare. Summarized, could one say that drillpipe failure imposes an overall low risk.

$$Risk = Probability \cdot Consequence \tag{7.1}$$

Table 7.1 presents a risk matrix with the probability of the components failing and the consequences involved. Afterward, risk mitigation has been implemented. Table 7.2 presents the risk matrix with the probability of the different components failing and the severity of the failure of a component after different measures have been taken. Risk mitigation could be; acquiring backup parts, having a redundancy plan available for changing the original design. The trend shifts from red and yellow part towards the green part of the table after the measures have been implemented. Table 7.2 is the summarized result of the final risk analysis for rig components. This analysis is essential to identify which components represent the highest risk of slowing down the project. Further explanation for each component will be provided in the following sections. If a component has been risk mitigated, this will be explained.

Table 7.1: Risk matrix for rig components before risk mitigation.

Probability	Consequences 1(low)	2	3	4	5(severe)
1(low)		Drill chuck and connection		Drillfloor stabilizer Drillpipe connections Drillpipe	Top drive and hoisting motor
2			Bent sub Lower stabilizer, packer and bit sub	Hydraulic swivel Drill bit	T-shaft Computers Upper stabilizer and sensor housing Sensor card
3				USB-cable and connections Azimuth torque sensor Rod	Azimuth motor and gearboxes
4					Rod connection
5(certain)					

Table 7.2: Risk matrix for rig components after risk mitigation.

Probability	Consequences 1(low)	2	3	4	5(severe)
1(low)		Drill chuck and connection Drillpipe connections Drillpipe		Drillfloor stabilizer	Top drive and hoisting motor Upper stabilizer and sensor housing
2		Drill bit	Sensor card Bent sub Lower stabilizer, packer and bit sub	Hydraulic swivel USB-cable and connections	Azimuth motor and gearboxes T-shaft Computers
3	Rod		Azimuth torque sensor		
4		Rod connection			
5(certain)					

7.1 Top Drive Motor and Hoisting Motor

The old top drive motor has been replaced by a motor similar to the hoisting motor. If one of the motors should fail, it isn't easy to get a new one because of the long delivery time and high cost. Hence would the consequence of one of the motors failing be severe. In such a case, the old top drive motor must be mounted back on the rig, which involves extensive modifications to the drilling system. There is no available backup for the hoisting motor, but because the motor has worked well for many years, the probability of it failing or not delivering the needed power output is low. In total, the top drive motor for the rod and hoisting motor are graded as a medium risk.

7.2 Drill Chuck and Drill Chuck Connection

The drill chuck and its connection to the top drive motor are a part of the new design for the rig. The drill chuck was ordered from a recognized company with a short delivery time. It is mechanically solid and represents a low risk of failure. The connection between the top drive motor and the chuck was made at the workshop at NTNU. These components have a low probability of failure but are both easy to replace should they fail.

7.3 Rotating Rod

The rod will be the primary transmitter of RPM from the top drive motor to the bit. The WOB force is projected onto the formation rock by the drillpipe, so this will further reduce the probability of fatigue failure due to less force present. Because the rig drills with relatively low WOB, in the range of 0-30kg-f, the probability of a rod buckling is determined to be small. The most present risk related to the rod is bending and twist-off. To reduce the probability of rod twisting off, it should experience as little friction as possible inside the T-shaft, swivel, and drillpipe. The most efficient risk mitigation measure was to grease the rod before it is slid into the swivel and T-shaft and connected in the drill chuck. Many rods were acquired in different materials as a backup. Because the rods were easily accessible, the component is graded as low risk.

7.4 Azimuth Motor and Gearboxes

The azimuth motor controlling the rotation of the drillpipe and BHA is new to the rig design. The azimuth system has been tested and proved to function. The azimuth components are sensitive to dust and water and should therefore be located as far from the hydraulic swivel as possible to reduce the risk of motor failure. To avoid dust and particles entering the components, they are frequently inspected and wiped. Water is an issue if there is leakage in the hydraulic system. During drilling operations, there will be a frequent inspection for any sign of leakage to mitigate the risk of motor failure. The azimuth system is expensive and has a long delivery time. If this system fails, the rig can only drill with constant azimuth and cannot hit targets requiring a varying azimuth. So the components are essential for achieving a satisfying result. In total, the azimuth components are graded as a high risk.

7.5 Azimuth Torque Sensor

Without the torque sensor, the torque experienced when changing azimuth will be unknown. This uncertainty could potentially lead to applying more rotation than what the system can handle, which could generate mechanical failures or other problems for the drilling system. The team members expected the torque sensor to be a robust component, but it failed once. The reason is not

apparent but could have happened either during drilling operation or when dismantling the system. As a consequence, two new torque sensors were acquired to have one in backup. If it should fail, drilling would still be possible, but there would be a limitation on the permissible amount of azimuth rotation because the actual amount of torque generated in the system is unknown. The azimuth torque sensor represents a medium risk for the project.

7.6 T-shaft

The T-shaft is a custom-made component that is complicated for the workshop engineers to manufacture. If the T-shaft fails when the engineers are busy with other projects, this could lead to a prolonged production time. In case of a failure, there is no backup alternative to vary the azimuth when drilling. The rod rotating inside the T-shaft at 900 RPM could potentially wear the inside of the shaft, thus losing its sealing effect. However, greasing the rod will reduce the risk of wear and can have a sealing effect. A medium probability of failure but severe consequences results in the T-shaft being graded as a high risk component.

7.7 Hydraulic Swivel

The hydraulic swivel was produced at the university workshop by the first competing team from NTNU and is recycled each year. Only the hollow shaft inside the swivel is new. Similar to the T-shaft, the hollow shaft is a complex part to manufacture. Problems with the swivel could be water leakage and misalignment of the shaft. The misalignment could lead to additional friction when varying the azimuth. Without a functioning swivel, the drilling would take place without a transporting drilling fluid. This would be an extensive disadvantage concerning wear, hole cleaning, and the drill bit's cooling and lubrication. Therefore it is graded as a medium risk.

7.8 Drillpipe Connections

The drillpipe connections in the swivel and BHA have been sufficient for several years, but because this rig operates at a higher RPM and torque, extra connections were ordered to have in spare. However, the drillpipe connections are defined as a low-risk component.

7.9 Drillpipe

The drillpipe should be the primary transmitter of WOB. However, it shall not experience high RPM values. Low RPM values minimize the risk for fatigue failure. Because the drillpipe is subjected to buckling and fatigue failure, many drillpipes were ordered for easy replacement in such scenarios. In total, the drillpipe is considered a component with low risk.

7.10 Drillfloor Stabilizer

The drill floor stabilizer promotes much better stability in the drilling system, especially when drilling the first few inches in the rock. The roller bearing stabilizes the drillpipe in the lateral direction and functions well, although it has been used for three years. Drilling without the drill floor stabilizer introduces increased drillstring vibrations that could damage other rig components and reduce drilling performance. Therefore, the project risk related to the drill floor stabilizer is considered medium level.

7.11 USB-cable and Connections

The USB cable and its connections are crucial for communication between the downhole sensor card and the control system. Should any problems cut communication with the topside system, the rig must drill without downhole measurements. This issue has been a problem in the earlier years, and several risk-mitigating measures have been implemented.

This year's new design introduces a new path for the USB cable connecting the sensor card to the topside. The cable is secured with tape on the outside of the drillpipe because of limited space inside the pipe due to the rod. A risk involved with the USB cable is the rotation of the BHA and drillpipe. The cable has some slack which allows for some winding around the drillpipe. This winding will be solved by rotating the azimuth system clockwise and then anti-clockwise repeatedly. Vibrations and water leakage via the cable and down to the connections at the sensor card, should be minimized. If the connection is broken, the repair is time-consuming and should be avoided at every cost. Many USB cables have been bought to have in reserve, but the primary issue will be the connections between the cable and sensor card. It has a low probability of failing and the consequences would be severe meaning these components are graded as a medium risk.

7.12 Upper Stabilizer and Sensor Housing

The upper stabilizer and the sensor housing are made of solid metal, but the sensor housing has a pocket for the sensor card in its wall. Hence will the strength be reduced to some degree. This is one reason why an upper stabilizer has been designed on top of the sensor housing. The USB cable will fit through a hole of 3-4 mm drilled through the upper stabilizer. This ensures that the connection in the upper stabilizer between the drillpipe and BHA is more solid due to a thicker wall than the sensor housing, which houses the sensor card. The sensor housing is more complicated to produce in the workshop than a regular straight housing. This is because of the pocket for the sensor card. This is milled out from both sides and needs high precision since the margin wall between the pocket and the inside and outside of the housing is quite

small. It is also a challenge to line the hole for the USB cable to the same position for both the upper stabilizer and the sensor housing. This system is crucial for having a downhole sensor, and therefore the consequences are severe if it does not work. The workshop has experience producing these components, and a close follow-up with them before making the parts were risk-mitigating measures. The probability of the workshop failing in production is low, but if they cant make it, the consequences will be no downhole communication which is severe. Therefore the project risk is rated to medium for these components.

7.13 Sensor Card

The sensor card is crucial for estimating the position of our system. Without a functioning sensor card, there is no downhole sensor, and the rig would automatically fail in the competition. Possible problems with the sensor card could be water damage, vibrations, and loose connections. Different designs have thus been discussed to protect the sensor card from water. Also, different methods to seal the sensor card have been discussed. A suitable design has been tested and worked well. Different epoxy types to cover the sensor card and possible waterways have been examined, and a suitable material has been chosen. When it comes to loose connections and vibrations, connections must be made correctly. To place the sensor card in its sensor pocket is a careful process that requires accuracy and concentration. In earlier years, sensor cards have been made in-house. This is a time-consuming process and limits the number of cards available. The limitations on the number of cards make the consequence of a failing sensor card quite severe since there are not many backup cards. To mitigate this risk, a sensor card that is an off-the-shelf component has been implemented. This card has all the required properties, fits in our sensor housing, and is cheap. In total, the risk is rated as medium. The sensor card represents a medium risk for the project.

7.14 Bent Sub

The bent sub is a solid metal piece that should withstand impacts in the well during drilling, and the probability that the bent sub fails is low. The complexity and time involved in producing the bent sub is the main challenge. A situation that could require a new bent sub is if the theoretically expected deviation from calculations does not match the deviation the drilling system gives us. Ideally, the bent sub should be used many times for testing and understanding what deviation it produces for different drilling parameters. This is not easy if a new bent sub must be made. The bent sub, therefore, represents a medium risk.

7.15 Rod Connection in BHA

Connecting the rod to the drive shaft is essential for rotating the bit. The system should transmit the rod rotation to the drill bit and must therefore not slip or break. The main threat to the connection is wear and tear. During many runs, the set-screws and sleeve will experience wear and tear, and therefore, several set-screws are stored in backup. The workshop produces the drive shaft with the universal joint, which requires at least two days. Problems with the drive shaft is expected, and if it fails, the consequence is a non-functional drilling rig. Due to this, a backup drive shaft is produced. Since a backup is produced, the consequences go from severe to medium, and with a medium probability of failure, this component is graded as a medium project risk.

7.16 Lower stabilizer, Packer and Bit Sub

The drive shaft is threaded in the bit sub and goes through the lower stabilizer and packer. The workshop produces all three parts. The lower stabilizer and bit sub are robust parts where there is a low probability of failure. For the packer, the main issue will be wear and tear because it allows for concentric rotation. Producing a new packer part is challenging for the workshop and should be avoided. The bit sub will rotate against steel from the lower stabilizer without the packer, which does not work very well. The lower stabilizer, packer, and bit sub are graded as a medium risk.

7.17 Drill Bit

The main risks with the bit are wear and tear from the drilling operations. Because the rock to be drilled has a relatively low compressive strength, these risks are low. To further avoid damage and extra torque, the NTNU bits are designed less aggressive than regular bits. After some time, wear could become a problem. Therefore there is a wide range of different bits available to the team. The probability of failure is reduced by varying the bits used. The consequences are not so severe because there are many drill bits in backup. Therefore, drill bit is graded as a low risk to the project.

7.18 Computers

Two different computers operate the drilling rig. One operates the GUI, and the other receives sensor card data. At the rig location, the computers are subjected to dust, dirt, and water. Any shortages or damage related to this can halt all operations, and backup files are frequently stored separately from the rig location. Acrylic glass separates the drilling operation in the derrick from the computer system to reduce the risk of water damage. The computers have been used a long time and should work properly in at rig location, and the probability of failure is low. Project risk

related to the computers is nevertheless rated as a high risk.

Power Consumption

The motors and components on the drilling rig contribute to the total power consumption of the rig. Power consumption was in this project limited to a total of 25 hp, which is equivalent to 18.64 kW. The main components contributing to this power consumption are the top drive motor, hoisting motor, azimuth motor, and computer. The power limit is relatively high for this project, meaning that it was not a limiting factor for building and operating the drilling rig. However, to ensure an energy-efficient drilling operation, the expected electrical consumption is estimated in this chapter.

8.1 Top Drive Motor

The top drive motor applies rotation and torque to the drill bit through the rod. The power consumption is thus due to these two parameters, and can be found by the following equations:

$$P = \frac{T\omega}{\eta} \tag{8.1}$$

$$\omega = \frac{2\pi N}{60} \tag{8.2}$$

where T [Nm] is the torque provided by the motor, ω is the angular velocity, N is the RPM, and η is the motor efficiency.

The top drive motor is rated with a maximum output of 3 400 RPM and 45 Nm, and a motor

efficiency of 96% [54]. Given that the top drive system operates at its limits, the power consumption is calculated with Equation 8.1 and 8.2 and concluded to be 16.70 kW. However, the helical gearbox limits the operational window to 1 300 RPM and 5 Nm. With these limits, the expected power consumption of the system is estimated to be 0.71 kW. This estimate is reasonable compared to the rated power of the gearbox motor of 0.75 kW. Due to mechanical limits, the motor is operated at around 900 RPM giving a power consumption of **0.49 kW**.

8.2 Hoisting Motor

The rotational force applied by the hoisting motor is transmitted into vertical force by the ball screw. The torque provided by the hoisting motor can be estimated with Equation 8.3.

$$T = \frac{F \cdot l}{2\pi\epsilon} \tag{8.3}$$

where $T[Nm]$ is the torque, $F[N]$ is the force from the weight of the system, l is the lead of the ball screw, and ϵ is the motor efficiency. The torque provided by the hoisting motor is calculated in Equation 8.4, with a rotary system weight of 490 N, lead of the ball screw equal to 5 mm, and a motor efficiency of 90%.

$$T = \frac{F \cdot l}{2\pi\epsilon} = \frac{490 \cdot 0.0050}{2\pi \cdot 0.90} = 0.43Nm \tag{8.4}$$

Equation 8.1 and 8.2 can then be used to calculate the power consumption at different RPMs, given that the motor torque provided is equal to 0.43 Nm. These result are given in Table 8.1

Table 8.1: Estimates of the hoisting motors power consumption at different RPM values.

Rotary Speed N [RPM]	Power Consumption P [W]
100	5
300	15
600	30
1200	60
2000	101
3000	151

The worst-case scenario is assumed to be when the motor is performing at its maximum, which results in power consumption of 151 W. The control system limits the ROP to 50 cm/min which is achieved with a motor 894 RPM. This is equal to a power consumption of **45 W**.

8.3 Azimuth System

The azimuth power system consists of a hollow shaft gearbox, two right-angled gearboxes and a motor. The hollow shaft gearbox is listed with a permissible torque of 30 Nm and a permissible table surface speed of 90 RPM. Assuming operation at its maximum and an efficiency of 90% the power consumption is equal to 314 W. However, the azimuth is expected to turn at a rate of no more than 40 deg/min equal to 1/9 RPM. This has proven to demand torque values around 10 Nm, and the expected power consumption is equal to **0.13 W**.

The azimuth servo motor is listed with a rated speed of 3000 RPM and a peak torque of 0.93 Nm. If the motor is operating under these conditions it has a power consumption of 324 W according to Equation 8.1 and 8.2. The azimuth system is operated in deg/min where the expected rotational velocity will be no more than 40 deg/min. This is equal to 1/9 RPM, and with a gear ratio of 1:270 the motor will have to operate at 30 RPM to achieve this. It is reasonable to assume that the torque experienced by the motor will be significantly less than the peak torque. Under the assumption of a torque value of 0.15 Nm, the motor will consume **0.52 W**.

8.4 Torque Sensor

The torque sensor is used to measure torque on the drill pipe when rotating relative to magnetic north. The chosen torque sensor is listed with a capacity of 5-50 Nm. It measures torque related to rotation provided by the azimuth motor, which is operated in deg/min. The upper limit for rotation is 360 deg/min equal to 1 RPM. The maximum power consumption of the torque sensor is estimated with Equation 8.1 and 8.2 to be 5.80 W, assuming an efficiency of 90%. However, the sensor is expected to operate at significantly lower torque of around 5-10 Nm. The competition requirement of 15 degrees azimuth change demands no more than a maximum of 40 deg/min of the system. This is equal to 1/9 RPM and gives an expected power consumption of **0.13 W**.

8.5 Computer

Two computers control the system of the miniature autonomous drilling rig. Both of them are miniature custom-built computers with similar specifications. The previously used computer was a OptiPlex 7440 AIO from Dell. Given that the miniature computers have specifications close to this computer and that they come from Dell, it is reasonable to assume that they will have the same power consumption. The OptiPlex 7440 AIO is listed with a maximum power consumption of 200 W [24]. Given that this is an All-in-One computer, it is fair to assume that the screen alone consumes 100 W worth of power. Under this assumption, the miniature computers consume 100 W each. Both of the computers have a screen connected to them. The main screen is a Dell

U3415W listed with a maximum power consumption of 130 W [22]. The secondary screen is a Dell U2711B listed with a typical power consumption of 113W [23]. Altogether, the computer setup has a power consumption of **443 W**.

8.6 Total Power Consumption

As mentioned, the total power consumption is limited to 18.34 kW. The expected power consumption from Table 8.2 is well below this limit.

Table 8.2: Overview of the expected and maximum power consumption for each component on the rig.

Rig Component	Expected Power Consumption [W]	Maximum Power Consumption [W]
Top Drive motor	491	709
Hoisting motor	45	151
Azimuth system	0.52	324
Torque Sensor	0.13	5.80
Computer	443	643
Total	2 729.65	3 582.8
Limit	18 340	18 340

Control System Design

Magnus Steinstø from the Department of Engineering Cybernetics (ITK) was responsible for the control system design in this thesis project. He performed thorough work with the Proportional Integral Derivative (PID) controllers, filtering, downhole sensor. He also constructed the control system with all its components. This chapter gives a brief description of his work related to the control system of the rig. A more detailed description of the theory and testing concerning the control system design can be found in his master thesis "Implementation of a Miniature Autonomous Directional Drilling Rig With NMPC Positional Control"(2021)[73].

9.1 Background Theory

This section presents the background theory relevant for understanding the basic principles of the presented control system.

9.1.1 PID Controller

Proportional Integral Derivative (PID) controllers are commonly used on control level within automation to regulate a parameter towards a set point. It is a closed-loop controller that uses a feedback mechanism to control process variables [64]. A PID controller consist of a proportional, integral, and derivative term which adjusts a control variable as shown in Equation 9.1:

$$u(t) = K_p e(t) + K_i \int_0^t e(\tau) d\tau + K_d \frac{de(t)}{dt} \tag{9.1}$$

The integral and derivative terms are often expressed by integral and derivative time, and Equation 9.1 can be rewritten as [15]:

$$u(t) = K \left(e(t) + \frac{1}{T_i} \int_0^t e(\tau) d\tau + T_d \frac{de(t)}{dt} \right) \quad (9.2)$$

Where $e(t) = r(t) - y(t)$ is the difference between the reference r and the output y . K_p , K_i and K_d are gains that can be tuned individually to obtain the desired control behavior. These three gains are tuned based on how the three terms work [64]:

1. **Proportional term** corrects a target proportional to the difference. From this mechanism, the desirable value will not be achieved because the correction will approach zero if the difference approaches zero.
2. **Integral term** attempts to correct this by accumulating error from the first step to increase the correction factor. This step attempts to drive cumulative error to zero, thus resulting in an overshoot.
3. **Derivative term** tries to minimize the overshoot from the integral term by slowing down the correction factor when the value approaches target value.

In other words, the proportional error is the difference between the process variable and the set point as shown in Figure 9.1.

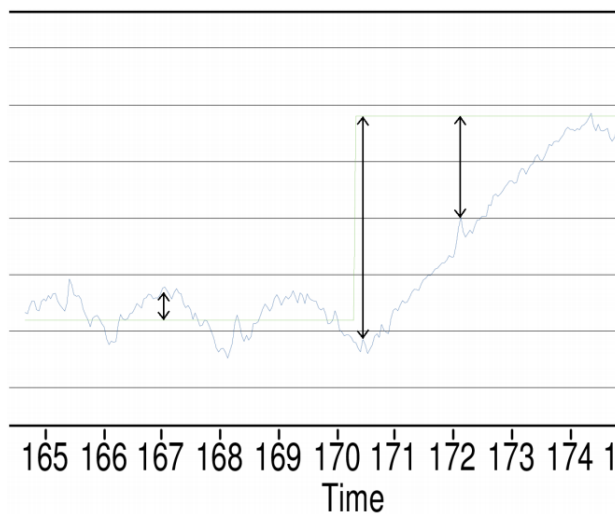


Figure 9.1: Illustration of the proportional error the process variable and the set point [42].

The integral error is the integral of the proportional error over time as shown in Figure 9.2.

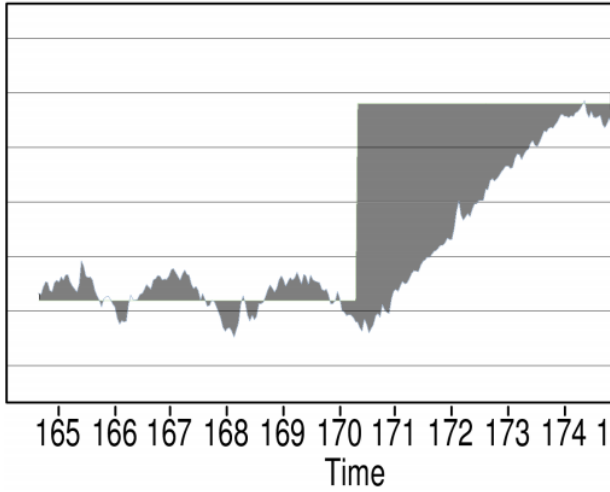


Figure 9.2: Illustration of the integral error [42].

The derivative error is the derivative of the integral error as shown in Figure 9.3.

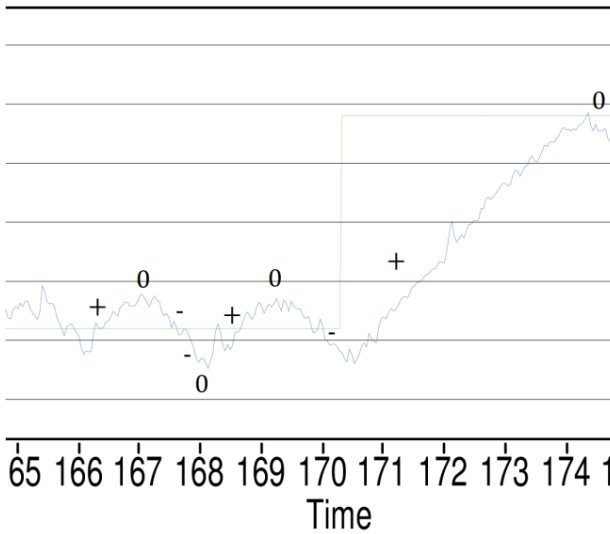


Figure 9.3: Illustration of the derivative error [42].

9.1.2 PID Tuning

The gains K_p , K_i and K_d in Equation 9.1 must be tuned before the PID controller can be implemented to control a system. The adjustments of these gains to get optimum performance from the controller is referred to as tuning. It is important to ensure a reliable, precise, and responsive PID controller.

The desired response from the controller varies with the system it is assigned to control Figure 9.4 illustrates different response types for a PID controller, where the critically damped response is often the desired one. Some desired traits are typical for a well-tuned PID controller. From one set point to another, it is desirable to have a slight overshoot. Overshoot is when the output shoots above the setpoint value and is desirable to keep small because it results in a slow controller resulting from slowly reaching the set point.

The controller should stabilize quickly at the desired set point with minimized oscillations. The time it takes for the controller to stabilize at the setpoint is referred to as settling time. The frequency of iterations must be modified to reduce wear on the actuators. There are several different ways of tuning a PID controller, some more advanced than others. For this project, a well-functioning PID controller can be achieved with the trial & error method once the purpose of each gain is known.

Tuning by trial & error typically begins by setting the integral and derivative gain equal to zero. The proportional term is then gradually increased until there is a minimum steady-state error, without excessive oscillations around the setpoint [53]. When the proportional gain gives this trend and a fast response is decided, the integral gain is increased to minimize the steady state. Lastly, the derivative gain is increased to reach the setpoint quickly and reduce the overshooting from the integral gain. Ideally, this will give a sufficient PID controller, but the integral and derivative term must be tuned depending on how the system reaches setpoint. The derivative gain must also be tuned with respect to system noise. This is because a sizeable derivative gain will result in the PID controller trying to correct for the system noise.

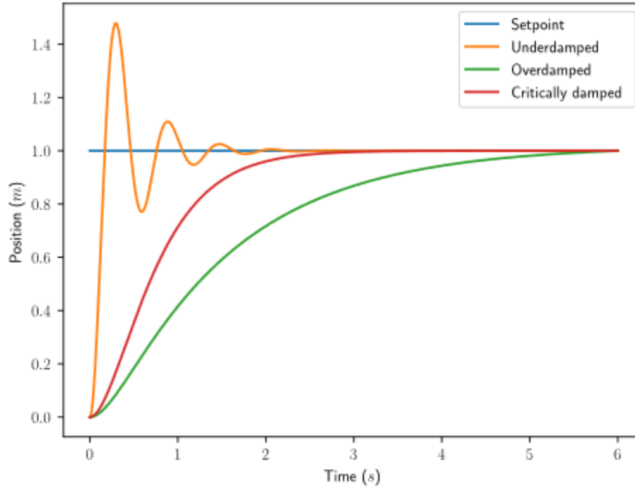


Figure 9.4: Response types for a PID controller system [78].

9.1.3 Kalman Filter

Kalman filters are described as state estimators for stochastic systems [58]. A Kalman filter is implemented to handle measurement uncertainty and process noise in a system. This filter type combines multiple sensor measurements with a model estimate where each measurement is weighted based on its co-variance [9]. Under the assumption of Gaussian noise distribution, the estimate with the smallest co-variance, and thus the optimal state estimate, can be found by a Kalman Filter.

The Kalman filter compares the estimate of the model to the output of the system on the basis of the linear state-space model:

$$\hat{x}_k = A\hat{x}_{k-1} + Bu_k + K_k(y_k - C(A\hat{x}_{k-1} + Bu_k)) \quad (9.3)$$

The filter prediction, \hat{x}_k^- , referred to as the prior estimate is the prediction of the next state estimate and often written as a separate equation:

$$\hat{x}_k^- = A\hat{x}_{k-1} + Bu_k \quad (9.4)$$

Based on the system matrix, process noise co-variance, Q , and the previous co-variance the co-variance of the state estimate is predicted using:

$$P_k^- = AP_{k-1}A^T + Q \quad (9.5)$$

The Kalman filter algorithm is updated each time-step, where the Kalman gain K_k , is calculated to minimize the variance of the optimal state estimate. The gain is inversely proportional to the noise co-variance R :

$$K_k = \frac{P_k^- C^T}{CP_k^- C^T + R} \quad (9.6)$$

The new estimated state is based on the new measurement and the prior estimate:

$$\hat{x}_k = \hat{x}_k^- + K_k(y_k - C\hat{x}_k^-) \quad (9.7)$$

An error co-variance matrix of the current best estimate can then be used to monitor expected deviation of the state estimate. The error co-variance matrix is calculated on the basis of the Kalman gain and the predicted co-variance:

$$P_k = (I - K_k C)P_k^- \quad (9.8)$$

9.1.4 Extended Kalman Filter

If a system is non-linear, it cannot be described directly by the equations in subsection 9.1.3 because it cannot be based on a linear state-space model. A non-linear system can be described by Equation 9.9 [59].

$$x_k = f(x_{k-1}, u_k) + w_k, \quad y_k = g(x_k) + v_k \quad (9.9)$$

For a Kalman function to converge, it requires a linear function. The Kalman filter also requires all noise to have a Gaussian distribution. If a Gaussian distribution is passed through a non-linear function, it normally does not provide a Gaussian distribution output. w_k and v_k in Equation 9.9, are noise values for the states and output at a specific time-step.

If a system is close to linear in a region near a point, some non-linear systems can be approximated by linearization near that point. When making prior predictions, the Kalman filter can use a linearized state-space model as described in Equation 9.10.

$$f(x) \approx f(\hat{x}) + f'(x)(x - \hat{x}) \quad (9.10)$$

When calculating the Jacobians of the state and output functions, the linear approximation can be implemented directly in the Kalman filter:

$$F = \frac{\partial f}{\partial x} \Big|_{\hat{x}_{k-1}, u_k}, \quad G = \frac{\partial g}{\partial x} \Big|_{\hat{x}_k} \quad (9.11)$$

If the states or outputs are linear, the state-space matrix can replace the Jacobian approximation. A Kalman model can be estimated using the Jacobians if both states and inputs are non-linear:

$$\Delta x_k \approx F \Delta x_{k-1} + w_k, \quad \Delta y_k \approx G \Delta x_k + v_k \quad (9.12)$$

9.1.5 Model Predictive Controller (MPC)

One advanced controller based on system model and optimization is the Model Predictive Controller (MPC). This type of controller uses the initial conditions to perform a complete optimization at every time step. The subsequent input is then applied to the plant, which is the system indicating the relation between input and output. Advantages with MPC are that it enables multi-variable control and strict enforcement of input constraints.

The MPC simulates a system model for a prediction horizon, at which states and outputs can be assigned weights. An optimization algorithm then finds a set of inputs to minimize the sum of the cost function of the duration of the prediction horizon. Weights are used to limit deviation and rate of change in state and output. This is commonly done with an optimization algorithm that penalizes the square of the deviation from the reference [73]:

$$\min_{x,u} J = \min_{x,u} \sum_{k=0}^{N-1} (x_k^T Q x_k + u_k^T R u_k) \quad (9.13)$$

Where Q and R are matrices with the weights for states and inputs, respectively. k is the current time-step and N is the length of the prediction horizon. Each input and state at every time step is a variable that is optimized for and checked towards any constraints.

Well Path Reference With Bezier Curve

An approach to have long-term planning and high-resolution, short-term control, is to create a reference well path for a short time-step controller. The reference well path can be generated before drilling or dynamically during the drilling operation.

Bezier curves are commonly used in the drilling industry when planning well trajectories. The mathematics behind it are relatively simple to implement in the control system and require a

low computational cost. Bezier curves are line segments with a curvature adjusted by one single parameter. Second-order Bezier curves used for well path planning are implemented using free endpoints. Third-order Bezier use set (or fixed) endpoints [51]. The goal is to generate a smooth well path that can intersect multiple target points within a set range for both azimuth and inclination.

Free-end Bezier curves do not have restrictions with regards to azimuth and inclination at their endpoints. The curves are used as the azimuth and inclination at the target points. An initial azimuth and inclination can be defined such that the initial orientation of one point will be the initial orientation of the succeeding point. The line segments each have a starting point, S , and an endpoint, E . A unit tangent vector t_s is drawn from the starting point [73]:

$$t_s = \begin{bmatrix} \cos \theta_s \\ \sin \theta_s \cdot \cos \phi_s \\ \sin \phi_s \end{bmatrix} \quad (9.14)$$

The starting point inclination and azimuth are denoted by θ_s and ϕ_s , respectively. A scalar, d_s adjusts the degree of curvature of the line segment. The scalar, which can be tuned, determines the position of the attractor point, C_s . The attractor point is an arbitrary control point used to construct the curvature. From the starting point to the attractor point, and from the attractor point to the endpoint, the line segment has been normalized to the range [0, 1]. These lengths are generally not the same, and this means that the range corresponds to a different movement. When moving along line segments with normalized step size, the tangent of the two connected points along the line will form a curve. Figure 9.5 illustrates the parameters and their context [73].

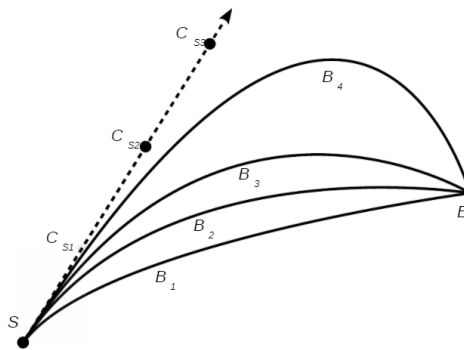


Figure 9.5: 2nd order bezier curves [51].

The attractor point is placed with respect to the tangent in Equation 9.15 , starting point and the scalar, d_s .

$$C_s = S + d_s \cdot t_s \quad (9.15)$$

A second-order Bezier curve can be described with Equation 9.16, where the movement along the normalized lines describes the position along the curve.

$$B(u) = (1 - u)^2 S + 2(1 - u)u \cdot C_s + u^2 E \quad (9.16)$$

Given a well path with multiple target points, it must be described by multiple free-end Bezier curves in succession at which the target points are the starting point for one segment and the endpoint for another. To achieve a continuous well path, the initial azimuth and inclination are set from the parameters at the endpoint of the previous line segment. Each line segment is given its unique tunable parameter d_s .

The inclination and azimuth are calculated from the unit tangent vector at a point along the Bezier curve described by Equation 9.16:

$$t = \frac{\dot{B}}{\sqrt{\dot{B} \cdot \dot{B}}} \quad (9.17)$$

Where \dot{B} is the derivative at a point of Equation 9.16:

$$\dot{B}(u) = -2(1 - u)S + 2(1 - 2u)C_s + 2uE \quad (9.18)$$

The inclination and azimuth in Equation 9.19a and 9.19b respectively is then found by trigonometric identities from the unit tangent vector in Equation 9.17.

$$\theta = \arccos t_z \quad (9.19a)$$

$$\phi = \text{atan2}(t_x, t_y) \quad (9.19b)$$

The desired well path can then be generated automatically with a cost function and an optimiza-

tion algorithm, described in the following section.

Cost Function

A cost function in combination with an optimization algorithm can be implemented to generate a suitable well path by penalizing unwanted characteristics of the well path. The optimal well path has a constant fixed Dogleg Severity (DLS) equal to the DLS characteristics of the Bottom Hole Assembly (BHA).

$$k = \frac{1}{\dot{B} \cdot \dot{B}} \ddot{B} - \frac{\dot{B} \cdot \ddot{B}}{(\dot{B} \cdot \dot{B})^2} \dot{B} \quad (9.20)$$

Where the double derivative, \ddot{B} , for free-end well paths is given by Equation 9.21:

$$\ddot{B}(u) = 2S - 4C_s + 2E \quad (9.21)$$

The DLS can be calculated at a given point using the magnitude of the well path curvature, k :

$$DLS = k \cdot \frac{180}{\pi} \quad (9.22)$$

In full-scale well path planning, the DLS is given by the degrees of curvature built over a distance of 100ft or 30m. For the miniature drilling rig, DLS have been defined as inclination built (in degrees) from 1 meter of drilling. The algorithm should penalize deviations between the estimated DLS and the target DLS. This deviation has been squared to prevent large deviations along the complete well path:

$$\min \sum_{n=1}^{m-1} ((q_1(DLS(n) - DLS_{target}))^2 + (q_2(DLS(n+1) - DLS(n)))^2) + (q_1(DLS(m) - DLS_{target}))^2 \quad (9.23)$$

A similar approach for penalizing change in azimuth and curvature was attempted. However, tuning the function for many potential paths proved difficult with more factors than the ones already present in Equation 9.23.

Optimization

The recommended MATLAB optimization function for smooth nonlinear functions is *fmincon* [46]. This optimization will be used by default with an interior-point solver by the nMPC. See the master thesis written by Magnus Steinstø for further detail [73].

9.1.6 Position Estimate

To intersect target points, a position controller must know the exact position and orientation of the BHA. However, precise measurements inside the rock sample have proven to be challenging. The BHA position has been estimated by using the orientation of the BHA and a model based on expected system behavior.

Model

A discrete time model is used because the sensor card samples data at discrete time intervals. The model is based on a continuous-time model to estimate inertial frame position. The main assumption is that the length between the center point of the BHA and bit center will have an angular velocity based on the orientation of the BHA bend and hoisting system velocity in True Vertical Depth (TVD). The BHA movements are relative to its frame and further translated into the inertial frame to, over time, lead to displacement inside the rock sample and change of orientation relative to the inertial frame.

Movement within the BHA frame depend on the bend angle and rate of change in orientation in the azimuth controller. Movements are planned because the BHA body orientation forces the bit against the well path because the BHA with its bend is wider than the BHA body alone. The model assumes the rate of change in rotation of the azimuth controller to be equal to the rate of change in orientation of the BHA body. Euler angles describe the orientation; roll, pitch and yaw:

$$\hat{\phi}_{BHA}[k + 1] = \hat{\phi}_{BHA}[k] = 0 \quad (9.24a)$$

$$\hat{\theta}_{BHA}[k + 1] = \Delta t \cdot DLS \cdot \dot{d}[k] + \hat{\theta}_{BHA}[k] \quad (9.24b)$$

$$\hat{\psi}_{BHA}[k + 1] = \Delta t \cdot \dot{\psi}_I[k] + \hat{\psi}_{BHA}[k] \quad (9.24c)$$

Where \dot{d} is the change in hoisting position and $\dot{\phi}$ is the rate of change in azimuth controller. For simplicity, Equation 9.24 are written as a vector:

$$\hat{\Theta}_{BHA}[k + 1] = \begin{bmatrix} \hat{\phi}_{BHA}[k + 1] \\ \hat{\theta}_{BHA}[k + 1] \\ \hat{\psi}_{BHA}[k + 1] \end{bmatrix} \quad (9.25)$$

The rate of change in BHA frame has to be converted to rate of change in the inertial frame. This is done with Equation 9.26.

$$\hat{\Theta}_I[k+1] = \frac{1}{\cos(\hat{\theta})} \begin{bmatrix} \cos(\hat{\theta}) & \sin(\hat{\phi}) \cdot \sin(\hat{\theta}) & \cos(\hat{\phi}) \cdot \sin(\hat{\theta}) \\ 0 & \cos(\hat{\phi}) \cdot \cos(\hat{\theta}) & -\sin(\hat{\phi}) \cdot \cos(\hat{\theta}) \\ 0 & \sin(\hat{\phi}) & \cos(\hat{\phi}) \end{bmatrix} \hat{\Theta}_{BHA}[k+1] + \hat{\Theta}_I[k] \quad (9.26)$$

All estimates of orientation are with respect to the inertial frame, and the current orientation is found by integrating the change in orientation given by:

$$p_I[k+1] = \Delta t \cdot \hat{R}_{BHA}^I \cdot \begin{bmatrix} 0 \\ 0 \\ \dot{d} \end{bmatrix} + p_I[k] \quad (9.27)$$

Orientation Estimate

The movement at each time-step is by the position estimation model assumed to be in the direction of the BHA orientation at the rate of change. The estimate of orientation uses an integration of unreliable values, which develop a high degree of uncertainty over time. Orientation can, however, be estimated with the downhole sensor data from the accelerometer and magnetometer because gravity is aligned with the inertial z-axis. A pitch and roll estimate can be obtained from trigonometric relations by comparing the measured gravity vector of the downhole sensor:

$$\hat{\phi}[k] = \text{atan2}(a_y[k], a_z[k]) \quad (9.28a)$$

$$\hat{\theta}[k] = \text{atan2}(a_x[k], a_z[k]) \quad (9.28b)$$

Yaw is estimated from magnetometer measurements where the vector points towards magnetic north. The magnetometer readings have both x and y -components that are used to estimate the yaw relative to magnetic north:

$$\hat{\psi}_{north}[k] = \text{atan2}(-m_y[k], m_x[k]) \quad (9.29)$$

Because of the location of the rig, it is not practical to align it with the magnetic north direction. An offset between the magnetic north and the inertial x-axis in the x and y direction are therefore

found before drilling and used as a bias:

$$\hat{\psi}[k] = \hat{\psi}_{north}[k] - \psi_{offset} \quad (9.30)$$

A large amount of process and measurement noise affect the downhole measurements. Raw data will give highly deviating estimations. The orientation changes slowly compared to the sampling rate, leading to slow changes in gravity and electromagnetic field in the sensor frame. A model observer for acceleration and magnetic field strength provides an estimate at each time-step to be further used in orientation estimation.

Gravity Field Model

The accelerometer measurements are affected by vibrations. An appropriate estimate of acceleration can be based on the current orientation estimate. The gravity field points in the direction of inertial z-axis. The gravity field in the sensor frame is therefor estimated as the inverse rotation matrix with the current inertial orientation estimate, multiplied with the z-axis unit vector:

$$\hat{a}[k] = (\hat{R}_{BHA}^I[k])^T \cdot \begin{bmatrix} 0 \\ 0 \\ 1 \end{bmatrix} \quad (9.31)$$

The gravity model has a low-pass and noise rejection effect on the acceleration measurements used to estimate the orientation.

Azimuth and Inclination

Roll, pitch, and yaw have to be converted into azimuth and inclination for the purpose of this project. Because both yaw and azimuth is the orientation relative to a reference direction, azimuth is, therefore, equal to the inertial yaw:

$$\alpha = \psi_I \quad (9.32)$$

The mentioned reference direction is the x-axis direction of the rock. Inclination can be defined with a combination of roll and pitch. The rotational matrices for roll and pitch are multiplied with a z-axis unit vector to create a vector in 2D-plane with an angular difference to the z-axis. The dot product of the two matrices are the inverse cosine of the matrix product:

$$\psi_{Inclination} = \arccos(\cos \phi_I \cdot \cos \theta_I) \quad (9.33)$$

9.2 Implementation in Control System

9.2.1 PID Controller

Simulink has a Proportional Integral Derivative (PID) block as an option for PID control. This block supports both continuous and discrete systems, and the component constants can be set directly in the block as shown in Figure 9.6 or by an external signal. Because the control system uses discrete time-steps, the discrete implementation had to be chosen for the PID block. Equation 9.34 shows the compensator formula used by Simulink.

$$u[k] = \left(K_P + K_I \cdot T_s \frac{1}{z-1} + K_D \frac{N}{1 + N \cdot T_s \frac{1}{z-1}} \right) \cdot e[k] \quad (9.34)$$

Where a large filter constant N is used for the derivative estimate.

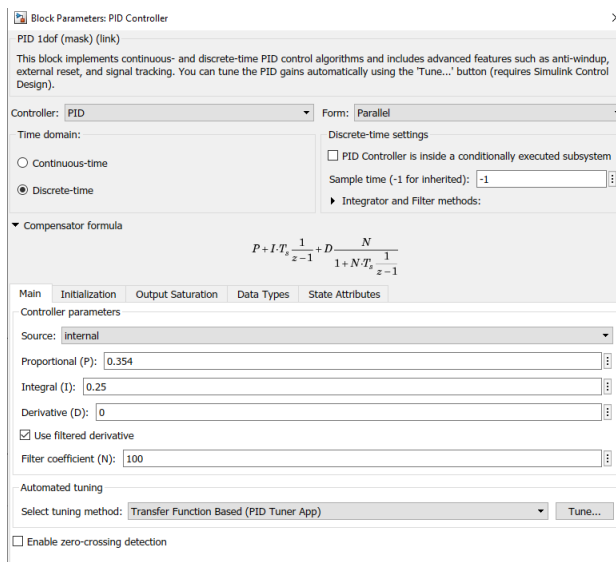


Figure 9.6: PID block in Simulink with tuned parameters.

To limit integral accumulation in the PID controller, an anti-windup scheme is implemented. A common method available directly in the PID block is back-calculation. Back-calculation prevents accumulation and slow response by discharging the integrator output when the controller hits its saturation limit [43]. This is achieved by feeding back the difference between the unsaturated and saturated control signal in the integrator.

Tuning

The optimal PID gains were found by using a closed-loop auto-tuning tool in Simulink. This block used the output of the PID controller to estimate the frequency response of the system and provide PID coefficients based on phase margin, and target bandwidth [44]. The controller remained unchanged during tuning, enabling it to remain stable. As shown in Figure 9.6, the tuned parameters for the WOB PID controller ended up in a pure PI-controller with the proportional gain, $P = 0.354$, and the integral gain, $I = 0.25$.

WOB PID Controller

Drilling requires a constant force on the bit to reduce mechanical stress and maximize ROP. Bit rotation against the rock causes a large amount of vibrations and variation in torque. To maintain a constant WOB, it is required constant regulation and quick response from the WOB PID controller. The velocity of the hoisting system is regulated based on measurements from the load cell. The output of the WOB controller is a ROP set-point, which is sent to the hoisting motor. The ROP output is limited to prevent the uncontrollable acceleration of the hoisting system when there is no bit-rock interaction. This mechanism is useful when tagging the rock or pulling out of the hole to prevent extensive pulling forces should the drillstring become stuck.

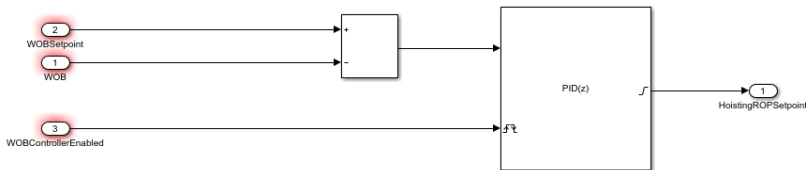


Figure 9.7: WOB PID Controller in Simulink.

The WOB controller is implemented with a Simulink PID block in a sub-system as shown in Figure 9.7. The error input is the difference between the measured WOB estimate from the load cell and the WOB set-point. A switch located in the GUI toggles the WOB controller, whereas another switch selects whether the set-point from the controller or the set-point from the velocity control is sent to the hoisting motor.

Azimuth Torque Controller

To change the drilling direction, the drill bit carves into the rock with additional rotational forces provided by the azimuth system. This generates torque spikes propagating through the BHA, drillpipe, and further to the azimuth control system. To prevent mechanical damage to these components, the torque is limited by a PID controller. Figure 9.8 illustrates the controller for

the azimuth system. Because the system can rotate clockwise and counter-clockwise, the torque limit is set-point is set in the direction of rotation. The PID controller output is normalized not to exceed an absolute value of 1 before it is multiplied by the absolute value of the set-point because counter-clockwise rotation is defined in the negative direction.

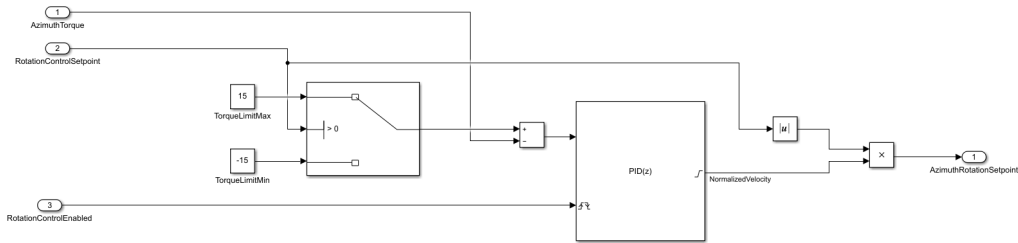


Figure 9.8: Azimuth controller system in Simulink.

9.2.2 Kalman Filter

Simulink has a designated Kalman filter blocks with Kalman filter functionality. These blocks include linear state-space filtering, extended filtering, and unscented filtering. The control system only uses extended Kalman filters because the system is non-linear and can be approximated around a linearization point. The extended Kalman filter block has one input to the model function, and a state estimate output by default as shown in Figure 9.9 [45].



Figure 9.9: Extended Kalman filter block in Simulink with input y_1 and state estimate output \hat{x} .

Hoisting Velocity Estimation

Monitoring the Rate of Penetration (ROP) during drilling is useful when evaluating the drilling performance. The ROP is measured based on the velocity estimate of the hoisting system. The estimate should react quickly to abrupt changes in movement while providing a consistent value at a consistent velocity. The velocity is further based on hoisting motor position, which is highly

accurate and frequently read from the motor. The change in position from one reading to another can be used to estimate the ROP, as shown in Figure 9.10. The velocity from time-step to time-step will vary because of limited resolution in the encoder. Therefore, the ROP estimations have to be filtered. A Kalman state observer is used to filter the estimations with the Simulink block. The ROP estimates are filtered by adjusting process noise and measurement noise.

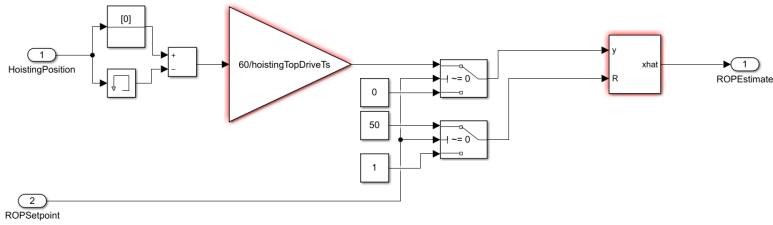


Figure 9.10: The ROP estimation with kalman filtering.

Azimuth Rotation Velocity Estimation

The azimuth motor outputs position with a high frequency in the same manner as the hoisting motor. Therefore, the estimate for azimuth rotation velocity can be filtered in the same way using a Kalman state observer. The Kalman filter adjusts process and measurement noise to provide the operator with an accurate indication of the current azimuth rotation velocity. Figure 9.11 shows the azimuth rotation velocity estimation and Kalman filtering.

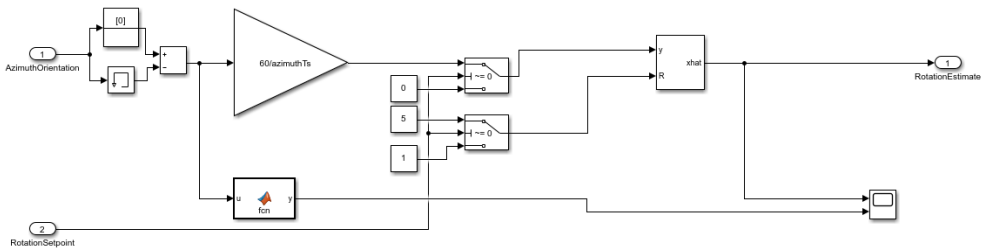


Figure 9.11: Azimuth rotation velocity estimation with kalman filtering.

9.2.3 Graphical User Interface (GUI)

The created control system Graphical User Interface (GUI) uses a MATLAB integrated tool "App Designer" - frequently used for creating applications and user interfaces. The main focus was to create a simple and self-descriptive GUI which enables operations without requiring background

information or introduction to the user.

The GUI, illustrated in Figure 9.12, consists of three tabs. The first tab manually operates the rig for testing the hardware components and control system mechanisms. In this tab, the user changes the hardware states and set-points. The second tab is the competition GUI tab to start and stop the autonomous drilling operation. The tab is used for surveillance and monitoring and only has an operable start and stop function. The third tab is used for OPC UA communication through the API described in chapter 10.

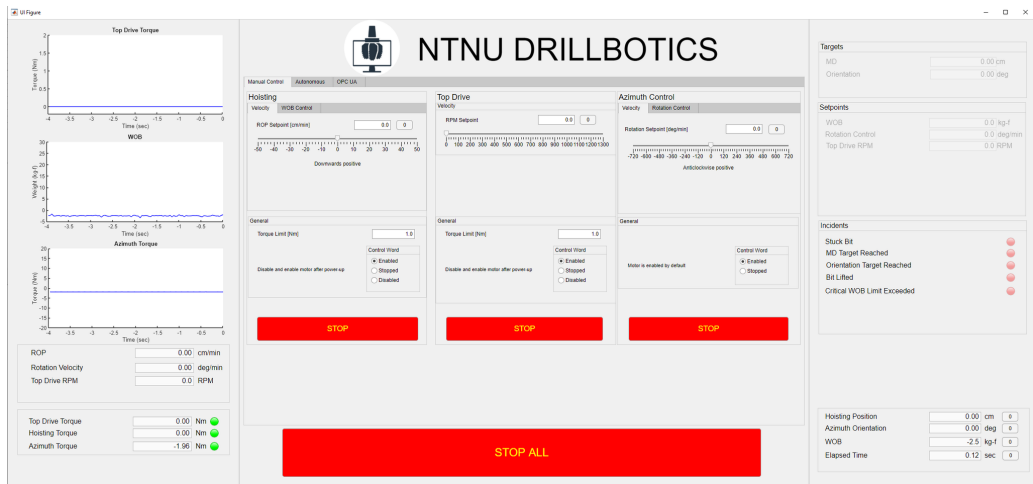


Figure 9.12: Graphical User Interface (GUI) for manual operation.

Important parameters such as WOB, bit, and drillpipe torque are carefully monitored with plots in the upper left corner of the GUI. The hoisting position, equal to () drilled in the rock, is monitored in the bottom right corner along with the azimuth orientation. The torque measurements are displayed in the bottom left corner. Warning lights indicate whether the readings are within the accepted range pre-set by the user. Values within range are displayed as green, values slightly outside the range are displayed in yellow, and unacceptable values near a limit are displayed in red. This easy monitoring enables quick actions if unacceptable incidents should occur. To further improve the reaction time and reduce incidents such as stuck bit and critical WOB are displayed to the far right. The warning lights related to such incidents light up if the system detects behavior that simulates an unacceptable incident. Some events, such as reaching target and azimuth, are also indicated. Large stop-buttons in red are implemented to shut down one or all motors. This is to prevent damage and wear in case of uncontrollable behavior. When the system and its behavior are known, the rig can be operated autonomously.

Figure 9.13 shows the GUI for autonomous operation. It is similar to the GUI for manual operation and monitors the same parameters. The main difference is the state progress observer that illustrates what state the state machine is operating in at any given time by lighting up green lights. The operation can be started by first choosing the initial state and end state of the process and then press the big green start button. For quick action in case of unexpected incidents, the stop button is also present in the autonomous GUI.

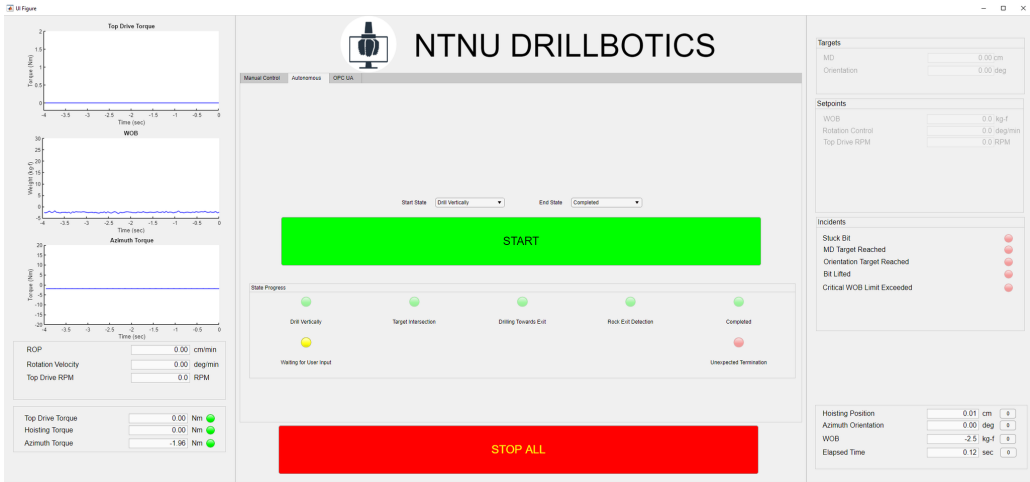


Figure 9.13: Graphical User Interface (GUI) for autonomous operation.

Due to limited time and priorities, the OPC UA tab was put on hold and not implemented. The communication and process state of the API is well monitored in UaExpert, and the server itself described in chapter 10.

9.2.4 Directional Model Predictive Controller (MPC) Model

The nonlinear Model Predictive Controller (MPC) in Simulink use a continuous time model by default. The rotational velocity of the azimuth system is the only input. Six states are kept track of; inertial Euler angles and Cartesian coordinates. The input to the model, u , is $\dot{\psi}_I$ given in radians per second. The angles in Equation 9.35a, 9.35b and 9.35c are the orientation of the BHA in the inertial frame.

$$\dot{\phi} = \frac{\cos \phi \cdot \sin \theta \cdot \dot{\psi}_I + DLS \cdot \exp\left(-\frac{\dot{\psi}_I^2}{q}\right) \cdot \sin \phi \cdot v_{nom}}{\cos \theta} \quad (9.35a)$$

$$\dot{\theta} = DLS \cdot \exp\left(-\frac{\dot{\psi}_I^2}{q}\right) \cdot \cos \phi \cdot v_{nom} - \sin \phi \cdot \dot{\psi}_I \quad (9.35b)$$

$$\dot{\psi} = \frac{\cos \phi \cdot \dot{\psi}_I + DLS \cdot \exp\left(-\frac{\dot{\psi}_I^2}{q}\right) \cdot \sin \phi \cdot v_{nom}}{\cos \theta} \quad (9.35c)$$

$$\dot{x} = v_{nom} \cdot (\sin \phi \cdot \sin \psi + \cos \phi \cdot \cos \psi \cdot \sin \theta) \quad (9.35d)$$

$$\dot{y} = -v_{nom} \cdot (\cos \psi \cdot \sin \phi - \cos \phi \cdot \sin \psi \cdot \sin \theta) \quad (9.35e)$$

$$\dot{z} = v_{nom} \cdot \cos \phi \cdot \cos \theta \quad (9.35f)$$

DLS and v_{nom} are constants based on the estimated build rate and nominal ROP in radians and centimeters per second.

Chapter 10

API

The API described in this chapter is based on the same principles as the API made by the Drillbotics team from University of Stavanger in 2019 [72]. Magnus Steinstø was a part of that team and contributed to the development of that specific API.

A new requirement to the competition in 2021 is the requirement to implement an Application Programming Interface (API). It is a software intermediary that enables two applications to talk to each other [61]. Implementation of such a system enables remote control of the drilling rig and provides a layer of security. An API integration can streamline processes by enabling cross-platform communication and tool exchange. Integration of third-party apps to optimize functionality and usability can reduce development costs. APIs are central in automation strategies where manual tasks are automated for a smooth transition between linked applications [14]. With APIs, government-level data and information are available to everyone with a level of security.

10.1 OPC UA

OPC Unified Architecture (UA) is a platform independent service-oriented architecture that integrates all the functionality of the individual OPC Classic specifications into one extensible framework. OPC UA is capable of the following [37]:

- **Discovery:** find available OPC Servers on local PC's or networks
- **Address space:** all data is represented hierarchically in files and folders to simplify understandability and usability for clients

- **On-demand:** read/write data/information based on accessibility
- **Subscriptions:** monitor data and information and report based on clients criteria
- **Events:** based on client's criteria, notify important information
- **Methods:** methods defined on the server allows for clients to execute programs

The Application Programming Interface (API) was implemented using Python because there was no sufficient option for implementation in MATLAB. Without commercial Software Development Kit (SDK) for OPC UA, the implementation was performed with an open-source package. The control system of this rig was written in Simulink, a graphical programming environment in MATLAB. This required an open-source package for Python-MATLAB communication to communicate across the platforms.

10.1.1 Information Model

The information model defines the server's address space and thus also describes the available nodes through the server. The server imports the model as a Extensible Markup Language (XML) Nodeset file. From this information model, the server can interpret the different elements and then add them to the hierarchically address space. The available information enables the server to create and manage the nodes, but the objects are not present. These nodes include properties such as method, data type, events, etc. The model is designed such that an object represents a rig request. Customized methods are linked to these objects as a child node, which are the methods that are called when the request is executed.

10.1.2 Server Implementation

The API is based on OPC UA because of the possibilities and availability it provides. In addition to the bullet points already mentioned, OPC UA is fire-wall friendly and provide security [37]:

- **Session Encryption:** messages are encrypted and transmitted securely
- **Message Signing:** the origin and integrity of received messages can be verified by the recipient with message signing
- **User Control:** users can be required to authenticate and then further be restricted with respect to access rights
- **Auditing:** activities by users and systems can be logged

The API is dependant on an OPC UA server available for clients to connect to. The server is initiated by creating a high-level server class object in the following manner:

```
1 server = Server()
```

The XML Nodeset file is then imported with the high-level server class method:

```
1 server.import_xml(r"file-path/filename.xml")
```

The address of the server is defined by an endpoint using the high-level server class method:

```
1 url = "opc.tcp://localhost:4844"
2 server.set_endpoint(url)
```

This way, the Uniform Resource Locator (URL) is handled by the server and the address is assigned to localhost to allow for simple local testing. The following method adds a namespace containing NodeIDs to the server:

```
1 addspace = server.register_namespace("Name")
```

After the namespace and endpoint are set up, the server is initiated with the following command:

```
1 server.start()
```

The server, and its accessible nodes, are now available for clients to connect locally or across networks.

10.1.3 Server Nodes

The objects from the information model are yet to be included in the server. All objects containing methods and events are rooted in the object node of the server. This is obtained through the following method:

```
1 node = server.get_objects_node()
```

Specific nodes can then be fetched by first returning the ObjectType node, which defines all the object types available. To fetch a specific node, the browse-name or the nodes ID must be specified and the namespace index of the desired node. In this server, the browse-name is used

to define and obtain a specific node. After receiving the request type of a specific node from the information model, the object has to be made by the server for clients to access it. To create a node, the node id has to be fetched and specified. All these commands which allow for object nodes to be fetched and created, are shown in the example code below for the ROPSetpoint request type:

```
1  ROPSetpoint_type_nodeid =
   ↪ server.get_node(ua.ObjectIds.BaseObjectType)...
2  .get_child(["%d:RigRequest_ROPSetpoint" % addspace]).nodeid
```

This object can now be added to the address space by calling the following method on the specific node:

```
1  ROPSetpoint = node.add_object(addspace, "ROPSetpoint",
   ↪ ROPSetpoint_type_nodeid)
```

The line of code above defines the standard for creating and adding objects to the server based on the information model. The method adds objects based on three parameters: address space, browse-name, and object type.

10.1.4 Rig Request

The API defines a rig request as a command the rig ought to execute. Every request node created contains a method child node. These method nodes are the actual method the clients call to execute the request to which they are linked. Method nodes can be retrieved by the *get_child()* command, in the same way, the request type nodes were fetched as a child node from the object node of the server:

```
1  ROPSetpointMethod = ROPSetpoint.get_child("2:SetROP")
```

The method types create information about input and output parameters but lack specific content to carry out when called by a client. For that reason, the method has to be linked to a Python function. This is done with the *link_method()* command that links an UA method to a Python method:

```
1  server.link_method(ROPSetpointMethod, api.ROPSetpoint)
```

By linking the methods with this command, the Python function is called with the same arguments as the UA method. Because the control system operates in MATLAB and Simulink, this Python

function must be linked to a MATLAB function again. This is achieved by setting up a MATLAB engine session with an open-source package:

```
1 engstart = matlab_engine.start_matlab()
2 eng = matlab.engine.connect_matlab()
```

The `connect_matlab()` command connects to a shared MATLAB session started in MATLAB with the following commands:

```
1 matlab.engine.shareEngine()
```

When a connection is established, the Python method calls MATLAB functions through the engine with parameters set by the client in a third-party app subsection 10.1.7. To follow up the example used through this chapter, the ROPSetpoint Python method calls the SetROP MATLAB function:

```
1 def ROPSetpoint(ObjectID, SetpointROP, RequestID):
2     print("ROPSetpoint successfully called.")
3
4     eng.SetROP(SetpointROP.Value)
5     TriggerEvent("ROPSetpoint", 0, 0, RequestID.Value)
6     return[]
```

10.1.5 Events

The server uses events to inform about changes related to the requests made by the client. These changes describe the status of the rig and what progress is under execution. Each request type node has a related event as a child node. This event type node is created similarly to the object type node, besides the fact that the base type is an EventType:

```
1 eRapProgressChange_type =
   ↳ server.get_node(ua.ObjectIds.BaseEventType)...
2   .get_child(["%d:eRapProgressChange" % addspace])
```

To connect an event to an object, an event generator is created by the `get_event_generator()` command. This way, the uniform event type can connect to specific object nodes:

```
1 ROPSetpointEvent =
   ↳ server.get_event_generator(eRapProgressChange_type, ROPSetpoint)
```

With this object, the server can set parameters of the event and trigger the event related to the object with the method *trigger()* as shown in the Python function in subsection 10.1.4.

10.1.6 Rig Data

Real-time rig data should be accessible through the API for surveillance and optimization purposes. Surveillance is essential to detect and prevent incidents such as stuck drillstring, buckling, etc. Optimization provides improvement to the drilling process based on real-time data. Real-time data and setpoint values are extracted in the same way that clients set parameters in subsection 10.1.3 and 10.1.4. The Python method linked to the object calls functions in MATLAB through the engine to gather relevant data. As an example, *GetMeasuredParameters* gathers the monitored drilling parameters:

```
1  @uamethod
2  def GetMeasuredParameters (Parent) :
3      return eng.readActualWOB(), eng.ReadActualRPM(),
           ↪ eng.readActualROP(), eng.readAzimuthMeasured()
```

The data returned by the function above is available for reading only and cannot be edited by the clients.

10.1.7 Third Party Tools

During the design and implementation of the OPC UA server and API, the two tools frequently used were Free OPC UA Modeler and UaExpert.

Free OPC UA Modeler

Free OPC UA Modeler is an open-source OPC UA address designer. It allows for users to create and interact with the information models [41]. The tool was used to visualize the information model in a hierarchy as illustrated in Figure 10.1 and to create and edit the objects and nodes easily. The designer takes a XML file as input and provides the same type of file as output. With this Python extension, it is easy to browse every parameter related to the API, such as methods, event types, and data types. It also allows for viewing and editing an object and its related children and references.

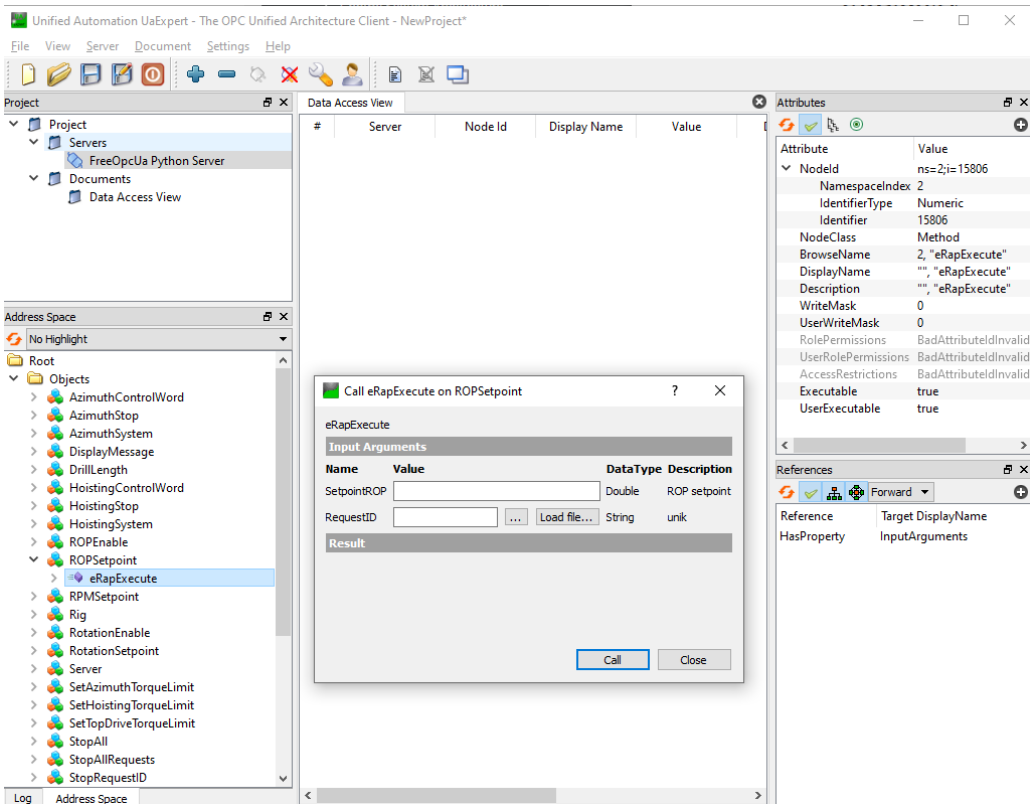


Figure 10.2: UaExpert main window. This screenshot shows a connection to the OPC UA server in python in the upper left corner. The available objects in the address space is shown in the bottom left corner. Data access is located in the middle, and the attributes of the chosen node is shown in the upper right corner. The prompt in this screenshot shows the input parameters for the ROPSetpoint request.

10.2 Connection to Rig Control System

10.2.1 Request Handling

Requests defined in the address space of the OPC UA server are linked to Python methods that handle the requests. These methods are responsible for linking the requests to the control system in MATLAB by sending commands to the rig or receiving data from the rig. A command is created by the method and sent to a module for execution. The method needs feedback stating that the command is sent and verifying whether the request is finished or failed for the request to be successfully executed. By comparing the received rig data related to the execution of the request with the data sent by the request, this can be verified. If the data match, the request has been successfully executed. If not, the request will wait for the data to match.

10.2.2 Events

A dictionary with available event generators is created after the event generators themselves are made by the OPC UA server. The rig control system can trigger events through this dictionary with the request name in string format as key value and the event generator as the value.

```
ROPSetpoint successfully called.
DEBUG:opcua.server.internal_subscription.78:<opcua.server.internal_subscription.MonitoredItemService object at 0x000001939A622F08> has no subscription for events CustomEvent(["EventId:Variant(val:b'1e7bf2f131a4437c8b6f3e896d9bf992',type:VariantType.ByteString)", 'EventType:NumericNodeId(ns=2;i=15377)', 'SourceNode:NumericNodeId(ns=2;i=15805)', 'SourceName:ROPSetpoint', 'Time:2021-04-16 14:12:50.116101', 'ReceiveTime:2021-04-16 14:12:50.116101', 'LocalTime:TimeZoneDataType(Offset:{self.Offset}, DaylightSavingInOffset:{self.DaylightSavingInOffset})', 'Message:LocalizedText(Encoding:0, Locale:None, Text:None)', 'Severity:1', 'Progress:0', 'Status:0', 'RequestID:ROPSetpoint_ID', '_freeze:True'] from node: NumericNodeId(ns=2;i=15805)
Event successfully updated!
```

Figure 10.3: Event related to ROPSetpoint request call. Progress, Status, and RequestID are written to console.

A response, as shown in Figure 10.3, is written to console when an event and method is successfully called. This is an informative response that includes interesting parameters such as the progress variable, the status of the request, and the RequestID linked to the specific request.

10.2.3 Sending and Receiving Rig Parameters

The operating parameters of the rig can be set with the OPC UA server. The server receives the set parameters in a dictionary, reads the values, and sends commands to the respective Python functions. These functions then send commands with the set values to the MATLAB function, which again links the values to the control system.

Two types of data from the rig system are interesting to the client operating it—the current set points of the system to link them to the current behavior and real-time data. The setpoints are imported by accessing the control system in the same way that setpoints are sent to the system. The MATLAB function is asked to read the current value and return it to the server. The real-time data changes unceasingly and has to be updated frequently. Data is still received in a dictionary, but new data is received and overwrites the old data at a specific interval. When the client requests a reading, the continuously updated data is simply read from the dictionary.

(This page is intentionally left blank)

Testing and Qualification

Testing of systems and components is beneficial to check the rig’s functionality and optimize the drilling performance based on the results. This chapter describes the testing of the functionality of different components on the rig.

An essential aspect of designing and implementing a fully autonomous drilling rig is to run tests on the system. Different parts of the system should be tested separately, and the rig consists of equipment that also should be tested separately. The whole system should be tested altogether. Determining the operating window and other constraints for the rig is a goal with testing. When testing the equipment, an industry procedure named Factory Acceptance Test (FAT) has been used. FAT is used to check whether the relevant equipment works as expected.

11.1 Factory Acceptance Test For Equipment

The main goal of testing the rig components was to verify their functionality with respect to their task. The components should deliver what is required to complete a fully autonomous drilling rig. A FAT is commonly performed during and after the assembly operation. This phase is the last part of the design and engineering phase. The tests should be divided into smaller parts of the system. This makes it easier to detect where a problem occurs. When testing the components, it is examined whether the instructions put in the software for the equipment are executed.

11.1.1 FAT Plan

A thorough FAT for the rig has been done by the earlier team from 2017 [63]. Many of the critical components are therefore already tested and approved for this project’s use. Only the new parts of

the rig have therefore been tested. New components to this year's rig to be tested are the azimuth rotation system, new emergency stop button, and new top drive.

11.1.2 Azimuth Rotation Test

The requirement stated in the guidelines requires an azimuth of 15 degrees equal to $1/25$ of a rotation. To meet the requirement, it is crucial that the azimuth system can rotate at a precise rate. The need for precision is amplified by the need for high accuracy when drilling towards the three targets given.

Test Setup and Procedure

A thin cardboard piece with measured angles was placed on the drill floor stabilizer as shown in Figure 11.1. Then a line was drawn on the drillpipe in the direction of zero degrees. The azimuth system was run at two different velocities. In the first run, it ran for a minute with a velocity of 15deg/min. In the second run, the velocity was increased to 180 deg/min. After one minute had passed, the system was shut off, and the direction of the line on the pipe was read.



Figure 11.1: Azimuth rotation test setup.

Results

Both of the tests seemed to give a fair result, where the position of the last test is shown in Figure 11.2.



Figure 11.2: Resulting direction after running 180/deg for a minute.

Errors and Discussion

The test was a simple test to verify if the system worked or not quickly. Thus the setup, especially the cardboard piece, was made by hand and may lead to human error. Under the restriction of the setup and assumptions made, the azimuth system seemed sufficiently accurate for the purpose.

11.1.3 Top Drive Rotation Test

The new top drive motor had to be tested to verify its functionality. It is not of utmost importance that the top drive rotational accuracy is exact, but it should be accurate within a few percent range.

Test Setup and Procedure

To run the test, an approach similar to the azimuth rotation test was used. A line was drawn on the drill chuck attached to the motor shaft, and a set screw in the T-shaft was used as a reference. The setup is shown in Figure 11.3. The motor was run on different RPM velocities for one minute at each velocity, and the number of rotations was counted. After one minute, the motor was stopped to check for offsets on the final rotation.

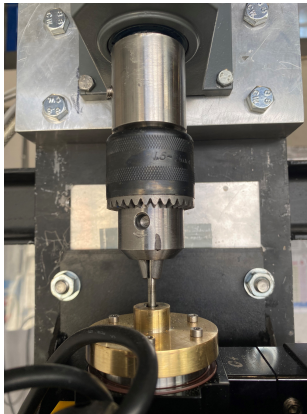


Figure 11.3: Top drive rotation test setup.

Results

The motor was rotated at three different velocities as shown in Table 11.1

Table 11.1: Top drive rotation test results.

Top Drive Velocity [RPM]	Rounds rotated in one minute	Deviation
1	3/4	25%
10	9 7/10	3%
20	19 3/4	1.25%

Errors and Discussion

The first test with a velocity of 1 RPM had a deviation of 25% as shown in Table 11.1. This was expected because the motor is calibrated for velocities up to 1 300 RPM. Because the velocity increased, the deviation decreased, thus supporting the assumption of better calibration and accuracy at higher velocities. Because a team member counted the rounds, it was hard to count rounds at higher velocities because of limitations in human capacity. Assuming that the trend observed from the three tests extrapolates to higher velocities, it is reasonable to assume the actual velocity to be approximately equal to the set-point velocity.

11.2 Pipe and Rod Limit Tests

This section presents the tests done to examine the actual limits of the pipe and rod that were calculated in section 4.3.

11.2.1 Buckling

The tested component is drillpipe in aluminum 7075-T6. The NTNU Drillbotics team in 2018 performed a similar test for aluminum drillpipe, but with the alloy 6061-T6 [52]. This test will be similar to the one in 2018 for being able to compare the results. The rod will not experience buckling effects because it is not subjected to WOB and will therefore not be tested. The purpose of the buckling test is to confirm the amount of weight that can be applied to the component before it buckles.

11.2.2 Test Setup and Procedure

The drillpipe is fixed to the drilling system using the nipple connection under the hydraulic swivel. The pipe is pinned using the upper stabilizer described in subsection 6.6.6. It is cut to make the length of pipe between the top connection and drill floor stabilizer 0.68 meter. This is the same length as the pipe maximum will be free when drilling at the end of the rock. It continues down through the riser and into a previously drilled shallow well in the cement block for extra support. The pipe will be hoisted down with a fixed speed, and then the WOB value will be observed in the GUI. A person will also observe the drillpipes' physical behavior. When the WOB starts to drop after increasing steadily, and the pipe deforms in a curve-like manner, buckling has occurred. The protection glass and full PPE will be used during the test.

11.2.3 Results

Table 11.2: Results from buckling tests on aluminium 7075 drillpipe.

L [m]	Buckling force [kg]
0.68	178
0.68	172

The test was performed two times, and the results are shown in Table 11.2. Figure 11.4 shows how the WOB increase until it drops and the pipe bends like in Figure 11.5. The reason that the WOB-values are not steadily rising is that the ROP velocity was changed during the test.

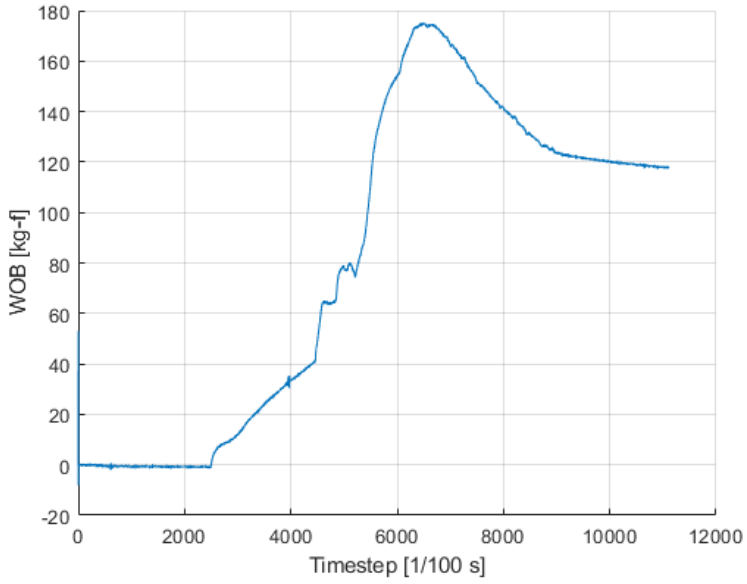


Figure 11.4: Buckling test of aluminium 7075 pipe.

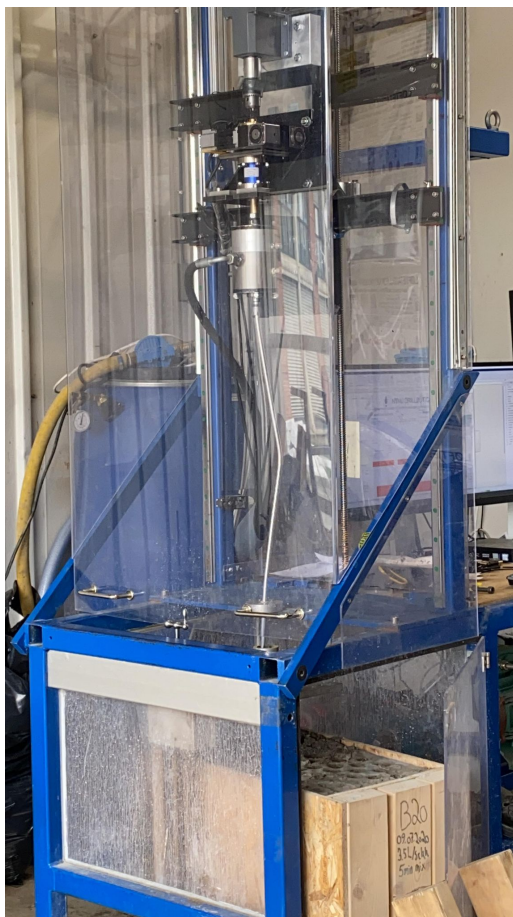


Figure 11.5: Drillpipe buckled.

11.2.4 Errors and discussion

The force needed to buckle the drillpipe where much higher than our operating range, and therefore only two tests were performed. The buckling force was also higher when using the aluminum 7075-T6 drillpipe instead of the aluminum 6061 drillpipe used in 2018. This was expected due to higher strength for the 7075 alloy but could also be due to differences in the testing procedure. The test is a static buckling test, which resulted in sinusoidal buckling.

Ideally, a dynamic buckling test should be performed, but since the buckling force for the static test was so much higher than our operating window, this was not done. Another reason for not doing a dynamic buckling test was that in the thesis from the NTNU 2018 Drillbotics team, it is stated that a dynamic buckling test is very damaging for the mechanical system [52].

11.2.5 Bending

The main purpose of the bending test is to verify that both the pipe and rod can handle a bend of 30 degrees. A simple test was done on the aluminum 7075-T6 pipe and the three available rods; aluminum 7075-T6, 316 stainless steel, and Grade 5 titanium.

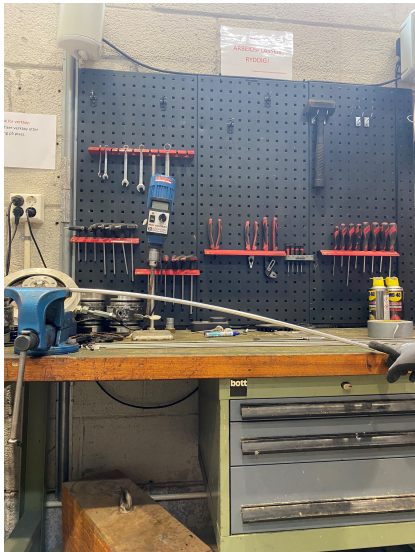
Test Setup and Procedure

A simple test was set up in the workshop as shown in Figure 11.6. The pipe and rods were fastened in a vice with the respective representative lengths hanging vertically out to resemble a fixed-free situation. The bent length of the pipe was the expected measured depth through the rock sample, 63 cm, plus the length from block surface to drill floor, 28 cm, minus the length of the BHA, 20 cm, resulting in a length of 71 cm. The bent length of the rod was conservatively assumed to be the same length plus the 10 cm from top of BHA to the universal joint, giving a length of 81 cm.

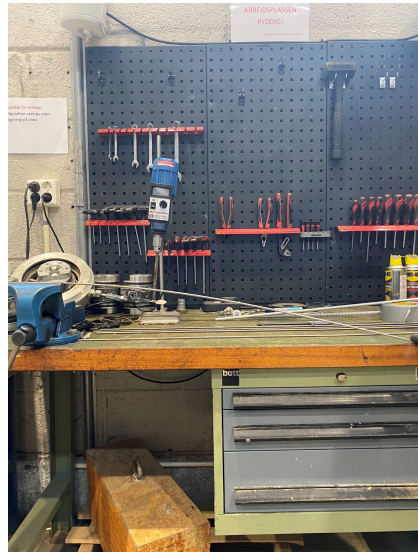


Figure 11.6: Setup of simple bending test.

To confirm if the materials could handle the expected bend of 30 degrees, they were pinned down at the end as shown in Figure 11.7. The expected vertical deviation after building 30 degrees is 13.60 cm as calculated in section 5.1. The distance from the vertical to the table in the picture was measured to be 14 cm. Thus the materials were bent down towards the table to give a conservative result.



(a) Bending of aluminum 7075-T6 pipe.



(b) Bending of 4 mm diameter 316 stainless steel rod.

Figure 11.7: Bending test resembling fixed-free scenario.

To further check if the material had been deformed, a "rolling test" illustrated in Figure 11.8 was conducted for each of the components. This test aims to see if the material is aligned with the flat surface when rolling it or if any space between the material and the surface can be spotted as a result of a bend in the material.



(a) Flat surface used to conduct "rolling test".



(b) Possible space between material and surface.

Figure 11.8: "Rolling test" to check the results of the bending test.

Results

The test was conducted for one type of pipe and six different rods as presented in Table 11.3. All the tested entities passed the test with no deformation, i.e., no space could be observed between the materials and the flat surface.

Table 11.3: Bending test results showing all the materials passed.

Type	Material	ID [mm]	OD [mm]	Length [cm]	Bend [cm]	Pass/Fail
Pipe	Aluminum 7075-T6	7.036	9.53	71	14	Pass
Rod	Aluminum 7075-T6	-	4	81	14	Pass
Rod	316 Stainless Steel	-	4	81	14	Pass
Rod	Grade 5 Titanium	-	4	81	14	Pass
Rod	316 Stainless Steel	-	4.5	81	14	Pass
Rod	Grade 5 Titanium	-	4.5	81	14	Pass
Rod	316 Stainless Steel	-	5	81	14	Pass

Errors and Discussion

With respect to the theoretical calculations conducted beforehand, it was expected that all the tested components would pass the test. It is not intuitive to define the length where the rods will be bent as they are not stabilized like the drillpipe on the drill floor. The drillpipe will have some

stabilizing effect on the rod, but the rod will still be able to bend inside the pipe up to the hydraulic system. This problem was solved simply by assuming that the bending happens below the drill floor stabilizer. This assumption will give the most conservative estimate, as a shorter length will be less resistant to bending.

The test will not mirror the environment during drilling, as several other parameters and forces are acting on the drill string. The borehole wall will have a stabilizing effect, the angle of bend and bent length will increase gradually, and there will be vertical forces compressing the string.

11.3 Twist-off

The rod is the only component discussed with respect to twist-off as the pipe will not be rotating to that extent. There were no explicit tests conducted for twist-off, but twist-off did occur multiple times during the initial testing of the mechanical setup and control system. The twist-off scenario below happened while drilling with a 4 mm diameter grade 5 titanium rod. According to the theoretical calculations in section 5.4 based on the shear strength of the material, the twist-off limit is 9.58 Nm. However, twist-off occurred at a significantly lower torque value as shown in Figure 11.9.

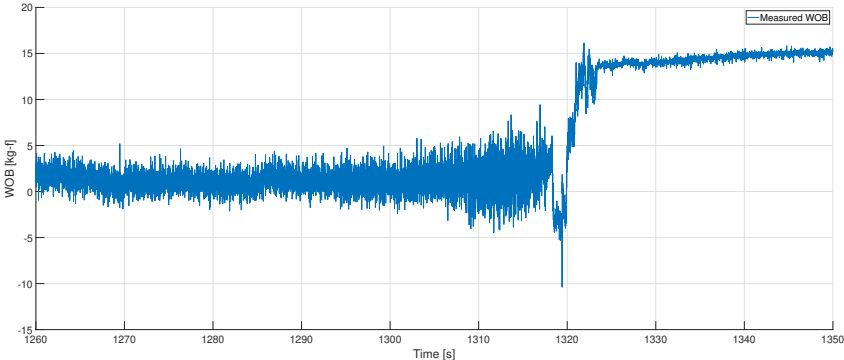


Figure 11.9: Twisted rod.

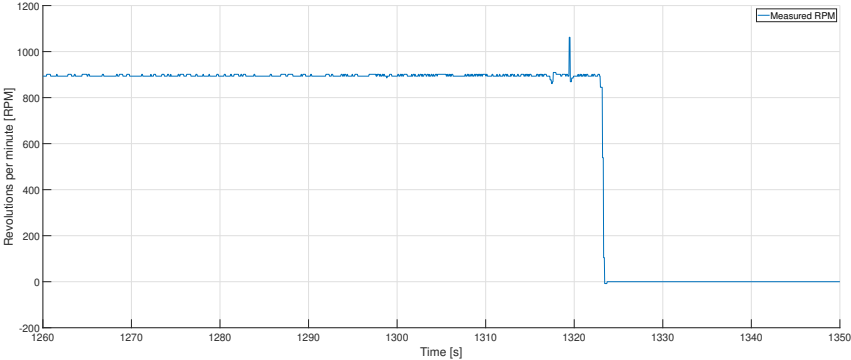
Figure 11.10 shows WOB, RPM and torque for a run where twist-off occurred. The twist-off occurred at the start of the run during pilot hole drilling. Several trends can be found in these plots. The measured WOB depicted in Figure 11.10(a) shows noisy measurements while drilling from 1 310 seconds on due to vibrations. When the rod twists off, there will not be any bit rotation and therefore slim to none vibrations. After approximately 1 316 seconds, the WOB drops because of the stuck bit detector that is set to decrease WOB to -5 kg-f when torque is consequently high over time. At 1 319 seconds, the rod twists, and the WOB abruptly increases due to compaction when the system hoists down with no bit rotation.

By looking at the RPM plot in Figure 11.10(b), it is clear to see where the rod twists off. The rotational velocity is constant at the setpoint of 900 RPM. At 1 319 seconds, the RPM spikes because it can rotate freely when the resistance in the rod disappears. It settles at the setpoint shortly after twisting until the motor is shut off at 1 324 seconds.

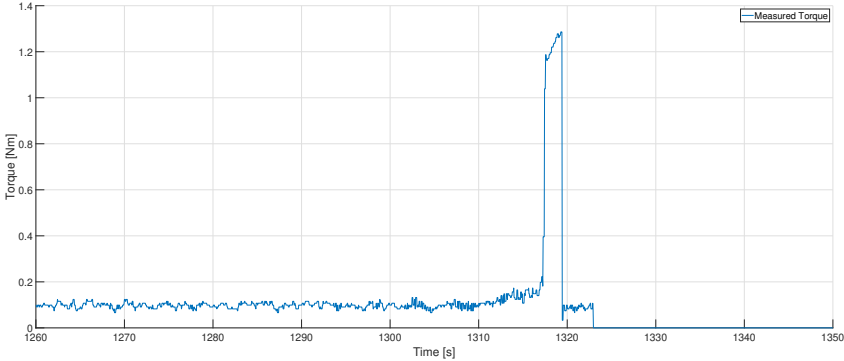
The most interesting plot with respect to twist off is the torque plot shown in Figure 11.10(c). A torque spike clearly visualizes the stuck-bit incident at 1 316 seconds. At 1 319 seconds, the rod twists off at a torque value of 1.3 Nm, and the torque plummets to the initial torque value in the motor itself. According to the twist-off limit calculated in section 5.4, the rod should not be close to twisting at this value. A couple of factors can explain this. The same rod had been used in several runs. During an average run of 45 minutes with a setpoint of 900 the rod rotates $900RPM \cdot 45min = 40\,500$ rounds. With torque spikes during multiple runs, fatigue will be experienced by the rod. 900 RPM is equal to 15 rotations each second. In this specific stuck-bit incident, the rod experienced a fixed-free situation for 3 seconds. This means that the rod rotated $15 \cdot 3 = 45$ times around its axis without rotating the bit. These two factors contribute to a lower twist-off value.



(a) WOB



(b) RPM



(c) Torque

Figure 11.10: WOB, RPM and torque plots from the run where twist-off occurred.

11.4 Rock Sample Cement Testing

The rock sample in which the competition requires the teams to drill through will be provided by DSATS on the competition day. The teams know that the sample rock is a homogenous sandstone and the range in which Uniaxial Compressive Strength (UCS) can be expected. Therefore, it is interesting to test the properties of the cement blocks self-made by the team to try to match the UCS. This way, the team can optimize and improve the drilling system for the sandstone provided on the competition day. To simplify and streamline the testing process, the volume of the cement block had to be scaled down to reduce resources and thickening time. The homemade cement for test drilling prior to the competition day requires approximately seven sacks of 25 kg cement.

Scaling down the recipe reduces the amount of cement needed to 335 grams of concrete, and the thickening time was reduced from two weeks to 24 hours. The competition rock sample is said to have the following dimensions: 24 inches tall, 12 inches wide, and 24 inches long. This corresponds to 60.96 cm, 30.48 cm, and 60.96 cm, respectively. This equals a rock volume of $4ft^3$, or $0.11 m^3$.

$$V_{block} = W \cdot L \cdot H = 30.48cm \cdot 60.96cm \cdot 60.96cm = 113267cm^3 \approx 0.1133m^3 \quad (11.1)$$

One sack of standard B20 cement weighs 25 kilograms and requires 3.5 litre of water when mixed. The density of B20 concrete when the slurry has hardened is normally 1 750 kg/m³ [65]. One sack of cement correspond to a volume of approximately $0.018m^3$:

$$V_{bag} = \frac{M_c}{\rho_c} + V_w = \frac{25kg}{1750kg/m^3} + 3.5 \cdot 10^{-3}m^3 \approx 0.018m^3 \quad (11.2)$$

From these calculations it is possible to derive the required amount of sacks and thus determine the mass of each sack of cement:

$$n_{bag} = \frac{V_{block}}{V_{bag}} = \frac{0.11m^3}{0.018m^3} \approx 6.37 \quad (11.3)$$

$$M_{c,tot} = n_{bag} \cdot M_c = 6.37 \cdot 25kg = 159.26kg$$

The amount of water required for mixing one block of cement corresponding to the dimensions previously mentioned, is:

$$V_{w,tot} = n_{bag} \cdot V_w = 6.37 \cdot 3.5L = 22.30L \quad (11.4)$$

The down-scaled cement sample was mixed in a blender and transferred to multiple cylindrical containers with a radius of 2.25 cm (approximately 1 inch) and a height of 15 cm (approximately 6 inches). The test cylinder is depicted in Figure 11.11.



Figure 11.11: Cement test cylinder

The volume ratio between the original cement block and the container is found by first deriving the volume of the cylinder:

$$V_{cylinder} = \pi \cdot r^2 \cdot h = \pi \cdot 2.25^2 \cdot 15 = 238.60 \text{ cm}^3 = 2.39 \cdot 10^{-4} \text{ m}^3 \quad (11.5)$$

Thus, the volume ratio is acquired:

$$\frac{V_{cylinder}}{V_{block}} = \frac{2.39 \cdot 10^{-4} \text{ m}^3}{0.11 \text{ m}^3} = 2.11 \cdot 10^{-3} \quad (11.6)$$

With this ratio, we can further derive the dry cement mass and volume of water needed for the cylinder while maintaining the same properties as the original cement block:

$$\begin{aligned} M_{c,cylinder} &= M_{c,tot} \cdot 2.11 \cdot 10^{-3} = 159.26 \text{ kg} \cdot 2.11 \cdot 10^{-3} = 335.40 \text{ g} \\ V_{w,cylinder} &= V_{w,tot} \cdot 2.11 \cdot 10^{-3} = 22.30 \text{ L} \cdot 2.11 \cdot 10^{-3} = 0.047 \text{ L} = 46.90 \text{ mL} \end{aligned} \quad (11.7)$$

With these parameters, nine cylindrical containers were filled with cement slurry. The amount of

water added to the slurry in the different cylinders represented the following three different ratios between cement and water; 3 L/25kg, 3.25 L/25kg, and 3.50 L/25kg. The purpose of filling nine containers is to check whether the slurry sample is consistent. Making three samples of each ratio will allow for the detection of any deviations in the samples.

11.4.1 Mixing and Test Procedure

To prevent the cement from adhering to the plastic cylinder, the cylinders were lubricated in advance. The nine samples were set to dry for 24 h before the hardened cement was easily removed from the cylinders.



Figure 11.12: Mixing of cement

The results are presented in Table 11.4.

Table 11.4: Results from testing of cement with different water to concrete ratio.

Sample	D [mm]	L [mm]	M [g]	ρ [kg/m ³]	UCS [MPa]	Ratio [L/25kg]
1	44.35	93.57	325.38	2251	NaN	3
2	44.24	93.44	318.71	2218.93	26.50	3
3	44.28	93.13	322.08	2245.79	27.03	3
4	44.25	93.58	319.39	2219.33	22.20	3.25
5	44.28	93.16	321.25	2239.28	22.80	3.25
6	44.23	93.15	319.21	2230.33	23.90	3.25
7	44.22	93.62	318.37	2214.30	18	3.50
8	44.24	93.60	317.03	2203.46	18.70	3.50
9	44.21	93.16	319.16	2231.76	17.00	3.50

11.4.2 Errors and Discussion

As shown in Table 11.4 the UCS varies with ratio, but is relatively consistent. Sample 1 was damaged in one end of the cylinder and could therefore not be tested. It is, on the other hand, reasonable to assume that the UCS value would be similar to sample 2 and 3 by looking at the consistency in the other samples.

11.5 Vertical Section

According to the guidelines, a vertical section of a minimum of 3 inches has to be drilled after drilling the pilot hole of 1 inch. The BHA has a fixed bent sub that does not allow for vertical drilling without rotating the entire assembly. For that reason, several tests have been conducted to find the best possible approach to this problem.

The first tests conducted were done with a constant WOB during the complete drilling run. For the vertical section, the azimuth controller was set to rotate at a velocity of 180 deg/min. Figure 11.13 shows the result of one of the tests conducted like this. A clear spiral and poor hole quality can be observed. This trend is probably caused by too high WOB giving to high ROP combined with too slow azimuth rotation velocity.



Figure 11.13: Poor hole quality with spiral pattern.

By interpretation of the results in Figure 11.13, it was decided to increase azimuth rotation velocity and decrease WOB to increase the surface area of the borehole that is cut by the bit. The azimuth rotation velocity was increased to 360 deg/min and the WOB was decreased to a WOB of 10 kg-f giving an average ROP of about 1.0 cm/min. Figure 11.14 shows the improved result with less of a spiral pattern.



Figure 11.14: Second attempt with improved hole quality.

Because the WOB controller did not react to and perform sufficiently on setpoints less than 10 kg-f, it was not possible to further decrease the WOB. The only option was, therefore, to increase the azimuth rotation velocity. It was increased to 540 deg/min, which gave a satisfying result as shown in Figure 11.15. With this approach, the borehole wall in the vertical section is smooth and builds an excellent base for kick-off in the desired direction.



Figure 11.15: Smooth vertical borehole with a clear kick-off point and direction.

11.6 Variation of DLS

Because the rig uses a fixed bent sub angle an approach to build less angle had to be found. The standard procedure with a fixed bent sub angle is to regulate the WOB or use a motor to rotate the BHA while drilling, which leads to straight drilling. These two approaches were tested with varying luck.

11.6.1 WOB approach

The WOB approach is based on applying a higher WOB to increase building angle. Through several drilling tests with varying WOB applied, it was examined if there was a pattern in inclination built. No clear pattern was observed. This could be due to a limitation on how much WOB could be applied. The drilling system can only handle around 30 kg-f WOB until torsional problems occur. For that reason, the WOB could only be varied in a range between zero to 30 kg-f WOB. This approach was also not beneficial with respect to the control system that is based on drilling with a constant WOB.

11.6.2 Full Azimuth Rotation Approach

The second approach that is based on industry-standard is to use the same principle applied when drilling the vertical section described in section 11.5. This was attempted, but when drilling with the complete BHA in the borehole, which led to very high tortuosity that led to a stuck drillstring.

A solution to this could be to reduce the WOB to limit the ROP, but this was not a possible feature in the implemented control system. Therefore another approach was tried and proved satisfactorily enough.

11.6.3 Little Azimuth Rotation Approach

The final approach tested is based on a trend observed when test drilling. This trend was that when applying little azimuth rotation levels at approximately 10-15 degrees/min, straight drilling was achieved. Based on this observation, the solution became to rotate the BHA with the azimuth system at 10-15 degrees/min while drilling. By doing this, the drilling system could drill straight for a short period resulting in a lower inclination if wanted. This approach is not perfect but was most feasible with the implemented control system and was therefore used.

11.7 Drill Bit

The competition guidelines allow for the use of any bit type, both the provided DSATS bit and any acquired or designed bit (Appendix A). For that reason, it is of high interest to test the bit performance to compare them and select the bit that is deemed to be the best. This determination is essential for further tuning of drilling parameters to achieve the best performance during the competition. It is also interesting to see which bit parameters are affecting the drilling operation the most on a small scale.

Five different bits were planned to be tested: the bit provided by DSATS (Appendix N), two different custom-designed bits described in section 6.10, and two different bits bought from Alibaba Express. These will from now on be referred to as DSATS bit, NTNU bit 1 and 2, and Alibaba bit 1 and 2 respectively and are shown in Figure 6.49.

When using the DSATS bit, the drilling system experienced several problems with respect to instability leading to vibrations. Broken set screws, drive shaft and a stuck drillstring occurred when using the DSATS bit. Because the Alibaba bit 2 worked better, the team decided not to use the DSATS bit anymore due to the risk of destroying parts of the drilling system. Since it was important for the control system to drill with constant drilling parameters, it was also prioritized to only drill with the Alibaba bit 2 and NTNU bit 2. The Alibaba bit 2 has been used for some time before these tests, while the NTNU bit arrived later and was tested later than the Alibaba bit 2. These circumstances led to that only testing of Alibaba bit 2 and NTNU bit 2 will be presented and discussed in this section.

The drilling tests were conducted autonomously to reflect the circumstances on the competition better. A pilot hole of 2.54 cm (1 inch) length was drilled with a straight BHA and a 5.08 cm (2 inches) diameter bit from Alibaba to provide stability and resemble the effective diameter of

the borehole when drilled with a bent sub. A vertical section was then drilled as explained in section 11.5 with a WOB setpoint of 11 kg-f. After the vertical section, the well path was kicked off with constant azimuth and drilled through the sample with a constant WOB setpoint of 14 kg-f for the Alibaba bit 2 and 26 kg-f for the NTNU bit 2. A constant RPM of 900 was used for the testing. All tests were conducted in rock samples made at the same time with the same concrete to water ratio and mixing time, 3.0L/25kg and 5 minutes, respectively. The measurements may vary, however, because of differences in bit-rock interaction or other factors. To best rule out unrepresentative data, trends are observed over time.

It is important to quantify the importance of different parameters when analyzing bit performance in a small-scale drilling rig and the environment it drills in. A commonly known trade-off is ROP and bit aggressiveness at the expense of stability, vulnerability to vibrations, and bit damage. Autonomous operations benefit from a consistent and reliable system, thus setting these criteria as a high priority in the bit tests. The bit parameters evaluated and compared are ROP, torque, vibrations, and hole quality.

11.7.1 Rate of Penetration (ROP)

The ROP data is an estimate based on the position and velocity of the hoisting system. Measurements are made at a time step of 1/25 s. Figure 11.16 shows ROP for Alibaba bit 2 as a function of time for the drilling test described above, while ROP for NTNU bit 2 is shown in Figure 11.22(c). For both plots, there is an interval of zero ROP. This interval is due to a break in drilling after the vertical section is drilled and KOP is reached. A difference in the plots is that for the NTNU bit 2 plot, ROP measurements after the KOP have a break in drilling for each 5 cm drilled. This is because the run in Figure 11.22(c) was done with a functioning sensor card, and survey points were taken. The fact that the run using Alibaba bit 2 has a WOB set point of 14 kg-f while the run using NTNU bit 2 uses WOB set point of 26 kg-f is a weakness with respect to comparing the runs. Still, it is an interesting observation that with the NTNU bit 2, it is possible to use such a high set point value. By examining the two plots, it is clear that the NTNU bit 2 is outperforming the Alibaba bit 2. The Alibaba bit 2 has a ROP ranging from around 0.5 cm/min to 2 cm/min while the NTNU bit 2 is ranging from 4 cm/min to 12 cm/min.

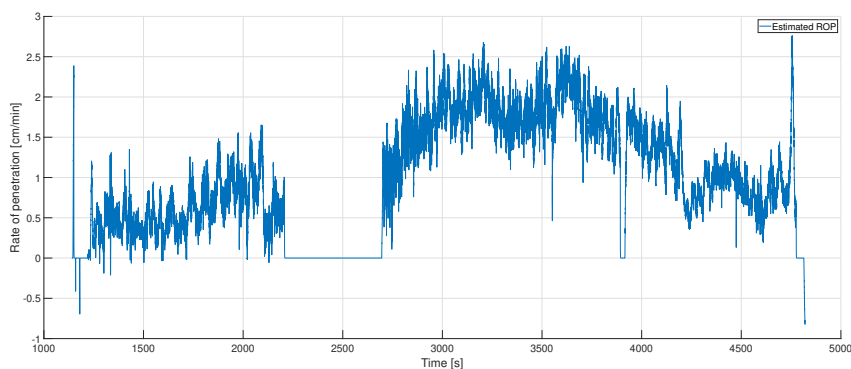


Figure 11.16: ROP measurements for Alibaba bit 2.

11.7.2 Torque

It is important to minimize the torque to avoid twist-off incidents, and torque variations such as significant spikes should be limited. The torque measurements are from the same run as the ROP measurements are based on. Figure 11.17 show the torque measurements for Alibaba bit 2 while Figure 11.22(b) show the torque measurements for NTNU bit 2. The torque ranges from 0.05 Nm to 0.3 Nm for the Alibaba bit 2. It is mostly fixed around 0.15 Nm for the building section that comes after the KOP. For NTNU bit 2, it ranges from 0.05 Nm to 0.35 Nm. For the building section, it is mostly fixed around 0.2 Nm. After each survey point, there is a great spike in the torque when starting drilling. This spike is not considered a problem and is explained by the rapid change from 0 to 900 RPM. The two plots show that the torque is much more stable for the NTNU bit 2, and it has much fewer large torque spikes than Alibaba bit 2. The torque measured for NTNU bit 2 is also with a WOB set point of 26 kg-f. To conclude, the NTNU bit 2 performs much better with respect to torque-related issues.

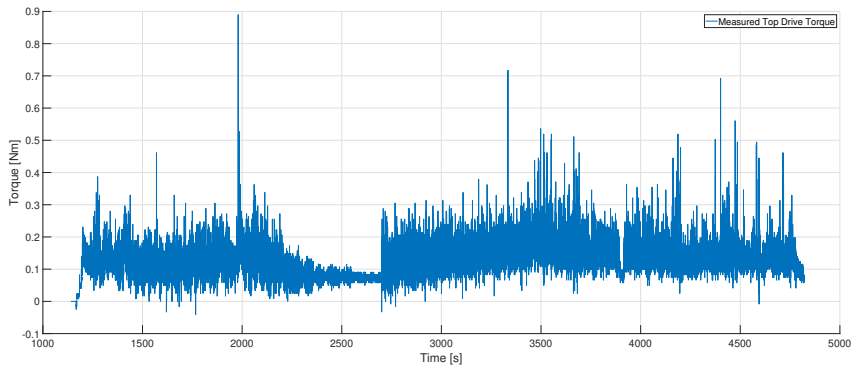


Figure 11.17: Torque measurements for Alibaba bit 2.

11.7.3 Vibrations and Hole Quality

Operation integrity must be maintained through good hole quality, leaving fast and efficient drilling irrelevant if not the case. Stability and vibrations are highly related to hole quality, where differences were observable between the bits. With a fixed bent sub and an azimuth system, the hole quality is more vulnerable due to increased effective diameter and extensive vibrations.

Vibrations are also an issue for the sensor data measurements. Figure 11.18 and Figure 11.19 shows the measured accelerometer data noise for the sensor card when drilling with the Alibaba bit 2 and NTNU bit 2. The plots show the noise for the building section that comes after the KOP. The intervals with no noise are at survey points. The run with Alibaba bit 2 has significantly more noise than the run with NTNU bit 2. Since the drilling rig only measures sensor data at survey points, this is not a problem with respect to sensor data, but if MWD were implemented, it would be much easier with the NTNU bit 2. A more interesting point with the plot is that it backs up the observations done when drilling. When drilling with Alibaba bit 2, the lateral vibrations were quite extensive, and it could be seen on the drillpipes movement. Drilling with NTNU bit 2 had close to no vibrations compared to the runs with Alibaba bit 2.

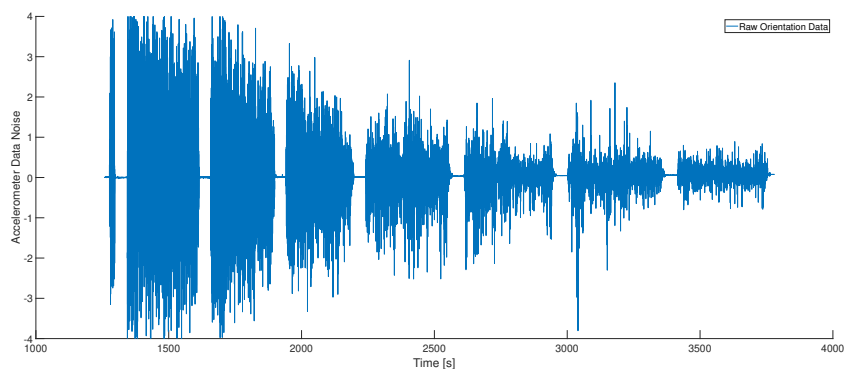


Figure 11.18: Accelerometer data noise for Alibaba bit 2.

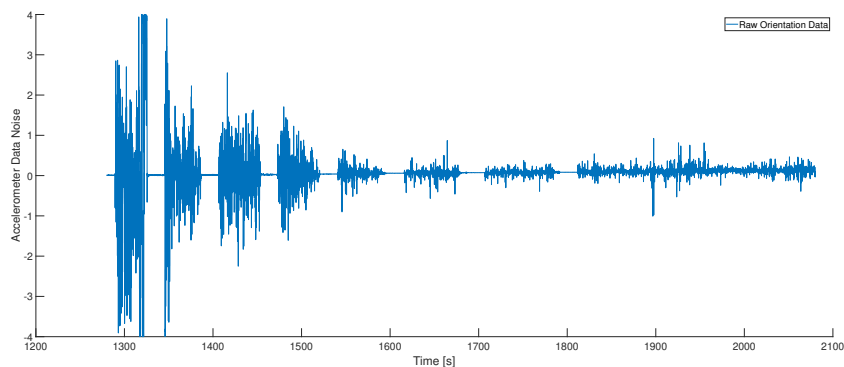


Figure 11.19: Accelerometer data noise for NTNU bit 2.

The bits did also perform quite differently with respect to hole quality. Figure 11.13 shows a vertical hole quality for the Alibaba bit 2 while Figure 11.15 shows the hole quality when drilling with NTNU bit 2. Measurements with a caliper also show that Alibaba bit 2 drilled an uneven hole when drilling with a constant azimuth. This could be due to the vibrations. NTNU bit 2 drilled a gauge hole with excellent hole quality. When the drilling operation was done it was necessary to use bit rotation to trip out of the well. This confirms that the borehole is a gauge hole. With respect to vibrations and hole quality NTNU bit 2 is outperforming Alibaba bit 2.

11.7.4 Overall Performance

The testing shows that the self-designed bit was much better than the other bits available. This confirms that the work investigated in making self-designed bits was time well spent. It was not

surprising that the self-made bit performed better due to the extensive work performed to obtain it. Although its excellent performance was not expected to that extent, this was a very positive feature that made the drilling system much better.

11.8 Sensor Card Tests

At the end of the Equinor-demo described in subsection 11.9.2, the position estimate was retrieved from the sensor data. To compare sensor data with actual drilled well path, the last measurement was compared to the total displacement in x-direction, which in this case, was the inclination direction. The sensor gave an estimate of displacement equal to 4.54 cm. The total displacement was measured with the method illustrated in Figure 11.25, and found to be 13 cm. This confirms that the sensor card estimates are highly inaccurate.

It can be different explanations for this. First off, the estimate is considered at a point extrapolated from the sensor card location to the bit depth location. This extrapolation might be inaccurate, causing reproduction defects as the system drills. With a reproduction defect in a constantly updated system like this, the error will increase in magnitude with time. In addition to that, the estimate does not take into account the additional inclination of 7° from the bent sub. Although the sensor card estimate is deviating from the actual value, it makes reasonable measurements that resemble the well path as shown in Figure 11.20. It plots a curve similar to the observed curve, only with a lower inclination.

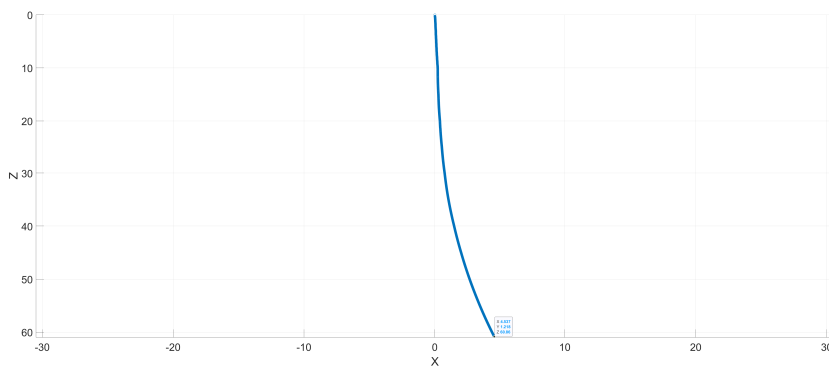


Figure 11.20: Plotted well path from the sensor card estimates of position.

11.9 Competition

11.9.1 Pilot Hole

According to the guidelines (Appendix A) the pilot hole should be located at the intersection point of the diagonals of the rock sample. The hole was pre-drilled with a straight BHA and a 2 inch bit to provide stability and room for a bent BHA to fit. Figure 11.21 shows the intersection point and the resulting pilot hole.



(a) Aligning the BHA with the intersection point.

(b) Finished 2.54 cm pilot hole.

Figure 11.21: Pilot hole procedure.

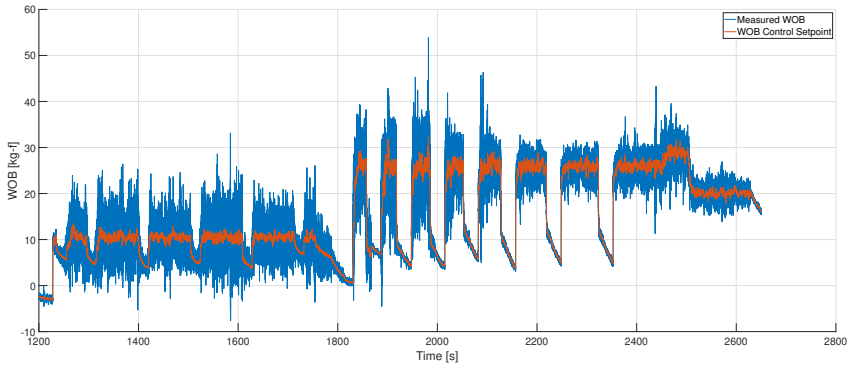
11.9.2 Competition Run

On the day of the competition, things were hectic. Due to the pandemic situation, everything had to be live-streamed with a minimum of three cameras through Microsoft Teams. The team had to provide commentary and monitor the chat for questions underway while monitoring the drilling process. In addition to this, the committee requested a second drilling run described in subsection 11.9.3, after the competition run. With this stressful situation, the operator forgot to save the drilling data from the actual competition run. This data was overwritten when the program was

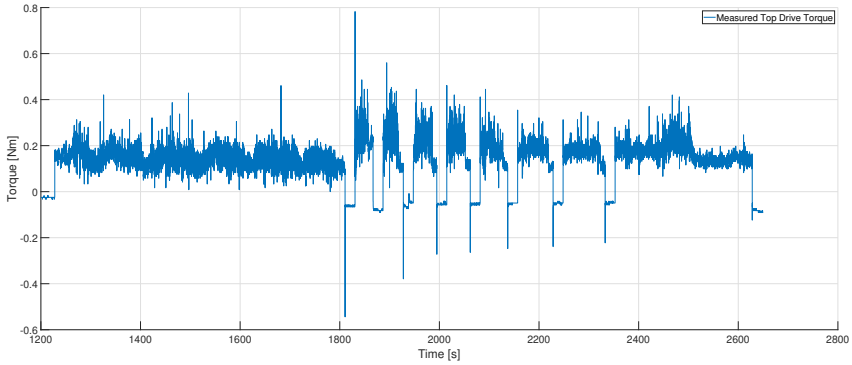
restarted for the extra run. Luckily the team had a drilling demo for Equinor the day after with the same setup. The results from this demo are presented in this section.

The autonomous run first drilled the vertical section with alternating azimuth rotation direction as observed in Figure 11.23(b). The alternating direction was done to prevent the USB cable from winding up. After the vertical section was drilled, the azimuth homed in on the initial azimuth direction to prepare for directional drilling. This can be observed around 1 800 s in Figure 11.23(b). After the homing, a survey point was taken before kicking off. Figure 11.22(c) illustrates that the ROP increases significantly after drilling the vertical section. The ROP in the vertical section was kept at a low value on purpose to give the bit cutters time to drill a smooth borehole. Figure 11.22 shows that surveys were taken at an interval of 5 cm where the motors were stopped to reduce vibrations and noise.

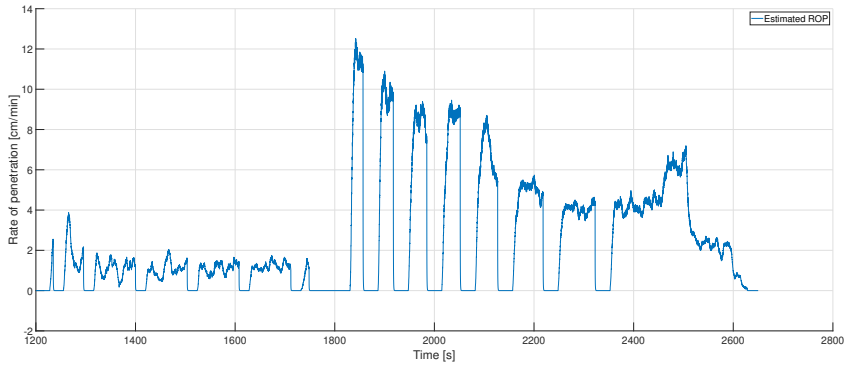
Figure 11.23(c) shows that the sensor card sent commands to adjust the azimuth to hit targets after kicking off. Measurements from the sensor card continuously updated the azimuth system with the offset from the target, slowly decreasing the azimuth adjustments while approaching the target. A decreasing trend can be observed in ROP in Figure 11.22(c). This can be explained by increasing drag as the BHA, and pipe descends in the rock sample. At 2500 seconds a drop in WOB can be observed in Figure 11.22(a). This was an intended WOB drop to decrease the ROP when approaching the rock exit phase. After 2 600 seconds, the rock exit detection state kicked in and shut down the system after a mean ROP value lower than 0.3 cm/min for 15 seconds as shown Figure 11.22(c). The complete drilling run from the vertical section to the rock exit took approximately 23 minutes.



(a) WOB

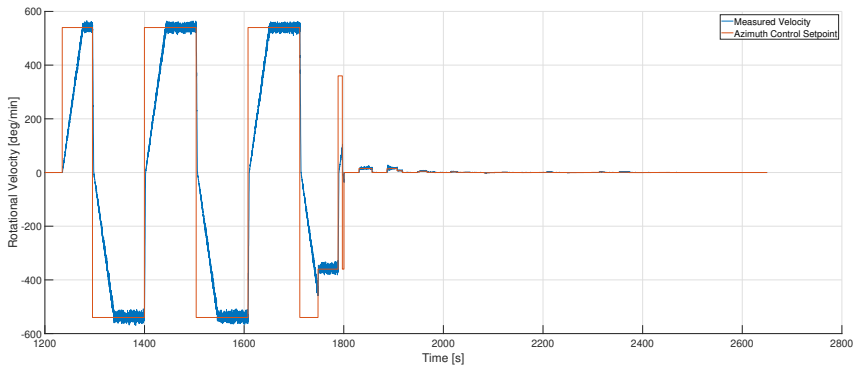


(b) Torque

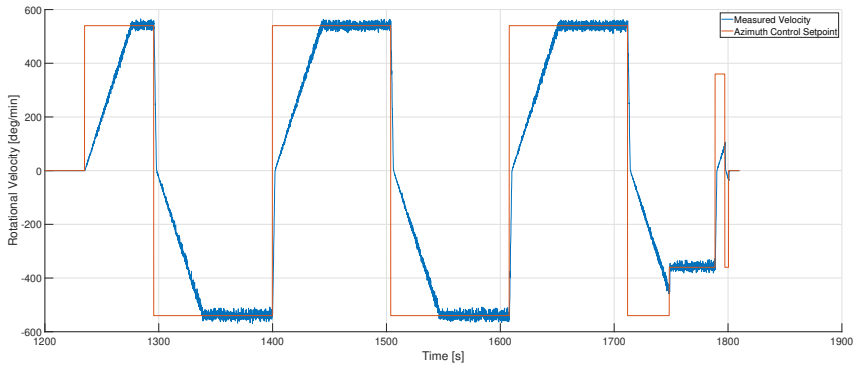


(c) ROP

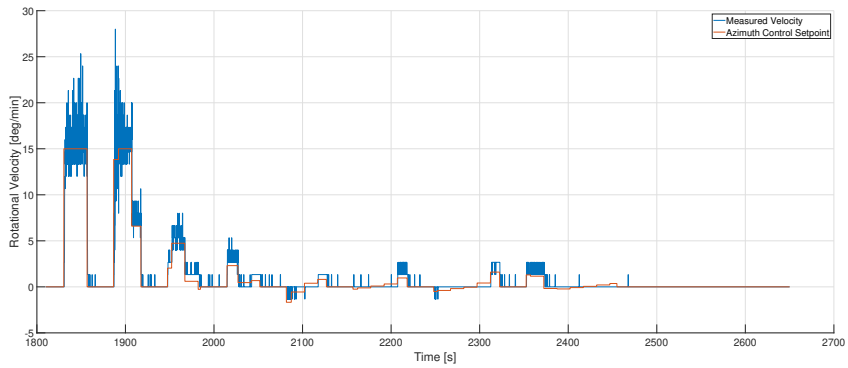
Figure 11.22: WOB, torque and ROP plots from the Equinor-demo run.



(a) Azimuth rotation full run.



(b) Azimuth rotation vertical section.

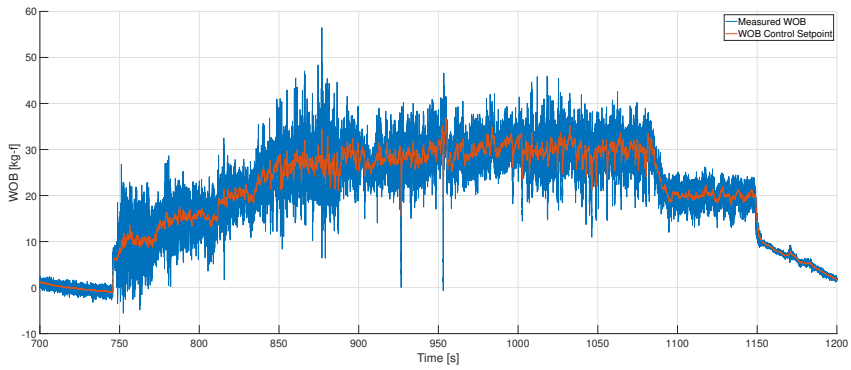


(c) Azimuth rotation after KOP.

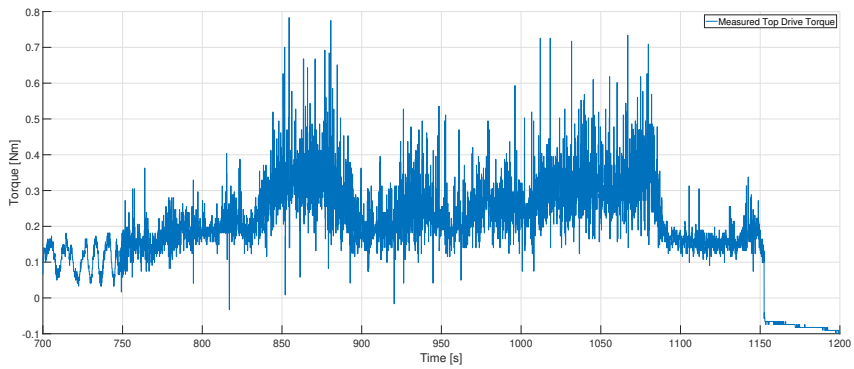
Figure 11.23: Measured azimuth rotational velocity during Equinor-demo run.

11.9.3 Extra Run

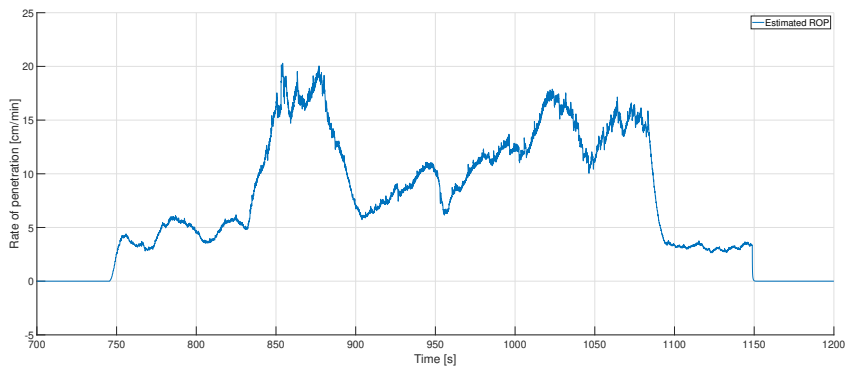
After the actual competition run with given points, the committee wanted to see how fast the rig could drill and how much inclination it could build. For that reason, the team executed another run without a pilot hole and vertical section, thus building an angle from top to bottom. The run was conducted manually with a constant RPM of 900 and gradually increasing the WOB to maximize the ROP.



(a) WOB



(b) Torque



(c) ROP

Figure 11.24: WOB, torque and ROP plots from the extra run during competition.

As illustrated in Figure 11.24(a), the WOB was gradually increased to 31 kg-f where it was

decided to stop the increase due to unfamiliar noises and torque spikes. At around 850 seconds the WOB approached 30 kg-f. Significant torque spikes at short intervals can be seen at this point in Figure 11.24(b). Although the WOB was maintained at around 30 kg-f, the ROP dropped from 18 cm/min to 6 cm/min at 870 seconds. A possible reason for this is that the upper stabilizer in the BHA was in tension in the riser due to the built angle. After drilling for some time, the ROP gradually increased to around 15 cm/min again as shown in Figure 11.24(c). The drop in ROP at 1 050 seconds is due to the operator lowering the WOB. At 1 190 sseconds the WOB was lowered to 20 kg-f to reduce the ROP at rock exit.

After finishing the run and pulling out of the hole, measurements were conducted to decide how much inclination the rig had built. The measurement process is shown in Figure 11.25. The measurements gave a displacement of 17 cm, which corresponds to an inclination of approximately 37°. This confirms that the theory described in section 13.5 is more accurate than previously assumed.



(a) Measured distance from well center equal to 30.5 cm. (b) Measured distance from end point equal to 13.5 cm.

Figure 11.25: Measured displacement of 17 cm.

(This page is intentionally left blank)

Chapter 12

Budget and Accounting

The budget related to this thesis project is limited to \$10,000 USD by the Drillbotics guidelines (Appendix A). NTNU and the Norwegian oil and gas operator company Equinor fund this project. The Drillbotics guidelines specify that the funding should cover expenses related to "hardware, software, and labor to construct and operate the team's equipment". Subsequently, the guidelines state that "In-kind" contributions will not be included in the team's project costs". This can be interpreted in various ways and may therefore be interpreted to benefit the project in the best ways. This chapter will cover the expenses included in the budget, expenses considered as "in-kind" contributions, and expenses related to labor[1].

12.1 In-house Contributions

The Drillbotics competition is a well-recognized competition for international universities around the world. It is a privilege to participate in the competition and represent NTNU. For this reason, many instances at the university are eager to contribute towards the common goal of winning the competition. Recycled materials and in-house equipment are not considered to contribute to the total cost of the project. Many rig components in this project have been recycled from previous years, and nearly all equipment used to assemble the rig was already in the workshop at NTNU. The BHA, mounting parts for all three motors, and the hydraulic swivel were made in-house with materials available in the workshop. The rock samples were created in wooden boxes made by previous teams.

Because this year's project team surpassed previous teams' accomplishments quite early, significantly more drilling sessions were completed, thus needing more rock samples. New wooden

boxes were made by unused workshop materials and therefore not considered a project expense. The cement used to create the rock samples is considered to go under the in-kind contribution category. Lyng Drilling fully sponsored the custom drill bits made in collaboration with Lyng Drilling. Two new computers were obtained to achieve the desired performance of the system. These are not considered in the budget because they remain the property of NTNU and can be used in other projects. Because the project does not consider recycled parts an expense, unused components ready for next year will also not be considered. The team acquired a significant amount of drillpipes and rods for the project. Only the amount by which the team actually used will be considered in the budget. The remaining parts are considered university property to be used in upcoming projects.

12.2 Labor

By interpretation of the guidelines, costs related to salaries for labor are not included in the budget. However, salaries contribute to a large percentage of cost estimates in a "real" project and should therefore be mapped. The project involves four students, four supervising professors, a support crew of two lab engineers, and two workshop engineers. The students are estimated to have spent an average of 50 working hours a week. The number of hours has varied throughout the project but will serve as a reasonable estimate. These working hours include meetings, project management, design, calculations, testing, and theses writing. The supervising professors have been available most times but mainly contributed through the one-hour-long meetings held every second week. The number of hours spent by the support crew varied considerably from one week to the other, depending on the challenges.

Table 12.1: Overview of the labor expenses related to the theses project with an exchange rate of 1 USD = 8.3 NOK as of 05.05.2021.

	Hours/week	# Weeks	Hourly wage [NOK]	# Employees	Total Cost [NOK]
Students	50	18	170	4	612 000
Supervisors	0.5	18	520	4	18 720
Support Crew	5	18	370	4	133 200
Total					763 920 NOK \$92 038 USD

From Table 12.1, it is apparent that a total budget of \$10,000 USD would be insufficient if labor expenses were included.

12.3 Funding

The Drillbotics guidelines state that "The students shall find a source of funding (...)" [1]. The budget of \$ 10,000 USD has typically been provided by a collaboration between NTNU and Equinor. This year, Equinor is funding the project with \$2,500 USD and NTNU and Better Resource Utilization in the 21st century (BRU21) funds the remaining part. Because of the pandemic virus Covid-19, it was recommended by the NTNU administration to keep expenditures at a minimum, preferably less than 75 000 NOK. However, should expenses exceed this, the \$10,000 USD would be fully covered by BRU21 and NTNU.

12.4 Expenses and accounting

This section presents the actual expenses in the project.

Table 12.2: Total cost throughout the project with an exchange rate of 1 USD = 8.26 NOK as of 08.06.2021.

Component	Price per item (USD)	Quantity	Total Cost (USD)
Drill Chuck	43.42	1	43.42
Hollow shaft gearbox	626	1	626
Shipping gearbox	135	1	135
Servomotor + Driver	602	1	602
Universal joint	27.4	4	109.6
Radial ball bearing	30.92	4	123.68
Aluminum drillpipes	2.57	110	282.7
Aluminum rod	1.1	120	132
Shipping drill pipe and rod	182	1	182
Generic drill bit 1	23	3	69
Generic drill bit 2	20	5	100
Sensor card and USB cable	41	5	205
Inspection camera	33	2	66
Azimuth gearbox	377.5	2	755
Lenze Ethernet I/P module	430	1	430
Torque sensor	156	3	468
Hard drive and cable	166.57	1	166.57
Drillpipe connector	39.25	4	157
Mixing nozzle glue	30	1	30
Pilot hole bit	31.67	3	95
Silicone material	304	1	304
Titanium and steel rod	9.65	75	724
Top Drive motor	1730	1	1730
Epoxy glue and sensor card	192	1	192
Total Cost (USD)			\$ 7 730
			NOK 63 850
Balance (NOK)			NOK 11 150

Table 12.2 shows all the expenses related to parts and components in the project. The exchange rate is 8.26 NOK/USD as of 08.06.2021. The balance is calculated with respect to the recommended budget of 75 000 NOK, ending up at 11 150 NOK. Considering that the new design required many new components, this balance is deemed acceptable.

Chapter 13

Challenges and Lessons Learned

A part of every technical project is unexpected challenges and how to handle them. Some have been comprehensible, while others have influenced the project timeline greatly. Nearly all problems were fixed permanently, but some required provisional solutions because of time and budget limitations. The challenges and solutions are presented in this chapter.

13.1 Project Management and Norwegian Holidays

The thesis project is a multi-disciplinary project with students from the Department of Geoscience and Petroleum (IGP) and the Department of Engineering Cybernetics (ITK). Because there was only one student from ITK and the directional requirements were more complex than previous years, some of the workload related to cybernetics was delegated to the petroleum students. To understand, operate and maintain the rig, the students from IGP faced a steep learning curve with respect to low-level control, communication protocols, and downhole measurements. For example, one of the petroleum students designed and implemented the API and because this was an unknown topic, the process was time-consuming but released workload for the ITK-student. The month of May 2021 had holidays that landed on the day before or after the weekend, which led to periods up to five days without the support team present. The project timeline was greatly affected when components broke during these periods.

13.2 Corona Virus

The coronavirus led to several challenges during the project's lifetime. Multiple virus mutations introduced stricter rules and guidelines for infection control and led to sporadic lockdowns

throughout this project. Limited access to the workshop caused setbacks and reduced productivity. Essential personnel involved were in and out of quarantine and home office because of the infection risk. The pandemic generated uncertainty surrounding the conduct of the competition. Guidelines and information related to the competition scenario were set by the DSATS committee, and their final confirmation was given only 18 days before competition day. The most significant change occurred nearly two weeks before the competition day. The initial plan was for DSATS to ship one rock sample to each university. However, all teams were instead requested to order a sandstone sample from a local producer. This led to a stressful situation because it was difficult to locate a homogeneous sandstone with the required dimensions and rock properties in such a limited amount of time. The solution was to use the same samples of cement block which the team has used for test drilling.

13.3 Locating A Torque Sensor

Increasing the gear ratio in the azimuth system required the authors to find a hollow, water-resistant torque sensor. The sensor had to be capable of measuring small deviations in torque and preferably match the mounting points on the hollow gearbox (see subsection 6.7.1). The initial plan was to install a thin plated, low-profile sensor to reduce the length of the T-shaft and mount it directly to the hydraulic swivel. However, such a sensor was proven difficult to locate "off the shelf". The solution was to use a hollow, cylindrical, static torque sensor.

13.4 Rig System Alignment

Aligning the rig systems has been a repetitive challenge each year of the competition. The rig is located in a workshop on ground level with a concrete floor. This floor has a varying tilt depending on the location in the workshop. All motor connections and drilling components have been designed to align with respect to the drill floor stabilizers. However, because of the tilted floor on which the rock sample sits on, all rig components must be re-aligned with respect to the drill floor.

The authors learned that aligning components is a time-consuming process. Mainly because frequent mechanical alterations on the rig required new alignments, having a domino effect. All the components that had to be aligned are presented in the following sections. The solutions made have been described in detail. All have been done with respect to the drill floor stabilizer.

13.4.1 Hydraulic System

The hydraulic swivel was modified to enable clock-wise and counter clock-wise rotation of the drilling system. The swivel holder was re-used from the previous design and supported with

steel plates to align with the rest of the rig components. The new mechanical rig design caused misalignment between the hollow swivel shaft and azimuth T-shaft and between the swivel and drillpipe. This led to a slight bend in the drillpipe. It also caused a leakage above the swivel because the O-ring between the shafts was not deformed enough to seal around the rotating rod. Two steel plates, shown in Figure 13.1, were added to adjust the swivel.



Figure 13.1: Hydraulic swivel alignment.

Leakages

When designing the swivel shaft, the idea was to seal around the rotating rod with an O-ring placed at the contact point between the swivel shaft and the T-shaft. In the design progress, however, the dimensions of the groove holding the O-ring were incorrect. This resulted from a lack of sealing knowledge and miscommunication between the team members and supervising engineer.

The initial design proposed an inner diameter of 7 mm throughout the swivel shaft. This would, however, increase the risk for water migrating up towards the T-shaft. The solution was to decrease the inner diameter to 5 mm above the water inlet and keeping it at 7 mm below the inlet. However, the groove on the swivel shaft was originally designed to fit an O-ring for the initial 7 mm design.

When choosing O-ring dimensions, one must account for its shape when deformed. The shape depends on the direction of forces applied on the O-ring, axial, or radial. Axial forces will deform the O-ring in the vertical direction and vice versa. The choice also depends on whether it seals

against a static or dynamic component. In the swivel shaft, the assumption was that the O-ring would seal against a rotating rod and be deformed by the rod and groove walls. This required a design for a dynamic seal with deformation in the axial direction.

However, it turned out that the actual force applied to the O-ring was supposed to be axial. The groove floor and the inside of the T-shaft should deform it in the radial direction, thus squeezing it around the rod. With a groove floor of 2.65 mm (after decreasing to an inner diameter of 5 mm) and groove wall of 2.70 mm, the O-ring was too thin to be squeezed in the axial direction. The solution was to make small disks of Teflon, cut by hand, with an outer diameter of 10.30 mm and an inner diameter of 4 mm. The disks were placed underneath the O-ring to increase its height and enable sealing around the rod and between the two shafts. The solution is illustrated in Figure 13.2, where the black circles are the O-ring, and the white boxes are the Teflon disk. Another solution to this challenge could have been to mill or file down the top of the groove. This solution would allow the use of the original O-ring without the Teflon disks.

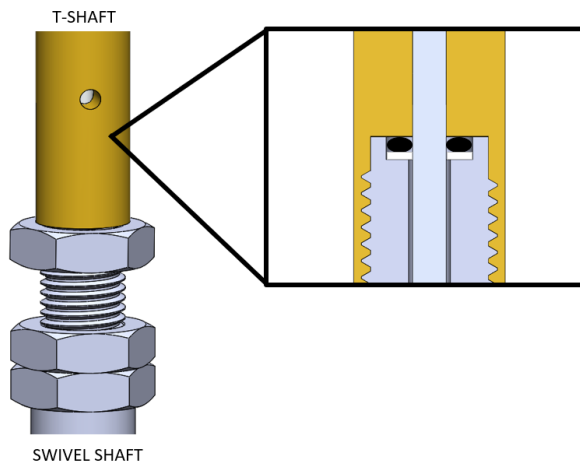


Figure 13.2: T-shaft and swivel shaft connection with O-ring and Teflon disk.

When designing grooves, the lesson learned was that one must account for their total deformation when all parts are mounted together. Also, the team learned was that designs could be subjected to changes along the way. It is wise to finish the design and manufacturing early, such that unexpected changes can be handled in a timely manner. The communication between the team members and engineers was good, and the discussion went back and forth multiple times. This was done over Teams due to the corona pandemic, which may have influenced the quality check before the design proposals were sent to the workshop.

13.4.2 Azimuth System

It was decided to recycle an old top drive shelf to anchor the azimuth system to the carriage mount. The shelf, which had minor offsets with respect to the swivel holder, increased the downhole torque between the drillpipe and borehole wall. The solution was to use thin steel plates, shown in Figure 13.3.



Figure 13.3: Alignment of azimuth system.

The azimuth motor and the right-angled gearboxes are only attached to the system using the hollow helical gearbox. The components are hanging in the air, thus generating a slight forward tilt to the system. Vibrations from drilling operations provoke the tilt as well. The solution was a 3D-printed pin in yellow, shown in Figure 13.3.

In addition to vertical alignment, the shelf needed additional plates to adjust the height of the azimuth system. The aluminum plate in Figure 13.4 functions as an adapter between the shelf and the torque sensor. The plate was made 2.5 mm thinner than intended because of limited materials available in the workshop. This led to a tensile load causing inaccurate measurements by the torque sensor and the risk of damaging the sensor during rotation. A simple fix to this was a 3D-printed disk in yellow, seen in Figure 13.4.

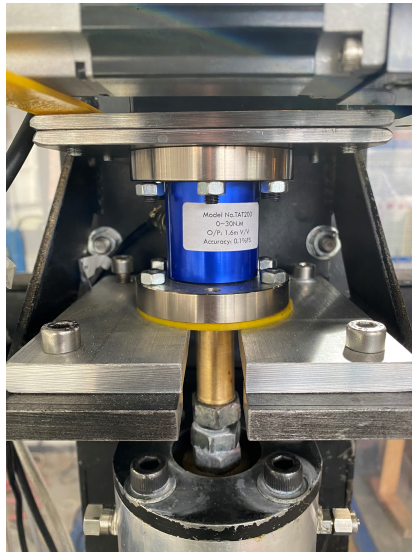


Figure 13.4: Azimuth system mount adapter.

13.4.3 Top Drive Motor

The new top drive motor (see subsection 6.6.2) required a new mount to fit the carriage mount on the rig. The hoisting motor mount inspired this design. An aluminum block was made to connect the motor to the carriage mount, shown in Figure 13.5. The block caused the drill chuck to grip the rod with only two out of three jaws, leading to slip motion and lack of torque and rotation transmission. It was fixed by reducing the thickness of the block.



Figure 13.5: Top drive adaptor block.

13.4.4 Rig Frame

Halfway through the project, the rig had to be moved to another location in the workshop due to maintenance of the workshop floor. Because the workshop floor is not leveled out evenly from one place to another, the rig frame was tilted a full 10-20° at the new location. Figure 13.6 shows how this problem was fixed. The rig frame has adjustable feet adjusted to level out the rig, thus not impacting all the other alignment measures.



(a) Adjusting rig frame feet.



(b) Spirit level used to align the frame.

Figure 13.6: Aligning of rig frame.

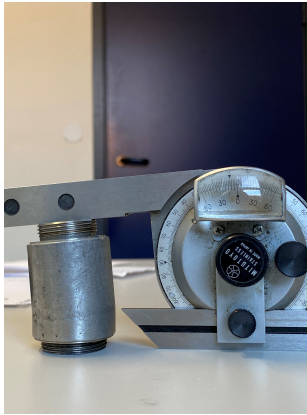


Figure 13.8: Measured angle of bent sub equal to approximately 5 degrees.

The assumption implies that the theoretical calculations have been too optimistic, resulting in a deviation of 6 degrees. To calculate the new angle and compensate for the deviation, Equation 4.1 and 5.2 can be combined to get:

$$\theta = \frac{\phi(L_1 + L_2)}{2 \cdot CL} \quad (13.1)$$

To compensate for the deviation in angle, 6 degrees are added to the required inclination of 30 degrees:

$$\theta = \frac{36^\circ(0.105m \cdot 0.1m)}{2 \cdot 0.534m} = 6.91^\circ \quad (13.2)$$

To simplify the process of making the new BHA and reduce the risk of accuracy failure, the new angle for the bend was 7 degrees. Figure 13.9 shows the verification test of the bent sub angle after production. The result was an angle close to 7 degrees.

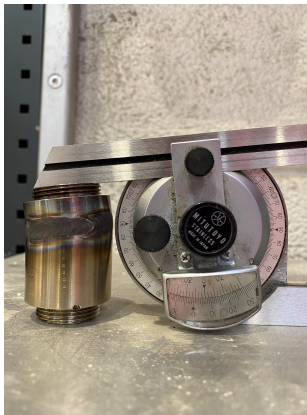


Figure 13.9: Verification of new bent sub equal angle.

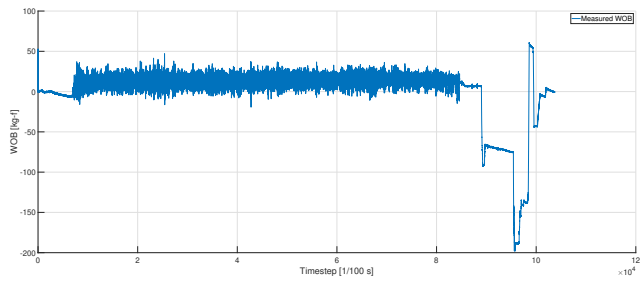
13.6 Challenges Related to Stuck Drillstring

Various methods were examined to increase azimuth during drilling. Drilling straight forward, i.e., drilling with constant inclination without changing direction, can lead to downhole challenges. A suggested method to drill straight was to turn the azimuth system while applying WOB and rotating bit. This would mean making a hyperbolic spiral (or reciprocal spiral) going down into the rock, drilling a slightly larger borehole. This was not feasible with the first top drive motor (see subsection 6.6.1). The RPM was too low, which resulted in high torque measurements downhole causing stuck bit and thus twisting off the rod.

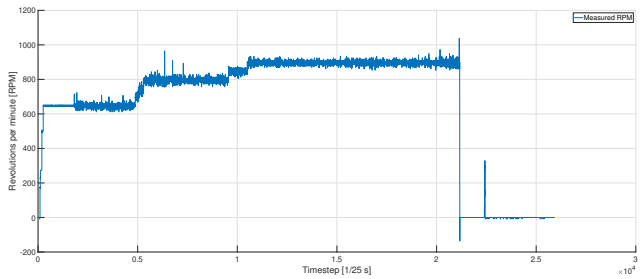
The new top drive motor (see subsection 6.6.2) yielded a higher RPM. The authors had previously experienced that a greater RPM decreased the overall torque and torque spikes during drilling. A drilling run was conducted to verify if the method was applicable with the new top drive motor. The run would also indicate which velocities it was possible to turn the azimuth direction successfully. It was run at a constant WOB of 12 [kg-f] and 900 RPM as shown in Figure 13.10, and then gradually increasing the rotational velocity of the azimuth system as shown in Figure 13.11.

Comparing the performance indicated by the ROP in Figure 13.10(d) with the rotational velocity in Figure 13.11, the rig performed without complications until reaching a velocity of approximately 70 deg/min. At this rate, the ROP decreased when increasing azimuth rotational velocity. Quickly after reaching 100 deg/min, the bit stuck, and a torque spike was observed in Figure 13.10(c). Because the WOB controller did not manage to release the bit, it was decided to stop all motors. The next attempt was to hoist the system up to inspect the borehole and to verify if the hole was vertical. This would ascertain that the method enabled straight drilling.

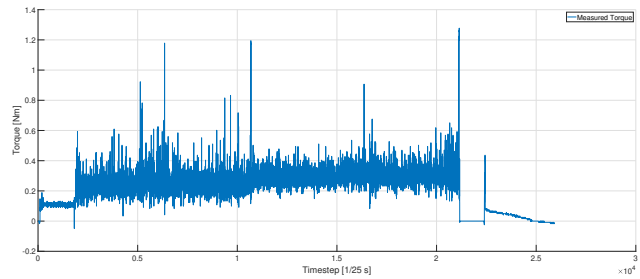
Because the system had been rotated several rotations while drilling, it was first attempted to back ream and rotate azimuth counter-clockwise to match the well path drilled. This can be seen in Figure 13.10 at which the WOB is negative and at a velocity of 300 RPM. A negative azimuth rotation in Figure 13.11 is also seen. This wasn't easy because the azimuth rotational velocity had been changed inconsistently. After hoisting up for a short period of time, the WOB fell drastically to -200 [kg-f], shown in Figure 13.10(a). This meant that the drilling system was stuck and stretched. The WOB was then increased to try and settle at a measured WOB of zero. After a few iterations, a WOB of approximately zero was reached, and the system was shut down.



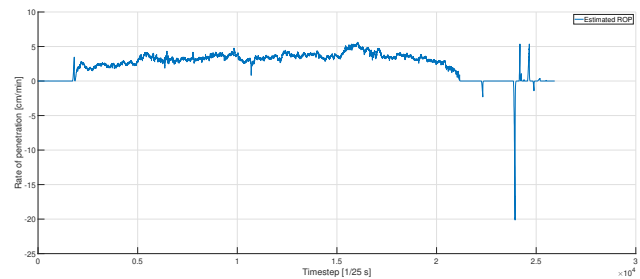
(a) Measured WOB with a setpoint of 12 [kg-f].



(b) Measured rotational velocity when ramping up to 900 RPM



(c) Bit torque during the test.



(d) Rate of penetration during the test.

Figure 13.10: Drilling parameters during the stuck pipe run.

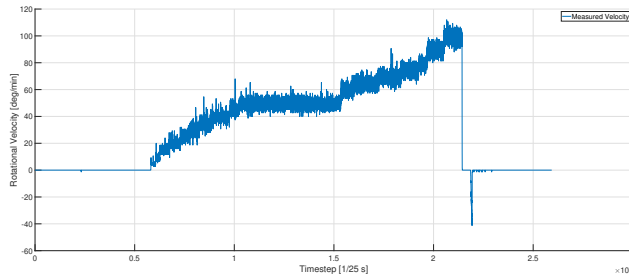


Figure 13.11: Measured azimuth rotation with gradually increasing set-point.

Because the system was stuck and there was limited space below the drill floor, it was decided to cut the pipe and rod with a hacksaw. This enabled the removal of the block and BHA. After moving the block, it was easy to remove the remaining pipe with the BHA attached simply by rotating and pulling by hand. This implied that the system had been misaligned while drilling, causing tension by the drillpipe stabilizer squeezing against edges created in the borehole by azimuth change. This test verified the "azimuth-change while drilling"-concept for a total maximum azimuth change of 15 degrees, which is the competition requirement. However, rotating the system while drilling to drill straight is problematic because of the problem encountered above.

13.7 BHA Integration of Sensor Card

The sensor card is sensitive to mechanical stress, water, dust particles, and metal during operation. It must be protected from these to ensure optimal performance and prevent disturbances or short-circuiting. The sensor is placed in a compartment in the sensor housing as shown in Figure 13.12. The USB cable, marked in white, is used for communication and power and exits the BHA through the upper stabilizer.

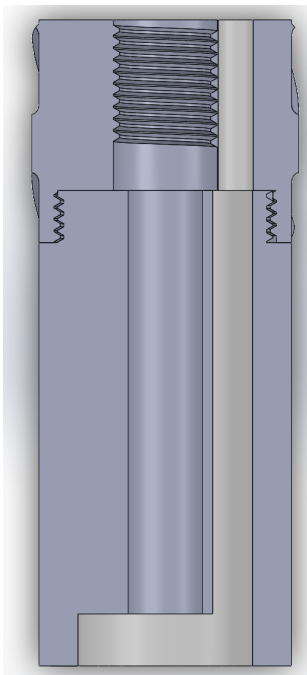


Figure 13.12: Location of downhole sensor card in the BHA.

13.7.1 Epoxy

The most critical measure to protect the sensor card is to prevent contact with water and dust, keep it from moving inside the BHA and touch the surrounding metal. Epoxy has previously proven successful for this purpose, and this design will continue to use it.



Figure 13.13: 3M Scotch-Weld Epoxy Adhesive DP110.

The specific epoxy mix used is 3M Scotch-Weld Epoxy Adhesive DP110 as shown in Figure 13.13. The reasons for choosing this epoxy is [3]:

- Provides strong, permanent bond even under vibration and impact
- Low viscosity; easy to apply and dispense
- Not electrically conductive (volume resistivity of $6.90 \cdot 10^{10}$ ohms-cm)
- Good adhesion to plastics and metals
- Water resistant (cold water)

13.7.2 Cabled Implementation

The first and easiest method for sensor card communication and power supply was through a USB cable. This solution required a considerable amount of space in the BHA. Hence, the first suggestion was to solder the card directly into a micro USB connector. This connector required very precise soldering and was therefore quickly ruled out.

The connection required the male micro USB cable to be connected directly to the card. Because the connectors on such cables are bulky, they did not fit into the BHA. The connector on the micro USB cable was therefore trimmed down to an absolute minimum using a knife. Such trimming required high precision to avoid cutting the wires inside the cable and was executed carefully. After trimming the connector, it was possible to fit it in the BHA.

First Sensor Card Iteration: Electrical Tape and Epoxy

For the first attempt, the sensor card sides were wrapped with electrical tape to prevent short-circuiting to the metal housing when placed inside the BHA. The sensor compartment was then filled with epoxy from the top and bottom. Filling the compartment from the top was challenging because of the limited space in the stabilizer where the USB cable was pulled through. Because of high viscosity, it was not possible to fill the compartment from the bottom only. Although the application was not optimal, the short hardening time of the epoxy forced the team to proceed. The epoxy was left overnight to dry. When connected to a computer, the functionality of the card had not changed. It was able to communicate using the USB cable and Bluetooth. The BHA with the sensor card integrated was then submerged in a sink, as depicted in Figure 13.14, for ten minutes. This was to test whether the epoxy sealing was waterproof. When re-connected to a computer after the test, the card was not detectable and appeared as an unrecognized device. It was concluded that the epoxy application was insufficient and that the epoxy seal surrounding the

sensor card had been broken. The BHA was then prepared for a second attempt by using a heat gun to remove the epoxy and sensor card.



Figure 13.14: Bottom hole assembly with sensor card submerged in water.

Second Sensor Card Iteration: Epoxy

The second epoxy application was carefully planned. First, the sensor card was covered in a thin layer of epoxy before it was inserted in the BHA. The approach using electrical tape was discontinued because it occupied a large part of the compartment. Only a small piece of tape was used to cover the microphone on the sensor card. The trimmed USB cable was pulled through after filling the compartment in the stabilizer and in the sensor housing with epoxy. After the cable was pulled through and the sensor card was pushed in place, the top and bottom compartment was filled with as much epoxy possible. Afterward, it was left to dry overnight.

When re-connected to a computer, the device was not recognized but could broadcast Bluetooth and send data. One of the two data transfer wires in the USB cable was likely damaged. This meant the USB cable was capable of only supplying power and not communication. Because this scenario was anticipated, the card was programmed beforehand. The BHA was then again submerged in the sink for ten minutes. This time, the seal proved to be water-resistant. The sensor card was then tested while drilling, in which the Bluetooth communication was proven reliable.



Figure 13.15: Bottom hole assembly with sensor card submerged in water during drilling.

However, after three successful runs, the downhole sensor card failed. The reason was unknown but assumed to be caused by a leakage through the epoxy seal.

Third Sensor Card Iteration: Shrinking Tubes and Epoxy

The sensor card was placed inside a shrinking tube and cautiously heated with a heat gun to prevent further water leakages. When the card had cooled down, the previous procedure with the epoxy application was attempted again. The most exposed area is the metal where the micro USB connector was trimmed. Two shrinking tubes were applied, one smaller around the connector and one larger around the sensor card. The larger tube failed to seal the sensor on both ends because of too low heat. Extreme heat could potentially damage the sensor card. Because of the shrinking tubes, the sensor card also became larger and more difficult to insert into the sensor housing compartment.

Although this attempt was difficult because epoxy proved to seal off the sensor card in iteration number two (for a while), epoxy was applied in the same way. A heating gun was consequently held towards the sensor compartment to ensure low viscosity of epoxy flowing into the compartment during application. It was left to dry overnight and re-connected to a computer. The sensor card was capable of transfer data using Bluetooth only. However, it frequently lost connection, and it could maintain a connection for only ten seconds at a time. The cause for this could be the tight fit of the sensor card. A screwdriver was used to force it to fit the card, most likely squeezing the connector in the other end, causing damage to the power wires.

Fourth Sensor Card Iteration: Plasti Dip and Epoxy

It was attempted to coat the sensor card in two different protective materials to secure a tight seal to ensure water resistance. Before applying epoxy, the sensor card was covered in several layers of "Plasti Dip". Plasti Dip is a rubber coating that is flexible, waterproof, and electrically insulating [25]. A picture of the bottle is seen in Figure 13.16. It was applied in thin layers before applying epoxy as previously done with a refined application process.

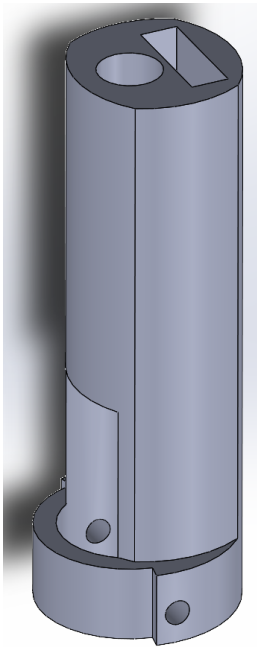


Figure 13.16: The Plasti Dip used to seal the downhole sensor card.

To avoid damaging the wires, the hole in the upper stabilizer was widened to fit the micro USB connection better. The sensor card was then carefully inserted into the compartment and sealed with a protective epoxy layer.

Backup Solution

With several failed attempts of integrating the downhole sensor card in the BHA, a backup solution was suggested. Figure 13.17 illustrates the intended design of the backup solution. Instead of integrating the card in the BHA, it was placed on top of the BHA in a 3D-printed housing. This enables direct insertion of the card without soldering the USB cable. It also facilitates the application process of epoxy. Using plastic as the material was advantageous because it removes a significant part of the magnetic distortion, thus providing better measurements. The backup solution placed the sensor card farther away from the bit and required that the card was on the opposite side of the drillstring bend to avoid contact with the borehole wall.



(a) SolidWorks drawing showing the design of the backup solution.



(b) Finished 3D-printed product.

Figure 13.17: Drive shaft and packer modifications.

13.8 Bottom Hole Assembly (BHA)

After testing the produced BHA in section 6.9, several components failed and had to be fixed. This section presents the repairs and replacements made in the BHA.

13.8.1 First Testing Stage

To be able to drill, the rod had to be appropriately attached to the universal joint to transfer torque and RPM. The rod had to be replaced frequently during initial testing, leading to welding or soldering not being an option. Neglecting these possible solutions was strengthened because aluminum and steel are not possible to weld together. For easy access and assembling, the rod was connected with a steel sleeve pressed together by two set screws as shown in Figure 13.18.



Figure 13.18: Connection between rod and joint made up of two set screws and a steel sleeve.

At the first stage of testing, the drive shaft that connects the rotating rod to the bit sub proved to be a few millimeters too long. This resulted in steel-to-steel friction between the universal joint and lower stabilizer when rotating before tagging the rock. This was solved with a bronze disc between the joint and the inside of the stabilizer as shown in Figure 13.19.



Figure 13.19: Bronze disc in lower stabilizer to minimize friction between joint and inside of stabilizer.

Another problem was that the Teflon packer unscrewed while drilling because the bit sub rotates clockwise while the Teflon packer has counter-clockwise threads. When WOB was applied, the friction increased enough for the packer to unscrew. The driveshaft could not rotate the bit due to being pinched between the packer and the inside of the stabilizer. The solution was to insert a set screw through the packer and the stabilizer as shown in Figure 13.20.



Figure 13.20: Set screw inserted through the packer and into the lower stabilizer to prevent packer from unscrewing.

A third challenge discovered while drilling was related to the threads between different components in the BHA. Because of vibrations propagating through the BHA during drilling, the threads that connect the different components began to unscrew, which resulted in tension in the rod and extensive vibrations. The solution was to implement set screws preventing the threads from unscrewing as shown in Figure 13.21.



Figure 13.21: Set screws to prevent threads from unscrewing in the joints between components.

13.8.2 Second Iteration

The problem related to pinching was solved after inserting the bronze disc and locking the packer in place with a set screw. The result was a compact system with minimal slack in the drill bit

attached to the driveshaft. As drilling proceeded, vibrations gradually increased. The vibrations were related to the relation between the steel and bronze roughness and the pressure between them. A slight offset in the horizontal direction placed the driveshaft in a bent position. Because steel is rougher than bronze and the force acted on a concentrated circular area during rotation, the steel joint grounded down the bronze disc. The worn bronze disc resulted in slack and extensive vibrations. A steel disc was glued to the joint to increase the contact area between the joint and the bronze disc, as shown in Figure 13.19.

After further drilling, slack and vibrations were yet again experienced. An issue was observed when the system was disassembled. As a result of sand production, the Teflon packer had been worn down around the driveshaft causing slack and giving the drive shaft space to position in a more bent position. In addition, the steel disc had loosened, which caused significant friction, and had worn the steel joint as shown in Figure 13.22.



Figure 13.22: Melted steel joint because of friction between the steel disc and the joint.

The solution was to produce a new driveshaft with an integrated steel disc as shown in Figure 13.23(a). The wear of Teflon was reduced by inserting a cylinder made up of Polyetheretherketone (PEEK) as shown in Figure 13.23(b).



(a) Drive shaft with integrated steel disc.



(b) PEEK cylinder inside teflon packer.

Figure 13.23: Drive shaft and packer modifications.

13.8.3 Third Iteration

After the second iteration of the BHA, it proved to perform well. Multiple drilling runs were executed with a maximum of 20 kg-f WOB and 380 RPM. It was suspected that the top drive motor provided too low RPM, and a new motor was purchased to increase the limitation. The new motor was capable of giving 1300 RPM. A new drilling run was performed with the new top drive motor, reaching rotational velocities of 1300 RPM and a WOB of 21 kg-f. At this combination of velocity and force, the universal joint in the BHA gave in as shown in Figure 13.24. After closer investigation, the universal joint was constructed to handle rotational velocities of up to 1 000 RPM [66]. Thus the new upper limitation for RPM was set to 1 000 RPM.



Figure 13.24: Snapped shaft in the universal joint because of to high rotational velocity.

13.8.4 Fourth Iteration

After limiting the rotational velocity to 1 000 RPM the joint held together, and further drilling tests proceeded. When one part of the system was fixed, another part experienced more load and

forces leading to more failures. Drilling was conducted with the 1.5 inch drill purchased bit from Alibaba in multiple runs before testing the Baker Hughes bit with the new top drive motor and titanium rod. The Baker Hughes bit induced more vibrations on the system than the Alibaba bit, which caused the driveshaft to snap above the threads.

The outer diameter of the driveshaft was increased from 10mm to 12mm. An extra 1 mm increase in wall thickness increased the overall strength of the drive shaft. In the consecutive run, the shaft performed well. However, the weak point had moved to the connection between the driveshaft and the universal joint instead. The M5 set screw fixing the driveshaft and joint together had snapped off during drilling. At this stage, it was not possible to further increase the set screw size due to lack of space. The solution was to weld the two parts together as shown in Figure 13.25.



Figure 13.25: Universal joint and drive shaft welded together.

13.8.5 Fifth Iteration

The two parts of the universal joint were connected using a hollow square cube and two shafts. The shafts are held in place by caps that allow the joints to rotate freely around the shafts. After welding the driveshaft to the joint in the fourth iteration, these caps tended to pop out during drilling. When the caps popped out, the shaft fell out, and the joint could not transmit rotation. To prevent the caps from popping out, they were spot-welded onto the universal joint body as shown in Figure 13.26.



Figure 13.26: Spot welded cap to prevent it from popping out.

When this iteration was made, the rig had drilled multiple runs which had worn the Teflon packer. The packer had been grounded down by the steel bit sub as well as hollowed out by the set screw mechanism described in subsection 13.8.1. This caused vibrations and axial forces that disrupted the drilling performance. The solution was to make an equivalent packer in Polyetheretherketone (PEEK). To further decrease the chance of something similar happening again, the set screw was replaced by two flat head screws as shown in Figure 13.27.



Figure 13.27: Packer made of PEEK with flat head screws to prevent it from unscrewing.

(This page is intentionally left blank)

Chapter 14

Conclusions

This thesis showcases the work done by the 2020/2021 NTNU Drillbotics team. The objective has been to design and implement an autonomous miniature drilling rig for directional drilling. The main goal was to steer the drilling system with downhole measurements from a sensor card as feedback control. The drilling concept was changed significantly to a more mechanically feasible concept to meet the objective and competition requirements. The most significant changes were implementing an azimuth system combined with a bent sub for directional opportunities and a rod for torque and rotation transmission from a top drive to the drill bit.

A novel control system was created in MATLAB and Simulink. A new GUI was designed for easy operation, both in manual and autonomous operation. A safety measure for stuck bit detection was implemented with autonomous mitigation that involved decreasing WOB when torque spikes were detected.

The main challenge encountered during the implementation of the new concept was twist-offs in the rod. This challenge was mitigated by acquiring a top drive with increased rotational capacity and designing a drill bit that minimizes torque spikes and increases stability. Changing the rod material from aluminum to titanium increased the material strength and reduced the twist-off risk.

Achieving downhole communication with a sensor card was successfully done after several attempts. The measurements were sent from an Arduino sensor card in the BHA through a USB cable to the control system. Valuable estimates of position and direction were continuously up-

dated with downhole data measurements at each survey points and used by the directional model. June 7th was the competition date. The team was assigned two different targets, and the rig drilled towards the targets fully autonomously after drilling a vertical section to the KOP. The rig drilled through the rock in 23 minutes in the competition run, but issues with the control system were encountered. These issues led to an offset between the drilled well and targets. The committee requested an extra run to experience the drilling rig's maximal capabilities because the initial run was successful, and the team had the only functional rig. This run took six minutes, achieving an inclination of 37 degrees when drilling without taking survey points. The fully autonomous miniature drilling rig has, throughout this project, successfully drilled 53 deviated wells within the requirements of the Drillbotics competition of 2021.

Chapter 15

Future Work

This thesis and project have focused on implementing ideas to the autonomous miniature drilling rig for the best performing concept possible with respect to the competition requirements. Most of the ideas have been successfully implemented, but the successive Drillbotics teams should investigate some ideas because of limited time and budget. Various problems and modification opportunities occurred when the team became more familiar with the system throughout the project's lifetime. There is room for improvements which will be briefly introduced and described in this chapter.

15.1 Easier Protective Glass

Today, the protective glass in front of the derrick moves along the derrick rails. However, in order to secure the glass in place at the top of the derrick, an additional person must stick one pin on each side while another holds the cabinet. A suggestion is to install a heavy counterweight connected to a wire and pulley for a safer lifting procedure. This makes a more agile and elegant solution while protecting the workers from damage from improper lifting.

15.2 Adjustable Bent Sub

The fixed bent sub in the BHA could be replaced with a bent sub with an adjustable angle for a more agile design. An adjustable bent sub will enable drilling of less deviated well paths when needed to reach targets at multiple coordinates within the rock sample. The most beneficial aspect is that it does not require a constant dogleg angle, which is the scenario for most cases with multiple targets. However, a bent sub with an adjustable angle requires a complex mechanical

design, possibly with a hydraulic system to activate pins or pads to change the angle. This would require extensive testing but would be a very relevant solution.

15.3 Whipstock

An intelligent solution for building the inclination is needed to improve and use the control system and mechanical system developed and presented in this project. Theoretical calculations for the required bit tilt in subsection 5.8.2 changed drastically when implementing azimuth rotation. The challenge was related to where the easiest well path was directed for the bit and BHA during drilling. When azimuth was changed in a new direction while rotating the drill bit, it failed to build the expected inclination. The reason may be because the wellbore diameter increased when the azimuth system rotated the BHA, thus giving room for the bit behind the desired direction. A solution is to implement a mechanical whipstock that forces the drill bit in the desired direction. If a whipstock is not desirable, the bit tilt must over-compensate drastically. Analysis has to be performed to find a pattern between azimuth rotation and inclination build.

15.4 Hydraulic System

A closed-loop hydraulic system should be implemented on the rig. The authors made a major change in the overall concept by dismissing the previous drilling concept with the PDM solution. This concept change required a lot of work. Because the new drilling system did not need high-pressure drilling fluid, a closed-loop system was not prioritized.

Dry cuttings accumulated on the floor can swirl up when people walk across the workshop, potentially entering people's lungs. Another related problem is cuttings accumulating on the acrylic protection glass. Figure 15.1 shows a picture where there is little to no vision through the glass and thus no opportunity to observe the ongoing operation.



Figure 15.1: Dirty acrylic glass from cuttings squirting when flushed out of rock.

This should be avoided and can be solved with a semi-close loop similar to the one used back in 2018 showed in Figure 15.2. A more elegant solution would be a fully closed-loop system with filtering, allowing for other types of drilling mud.



Figure 15.2: Semi-closed loop mud system from 2018 where the interface between rock and riser is sealed to guide flushing up through the rubber hose directly to the drain [52].

15.4.1 Swivel Design

The hydraulic swivel design has been a part of the design since the first NTNU team with the modifications described in section 6.8. The most urgent challenge to address is the O-ring located between the T-shaft and the swivel shaft. The O-ring must be changed after multiple runs because it becomes damaged, which leads to leakages through the safety outlet in the T-shaft. With excessive wear, water can migrate up the T-shaft and exit near the azimuth system. Frequently changing the O-ring solved this problem, but this is a time-consuming process. Many components must be dismantled to access the O-ring. The next team is advised to modify or improve the design for easier access to the O-ring.

15.5 Computer Space

The requirements for directional drilling introduced a complex control system in which required a high-performance computer. Together with real-time data gathering from the sensor card, the computer used in this rig cannot perform sufficiently and lags. Because of budget limitations, a computer with improved specifications was not acquired. The temporary solution was to run the sensor card and control system on separate computers and communicate between them to isolate the processes. This led to a full computer desk, such that one of the computers was placed on top of the electrical cabinet as depicted in Figure 15.3.



Figure 15.3: Picture showing limited space on the rig when working with two computers.

The competition next year may require a more complex control system and autonomy. The authors, therefore, suggest investing in an improved computer with better specifications. An alternative is to order computer parts and build a customized computer. This solution enables easy modifications and replacements of computer parts while saving space.

15.6 Rock Sample Space

Because the team drills multiple wellbores in one rock sample, the sample is placed at different positions under the rig for each run. The riser system and rig frame limit the accessibility of the rock sample. The complete derrick design must be changed to access more of the rock surface, which may be a demanding job. Extra height under the drill floor would provide the rig with a better workspace between the rock surface and the riser and drill floor stabilizer. This was a problem because of the increased bit diameter, and consecutively, the overall length of the BHA was increased. In addition, the rock sample was unstable when placed directly on the floor. This reduced the stabilizing effect of the wellbore when vibrations propagated through the rock and vibrated the entire sample. Strapping the block to the floor could prevent this.

15.7 Electromagnet

The measurements made by the magnetometer in the sensor card are essential for directional drilling with this design. Yaw of the drill bit is normally obtained by magnetometer data and can be used as an excellent approximation to the azimuth orientation of the BHA. Ideally, the magnetometer would estimate the yaw based on a reference to Earth's magnetic field. Earth's magnetic field varies in magnitude and inclination with location, and is about 0.52 gauss in Trondheim, Norway [56]. This strength, combined with the inclination of 74° , has shown the magnetometer to be insufficient. The magnetometer is sensitive to interference from other magnetic fields, metal objects and has proven not to give reliable and valuable data.

A suggestion is to install a new magnetic field as a reference using an electromagnet. A strong electromagnet placed close to the rock sample would act as a new magnetic north, thus creating a local magnetic field strong enough to produce reliable data measurements. The electromagnet should be fixed in a permanent spot to provide the same magnetic field and reference to the north, independently of the rock samples' position. To produce the most accurate measurements, the magnet should be placed as close to the sensor tool as possible. This is because the magnetic strength varies with the inverse of the squared distance to the magnet source. Figure 15.4 shows an illustration of a suggested setup.

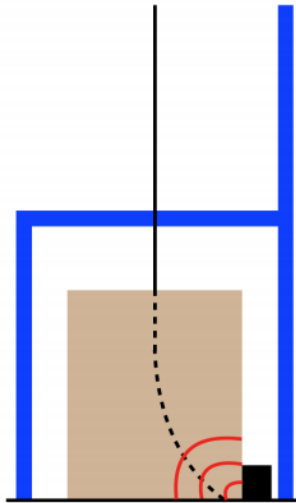


Figure 15.4: Setup of magnetic field with an electromagnet (black) [42].

15.8 Sensor Card

As mentioned in section 13.7, problems were encountered when attempting to integrate the sensor card in the BHA. Issues were related to space, sealing, communication, and power transmission. It is advised to locate a smaller downhole sensor card than the one used in the presented design.

The solution to use epoxy to seal the sensor card has proved sufficient and introduces some weaknesses. It isn't easy to apply the chosen epoxy in tight spots because of its high viscosity. The hardened epoxy can become brittle over time, introducing the risk of cracks with extensive vibrations. An improved solution is to seal the sensor cards completely using a metal cap. However, this requires a wireless solution to communicate with the card. Bluetooth communication works, but the signal strength is weakened from time to time. The sensor card also requires a power source, which is the computer for the time being. The power cord (USB cable) can be removed by implementing a battery package with rechargeable batteries. This will ultimately ease the problems with space and sealing. A suggestion is to charge the batteries with a wireless charging pad.

15.9 Kick-Off Point (KOP)

The Kick-Off Point (KOP) can be located at any depth greater than the 10.16 cm vertical hole. The system described in this thesis has set the KOP to be at 10.16 cm exactly, which led to problems drilling low inclination well paths. If the first target is located along the vertical hole's

center axis, it is hard to hit it when kicking off above the point. It would be smart to implement an autonomous process that decides whether to proceed with vertical drilling or not after the vertical section depending on the targets put in. In this way, the KOP can be adjusted according to the target points, allowing for more opportunities with respect to the well path. An even more manageable approach to this problem would be implementing different kick-off points in the Bezier calculation before starting the drilling process. In this way, the Bezier optimization can decide where to kick-off for the smoothest possible well path.

(This page is intentionally left blank)

References

- [1] Drilling Systems Automation Technical Section (DSATS). *Drillbotics® Guidelines*. Sept. 2020. URL: <https://drillbotics.com/wp-content/uploads/simple-file-list/Guidelines/Guidelines-2021/2021-Drillbotics-Guidelines-v3.pdf>.
- [2] victorromeo (GitHub username). *PDM library*. URL: <https://github.com/victorromeo/ArduinoPDM>. Accessed: 22.04.2021.
- [3] 3M. *3M™ Scotch-Weld™ Epoxy Adhesive DP110 Gray*. URL: https://www.3m.com/3M/en_US/company-us/all-3m-products/~ / 3M-Scotch-Weld-Epoxy-Adhesive-DP110-Gray/?N=5002385+3293242433&rt=rud. 05.05.2021.
- [4] AEP. *TC4 AMP*. URL: <https://www.aep.it/wp-content/uploads/2020/02/TC4AMP.pdf>. 24.03.2021.
- [5] *AISI Type 316L Stainless Steel, annealed sheet*. URL: <http://www.matweb.com/search/DataSheet.aspx?MatGUID=1336be6d0c594b55afb5ca8bf1f3e042>. 05.06.2021.
- [6] A.J. Adams et al. “The Barlow Equation for Tubular Burst: A muddled History”. In: *Society of Petroleum Engineers* (Mar. 6, 2018). URL: <https://doi.org/10.2118/189681-MS>.
- [7] A.T. Bourgoyne Jr et al. *Applied Drilling Engineering*. 2nd ed. Society of Petroleum Engineers, 1991.
- [8] B. Brechan et al. *Drilling, Completion, Intervention and PA - design and operations*. Department of Geoscience and Petroleum, 2017.
- [9] G. Hånsnar et al. *Design Report NTNU - Drillbotics 2021 Phase I*. Specialization Project. Department of Geoscience and Petroleum, 2020.

-
- [10] H.E. Helle et al. *Design Report NTNU - Drillbotics 2018 Phase I*. Specialization Project. Department of Geoscience and Petroleum, 2018.
- [11] J. Mannsverk et al. *Design Report NTNU - Drillbotics™ 2020 Phase I*. Specialization Project. Department of Geoscience and Petroleum, 2019.
- [12] *Aluminum 6061-T6; 6061-T651*. URL: <http://www.matweb.com/search/DataSheet.aspx?MatGUID=b8d536e0b9b54bd7b69e4124d8f1d20a>. 05.06.2021.
- [13] *Aluminum 7075-T6; 7075-T651*. URL: <http://www.matweb.com/search/DataSheet.aspx?MatGUID=4f19a42be94546b686bbf43f79c51b7d&ckck=1>. 05.06.2021.
- [14] *API Integrations: 5 Ways they can benefit your business*. URL: <https://mydatascope.com/blog/en/api-integrations-5-ways-they-can-benefit-your-business/>. 07.06.2021.
- [15] T. Åström and Karl J. Hägglund. *PID Controllers- Theory, Design and Tuning*. ISA, 1995.
- [16] A. Austin and J.H. Swannell. “Stresses in a pipe bend of oval cross-section and varying wall thickness loaded by internal pressure”. In: *International Journal of Pressure Vessels and Piping* 7.3 (1979), pp. 167–182. ISSN: 0308-0161. DOI: [https://doi.org/https://doi.org/10.1016/0308-0161\(79\)90016-4](https://doi.org/https://doi.org/10.1016/0308-0161(79)90016-4). URL: <http://www.sciencedirect.com/science/article/pii/0308016179900164>.
- [17] Unified Automation. *UaExpert - A Full-Featured OPC UA Client*. URL: <https://www.unified-automation.com/products/development-tools/uaexpert.html>. Accessed: 13.04.2021.
- [18] J.J. Azar and G. Robello Samuel. *Drilling Engineering*. PennWell Books, 2007.
- [19] Parts Badger. *Properties of Titanium Ti-6Al-4V (Grade 5)*: URL: <https://parts-badger.com/properties-of-grade-5-titanium/>. 25.05.2021.
- [20] *Beryllium Copper, UNS C17200, TH04 Temper rod, bar, plate, tubing, >25 mm*. URL: <http://www.matweb.com/search/datasheet.aspx?matguid=bbe220809bb144eb9c2f3672d>. 05.06.2021.
- [21] Alain Besson, Bruce Burr and Scott Dillard. *On the Cutting Edge*. 2000. URL: <https://www.slb.com/-/media/files/oilfield-review/p36-57-3-english>.
- [22] Dell. *Dell UltraSharp 34 Curved Ultrawide Monitor: U3415W*. URL: <https://www.dell.com/hr/business/p/dell-u3415w-monitor/pd>. 04.05.2021.
- [23] Dell. *Dell UltraSharp 34 Curved Ultrawide Monitor: U3415W*. URL: <https://www.dell.com/hr/business/p/dell-u3415w-monitor/pd>. 04.05.2021.
- [24] Dell. *OptiPlex 24 7000 Series All-in-One (7440)*. URL: <https://dustinimages.azureedge.net/media/d200001004269838/optiplex-7440-aio.pdf>. 04.05.2021.
-

REFERENCES

- [25] Plasti Dip. *Plasti Dip® Spray Bruksområder*. URL: <https://plastidip.online/produkt-kategori/plastidip/plasti-dip-spray/>. 24.05.2021.
- [26] Wiki ed. *Darcy friction factor formulae*. URL: https://en.wikipedia.org/wiki/Darcy_friction_factor_formulae#Swamee%E2%80%93Jain_equation. 24.04.2021.
- [27] Enggcyclopedia ed. *Absolute Pipe Roughness*. URL: <https://www.enggcyclopedia.com/2011/09/absolute-roughness/>. Accessed: 29.05.2021.
- [28] Helsenorge ed. *How to prevent transmission*. URL: <https://www.helsenorge.no/en/coronavirus/how-to-prevent-transmission/>. Accessed: 15.03.2021.
- [29] MechaniCalc ed. *Column Buckling*. URL: <https://mechanicalc.com/reference/column-buckling>. Accessed: 12.03.2021.
- [30] MechaniCalc ed. *Cross Section Properties*. URL: <https://mechanicalc.com/reference/cross-sections#radius-of-gyration>. Accessed: 12.03.2021.
- [31] Micon Downhole Tools ed. *Positive Displacement Motors (PDM)*. URL: https://micon-drilling.de/Download/Catalog_PDM_EN.pdf. Accessed: 17.03.2021.
- [32] NIOSH ed. *Hierarchy of Controls*. URL: <https://www.cdc.gov/niosh/topics/hierarchy/default.html>. Accessed: 15.03.2021.
- [33] Petrowiki ed. *Cuttings transport*. URL: https://petrowiki.org/Cuttings_transport. Accessed: 09.06.2020.
- [34] Petrowiki ed. *PDC bit design*. URL: https://petrowiki.spe.org/PDC_bit_design. 06.05.2021.
- [35] Schlumberger ed. "Drill bit cutting structure - Basic information". Schlumberger private. -.
- [36] Drilling Formulas. *What You Need To Know About Drilling Bit Balling Up and How To Troubleshooting It*. URL: <http://www.drillingformulas.com/what-you-need-to-know-about-drilling-bit-balling-up-and-how-to-troubleshooting-it>. Accessed: 15.03.2021.
- [37] OPC Foundation. *Unified Architecture*. URL: <https://opcfoundation.org/about/opc-technologies/opc-ua/>. Accessed: 07.04.2021.
- [38] Gigager. *GSH Hypoid Gear Rotary Table*. URL: <https://5.imimg.com/data5/VT/DC/CF/SELLER-2308089/hypoid-gear-rotary-table.pdf>. 08.05.2021.
- [39] Gigager. *Right Angle Gearboxes*. URL: <https://www.gigager.net/right-angle-gearbox/right-angle-gearboxes.html>. 09.06.2021.

-
- [40] Gigager. *Right Angle Reducer*. URL: <https://www.gigager.net/uploads/201919612/Right-Angle-Gearboxes.pdf?rnd=479>. 15.05.2021.
- [41] GitHub. *FreeOpcUa/opcuamodeler*. URL: <https://github.com/FreeOpcUa/opcuamodeler>. Accessed: 12.04.2021.
- [42] M.U. Azam H.E. Helle and J.M. Montoza. *Design and Implementation of an Autonomous Miniature Drilling Rig for Directional Drilling*. Thesis. Department of Geoscience and Petroleum, 2019.
- [43] The MathWorks Inc. *Anti-Windup Control Using a PID Controller*. URL: <https://se.mathworks.com/help/simulink/slref/anti-windup-control-using-a-pid-controller.html>. 03.05.2021.
- [44] The MathWorks Inc. *Closed-Loop PID Autotuner*. URL: <https://se.mathworks.com/help/slcontrol/ug/closedlooppidautotuner.html>. 03.05.2021.
- [45] The MathWorks Inc. *Extended Kalman Filter*. URL: https://se.mathworks.com/help/control/ref/ekf_block.html. Accessed: 21.04.2021.
- [46] The MathWorks Inc. *fmincon*. URL: <https://se.mathworks.com/help/optim/ug/fmincon.html>. 07.06.2021.
- [47] Moons Industries. *SM0402AE4-KCD-NNV*. URL: <https://www.moonsindustries.com/p/m2dv-series-ac-servo-motors/sm0402ae4-kcd-nnv-000004611170000217>. 09.06.2021.
- [48] National Instruments. *USB-6212*. URL: <https://www.ni.com/en-no/support/model.usb-6212.html>. 25.03.2021.
- [49] Fridtjov Irgens. *Fasthetslære*. 7th ed. Tapir Akademisk Forlag, 2006.
- [50] Henning Johansen. *Aksler*. URL: <https://materialteknologi.files.wordpress.com/2018/01/sb-aksler-kompendium.pdf>. Accessed: 15.03.2021.
- [51] J. H. B. Sampaio Jr. "Designing 3D Directional Well Trajectories Using Bezier Curves". In: *ResearchGate* (2016).
- [52] S. Knoop. *Design and optimization of a miniature autonomous drilling rig contribution to the drillbotics competition 2018*. Master's Thesis, NTNU, 2018.
- [53] B. Larsen. *Måle- og reguleringssteknikk*. Instrutek A/S, 1994.
- [54] Lenze. *Automation systems Drive solutions, Control Inverter Motors Gearboxes Engineering Tools*. URL: https://download.lenze.com/TD/g500-BHS%5C%20geared%5C%20AC%5C%20motors%5C%20MF%5C%20inverter-optimised__v1-0__EN.pdf. 07.05.2021.
-

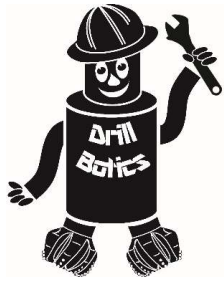
REFERENCES

- [55] Lenze. *Inverter Drives 8400 TopLine C*. URL: https://download.lenze.com/TD/E84AVTCx__8400%5C%20TopLine%5C%20C__v11-1__EN.pdf. Accessed: 24.03.2021.
- [56] Magnetic-Declination.com. *What is magnetic declination in Trondheim, Norway?* URL: <https://www.magnetic-declination.com/Norway/Trondheim/1877858.html>. 23.05.2021.
- [57] MaplePrimes. *The vibration of continuous structures*. URL: https://www.mapleprimes.com/DocumentFiles/206657_question/Transverse_vibration_of_beams.pdf. Accessed: 22.02.2021.
- [58] MathWorks. *Understanding Kalman Filters: An optimal estimator algorithm*. URL: <https://www.mathworks.com/videos/understanding-kalman-filters-part-3-optimal-state-estimator--1490710645421.html>. Accessed: 21.04.2021.
- [59] MathWorks. *Understanding Kalman Filters: Nonlinear state estimators*. URL: <https://www.mathworks.com/videos/understanding-kalman-filters-part-5-nonlinear-state-estimators-1495052905460.html>. Accessed: 21.04.2021.
- [60] S. Menand (Armines/Ecole des Mines de Paris) | H. Sellami (Armines/Ecole des Mines de Paris) | C. Simon (DrillScan). *PDC Bit Classification According to Steerability*. URL: <https://doi.org/10.2118/87837-PA>. Accessed: 07.05.2021.
- [61] MuleSoft. *What is an API? (Application Programming Interface)*. URL: <https://www.mulesoft.com/resources/api/what-is-an-api>. Accessed: 06.04.2021.
- [62] Oljedirektoratet. “Oljedirektoratet”. In: (2020). URL: <https://www.npd.no/en/>.
- [63] M.A. Olsen et al. *Design and optimization of a miniature autonomous drilling rig contribution to the drillbotics competition 2018*. Master’s Thesis, NTNU, 2017.
- [64] Omega. *What is a PID Controller?* URL: <https://www.omega.co.uk/prodinfo/pid-controllers.html>. Accessed: 06.04.2020.
- [65] Optimera. *Tørrbetong B20*. URL: <https://www.monter.no/globalassets/importedresources/2/pdf/205857.pdf>. Accessed: 20.04.2021.
- [66] RS Pro. *RS PRO Universal Joint, Single, Plain, Bore 6mm, 34mm Length*. URL: <https://no.rs-online.com/web/p/universal-joints/7906699/>. 04.05.2021.
- [67] S. Chen | R. Arfele | S. Anderle | J. Romero. *A new theory on cutter layout for improving PDC-Bit performance in hard-and transit-foramtion drilling*. URL: <https://www.onepetro.org/download/journal-paper/SPE-168224-PA?id=journal-paper%5C%2FSPE-168224-PA>. Accessed: 06.05.2021.
- [68] B. Brechan S. Hovda and P. Skalle. *Introduction to Drilling Engineering*. Department of Geoscience and Petroleum, Feb. 12, 2019.

-
- [69] Bjørn A. Brechan | Anisa N. Corina | Tor B. Gjersvik | Sigbjørn Sangesland | Pål Skalle. “Compendium TPG4215 Drilling Engineering”. University compendium. 2017.
- [70] Sandy Smith. *Safety Practices in the Oil and Gas Industry (Infographic)*. URL: <https://www.ehstoday.com/safety/article/21919443/safety-practices-in-the-oil-and-gas-industry-infographic>. Accessed: 15.03.2021.
- [71] *Sound Speeds in Water, Liquid and Materials*. URL: <https://www.rshydro.co.uk/sound-speeds/>. 29.05.2021.
- [72] Carsten Berge Guggedal | Magnus Steinstå. “Control System Architecture and API Integration”. Bachelor’s Thesis. 2019.
- [73] Magnus Steinstå. *Implementation of a Miniature Autonomous Directional Drilling Rig With NMPC Positional Control*. Master Thesis. Department of Engineering Cybernetics, 2021.
- [74] STMicroelectronics. *HTS221*. URL: https://content.arduino.cc/assets/Nano_BLE_Sense_HTS221.pdf. Accessed: 22.04.2021.
- [75] STMicroelectronics. *LPS22HB*. URL: https://content.arduino.cc/assets/Nano_BLE_Sense_lps22hb.pdf. Accessed: 22.04.2021.
- [76] STMicroelectronics. *LSM9DS1*. URL: https://content.arduino.cc/assets/Nano_BLE_Sense_lsm9ds1.pdf. Accessed: 22.04.2021.
- [77] Arduino Official Store. *Arduino Nano 33 BLE Sense*. URL: <https://store.arduino.cc/arduino-nano-33-ble-sense>. Accessed: 22.04.2021.
- [78] WPI FIRST Robotics Competition Control System. *Introduction to PID*. URL: <https://docs.wpilib.org/pt/latest/docs/software/advanced-controls/introduction/introduction-to-pid.html>. Accessed: 07.06.2021.
- [79] *The Future of Drilling Wells*. 2020. URL: <https://www.slb.com/drilling/bottomhole-assemblies/directional-drilling/autonomous-directional-drilling>.
- [80] *Titanium Alloys - Ti6Al4V Grade 5*. URL: <https://www.azom.com/properties.aspx?ArticleID=1547>. 05.06.2021.
- [81] *Tungsten carbide*. Apr. 2021. URL: https://en.wikipedia.org/wiki/Tungsten_carbide.

Appendix **A**

Drillbotics Guidelines 2021



Society of Petroleum Engineers
Drilling Systems Automation
Technical Section (DSATS)
International University Competition
2020-2021



Drillbotics® Guidelines

Revised 30 September 2020

1. Introduction

This year marks the seventh competition for the title of Drillbotics® champion and a chance for students to learn about the drilling process from industry experts and for winning team(s) to travel and present a paper at the next SPE/IADC Drilling Conference and at an event organized by DSATS. The past years involved undergraduates, masters and doctoral students from a variety of disciplines who built innovative drilling machines and downhole tools while developing a deeper understanding of automating the drilling process. The university teams freely share lessons learned, which more rapidly advances the science of drilling automation. Everyone involved claims to have had a lot of fun while learning things that are not in the textbooks or published papers. Students also participated in related events at conferences, workshop meetings and networking with industry leaders in drilling automation. This year's contest promises to be just as challenging and hopefully as much fun.

This year's competition will be to create a virtual rig, including drill string/BHA and wellbore interaction, and to demonstrate the model using a control model developed by each team. Due to the COVID-19 pandemic, the Drillbotics challenge committee decided to focus this year's competition on a virtual rig in an effort to facilitate competition success while teams work together remotely. If school policies allow a team to design and build a physical rig and there are a sufficient number of teams capable of building a physical rig, the Committee will allow these teams to compete as a second group as mentioned below and referred to as Group B. The competition guidelines for the Group B competition is listed in Appendix C.

How did the competition first come about? (Florence et al., 2000). The origins began in 2008 when several SPE members established the Drilling Systems Automation Technical Section (DSATS) to help accelerate the uptake of automation in the drilling industry. DSATS' goal was to link the surface machines with downhole machines, tools, and measurements in drilling systems automation (DSA), thereby improving drilling safety and efficiency. Later, at an SPE Forum in Paris, the idea of a student competition began to take shape; a DSATS sub-committee was formed to develop the competition format and guidelines further. Several universities were polled to find out the ability of academic institutions to create and manage multi-

Version	Date	Section	Description
2021.01		All	Updated all sections to reflect virtual rig model+controls. Physical rig guideline is moved to appendix.
2021-02	23 Sept 2020	4.5	Removed restriction
2021-03	30 Sept 2020	Appx Objectives and 1.6 and All	Clarification Fix broken links and update Committee members

disciplinary teams. The Drillbotics committee began small in 2014-2015 to see if the format could succeed. With fine tuning, we continue along those lines as we start the 2021 process.

Competition Overview:

- The challenge requires teams to develop a full-scale drilling system model, including its corresponding control scheme, to virtually drill a directional well following a given trajectory.
- The teams will design a control system that will virtually control the full-scale drilling system model to test and demonstrate the automated system. The teams should incorporate virtual downhole sensors, in addition to surface sensors in their automation and controls scheme.

The DSATS technical section believes that this challenge benefits students in several ways. Petroleum, mechanical, electrical, and control engineers gain hands-on experience in each person’s area of expertise that forms a solid foundation for post-graduate careers. They also develop experience working in multi-disciplinary teams, which is essential in today’s technology-driven industries. Winning teams must possess a variety of skills. The mechanical and electrical engineers need to build a stable, reliable, and functional drilling rig. Control engineers need to architect a system for real-time control, including a selection of sensors, data handling, and fast-acting control algorithms. The petroleum engineers need an understanding of drilling dysfunctions and mitigation techniques. Everyone must work collectively to establish functional system requirements, often fully understood by each team member to accurately model the drilling issues and create an integrated package working seamlessly together.

The oil and gas industry today seeks lower costs through efficiency and innovation. Many student competitors may discover innovative tools and control processes that will assist drillers in speeding the time to drill and complete a well. This includes more than a faster ROP, such as problem avoidance for dysfunctions like excessive vibrations, stuck pipe, and wellbore stability issues. Student teams built new downhole tools using 3D printing techniques of designs that would be difficult, if not impossible to machine. They used creative hoisting and lowering systems. Teams modeled drilling performance in particular formations and adjusted the drilling parameters accordingly for changing downhole conditions. While they have a lot to learn yet about our business, we have a lot to learn about their fresh approach to today’s problems. Good Luck!

Drillbotics® Committee

Challenge Team

Mike Attrell
Fred Florence
Salem H. Al-Gharbi
Jayesh Jain
Enrique Z Losoya
Bader Al-Otaibi
Reed Spencer
Shashi Talya

Judges

DSATS

Shashi Talya (Chair)	Duane Cuku	Jayesh Jain	Scott Petrie
Fred Florence (Co-Chair)	Dmitriy Dashevskiy	Mathew Keller	Tony Pink
Mike Attrell	Mohamed Ali Ibrahim Hassan	Enrique Z Losoya	Dimitrios Pirovolou
Vimlesh Bavadiya	Jana Hochard	Alex Ngan	Ritthy Son
Eric Cayeux	Oliver Hoehn	Nii Ahele Nunoo	Victor Soriano

DUPTS

Salem H. Al-Gharbi (Chair)
Bader Al-Otaibi

Contents

1. Introduction	1
2. Background	6
3. Group A Competition Guidelines	7
3.1. Challenge overview for the 2020-2021 competition:.....	7
3.2. Design:	7
3.3. Modeling:.....	8
3.4. Controls:	9
3.5. Coding:.....	10
3.6. Evaluation:	10
3.7. Deliverables:	11
3.8. Useful resources:	11
4. Team Members	12
5. Expenditures	13
6. Other Considerations.....	13
7. Project Timeline.....	14
8. Project report	15
9. Evaluation Criteria.....	16
10. Final report and paper.....	19
11. Terms and conditions	20
12. Marketing.....	21
Appendix	22
A. Directional Objective Requirements	22
B. Safety	24
C. Group B Competition Guidelines.....	24
1.0. Physical Rig Considerations: 2020-2021 High Level Challenge and Judging Changes	24
1.1. Two Project Phases	25
1.2. Phase I – Design Competition	25
1.3. Phase II – Drilling Competition	29
1.4. Rock Samples	30
1.5. Bits	31

1.6. Drillpipe	32
1.7. Tool joints	32
1.8. Bit sub/drill collar/stabilizers.....	33
1.9. Automated Drilling	33
1.10. Sensors	34
1.11. Data collection and handling.....	34
1.12. Data visualization	34
1.13. Measure and analyze the performance	35
1.14. The test well:	35
1.15. Not included in the 2020-2021 competition.....	36
1.17. Presentation to judges at Phase II Testing	37
1.18. Project report	37
1.19. Final report and paper.....	41

Objectives for the 2021 Competition

- 1.1. During the school year beginning in the fall of 2020, a team of students will organize themselves to solve a drilling-related problem outlined in Section 3 below. The team should preferably be a multi-disciplinary team that will bring unique skills to the group to allow them to design and construct hardware and software to demonstrate that they understand the underlying physics, the drilling issues and the usual means to mitigate the issues. We cannot stress enough the need to involve students with different technical training and backgrounds. They will need to develop skills to understand drilling dysfunctions and mitigation strategies, but they must also have the mechanical engineering and controls capabilities to model, design the rig/drilling package and develop the controls system. In past years, some entrants have not adequately considered the control network and algorithms needed for autonomous drilling. They have often misunderstood the need for calibrated sensors and fast, accurate data handling. All of this and more is needed to build and operate a complete automated drilling system.
- 1.2. The students could produce novel ideas leading to new drilling models, improved drilling machines and sensors, and the ability to integrate the data, models and machines that will hopefully create new, more efficient ways to drill wells in the future. Any such innovation will belong to the students and their university in accordance with the university's written policies. DSATS and SPE waive any claims to students' intellectual property.
- 1.3. The students, working as a multi-disciplinary team, will gain hands-on experience that will be directly applicable to a career in the upstream drilling industry.

2. Background

2.1. What is DSATS?

- 2.1.1. DSATS is a technical section of the Society of Petroleum Engineers (SPE) organized to promote the adoption of automation techniques using surface and downhole machines and instrumentation to improve the safety and efficiency of the drilling process. More information is available about DSATS at the DSATS homepage (<http://connect.spe.org/DSATS/Home/>).
- 2.1.2. The Drillbotics website at www.Drillbotics.com includes official updates to the competition guidelines and schedule, as well as FAQs, photos, and previous entrants' submittals and reports. Any updates to the guidelines posted on the Drillbotics website via blog entries from the Committee are considered to be an official revision to these Guidelines. Questions and suggestions can be posted there, or teams can email the sub-committee at 2021@Drillbotics.com.

2.2. Why an international competition?

2.2.1. DSATS, as part of the SPE, is a group of volunteers from many nations, connected by their belief that drilling automation will have a long-term, positive influence on the drilling industry. This diversity helped to shape the direction of the organization. The group feels that the industry needs to attract young professionals from all cultures and disciplines to advance drilling practices in all areas of the world. The winners of the Group A competition will receive a grant for economy class transportation and accommodations to attend the next SPE Drilling Conference and will present an SPE paper that will be added to the SPE archives of One Petro¹. Winners of Group B will publicly receive recognition of their achievement and have the opportunity to publish an SPE paper that will be added to the SPE archives of One Petro. DSATS believes recognition at one of the industry's leading technical conferences will help encourage student participation. Also, the practical experience with drilling automation systems increases the students' visibility to the companies that are leading automation activities.

3. *Group A Competition Guidelines*

3.1. **Challenge overview for the 2020-2021 competition:** The Group A challenge requires teams to develop a drilling system model that represents a full-scale system and corresponding control scheme to virtually drill a directional well to a given trajectory. The Group A challenge does not involve building a rig or drilling system. The teams will design automation and control but will develop a virtual drilling system (i.e. computer models) to test and demonstrate the controls. Therefore, in addition to the guidelines specified below (Group A Competition Guidelines) in general, applicable guidelines from Appendix C (Physical Rig Considerations), should also be referred. While the teams will have to meet minimum competition requirements, any "above and beyond" work along the main theme will be rewarded additional points to encourage creativity and innovation.

3.2. **Design:** Since the challenge does not require rig construction, the scope of the design portion is limited. The teams are not expected to carry out detailed mechanical design of the rig but are expected to perform basic calculations for a realistic system. The scope includes selecting essential elements such as drive mechanism, drill pipe, BHA, surface systems for application of WOB and RPM, and other required components for the virtual system. Please refer to Appendix C for considerations for physical rig design.

¹ Publication is subject to the SPE program committee's acceptance of the abstract/paper. If the abstract is not accepted, DSATS will solicit other SPE events try to get the paper into OnePetro.

3.3. Modeling:

- 3.3.1. Rig model: The rig model will consist of a drum controlling the drawworks, a top drive controlling the torque and RPM. The RPM, Torque, and Hookload are measurements taken at the rig model and will be inputs into the Control System.
- 3.3.2. The downhole drilling system model should predict bit trajectory for given WOB, RPM, drive mechanism parameters (e.g. steering force, AKO angle), and rock strength – as a function of measured depth. While the teams are empowered to decide on the complexity of the simulation model, the minimum requirements are stated below.
- 3.3.3. Bit model: The bit model can be as simple as the equivalent model of Pessier et al. (1992) with appropriate framework for steerability such as bit anisotropy and bit tilt such as Menand et al. (2012). Effect of key parameters such as gage length, drilling efficiency (MSE-DOC relationship) should be included. Inclusion of bit wear effects is not mandatory. For the purposes of this challenge, the bit model will be provided.
- 3.3.4. Rock/wellbore: The rock model should be defined by rock type, UCS, and confining pressure. At each simulation step increment, the bit drills and extends the wellbore. While calculation of explicit contact forces with the wellbore are not mandatory, the build rate will still change due to newly formed wellbore geometry and changing rock strength. This phenomenon must be taken into effect accurately. Teams can assume a 2D wellbore and thus develop a 2D drilling propagation model.
- 3.3.5. BHA: The BHA must be modeled so that contact force at the bit and bit tilt are computed to be used in the steering model. Generally speaking, 100 ft. of the BHA within the wellbore needs to be modeled in order for correct bit side force and bit tilt computations. The resulting behavior of drive mechanism should be modeled. The BHA should also (virtually) measure certain parameters (such as inclination, RPM, vibration etc.) and return to the surface or the control system. The bit-to-sensor distance as well as measurement frequency (i.e. intermittent vs continuous survey) should be a configurable parameters in the design.
- 3.3.6. Steering Model: The steering model takes inputs from the Bit Model and BHA Model to predict trajectory. A Control System will also interface with the Steering Model and update parameters (such as pad force, AKO orientation, WOB, RPM, etc) accordingly.
- 3.3.7. Drillstring: The Drillstring may be represented by one or more models. These models will have to do the following:

1. Calculate torque and drag for a 3D survey, with hook load, mud weight, drill string/BHA dimensions, sheave friction and variable friction factors along the wellbore as inputs. Using this data, the model will be able to predict downhole WOB and available torque at the bit, which will be used as input to the Bit Models.
2. The Drillstring Model(s) must also calculate buckling conditions. Drilling ahead in simulation will not be allowed if the Drillstring is buckling at any point along the Drillstring.
3. The Drillstring Model(s) must be able to simulate torsional oscillations (slow ones, like stick slip). It must be made up of multiple torsional spring elements and have friction damping from wellbore contact. Bit behavior in different rocks and at different WOB/RPM settings will cause stick slip, and the Control System for the top drive must be able to counter act stick slip automatically when it appears.
4. Please do not attempt to model lateral vibrations of the Drillstring or BHA.

3.3.8. The directional bit behavior modeling assumptions should be clearly stated. The implementation (or sub-models) should be verified against published data such as Menand et al. (2012).

3.4. **Controls:** The control system may include the following elements

- 3.4.1. **Drilling Optimization:** Optimize set point commands for drilling parameters such as WOB, RPM, etc. such that drilling performance and steering are optimized (according to each team's definition of "optimized performance"). Such real-time optimization should be done automatically.
- 3.4.2. **Trajectory Control:** Steer the well according to the given well plan. The objective is both to minimize trajectory error and wellbore tortuosity. Virtual surveys should be acquired and be used as feedback for the steering control logic. Be prepared to model a push-the-bit RSS and a bent motor AKO. The steering model should include considerations for how often the survey is taken and how far from the bit the sensors are placed (e.g. projecting from the survey depth to the bit, and the control system using survey information to decide steering parameters).
- 3.4.3. **Rig Display:** Real-time display of the drilling parameters and wellbore positioning during the final testing is mandatory. End of well report immediately after the competition is mandatory.
- 3.4.4. **Set Point Control:** Although set point control, i.e. automatic control of drilling parameters as per optimal set points, is an integral element of the drilling systems, this competition does not make it mandatory to reduce complexity. It can be assumed that the surface parameters such as WOB and RPM reach the BHA, making quasi-static modeling sufficient. However, the teams are

encouraged to go “above and beyond” and demonstrate set point control independent of trajectory drilling. For example, the WOB and RPM control could be implemented for the virtual drill rig with a suitable mechanism for applying WOB (e.g. dead weight and drawworks), RPM (e.g. top drive), etc. Characteristics for each sub-system could be assumed realistically (e.g. top drive motor characteristics with RPM-torque relationship). Other examples include slide/rotate mode control.

3.5. Coding:

3.5.1. The entire code should be written with a modular design with functions/subroutines for each sub-system. The drilling system model should be a separate application that interacts with the control system. Appropriate interfaces (APIs) should be developed for interoperability and deployment.

3.5.2. Teams are encouraged to share their code to promote the learning spirit. Such sharing can occur during or after the final presentations, or after securing any IP protection, at the discretion of the teams. However, release of codes is not mandatory and will not count towards the final score.

3.6. Evaluation:

3.6.1. The drilling plan will be presented to the teams on the day of competition. The rock properties will be provided as a function of true vertical depth or measured depth. The teams are given maximum of three hours to virtually drill the well. Students are allowed to debug/modify the code and use multiple attempts within the allotted time.

3.6.2. An RSS or AKO motor BHA will be specified on the day of the competition. Thus, the model should be capable of simulating both steering systems.

3.6.3. Drillbotics may provide data to calibrate sub-models such as the bit model. Additional details will be released during Phase II.

3.6.4. While sharing of code is not mandatory, the presentations should include the details of the control schemes. Organizers can be contacted in case of any confidentiality requirements.

3.6.5. Teams will be evaluated on a per model basis. Points will be given for having each model or control system present and functioning in a realistic manner. A team that predicts the trajectory the best but is missing a model of the rig will earn fewer points than a team that has all the models and control systems from bit to rig. The purpose is to model the entire system and have the sub-models behave realistically.

3.6.6. The set point control is not a mandatory item for the competition. Any demonstration of such capability will attract extra points in “above and beyond” category.

3.7. Deliverables:

3.7.1. Phase I: A detailed report containing detailed literature review, model assumptions, overall plan of the virtual system, including the system architecture, different layers (such as data layer, control layer etc.), mathematical framework for modeling and control schemes, a plan for implementation, and relevant details. It is preferable to include special section for the API, if other system need to interact with your system. Preliminary results from the virtual drilling rig model should be included, along with a discussion on the results.

3.7.2. Phase II: A deployable application that drills a directional well to a given trajectory plan using autonomous control of a virtual drilling system.

3.8. Useful resources:

3.8.1. Florence, F., Losoya, E., Drillbotics with Fred Florence and Enrique Losoya (2020, August 18), SPE Podcast, [Link](#).

3.8.2. Pessier, R. C., & Fear, M. J. (1992, January 1). Quantifying Common Drilling Problems With Mechanical Specific Energy and a Bit-Specific Coefficient of Sliding Friction. Society of Petroleum Engineers. doi:10.2118/24584-MS

3.8.3. Menand, S., Simon, C., Gerbaud, L., Ben Hamida, M., Denoix, H. J., Cuillier, B., Sinardet, H. (2012, January 1). PDC Bit Steerability Modeling and Testing for Push-the-bit and Point-the-bit RSS. Society of Petroleum Engineers. doi:10.2118/151283-MS

3.8.4. Pehlivantürk, C., D'Angelo, J., Cao, D., Chen, D., Ashok, P., & Van Oort, E. (2019, March 4). Slide Drilling Guidance System for Directional Drilling Path Optimization. Society of Petroleum Engineers. doi:10.2118/194096-MS

3.8.5. Marck, J., Detournay, E., Perturbation to Borehole Trajectory across an Interface, ARMA-2014-7479, 48th US Rock Mechanics/Geomechanics Symposium, Minneapolis, Minnesota, June 1-4, 2014.

3.8.6. Zalluhoglu, U., Marck, J., Gharib, H., & Zhao Y. (2019) Borehole Propagation with Undergaged Stabilizers: Theory and Validation. ASME Journal of Dynamic Systems, Measurement and Control, vol. 141, no. 5: 051013. doi: 10.1115/1.4042380

- 3.8.7. Perneder, L., Marck, J. and Detournay, E., 2017. A model of planar borehole propagation. *SIAM Journal on Applied Mathematics*, 77(4), pp.1089-1114. doi: 10.1137/16M1094518
- 3.8.8. Zalluhoglu, U., Demirer, N., Marck, J., Gharib, H., & Darbe, R. (2019) Steering advisory system for rotary steerable systems. *SPE/IADC Drilling Conference and Exhibition*, 5-7 March, The Hague, The Netherlands. SPE-194090-MS, doi: 10.2118/194090-MS
- 3.8.9. Zalluhoglu, U., Gharib, H., Marck, J., Demirer, N., & Darbe, R. (2019) Steering advisory system for mud motors. *SPE/IADC Drilling Conference and Exhibition*, 5-7 March, The Hague, The Netherlands. SPE-194077-MS. doi: 10.2118/194077-MS
- 3.8.10. Franklin, G. F., Powell, J. D., Emami-Naeini, A., & Powell, J. D. (1994). *Feedback control of dynamic systems*, 3rd Edition, Reading, MA: Addison-Wesley.
- 3.8.11. Ogata, K. (2003). *System dynamics*, 4th Edition, Upper Saddle River, NJ: Prentice Hall.
- 3.8.12. Ogata, K. (2009). *Modern control engineering*, 5th Edition, Upper Saddle River, NJ: Prentice Hall.
- 3.8.13. Li, Y., Ang, K. H., & Chong, G. C. (2006). PID control system analysis and design. *IEEE Control Systems Magazine*, 26(1), 32-41.
- 3.8.14. Rawlings, J. B. (2000). Tutorial overview of model predictive control. *IEEE control systems magazine*, 20(3), 38-52.
- 3.8.15. Webinar: Machine Learning and Physics-based Solutions for Drilling Automation by SPE Distinguished Lecturer Prof. John Hedengren, Brigham Young University, YouTube [Video](#).
- 3.8.16. Webinar: Drilling Automation and Downhole Monitoring with Physics-based Models. [Link](#).
- 3.8.17. Video and Webinar Series: Understanding Control Systems by Mathworks. [Link](#).

4. *Team Members*

- 4.1. DSATS envisions that the students would be at least senior undergraduate or Masters level, well versed in the disciplines needed for such a project. The maximum number of students per team is five (5) and the minimum shall be three (3). Any team that loses team members during the project can recruit a replacement.
- 4.2. At least one member of the team must be a Petroleum Engineering candidate with sufficient coursework completed to understand the physics relating to the drilling problems and the normal industry practices used to mitigate the problem.

- 4.3. Students with a background in mining, applied mathematics, mechanical and electrical engineering, as well as controls, mechatronics and automation or software development, are the most likely candidates, but students with any applicable background is encouraged.
- 4.4. A multi-disciplinary team simulates the working environment in the drilling industry today, as most products and services are produced with the cooperation of technical personnel from differing backgrounds and cultures.
- 4.5. A university may sponsor more than one team in a group and may enter teams in one or both groups.
- 4.6. Students shall register their team not later than 1 November using the registration form on the Drillbotics website. Any changes to the team members or university supervisor over the course of the competition should be reported in the monthly reports.

5. *Expenditures*

- 5.1. Teams selected to advance to the second phase must limit the cost of the physical or virtual rig and materials to US\$ 10,000 or its equivalent in other currencies. The students shall find a source of funding and report the source in the Phase I proposal. All funding and procurement should comply with university policy. These funds are intended to cover the majority of expenses for hardware, software and labor to construct and operate the team's equipment. DSATS shall not be liable for any expenditure other than DSATS provided material and specified travel expenses.
- 5.2. DSATS will assist when possible to obtain free PLCs or similar control devices from suppliers affiliated with the DSATS organization. Such "in-kind" donations shall not be included in the team's project costs.
- 5.3. Students and universities may use other "in-kind" contributions which will not be included in the team's project costs. Such contributions may include modeling software, laboratory equipment and supplies, and similar paraphernalia usually associated with university laboratory projects.
- 5.4. Any team spending more than US\$ 10,000, or its equivalent in other currencies, may be penalized for running over budget.
- 5.5. DSATS reserves the right to audit the team's and university's expenditures on this project.
- 5.6. Any devices built for the project will become the property of the university and can be used in future research and competitions. Any maintenance or operating costs incurred after the competition will not be paid by DSATS.

6. *Other Considerations*

- 6.1. University coursework and credit: Each university will decide whether or not this project qualifies as a credit(s) towards any degree program.

7. Project Timeline

Phase I - Design:	Fall 2020
Submit monthly reports	On or before the final day of each month
Submit final design to DSATS	31 Dec 2020, midnight UTC
Submit an abstract to DSATS*	31 Dec 2020, midnight UTC

*DSATS will submit an abstract to the SPE that will include excerpts from the student abstracts by the conference paper-submittal deadline, typically in mid-summer, for consideration of a paper by the conference program committee.

Phase II – Model enhancement/testing and controls development	Spring 2021
DSATS to announce finalists	On or about 31 Jan 2021
Model & controls development/Construction	Spring 2021
Monthly reports	On or before the final day of each month
Final demonstration	The final demonstration will typically occur in late May or early June. Additional details on the logistics for the final demonstration will be shared in early 2021.

8. Project report

1.1.1. Starting in the fall term, the student team shall submit to DSATS a short monthly project report that is no more than one page in length (additional pages will be ignored) due on or before the last day of each month. Send it via email to 2021@Drillbotics.com. The monthly report should include:

1.1.2. Phase I

- Key project activities over the past month.
- Literature survey, rig modeling considerations, trade-offs, critical decision points etc.
- Cost updates
- Significant new learning, if any

1.1.3. Phase II

- Model enhancements, controls development updates.
- Preliminary results of exercising the drilling model and controls
- Other items of interest

1.1.4. Report content

1.1.4.1. To teach students that their work involves economic trade-offs, the monthly report should include at a minimum a summary estimate of team member labor hours for each step in the project: modeling, controls, testing etc. and a cost summary for software related expenditures. Also include labor for non-students that affect the cost of the project. Labor rates are not considered, as to eliminate international currency effects. Labor is not considered in the cost limits of item 6.1, but should be discussed in the report and paper.

1.1.4.2. Design reports must contain the following tables and place them in their design report appendices:

A. Student Biographies

- Name
- Previous degree attained – major
- Current degree and expected graduation date (month/year)
- Main area of contribution to the project
- Other information as deemed appropriate by the team

B. Summary of Calculations, model details, controls algorithm etc.

9. *Evaluation Criteria*

9.1. DSATS will select an evaluation committee from its membership

9.2. Criteria/Weighting for Group A (see table below):

Criteria	Metrics	Weight
Drilling system model	Does steering model consider steering method, geometry (e.g. projection-to-bit algorithm), bit side force/tilt, new wellbore, etc.? Are string elasticity, wellbore friction modeled?	30
Control scheme	Does trajectory control algorithm use realistic constraints? Does it use realistic virtual-measurements? Does it consider surveying uncertainties and noise? Does the model utilize a re-planning to target process based on as-drilled surveys? Is basic drilling optimization algorithm implemented? Are rig controls simulated? (e.g. slide vs rotate)	30
The Virtual Drilling App	Features, modularity, and robustness of the app, real-time display, end of well report	20
Performance	Demonstration of the app and the degree to which drilling objectives are met	20
Bonus	Considerations above and beyond the minimum requirements that demonstrate thoroughness and creativity	10
	Maximum achievable score out of 100	110

9.3. Phase II Criteria/Weighting for Group B (see table below):

Criteria	Parameter	Weighting
Phase I:		
a. Safety	Safety: construction and operation	10
b. Mobility of rig	Rig up, move, rig down	5
c. Design considerations and lessons learned		10
d. Mechanical design and functionality, versatility		25
e. Simulation/Model/Algorithm		25
f. Control scheme	Data, controls, response times	25
	Total	100%
Phase II:		
a. Creative Ability	Analysis, concepts, development	10
B. Engineering Skills	Problem/Goal, design criteria, feasibility	10
c. Construction Quality		10
d. Cost Control		10
e. Performance		30
Various parameters such as:	ROP, MSE, Landing Bit, Inclination, and other	
Are these used within the control algorithms		
Accuracy of drilled wellbore trajectory (see Appendix "A" for details)	Proximity of drilled wellbore to required target X/Y coordinates and vertical depths	
f. Quality of wellbore	Tested using the Go-No-Go flexible 'Casing'	10
	Verticality, tortuosity, caliper, other	
g. Data	Data handling, data visualization, data comparison to judges' wellbore logs, and other	20
h. Downhole Sensor Data Used in Control Algorithm	Pass/Fail	Pass/Fail
	Total	100%
Intangibles	Additional score may be added or subtracted by the judges at their discretion	

9.4. Group A Prizes

9.4.1. The winning team of Group A will be sponsored by DSATS to attend the next SPE/IADC Drilling Conference to present a paper that explains their project in detail.

9.4.1.1. The program committee of the Drilling Conference awarded the Drillbotics subcommittee a permanent slot in one of the drilling sessions at the conference. As per SPE's customary procedures, the paper will be archived in OnePetro. In addition, SPE has agreed to furnish a booth in the exhibition area during the conference where the team can erect their rig and describe its operation to the conference attendees. This is an excellent opportunity for students to network with the industry.

9.4.2. Upon submittal to DSATS of a valid expense statement (typically a spreadsheet supported by written receipts) of covered expenses will be reimbursed by the treasurer of DSATS for the following:

9.4.2.1. Round trip economy airfare for the team and one university sponsor/supervisor to the gateway city of the next SPE/IADC Drilling Conference. Entrants should use the SPE approved carrier where possible to minimize cost. Airfares that exceed the SPE rate must be pre-approved by the committee or the reimbursement will be limited to the SPE rate. Information of reduced fare flights is available on the conference website. Please note that reservations must be made before the SPE published deadline. The departure point will be a city near the university, the student's home, or current place of work, subject to review by the Committee. Alternately, a mileage reimbursement will be made in lieu of airfare should the entrants decide to drive rather than fly to the conference. The reimbursement is based on current allowable mileage rates authorized by the US Internal Revenue Service.

9.4.3. One rental car/van at the gateway city for those teams that fly to the conference.

9.4.4. Lodging related to one hotel room per team member will be reimbursed at a rate not to exceed the SPE rate. Note that the room reservations are limited, so entrants must book their rooms early. Room and taxes for the night before the DSATS symposium, the night of the symposium and for the nights of the conference are covered. Charges for the room on the last day of the conference need to be pre-approved by the Committee as most conference attendees depart on the last day of the conference unless there are unusual circumstances.

9.4.5.A per diem will be pre-approved by the Committee each year, which will vary with the cost of living in the gateway city. The per diem is intended to cover average meals (breakfast, lunch and dinner) and incidentals.

9.4.6.ATCE registration will be reimbursed. Students should register for the conference at the student rate. Early registration is appreciated.

9.4.7.Individual award certificates will be presented to all participants upon request, with special certificates given to all finalists.

9.4.8.DSATS may provide additional awards, at its sole discretion.

9.4.9.The evaluation and all decisions on any matter in the competition by the DSATS judges and DSATS board are final.

9.5. Group B Prizes

9.5.1.The winning team of Group B may submit a SPE whitepaper that explains their project in detail.

If the quality of the abstract is approved by the SPE Conference Program Committee, as per SPE's customary procedures, the paper will be archived in OnePetro

9.6. Other prize information

9.6.1.Individual award certificates will be presented to all participants upon request, with special certificates given to all finalists.

9.6.2.DSATS may provide additional awards, at its sole discretion.

9.6.3.The evaluation and all decisions on any matter in the competition by the DSATS judges and DSATS board are final.

10. Final report and paper

10.1. The finalists shall prepare a project report that addresses the items below. We suggest you use the format of most SPE papers. For reference, please see <http://spe.org/authors/resources/>

10.2. The winning team of Group A shall update the report as needed to comply with SPE paper submittal guidelines to write a technical paper for publication by the SPE at its Annual Drilling Conference. SPE typically requires that the manuscript is due in the fall following the Phase II test. While the Drillbotics committee will make every effort to have the paper presented during the Drilling Conference, the SPE Program Committee has authority over which papers will be accepted by the conference. If the paper is not accepted by the conference, the Drillbotics committee will endeavor

to have it presented at the DSATS Symposium and will use its contacts to have the paper published via other related SPE conferences.

- 10.3. The report, paper and all communications with DSATS shall be in the English language. The presentation will be made by at least one member of the student team.
- 10.4. The timing for submittal of the abstract and paper will be the published deadlines per the call for papers and conference guidelines as posted on the SPE's website (www.spe.org).
- 10.5. The abstract must generate sufficient interest with the SPE review committees to warrant publication, although DSATS will help promote acceptance where possible
- 10.6. The paper should address at a minimum
 - 10.6.1. The technical details of the drill system model, assumptions and architecture. Results of the model prediction and discussion of the model results.
 - 10.6.2. Details of the controls scheme, including block diagram and control algorithm. Challenges and trade-offs associated with use of specific control schemes.
 - 10.6.3. Results of the final demonstration and discussion on future work/enhancements.
 - 10.6.4. Recommendations for improvements by DSATS of the competition guidelines, scheduling and provided material.
 - 10.6.5. Areas of learning gained through the competition not covered in the university course material.
 - 10.6.6. A brief bio or CV of the team members and their sponsoring faculty.

11. *Terms and conditions*

- 11.1. In no event will SPE, including its directors, officers, employees and agents, as well as DSATS members and officers, and sponsors of the competition, be liable for any damages whatsoever, including without limitation, direct, indirect, special, incidental, consequential, lost profits, or punitive, whether based on contract, tort or any other legal theory, even if SPE or DSATS has been advised of the possibility of such damages.
- 11.2. By entering this competition,
 - 11.2.1. Participants and Universities agree to indemnify and hold harmless SPE, its directors, officers, employees and agents, as well as DSATS members and officers, and sponsors of the competition, from all liability, injuries, loss damages, costs or expenses (including attorneys' fees) which are sustained, incurred or required arising out of participation by any parties involved in the competition.

11.2.2. Participants and Universities agree and acknowledge that participation in the competition is an agreement to all of the rules, regulations, terms and conditions in this document, including revisions and FAQs posted to the DSATS and Drillbotics websites (see section [2.1](#)).

11.2.3. Winning teams and finalists must agree to the publication of their names, photographs and final paper on the DSATS web site.

11.3. All entries will be distributed to the Drillbotics Committee for the purpose of judging the competition. Design features will not be published until after all teams have been judged and a winner is announced. Previous years' submittals, reports, photos and similar documentation will be publicly available to foster an open exchange of information that will hopefully lead to faster learning for all participants, both new and experienced.

11.4. DSATS and the SPE cannot provide funding to sanctioned individuals and organization per current US law.

11.5. Participants must comply with all local laws applicable to this contest.

12. Marketing

12.1. Upon request, DSATS will provide a link on its website to all participating universities.

12.2. If university policy allows, various industry journals may send a reporter to witness the tests and interview students to publicize the project.

12.3. Drillbotics is now a registered trademark. According to international law, the proper reference is to use Drillbotics® instead of Drillbotics™. The trademark reference is only needed the first time Drillbotics is referenced.

12.4. Any team that wishes to use the trademark on signs, tee shirts, technical papers or for other purposes may receive a no-cost license upon request. Send the request by email to the committee at 2021@Drillbotics.com. Upon completion of the license agreement, access to the files with the logo will become available.

Appendix

A. Directional Objective Requirements

The following attached pages describe the directional objectives as well as the data/deliverables requirements. Scoring for the directional competition objective will be primarily based on how accurately the directional targets are intersected by the calculated well trajectory.

Objectives

- Hit one or more targets at one or more vertical depth(s) and X/Y coordinates
- For the Group B competition, the starting directional plan to hit the targets will not require wellbore inclinations in excess of 30° from vertical, 15° change in azimuth, or 10" displacement (departure from the vertical axis at well center) The max displacement/inclination/azimuth are total/accumulated from the start to the end of the well path.
- Please note: Teams should be prepared to drill any given trajectory within the specified parameters, so the coordinates will not be provided in advance of the test.

Automation Requirements

- Drilling mode/survey mode switching must be automated (i.e. built-in survey interval and drill string movement for on/off-bottom, slide/rotation mode switching)
- Steering requirements (e.g. toolface direction, slide length) must be calculated autonomously
 - NOTE: Steering mechanism can still require human intervention for placement and/or retrieval (e.g. whipstock) but orientation of steering mechanism must be calculated by the system and shown on the rig floor display.
- Directional surveying process must be entirely autonomous
 - Survey qualification must be done autonomously, however secondary qualification/verification/override can be made by a human
- Dogleg severity required to hit target(s), distance/direction to plan must be autonomously calculated at each survey station and shown on the rig floor display

Deliverables Requirements (Magnetic surveying)

- All teams are required to provide a definitive directional survey (TXT, LAS, or CSV format) meeting the following minimum requirements:
 - Header info to include:
 - Team/school name
 - Directional Survey Date
 - Well Center Coordinates (WGS84 Latitude & Longitude)
 - True Vertical Depth Reference (in depth units above block level)
 - Grid Convergence
 - Geomagnetic model used (if applicable)
 - Magnetic declination applied (Geomagnetic model or in-field referenced)
 - Total Azimuth Correction
 - Magnetic field dip reference (Geomagnetic model or in-field referenced)
 - Total magnetic field strength reference (Geomagnetic model or in-field referenced)

B. Safety

The team's safety plan should consider all foreseeable hazards and methods to mitigate them. Personal protective equipment is part of a safety plan but is far from sufficient. Teams must consider risks due to handling the rock, rotating machinery, electrical shock and others. How the team communicates with each other before and during rig operations is also important. Judges will grade each team on its comprehensive safety case.

Because most of the rigs have equipment spinning at high RPMs, some form of protective cover must be included in the team's rig design. A broken coupling, a loose screw or similar item becomes a projectile that can lead to serious injury to the team members, judges or visitors. Judges may decide to deny a team from competing if their design is unsafe.

The following links are a good starting point, but is by no means a comprehensive list of links:

- OSHA Pocket Guide, Worker Safety Series: <https://www.osha.gov/Publications/OSHA3252/3252.html>
- OSHA Checklist for General Industry: <http://www.scohsa.llronline.com/pdfs/genind.pdf>

C. Group B Competition Guidelines

The Group B competition applies to the automation of a physical rig. This Appendix C 1.0 (physical rig) replaces [Section 3.0](#) (virtual rig) for those teams who wish to compete in Group B.

1.0. Physical Rig Considerations: 2020-2021 High Level Challenge and Judging Changes

- 1.0.1.* Directional steering is a more critical part of the competition for 2021. (see 3.6) The wellbore must be started vertically and then kicked off below a specified depth to hit multiple directional targets (at varying X/Y coordinates and vertical depths). Teams score more points based on how accurately each directional target is hit (see 9.3 for scoring details)
- 1.0.2.* Downhole sensors are mandatory, and it is also mandatory to implement their data into the control algorithm of the rig. A severe penalty will be applied to teams who do not use downhole sensors. Closed loop control of the rig based on downhole data is mandatory in this year's competition and not integrating this data set into the control algorithm is considered a "F- Failing grade" in this year's competition.
- 1.0.3.* A homogeneous sandstone Rock Sample will be provided by Drillbotics (see A 1.4)
- 1.0.4.* DSATS to provide a new bit. The bit will be 1.5" diameter and 2" length. Students are permitted to use their own drill bit for the 2021 competition. (see A 1.5)
- 1.0.5.* Additional information regarding the judging of the competition is detailed in section 1.16.

1.1. Two Project Phases

Fall Semester 2020

The first phase of the project is to organize a team to design an automatic drilling machine to solve the project problem. It is not necessary to build any equipment in this phase, but it is okay to do so. Design considerations should include current industry practices and the team should evaluate the advantages and shortcomings of today's devices. The design effort may be assisted by university faculty, but the students are encouraged to introduce novel designs for consideration. The design should also include consideration for downhole sensor and the control system to automatically control the drilling process. The level of student, faculty and technical staff involvement shall be reported when submitting the design. For returning teams, the Phase I Design should include an analysis of data and learnings from previous ("offset") wells drilled.

Spring Semester 2021

During the second phase, the finalist teams selected by DSATS proceed to the construction and drilling operation will use the previous semester's design to build an automated drilling machine. As per industry practices, it is common during construction and initial operations to run into problems that require a re-design. The team may change the design as needed in order to solve the problem subject to section 3.3. Teams may use all or part of a previous year's rig.

See section 6 for detailed timeline information.

1.2. Phase I – Design Competition

Design an automated drilling machine in accordance with the rules below.

1.2.1. DSATS envisions a small (perhaps 2 meters high) drilling machine that can physically imitate the functionality of full-scale rig machinery. (Since the winning machines will be presented at the SPE conference, there may be height restrictions imposed by the conference facility, so machines that are too tall may not be allowed on the exhibit floor.) The machine will be the property of the university and can be used in future research and competitions. New and novel approaches that improve on existing industry designs are preferred. While innovative designs are welcome, they should have a practical application to drilling for oil and gas.

1.2.2. The drilling machine will use electrical power from the local grid not to exceed 25 horsepower. Lower power consumption resulting from energy efficient designs will receive additional consideration.

1.2.3. The design must provide an accurate and continuous measurement of Weight-On-Bit (WOB), inclination, azimuth, and depth; as well as other drilling parameters (see Appendix "A" for directional surveying-specific data requirements), that should be presented as a digital record across the period of the test. All depth related measurements shall use the rig floor as the datum, not the top of the rock (the offset between the rock surface and the rig floor must be adequately processed within the control algorithms). Appropriate statistical measurements should be made at frequencies and with an accuracy and appropriate frequency content for the dynamics of the drilling system both at surface and downhole. Discussion of such choices should be included in the design report.

1.2.3.1. Distinguish in all data and documentation the difference between Weight-On-Bit and Hook Load; be specific when referring to these parameters

1.2.4. The proposed design must be offered in Phase I of the project, but changes are allowed in Phase II, as long as they are reported to the Committee via students' monthly reports. A summary of all significant changes, including the reason modifications were necessary, must be included in the students' final report.

1.2.5. Design submittal by the students shall include:

1.2.5.1. Engineering drawings of the rig concept, mechanical and electrical and auxiliary systems, if any

1.2.5.2. Design notes and calculations

1.2.5.2.1. All engineering calculations shall be included in the Phase I report, even if the rig is built using previous years' designs. This ensures that the 2021 team reviewed and understood the previous design assumptions and calculations.

Calculations should include each formula considered in the design, a reference that shows the origins of the formula, why it was chosen, what engineering assumptions were made, a definition of all variables and the values used in the calculation.

Example

Buckling limit Euler’s Equation (1) cite a reference here or in the reference section of your design report

The critical buckling load, *P_{bcr}*, is calculated:

$$P_{bcr} = \pi^2 * E * I / (K * L)^2$$

- P_{bcr}*: Critical buckling load
- E*: Modulus elasticity of the aluminum drill pipe
- I*: Area moment of inertia
- L*: Length of the column
- K*: Column effective length factor (explain how you chose the appropriate k or n factor)

1.2.5.2.2. The report should include a table that summarizes ALL calculations.

Example

<i>Calculations</i>	<i>Formula</i>	<i>Reference</i>	<i>Results</i>
<i>Moment of Inertia</i>	$I = \pi / 64 (dp^4 - idp^4)$	<i>Thin wall approx. or ID/OD calc separately or other? List your reference</i>	<i>0.000546 in⁴</i>
<i>Buckling Limit</i>	$P_{bcr} = \pi^2 * E * I / (K * L)^2$	<i>Euler’s Eq</i>	<i>18.9 kg</i>

- 1.2.5.3. Control system architecture. (The response time of measurements, data aggregation and control algorithms should be estimated.)
- 1.2.5.4. Key features for any models and control software.
- 1.2.5.5. Proposed data handling and display.
- 1.2.5.6. Specification for sensors, signal processing and instrumentation, (verifying their accuracy, precision, frequency response and environmental stability), including the methods planned for calibration before and after the Phase II testing.

- 1.2.5.7. Plan for instrumentation of sensors in the BHA, as well as a method to synchronize all measurements and utilize both the surface and downhole sensors for real-time control of the drilling process.
- 1.2.5.8. An explanation of the implementation of the output of the BHA sensors to improve the trajectory of the wellbore, drilling efficiency and other drilling concerns.
- 1.2.5.9. An explanation of the algorithm used to autonomously control the drilling rig based on the output of the BHA sensors
- 1.2.5.10. An explanation of the principles being applied to directionally steer the wellbore and hit the required targets (see Appendix "A") with the intent to score the maximum amount of points
- 1.2.5.11. Cost estimate and funding plan
- 1.2.5.12. A design summary video used to outline the design submittal not to exceed five (5) minutes in length. Videos shall be the property of the university, but DSATS shall have the rights to use the videos on its websites and in its meetings or events.
- 1.2.5.13. All design, construction and operation of the project are subject to the terms and conditions of section 10.
- 1.2.5.14. A safety case shall be part of the Phase I design (see Appendix "B"). Include a review of potential hazards during the planned construction and operation of the rig, and for the unloading and handling of any rock samples or other heavy items. An example of a safety case will be posted on the Drillbotics.com website.
- 1.2.5.15. The Phase I design report should include a discussion regarding the major design features proposed (mechanical and otherwise) - are they scalable to today's working rigs? If not, what would be needed to allow implementation?
- 1.2.5.16. The Phase I design report should include a discussion regarding the control scheme and algorithm - How is each individual measurement used in the control code? Are they all given equal weight, and if not, what criteria is used to assign importance? What is the expected response time of the control system's key components? How will this affect equipment selection? The teams are encouraged to perform control simulations to verify the control scheme.

1.2.6.A committee of DSATS members (the Committee) will review the Phase I designs and select the top five (5) teams² who will progress to Phase II of the competition.

1.2.7.DSATS shall also award a certificate of recognition and publication on its website for the most innovative design. The design video will also be shown at the DSATS automation symposium at SPE conferences.

1.2.8.DSATS will not fund any equipment, tools, software or other material, including labor, for the construction of the rig. Student teams are encouraged to find external funding from industry participants and suppliers.

1.3. Phase II – Drilling Competition

1.3.1.In the spring term of 2021, qualifying teams will build the rig and use it to drill rock samples provided by DSATS. Drilling a deviated well to hit the required targets (see Appendix “A”), efficiently through the sample while controlling drilling dysfunctions is the primary technical objective of the competition. Scoring of the directional drilling component will be primarily based on the horizontal distance from the target coordinate at which each target vertical depth was intersected. The use of both surface and downhole measurements to control the drilling process in real-time is mandatory, failure to do so will result in a failing grade. To avoid disqualification due to a downhole sensor failure, redundant or immediately replaceable items should be part of the design and implementation. Time to replace a sensor will be added to the drilling time for calculation of ROP.

1.3.2. The teams are to use manual control to pre-drill a vertical pilot hole not more than 1” deep measured from the rock’s top face. This hole is to be drilled using the competition drilling rig. Location of this pilot hole will be marked on each sample by the committee at the intersection of two lines drawn from opposite corners of the rock sample.

1.3.3. Teams may use glue or use a mechanical fastener to attach a bell nipple or diverter housing to the top of the rock to allow connection of a flowline for return mud flow. The maximum allowable length of the bell nipple is 8 inches. If you use a fastener, be careful not to break the rock.

² The number of finalists could be increased or decreased by the DSATS Board of Directors.

1.3.4. When the competition drilling begins, teams will be required to continue to drill the pilot hole vertically to the kick off point. The kick off point may be at any depth greater than 4" below the surface of the rock.

1.3.5. Navigation shall be done autonomously

1.3.5.1. Manual intervention to add and/or remove a steering mechanism (e.g. whipstock) is permitted, however the determination/calculation of the orientation setting of the mechanism is required to be autonomous and must be shown on the rig floor display during each steering mechanism manipulation activity. The time to change orientation will affect the team's ROP calculation.

1.3.6. No lateral forces are allowed to be applied above the top face of the rock.

1.3.7. No forces are allowed to be applied external to the rock that will force the drill bit in a particular direction

1.3.8. External magnetic field effects from the drilling rigs will be present on the directional sensors used to drill the wellbore. The industry has accepted practice of magnetic ranging. This may be a technique worth investigating to improve the signal to noise of magnetic measurements

1.3.9. Once drilling commences, the test will continue until the drill bit exits the rock sample, or three (3) hours, whichever comes first

1.3.10. Drilling performance will be observed and measured by Drillbotics judges invited to attend and witness the test. This could be a virtual event depending on travel restrictions. The details will be announced in early 2021.

1.3.11. DSATS will judge the competitors primarily on their ability to hit the required targets as accurately (i.e. as close to target center at the given target vertical depth) as possible (see Appendix "A" for details)

1.3.12. The final test will be scheduled late in the school year.

1.4. Rock Samples

1.4.1. DSATS will prepare a set of nearly identical homogeneous sandstone samples appx. 12"W x 24"L x 24"H (30 x 60 x 60 cm) for the final demonstration

1.4.2. The rock sample will be homogeneous sandstone, and rock compressive strength values will be provided for the sandstone samples furnished by DSATS in early 2021. The Drillbotics committee will mark the surface of rock to indicate the well center where drilling will start. It will be located at the intersection of two lines drawn from opposite corners of the rock sample.

1.4.3. The university and/or students may acquire or produce at their own cost rock samples as needed to verify the design and allow students to practice using their machine prior to the test. Drilling of any samples provided by DSATS prior to Phase II testing is not allowed and could lead to disqualification, except for the pilot hole to be drilled at the test location.

1.5. Bits

1.5.1. Upon request, DSATS will send a bit to the finalist teams for use in Phase II. It is expected that the BHA and pipe will cause some difficulty, both for initiating drilling dysfunction and for sensor integration and data telemetry. The judges will look for creative concepts supported by sound reasoning showing an understanding of how the BHA, bit and drillstring function together, and how the downhole system measures, samples and transmits the drilling data.

1.5.2. Upon request, the bit shall be returned to the Committee following Phase II testing for reconditioning for use in future competitions.

1.5.3. One (1) PDC bit will be provided by DSATS to be used during the Phase II tests. For 2020-2021 the bit will be:

1.5.3.1. A micro-bit 1.5" in (38.1 mm) diameter and 2.0" in total length.

1.5.3.2. Low axial aggressiveness and high side aggressiveness (i.e. high bit anisotropy).

1.5.4. Students are encouraged to consider bit wear prior to the final test and its impact on drilling performance during the onsite testing. Based on prior competitions, bit wear should be minimal but some cutter damage is always possible.

1.5.5. Student teams may build or buy similar drill bits to test their design with the rock samples they sourced. The students must not engage any third parties or receive professional assistance in designing their own bit, however manufacturing can be performed by a third party.

1.5.6. For the final competition, the students may use the directional drill bit provided by DSATS or use their own bit design. However, the dimensions of their bits must not exceed 1.5 inches in diameter and 2 inches long. This provision is made to enable students to fully optimize the bit design for their specific directional system.

1.6. Drillpipe

- 1.6.1. Preliminary typical tubing specifications for aluminum tubing are listed below to assist with the mechanical and electrical design of the rig. Stainless steel tubing or aluminum tubing is permitted for the competition but must use the same dimensions as below, or the nearest metric equivalent. Teams may choose durability over flexibility and shall explain their choice in the design report.
- 1.6.2. The drill pipe specifications for the 2020-2021 competition are subject to change, but should be:
- 1.6.2.1. Round Aluminum Tube 3/8 inch diameter x 36 inches long; 0.049 inch wall or equivalent
 - 1.6.2.2. The material from KS Precision Metals is a typical low alloy material: "Our Aluminum tubing with wall thickness of .035 or .049 is 6061 T6"
- 1.6.3. DSATS will not be providing tubing to the competition teams.
- 1.6.4. The use of a metric equivalent of the tubing is permitted.
- 1.6.5. Tubing is usually available from various hobby shops such as K-S Hobby and Craft Metal Tubing and via Amazon and other suppliers.

<http://www.hobbylinc.com/htm/k+s/k+s9409.htm>

1.7. Tool joints

- 1.7.1. Students may design their own tool joints as long as the design concept is included in the Phase I proposal.
- 1.7.2. Alternately, students may use commercially available connectors/fittings attached to the drillpipe using threads, epoxy cement or other material, and/or may use retaining screws if desired, as long as the design concept is included in the Phase I proposal.
- 1.7.2.1. A fitting used somewhat successfully in 2017 is available from Swagelock. In 2018, the winning team used a fitting from Vertex.
 - 1.7.2.2. A fitting used successfully in 2016, but which did not work well in 2017, is available from Lenz (<http://lenzinc.com/products/o-ring-seal-hydraulic-tube-fitting/hydraulic-straight-connectors>) that uses a split-ring to allow a torque transfer across the fitting.
- 1.7.3. Students must state WHY they choose a tooljoint design in the Phase I proposal.



1.8. Bit sub/drill collar/stabilizers

- 1.8.1. It is expected that each team will design and build their own bit sub. Instrumentation of the bit sub is ideal for directional sensors.
- 1.8.2. Additional weight may be added to the bit sub, or surface weight/force (above the rock sample) may be applied to provide weight on bit and drill pipe tension
- 1.8.3. Stabilizers are permitted but will be limited in length at the discretion of the Challenge Committee. Advise the committee of your choice and why and include this in the Phase I design for committee consideration.
- 1.8.4. Students must add sensors to the drillstring but are not permitted to instrument the rock samples. They must have a smaller diameter than the stabilizers and bit by at least 10%. Please include design concepts in the Phase I design.
- 1.8.5. The addition of along-string sensors to measure vibrations, verticality and/or tortuosity or other parameters will receive extra consideration. They must have a smaller diameter than the stabilizers and bit by at least 10%.

1.9. Automated Drilling

- 1.9.1. Drilling automation should be considered a combination of data, control AND dynamic modeling so that the control algorithm can determine how to respond to differences between the expected and actual performance. Process state detection can often enhance automation performance. Refer to documents posted on the DSATS website for more information.
- 1.9.2. Once drilling of the sample commences, the machine should operate autonomously. Remote operation and/or intervention is not allowed.
- 1.9.3. All directional control operations should be autonomously controlled by the drilling rig
 - 1.9.3.1. Manual intervention to add and/or remove a steering mechanism (e.g. whipstock) is permitted, however the determination/calculation of the orientation setting of the mechanism is required to be autonomous and must be shown on the rig floor display during each steering mechanism manipulation activity
 - 1.9.3.2. Length and timing of drilling modes (e.g. switching from slide drilling to rotational drilling, initiating the directional surveying procedure at the appropriate survey interval), must be autonomously determined/calculated and controlled

1.9.3.3. Directional surveys acquired by the system need to be used as feedback for the steering control (and/or calculation of the steering requirements) logic.

1.9.4. Set-point commands for drilling parameters (WOB, RPM, ROP, etc.) should be optimized such that drilling dysfunctions are avoided, and drilling can be completed within the given time frame. Real-time optimization should be done automatically. The controllers need to ensure that the drilling parameters respond once the set points are altered.

1.10. Sensors

1.10.1. The team may elect to use existing oilfield sensors or may look to other industries for alternate sensors.

1.10.2. The team may develop its own sensors if so desired.

1.10.3. Sensor quality differs from data quality. Both are important considerations in this competition.

1.10.4. The final report shall address which sensors were selected and why. The sensor calibration process shall also be explained.

1.11. Data collection and handling

1.11.1. The team may elect to use standard data collection and recording techniques or may develop their own. Data handling techniques and why they were chosen should be described in the Phase I submittal.

1.11.2. The final report shall address which data systems were selected and why.

1.11.3. The observed response time of measurements, data aggregation and control algorithms should be compared to the Phase I estimates and published in the final report.

1.11.4. Describe how data is measured, aggregated, stored and retrieved. Describe calibration and data validation techniques used.

1.12. Data visualization

1.12.1. Novel ways of presenting the data and progress of drilling in real time while drilling will receive particular attention from the judges.

1.12.2. Visualization of the processes (automation, optimization, drilling state, etc.) should be intuitive and easily understood by the judges, who will view this from the perspective of the driller operating a rig equipped with automated controls.

- 1.12.3. Data must be presented in a format that allows the judges to easily determine bit depth, elapsed drilling time, ROP, MSE, verticality/inclination, vibration, and any other calculated or measured variable used to outline the drilling rigs performance to the judges. Lack of an appealing and usable Graphic User Interface (GUI) will be noted to the detriment of the team.
- 1.12.4. All depths shall use the industry-standard datum of rotary/kelly bushing interface (RKB), which should be the top of the rig's "drill floor."
- 1.12.5. An End of Well (EOW) report should be provided to the judges at the conclusion of drilling.
- 1.12.6. See Appendix "A" for directional surveying-specific data visualization requirements

1.13. Measure and analyze the performance

- 1.13.1. The drilling machine should react to changing "downhole" conditions to select the optimal drilling parameters for improved performance, as measured by the rate of penetration (ROP), mechanical specific energy (MSE), verticality, cost per foot or meter, and other standard drilling measures or key performance indicators. Adding parameters such as MSE, or similar features, to the control algorithms will receive special attention from the judges.
- 1.13.2. Design limits of the drilling machine shall be determined and shall be incorporated in the programming of the controls during the construction phase.
- 1.13.3. Downhole measurements from directional sensors are to be used for adjusting drilling parameters and control of drilling machines used to aid in directional drilling
- 1.13.4. The final report (see Clause **Error! Reference source not found.**) shall outline drilling performance and efficiency criteria and measured results.
- 1.13.5. One of DSATS' goals is to promote plug and play capability to accelerate the implementation of drilling automation. A DSATS committee is preparing definitions and examples of proposed data communication protocols and interfaces. Once this is available, the Drillbotics competition will require the use of these standard protocols. This will not be a requirement for 2021 but it will be included in future competitions. Links to these standards will be added to the Drillbotics.com website when they are published.

1.14. The test well:

- 1.14.1. The location and logistics for the final demonstration will be announced in early 2021.
- 1.14.2. Prior to the commencement of the test, teams will attach a bell nipple (per 1.33). They will then manually drill the pilot hole not to exceed 1" deep.

- 1.14.3. When the test begins, the teams will start drilling autonomously by continuing to drill the pilot hole, keeping the wellbore as vertical as possible until reaching the kick-off point. All rigs start the drilling competition at the same time.
- 1.14.4. The teams will kick off from vertical at any depth below the 4" vertical surface hole
- 1.14.5. The teams will attempt to hit multiple targets (varying X/Y coordinates and vertical depths) by following a provided directional plan/trajectory. Directional objective scoring will be based on the accuracy of the target depth intersection (i.e. horizontal distance from the target coordinate at the given target vertical depth). Refer to Appendix "A" for additional directional objective details.
- 1.14.6. No lateral forces may be applied above the rock or to the rock.
- 1.14.7. Drilling will stop at 3 hours or when the last team exits the rock sample.
- 1.14.8. A closed-loop fluid circulation system is not required, but could be of advantage for directional drilling, the bit and machinery should be cooled with air or fluid/water if needed. The design of the fluid system, if any, should be included in the Phase I design.
- 1.14.9. The rock sample will be homogeneous and will be capable of aiding in closed-loop fluid circulation. Note that the rock samples will leak once the drillbit punctures a rock face, so a rig design that includes a containment system is required.
- 1.14.10. Casing must fit in the directional wellbore. The ability to "run casing" is the secondary judging metric. Judges will run a "flexible" casing used as a gauge of borehole quality
- 1.14.11. A rig move, walking or skidding is not required, but the mobility of the rig will be considered in the design phase. The chargeable weight of the rig is an important consideration by the judges. See C 1.18.4.2 F regarding how this is calculated.
- 1.15. **Not included in the 2020-2021 competition**
- 1.15.1. The drilling will not include automating the making or breaking of connections. If connections are necessary due to the rig and drillstring design, connections should be made manually, and the time involved with the connections will be included with respect to its effect on drilling performance (rate of penetration reduction).
- 1.16. **Other Considerations**
- 1.16.1. The design concepts shall be developed by the student team under the supervision of the faculty. Faculty and lab assistants should review the designs to ensure student safety (see Appendix B).

1.16.2. Construction of the equipment shall be supervised by the student team, but may use skilled labor such as welders and lab technicians. The use of outside assistance shall be discussed in the reports and the final paper. DSATS encourages the students to gain hands-on experience with the construction of the rig since this experience will be helpful to the career of individuals in the drilling industry.

1.17. Presentation to judges at Phase II Testing

1.17.1. The students will present a BRIEF summary of their final design, highlighting changes from their Phase I design, if any. Include an explanation of why any changes were necessary, as this indicates to the judges how much students learned during the design and construction process. Explain what measurement and control features have been deployed. Describe novel developments or just something learned that was worthwhile. Also include how actual expenses compared with the initial estimate. (Previous teams used a short PowerPoint presentation of about ten slides or so. Use any format you like.) At some time during your talk, let us know who the team members are and what background they have that pertains to the project. Be sure to include all your team members as presenters, not just one spokesperson. The committee wants to see if all team members have a good understanding of key issues.

1.17.2. Judges will ask questions to ascertain additional details about the design and construction process and to see if all team members have a reasonable understanding how all the various disciplines used for the rig design and construction fit together.

1.17.3. All teams may sit in for the presentations and Q&A of the other teams. The order of presentation will be determined by drawing lots.

1.18. Project report

1.18.1. Starting in the fall term, the student team shall submit to DSATS a short monthly project report that is no more than one page in length (additional pages will be ignored) due on or before the last day of each month. Send it via email to 2021@Drilbotics.com. The monthly report should include:

1.18.2. Phase I

- Key project activities over the past month.
- Rig design criteria, constraints, tradeoffs, and how critical decisions were determined
- Cost updates
- Significant new learning, if any

1.18.3. Phase II

- Construction issues and resolution
- Summary of recorded data and key events
- Drilling parameters [such as WOB] and how they impact the test
- Other items of interest

1.18.4. Report content

1.18.4.1. To teach students that their work involves economic trade-offs, the monthly report should include at a minimum a summary estimate of team member labor hours for each step in the project: design, construction, testing, reporting, and a cost summary for hardware and software related expenditures. Also include labor for non-students that affect the cost of the project. Labor rates are not considered, as to eliminate international currency effects. Labor is not considered in the cost limits of item 6.1, but should be discussed in the report and paper.

1.18.4.2. Design reports must contain the following tables and place them in their design report appendices:

B. Student Biographies

- Name
- Previous degree attained – major
- Current degree and expected graduation date (month/year)
- Main area of contribution to the project
- Other information as deemed appropriate by the team

C. Summary of Calculations (list these at a minimum, list other in a similar format)

Parameter	Symbol	Calculated Results		Safety Factor	Max Allowable		Reference	(Other as needed)
		Field Units	Metric Units		Field Units	Metric Units		
Critical buckling load								
Burst limit								
Torque limit								
... Other								

D. Power Consumption (rename devices as appropriate)

Device	Voltage	Current	Estimated		Single or Three ϕ	(Other as needed)
			HP	Watts		
Rotation						
Hoist						
Pump						
... Other						
Controls						
Displays						
...						
Total						

E. Diagram showing maximum dimensions of rig when operational (Include all auxiliaries) [Needed to determine size of display area as the Drilling Conference and confirm the height is within the limits imposed by the conference organizers]

F. Chargeable Weight of Rig (include shipping crates/boxes for rig and auxiliaries)

- The Chargeable Weight of Freight shipments are calculated as the Actual Weight (Gross Weight) or the Volumetric (also called Volume or

Dimensional) Weight of the shipment, whichever is the greater. This uses an estimated weight that is calculated based on the dimensions (length, width and height) of a package (shipments are always shown in the order of L x W x H). Typically, large items with a light overall weight take up more space on an aircraft than a small, heavy item. That's why the shippers charge according to Chargeable Weight.

- Multiply the length by the width by the height (L x W x H) in inches to obtain the cubic inches, then:
- To obtain the dimensional weight in pounds using inches, divide the cubic inch result by 166
- To obtain the dimensional weight in kilograms using inches, divide the cubic inch result by 366
- Using Dimensions in Centimeters: To obtain the dimensional weight in kilograms using centimeters, multiply the length by the width by the height (L x W x H) in centimeters and divide the result by 6000

1.18.5. File naming convention

1.18.5.1. To avoid extra work by the committee to rename all files, please use this convention for:

1.18.5.1.1. Monthly reports

Year-Month# University Name (abbreviated)

(note this is the competition year (spring term))

Example 2021-09 UDC

1.18.5.1.2. Design reports

Year University Name (abbreviated)

(note this is the competition year (spring term))

Example 2021 University of Drillbotics Competition

1.19. Final report and paper

- 1.19.1.* The finalists shall prepare a project report that addresses the items below. We suggest you use the format of most SPE papers. For reference, please see <http://spe.org/authors/resources/>
- 1.19.2.* The winning team of Group B is encouraged to update the report as needed to comply with SPE paper submittal guidelines and to submit a technical paper for publication by the SPE at its Annual Drilling Conference. SPE typically requires that the manuscript is due in the fall following the Phase II test.
- 1.19.3.* The timing for submittal of the abstract and paper will be the published deadlines per the call for papers and conference guidelines as posted on the SPE's website (www.spe.org).
- 1.19.4.* The abstract must generate sufficient interest with the SPE review committees to warrant publication, although DSATS will help promote acceptance where possible
- 1.19.5.* The paper should address at a minimum
 - 1.19.5.1.* The technical and economic considerations for the control system, rig, and BHA design, including why certain features were chosen and why others were rejected.
 - 1.19.5.2.* The setup of the experimental test, the results and shortcomings.
 - 1.19.5.3.* Recommendations for improvements to the design and testing procedures.
 - 1.19.5.4.* Recommendations for improvements by DSATS of the competition guidelines, scheduling and provided material.
 - 1.19.5.5.* Areas of learning gained through the competition not covered in the university course material.
 - 1.19.5.6.* A brief bio or CV of the team members and their sponsoring faculty.

Appendix **B**

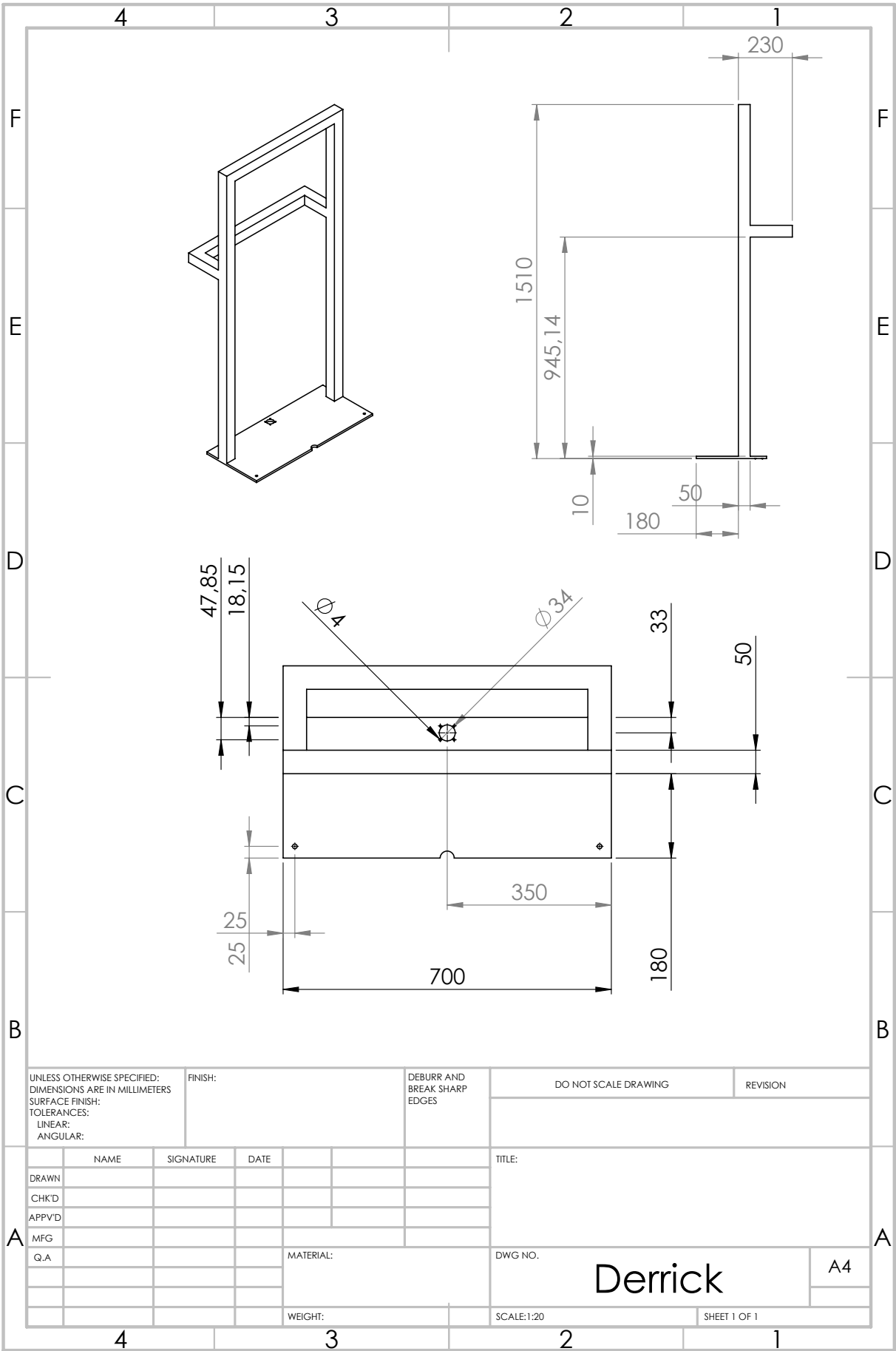
Labview/Simulink Control system

LEGGE INN STORE FINE BIDLER

(This page is intentionally left blank)

Appendix **C**

Framework and Cabinet



UNLESS OTHERWISE SPECIFIED:
 DIMENSIONS ARE IN MILLIMETERS
 SURFACE FINISH:
 TOLERANCES:
 LINEAR:
 ANGULAR:

FINISH:

DEBURR AND
 BREAK SHARP
 EDGES

DO NOT SCALE DRAWING

REVISION

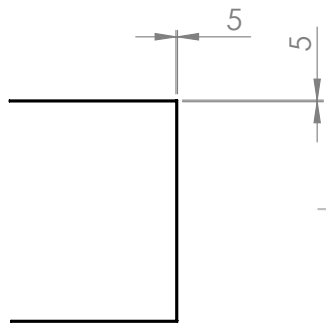
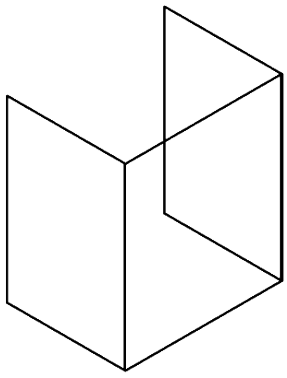
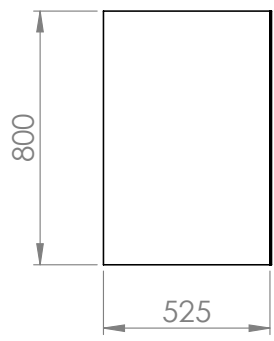
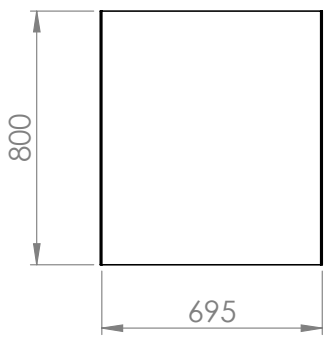
	NAME	SIGNATURE	DATE
DRAWN			
CHKD			
APPV'D			
MFG			
Q.A.			

TITLE:

DWG NO. **Derrick**

SCALE: 1:20

SHEET 1 OF 1



UNLESS OTHERWISE SPECIFIED: FINISH: DEBURR AND BREAK SHARP EDGES
 DIMENSIONS ARE IN MILLIMETERS DO NOT SCALE DRAWING REVISION
 SURFACE FINISH: TOLERANCES: LINEAR: ANGULAR:

	NAME	SIGNATURE	DATE		
DRAWN					
CHKD					
APPV'D					
MFG					
Q.A				MATERIAL:	
				WEIGHT:	

TITLE:
 DWG NO. Shower_cabinet A4
 SCALE: 1:20 SHEET 1 OF 1

(This page is intentionally left blank)

Appendix **D**

Hoisting Motor Specifications

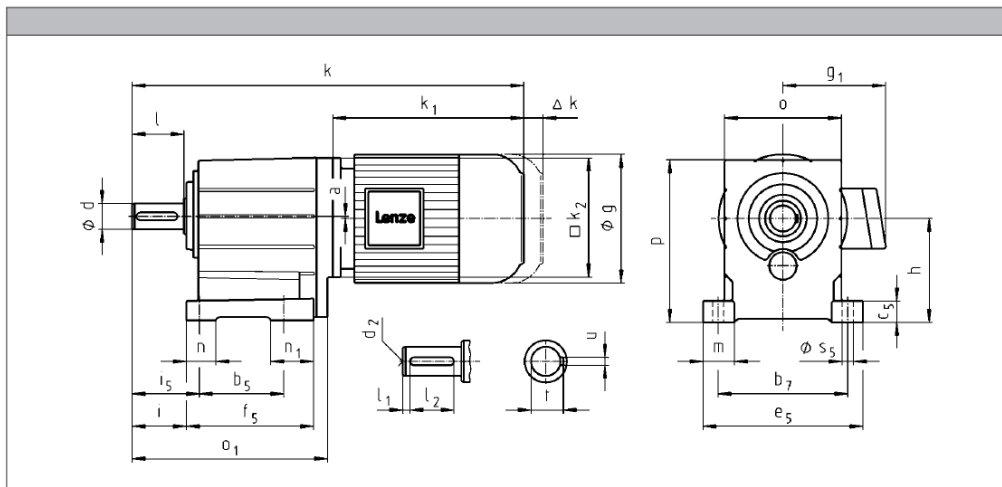
GST helical gearboxes

Technical data



Dimensions

GST□□-2M VBR



APPENDIX D. HOISTING MOTOR SPECIFICATIONS

		063C42	071C11	071C13 071C31	071C32	071C33	071C42	080C13 080C33
g		123			139			156
g ₁	MDEMAXX MDSMAXX	100			109			150
	MDEMABR MDSMABR	107			118			132
k ₁	MDEMAXX MDSMAXX	187			207			224.5
k ₂				120				145
Δ k	MDEMABR MDSMABR	40			52			73
	MDFMAXX MDFMABR	170			128 165			183
	k							
	GST03	329			349		349	
GST04	371			391			413	
GST05	401			421			443	
GST06	427			447			469	
GST07							525	

	a	h ¹⁾	o ¹⁾	p ¹⁾
GST03	2	65	90	101
GST04	0	80	100	132
GST05	1	100	115	158.5
GST06	2	125	145	198
GST07	3	160	180	251

	d	d ₂	l	l ₁	l ₂	u	t	i	i ₅	o ₁	b ₅	b ₇	c ₅	e ₅	f ₅	m	n	n ₁	s ₅	
	k6																			
GST03	14 20	M5 M6	28 40	4 5	20 28	5 6	16 22.5	34 46	40 52	127 139	60	91	11	105	84	20				6.6
GST04	20	M6	40	5	28	6	22.5	43	53	174	76	105	18	129	112	24.5	20	36	9	
GST05	25	M10	50	4	40	8	28	53	66	214	90	125	23	155	139	32.5	26	49	11	
GST06	30	M10	60	6	45	8	33	64	79	243	106	160	28	196	157	38	35	52	13.5	
GST07	40	M16	80	7	63	12	43	84	104	302	130	200	34	247	196	48.5	45	66	18	

¹⁾ k₂ !

Appendix E

Top Drive Motor Specifications

Motor data MF

Technical data



Rated data for 120 Hz

4-pole motors

Product	P_N [kW]	n_N [r/min]	M_N [Nm]	M_{max} [Nm]	$J^{(1)}$ [kgcm ²]	$m^{(1)}$ [kg]
MF□MA□□063-32	0.55	3440	1.53	6.00	3.70	4.40
MF□MA□□063-42	0.75	3400	2.11	8.00	3.70	4.40
MF□MA□□071-32	1.10	3490	3.01	12.0	12.8	6.40
MF□MA□□071-42	1.50	3450	4.15	16.0	12.8	6.40
MF□MA□□080-32	2.20	3500	6.00	24.0	28.0	11.0
MF□MA□□080-42	3.00	3480	8.20	32.0	28.0	11.0
MF□MA□□090-32	4.00	3480	10.9	44.0	32.0	18.0
MF□MA□□100-12	5.50	3525	14.9	60.0	61.0	26.5
MF□MA□□100-32	7.50	3515	20.3	80.0	61.0	26.5
MF□MA□□112-22	11.0	3530	29.7	120	107	38.0

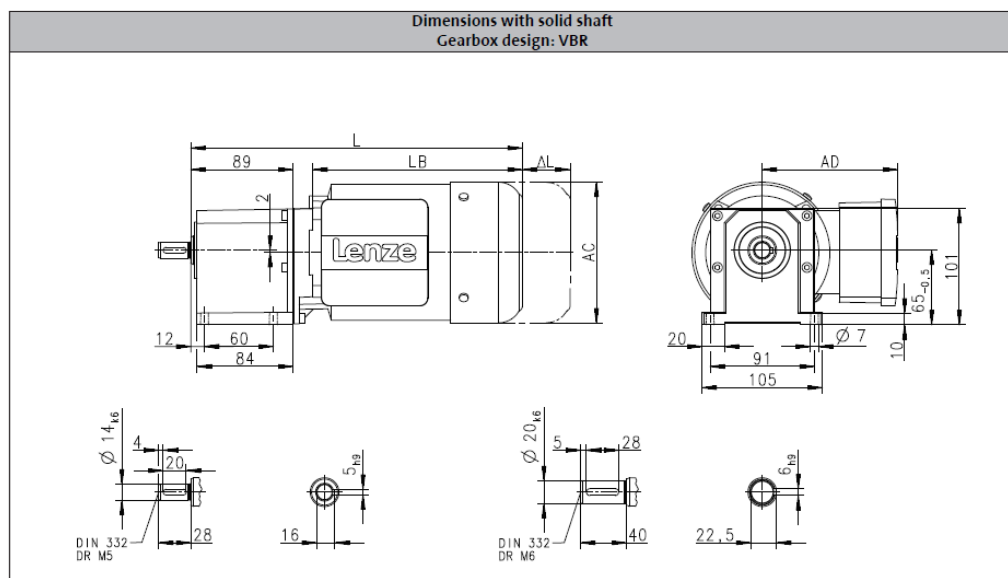
g500-H helical geared motors

Technical data



Dimensions, 4-pole motors

g500-H45



Appendix **F**

Drill Chuck Specifications

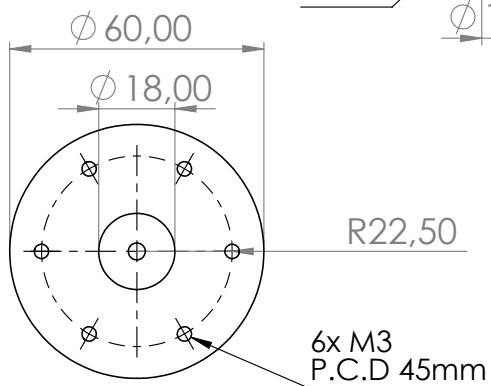
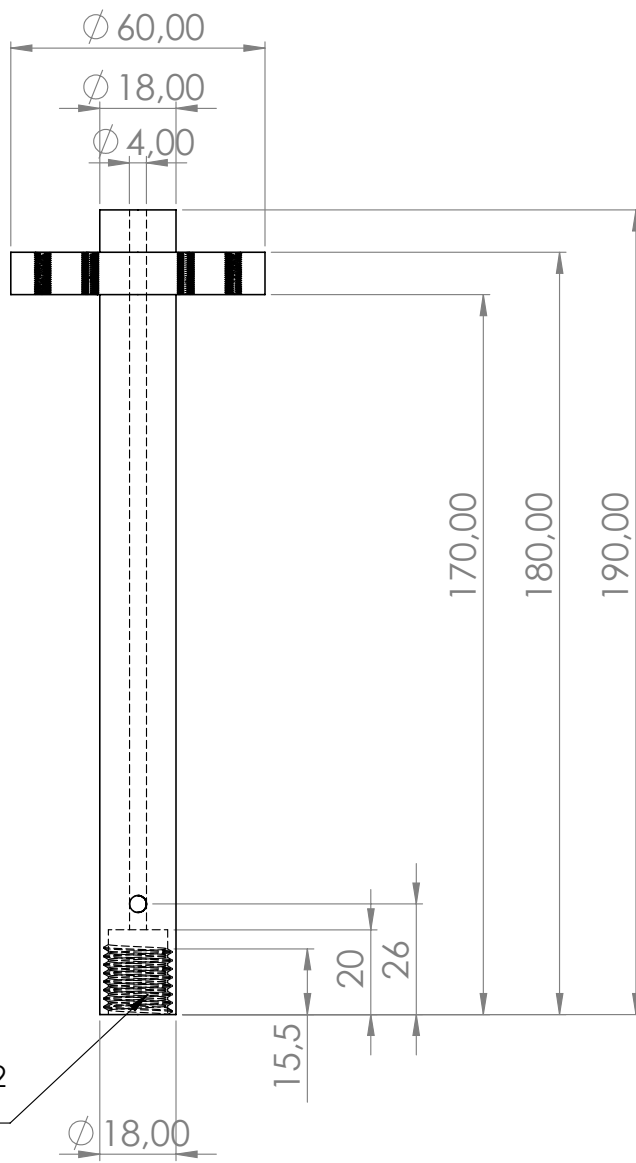
Keyed chuck up to 13 mm

Replacement key	Forward/reverse operation	Locking mechanism	Bench-mounted drill	Drill	Impact drill	Cordless drill	Cordless masonry drill	Cordless screwdriver	Illustration, No.	Product description	SPQ	DPQ	Part number	Barcode 3165140...
D	•		•	•	•				1	1,5 - 13 mm, 1/2" - 20	1	1	1 608 571 062	002639
D			•	•	•	•	•	•	1	1,5 - 13 mm, 1/2" - 20	1	1	2 608 571 079	347129



Appendix **G**

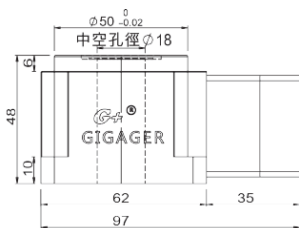
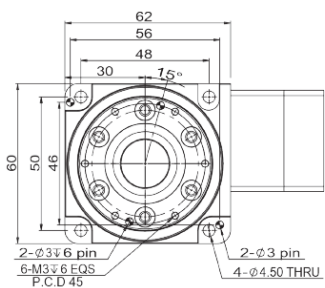
T-shaft Specifications



Appendix H

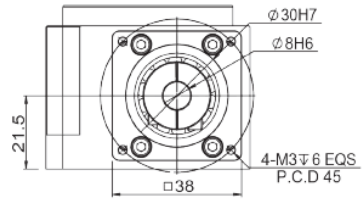
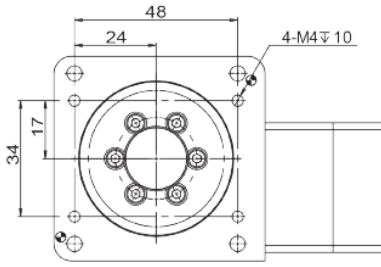
Hypoid Hollow Shaft Gearbox

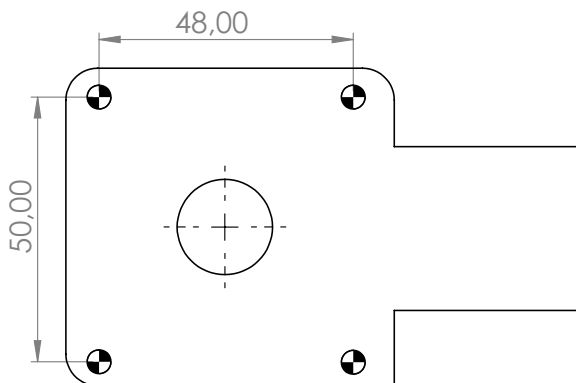
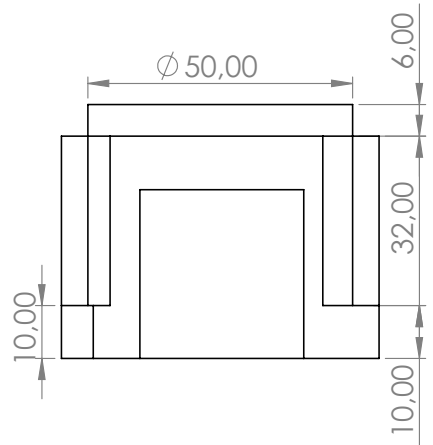
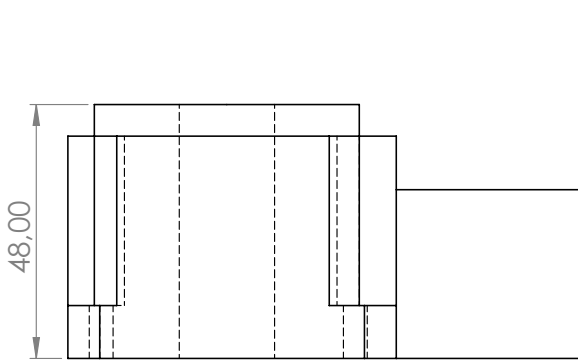
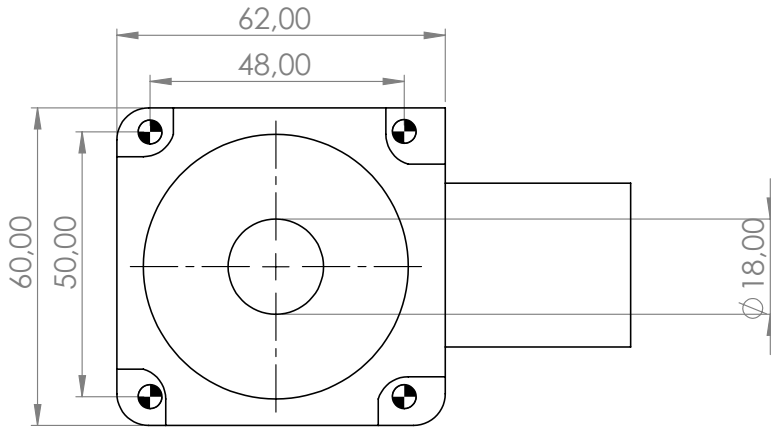
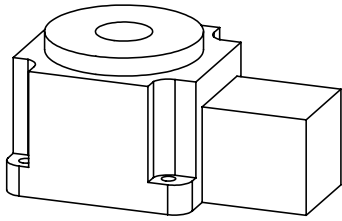
Series	Size	Ratio	Motor Model
GSH	60	30K	SV1
	60 100 150 200		SV1 : Servo Ø8 PCD45,M3 SV2 : Servo Ø8 PCD46,M4 suit for any brand 100W AC servo motor ST1 : Stepper Ø5 PCD43.8,M3 ST2 : Stepper Ø6 PCD43.8,M3 suit for any brand 42 stepper motor



Parameter

Bearing	Cross Roller Bearing	
Permissible Torque	N.m	30
Permissible Table Surface Speed	rpm	90
Gear Ratio	i	30
Repeatability	arc-sec	≤ 10
Positioning Accuracy	arc-sec	≤ 50
Permissible Axial Load	N.m	300
Table Flatness	mm	≤ 0.01
Table Concentricity	mm	≤ 0.01
Precision Life hr (Intermittent)		30000
IP Grade	IP	40
Weight	kg	0.9



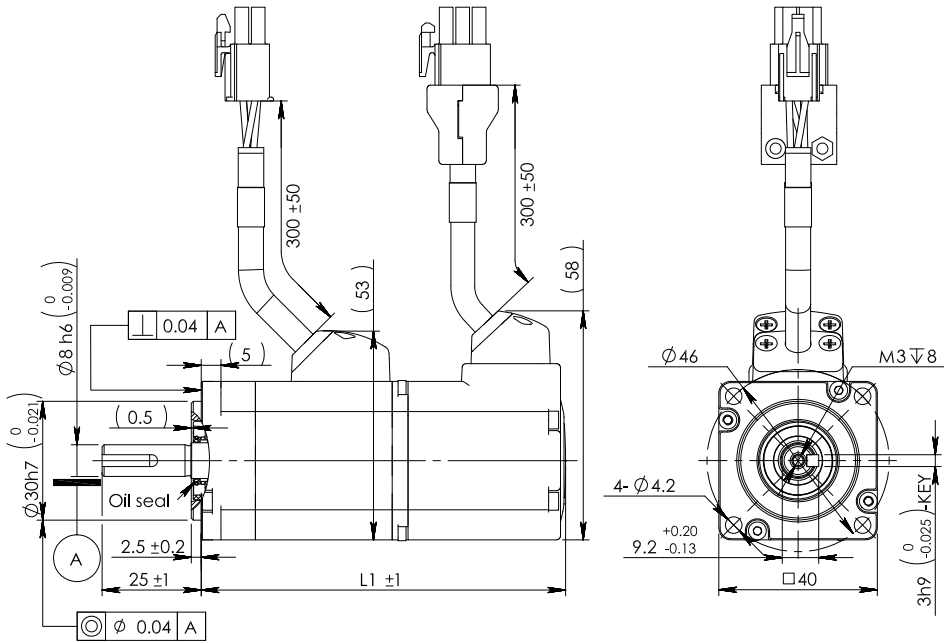


(This page is intentionally left blank)

Appendix **I**

Azimuth Servo Motor

MotorFeedback



L1尺寸 (mm)	
SM0401-E4-KCD-NNV	92
SM0402-E4-KCD-NNV	109

				60W SM0401□E4-KCD-NNV	
				100W SM040□AE4-KCD-NNV	
M0	标记	数量	更改序号	日期	出图阶段
设计			工艺		质量
标准化			审核		比例
校核			批准		第 1 张共 1 张
			日期		

上海安浦鸣志自动化设备有限公司

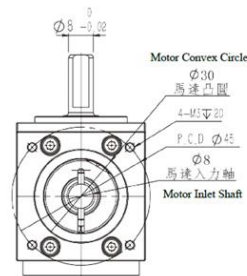
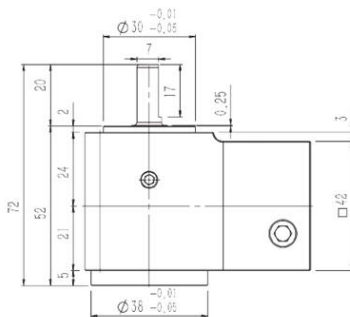
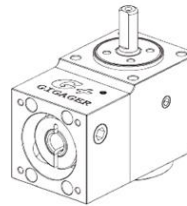
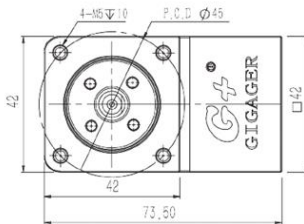
首次使用机型

个 / 台

Appendix **J**

Azimuth Right-Angle Gearbox

■ GSZ42-03K-SV

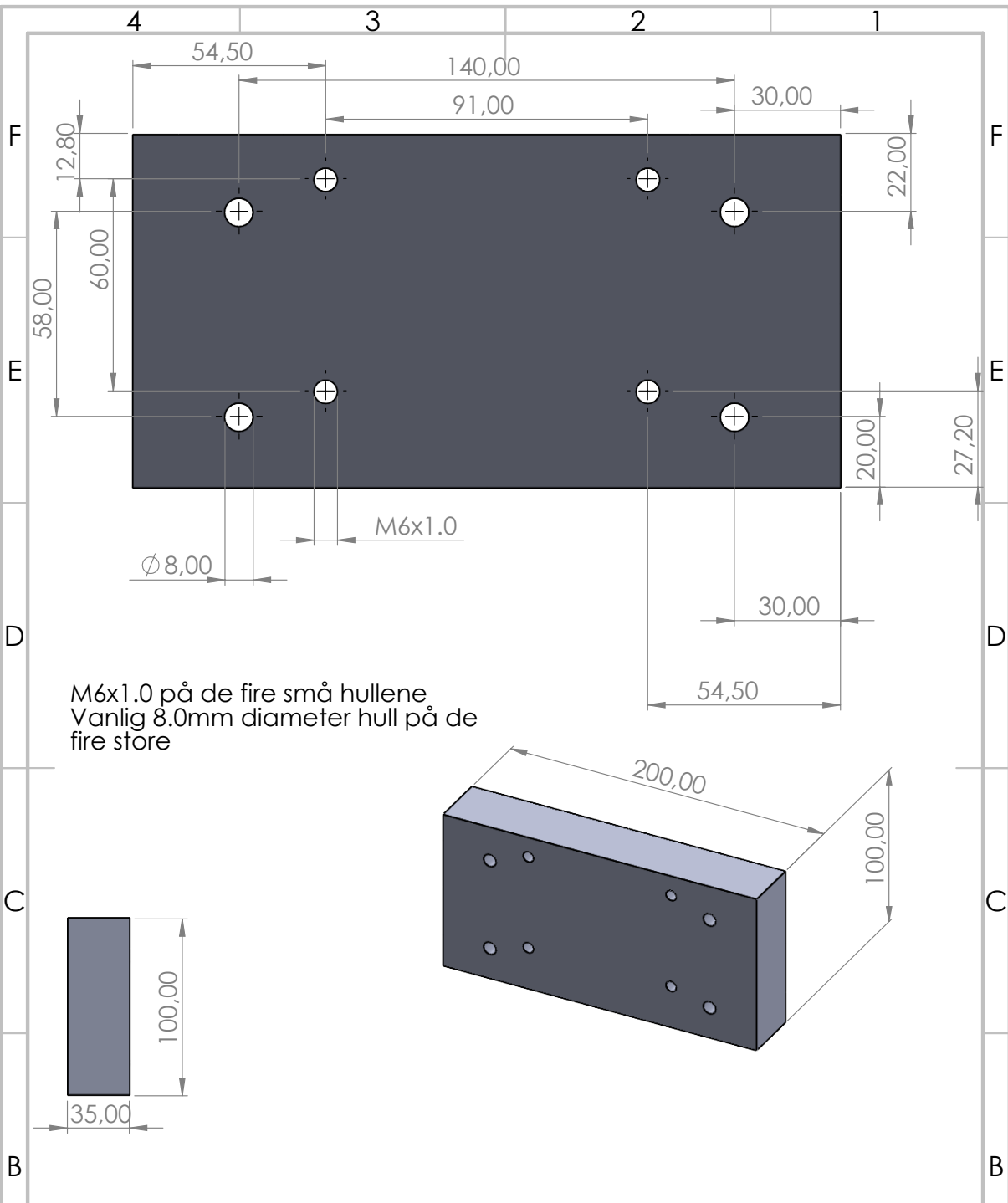


Parameter		
Gear Ratio	1:3	
Permissible Torque	N.m	12
Destructive torque	N.m	40
Permissible Input Speed	rpm	2500
Backlash	min	0.5
Weight	kg	0.45

Figure J.1: Right-angled gearbox from Gigager.

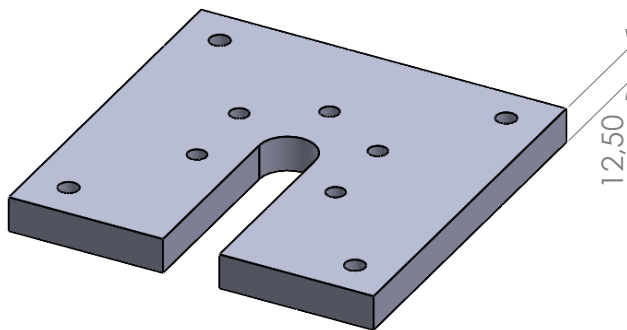
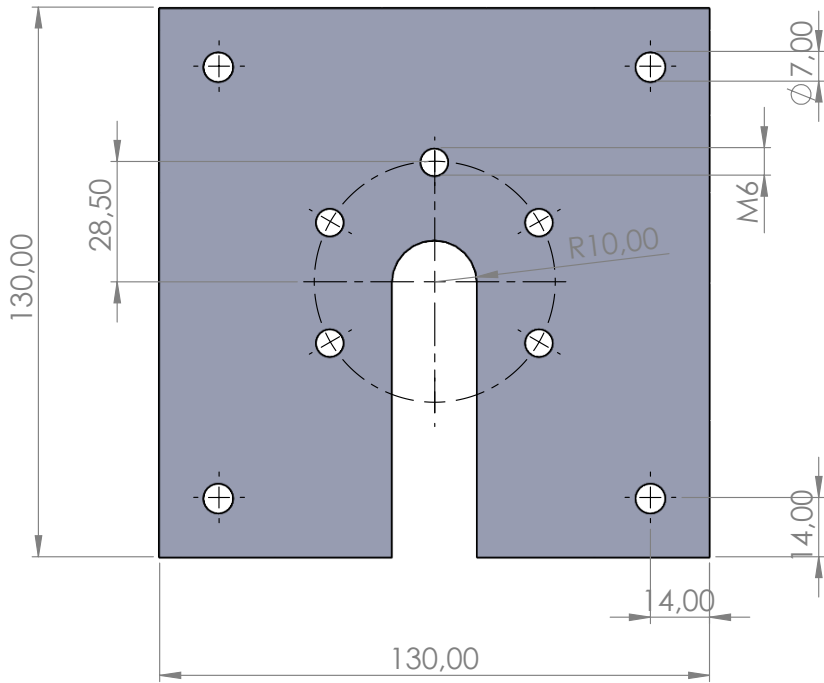
Appendix **K**

Adaptor Plates



M6x1.0 på de fire små hullene
 Vanlig 8.0mm diameter hull på de fire store

UNLESS OTHERWISE SPECIFIED: DIMENSIONS ARE IN MILLIMETERS		FINISH:		DEBURR AND BREAK SHARP EDGES		DO NOT SCALE DRAWING		REVISION	
SURFACE FINISH:									
TOLERANCES:									
LINEAR:									
ANGULAR:									
NAME		SIGNATURE		DATE		TITLE:			
DRAWN									
CHK'D									
APP'V'D									
MFG									
Q.A						MATERIAL:		DWG NO.	
						Aluminium		TD_connector	
						WEIGHT:		SCALE:1:5	
								SHEET 1 OF 1	

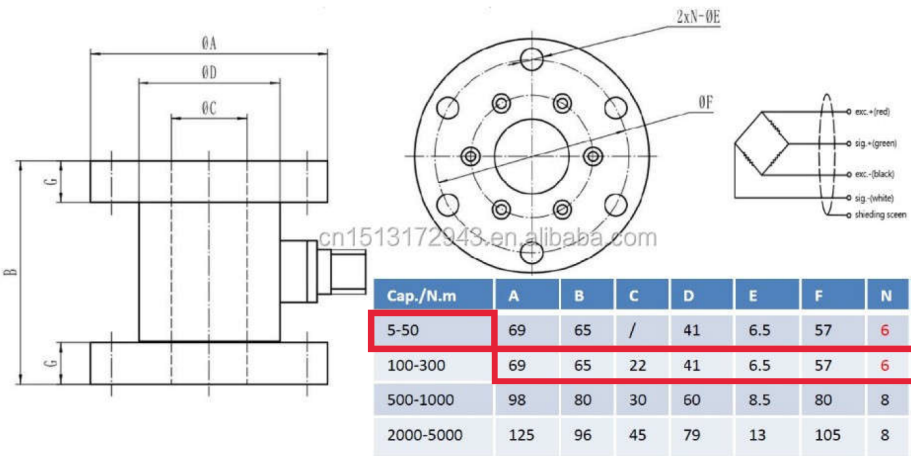


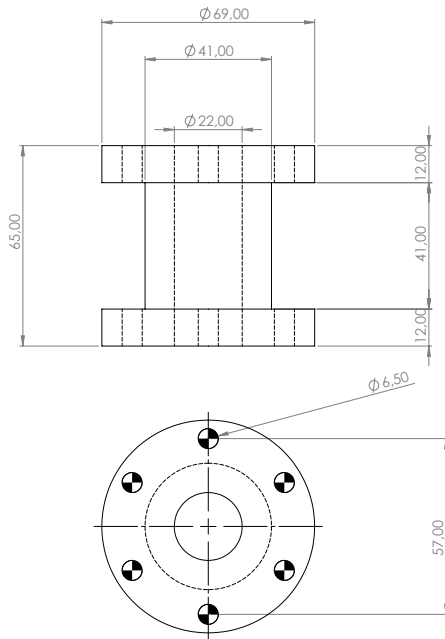
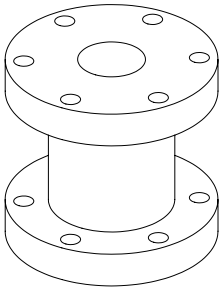
UNLESS OTHERWISE SPECIFIED: DIMENSIONS ARE IN MILLIMETERS SURFACE FINISH: TOLERANCES: LINEAR: ANGULAR:		FINISH:		DEBURR AND BREAK SHARP EDGES		DO NOT SCALE DRAWING		REVISION	
NAME		SIGNATURE		DATE		TITLE:			
DRAWN									
CHK'D									
APP'VD									
MFG									
Q.A				MATERIAL:		DWG NO.			
						Adapter_azimuthfeste			
				WEIGHT:		SCALE:1:5		SHEET 1 OF 1	

(This page is intentionally left blank)

Appendix L

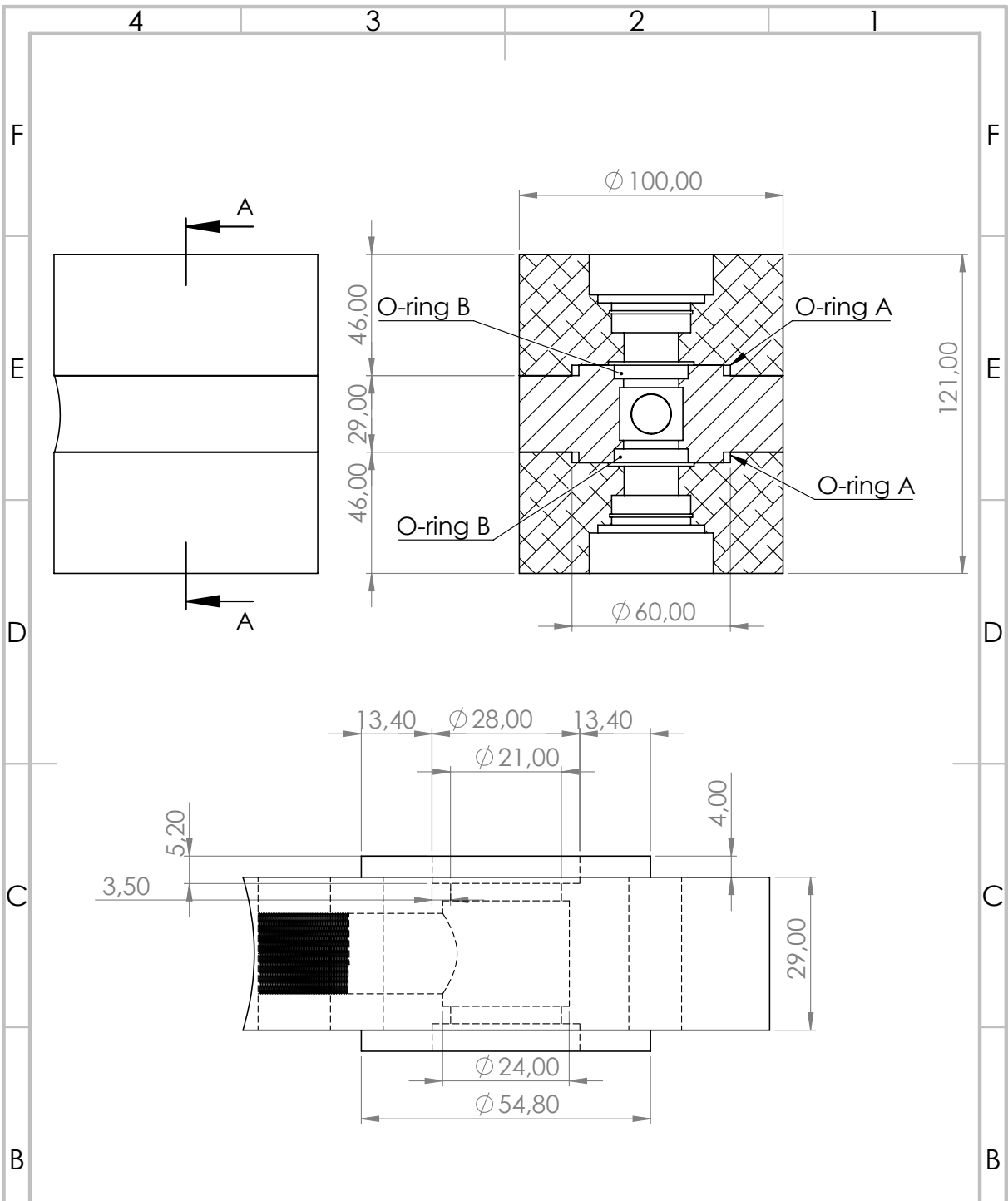
Torque Sensor Specifications





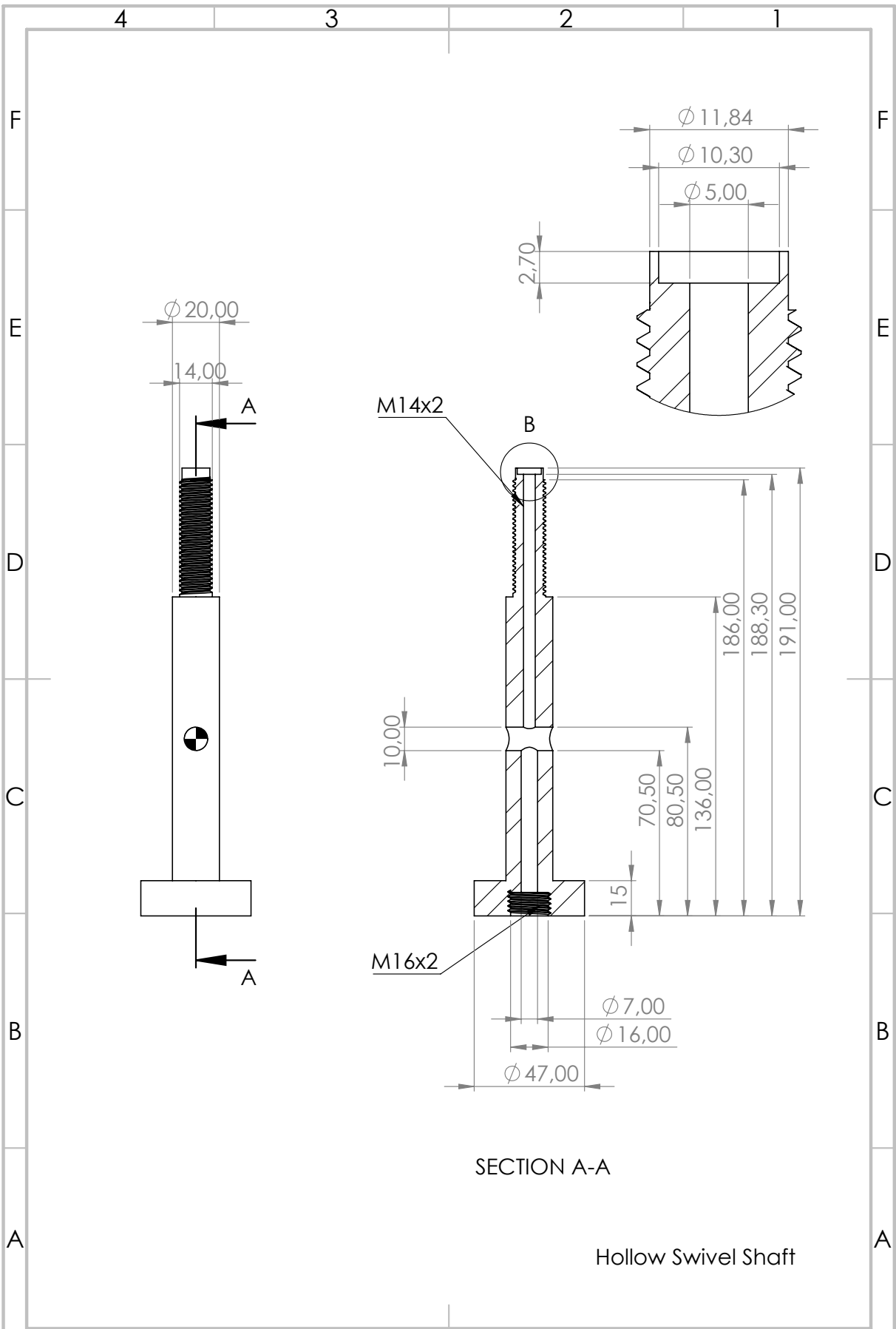
Appendix **M**

Hydraulic Swivel Specifications



UNLESS OTHERWISE SPECIFIED: DIMENSIONS ARE IN MILLIMETERS SURFACE FINISH: TOLERANCES: LINEAR: ANGULAR:		FINISH:		DEBURR AND BREAK SHARP EDGES		DO NOT SCALE DRAWING		REVISION	
DRAWN		SIGNATURE		DATE		TITLE:			
CHK'D									
APPV'D									
MFG									
Q.A.				MATERIAL:		DWG NO.		A4	
				WEIGHT:		SCALE:1:2		SHEET 1 OF 1	

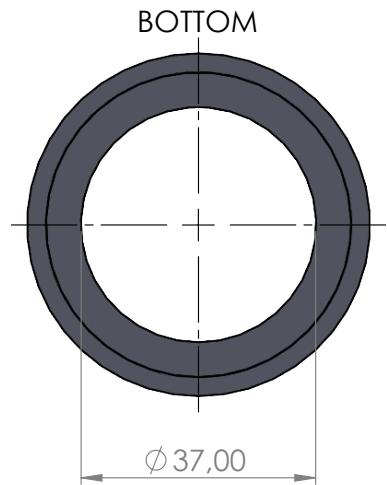
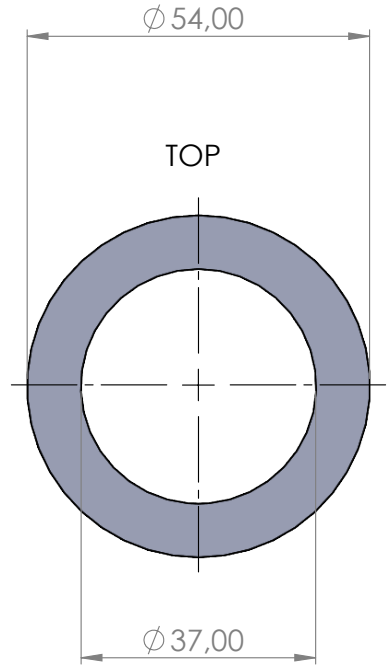
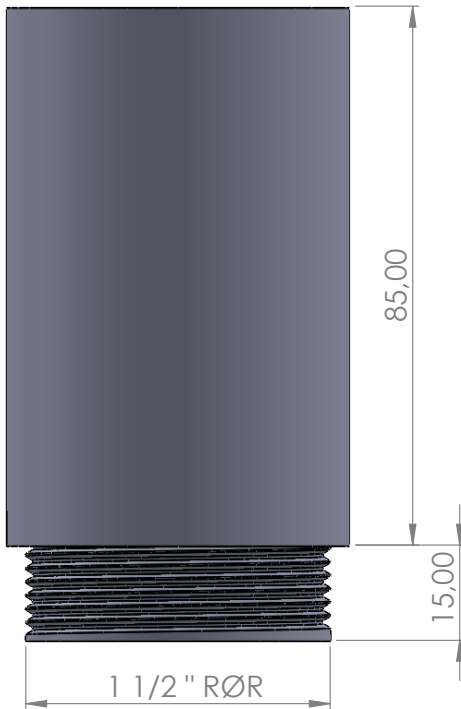
Svivelhus



(This page is intentionally left blank)

Appendix **N**

Riser Design



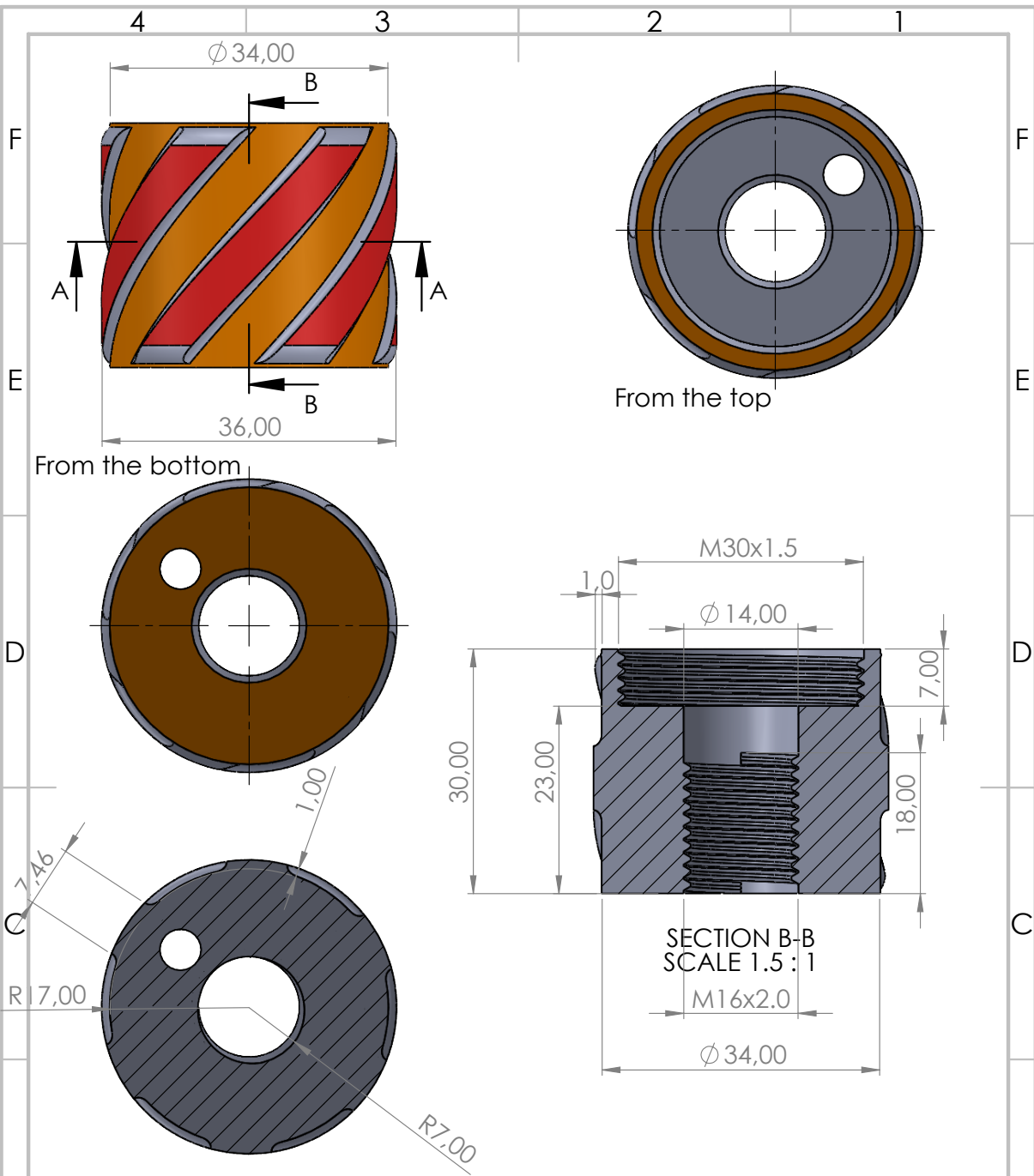
UNLESS OTHERWISE SPECIFIED: DIMENSIONS ARE IN MILLIMETERS SURFACE FINISH: TOLERANCES: LINEAR: ANGULAR:	FINISH:		DEBURR AND BREAK SHARP EDGES		DO NOT SCALE DRAWING	REVISION

	NAME	SIGNATURE	DATE		TITLE:
DRAWN					
CHKD					
APPV'D					
MFG					
Q.A				MATERIAL: STÅL	DWG NO. Riser_element
				WEIGHT:	SCALE:1:1
					SHEET 1 OF 1

(This page is intentionally left blank)

Appendix **O**

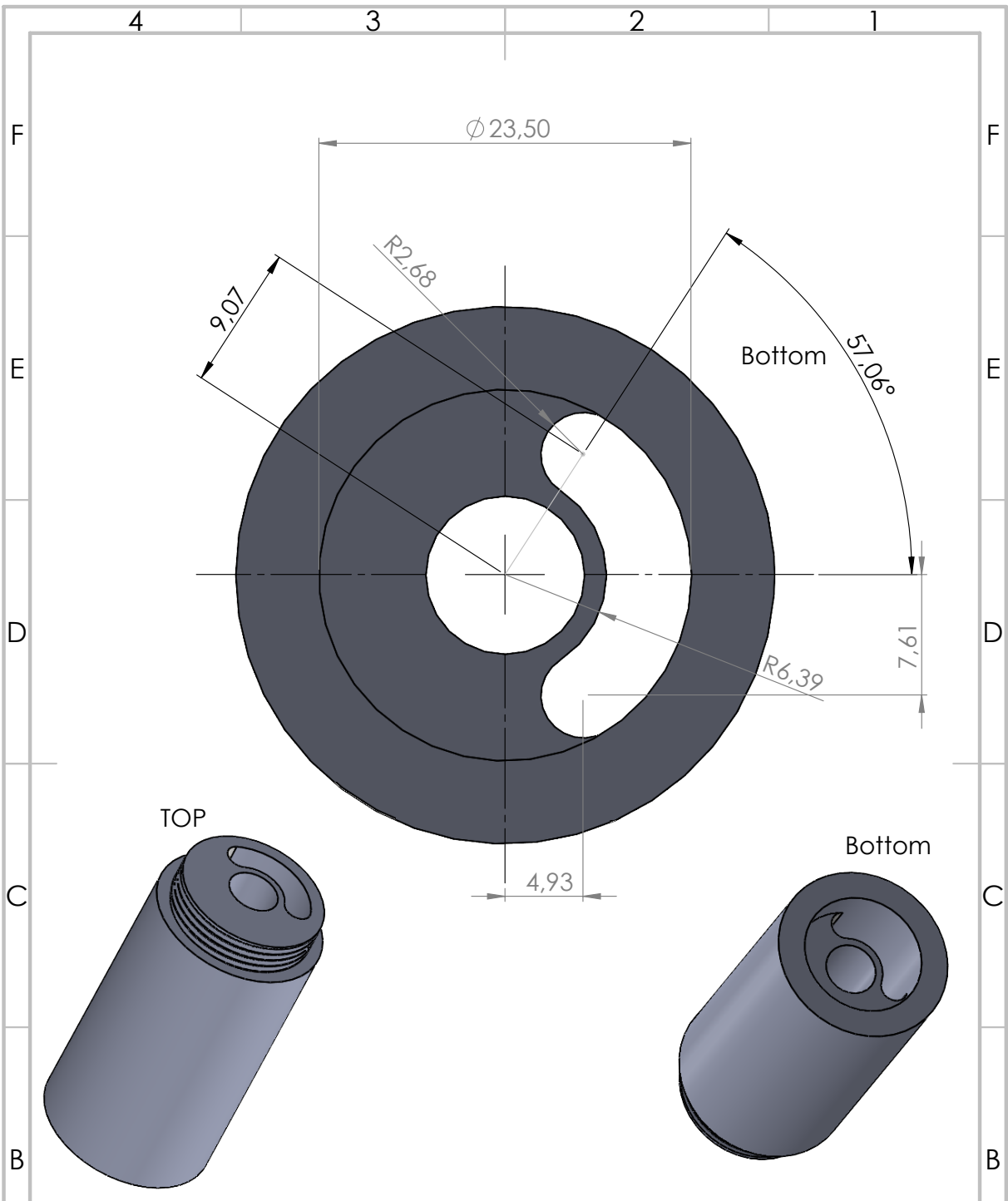
Bottom Hole Assembly (BHA) Specifications



SECTION A-A
SCALE 1.5:1

SECTION B-B
SCALE 1.5:1

UNLESS OTHERWISE SPECIFIED: DIMENSIONS ARE IN MILLIMETERS		FINISH:		DEBURR AND BREAK SHARP EDGES		DO NOT SCALE DRAWING		REVISION	
SURFACE FINISH:									
TOLERANCES:									
LINEAR:									
ANGULAR:									
NAME		SIGNATURE		DATE		TITLE:			
DRAWN									
CHK'D									
APP'VD									
MFG									
Q.A.						DWG NO.		A4	
		MATERIAL:		STÅL		Upper stabilizer			
		WEIGHT:				SCALE:1:1		SHEET 1 OF 1	



UNLESS OTHERWISE SPECIFIED: DIMENSIONS ARE IN MILLIMETERS
 SURFACE FINISH:
 TOLERANCES:
 LINEAR:
 ANGULAR:

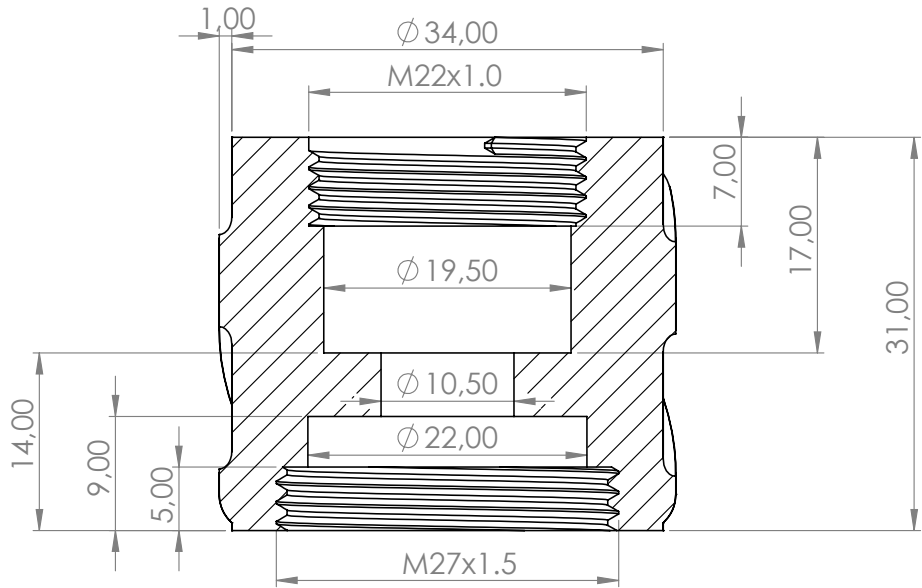
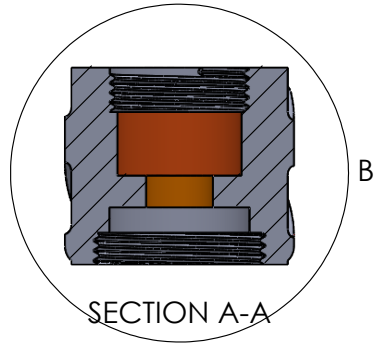
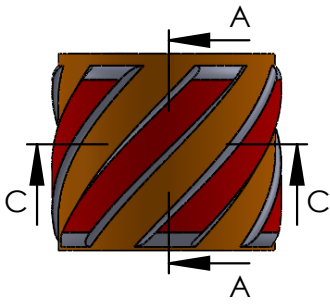
FINISH:

DEBURR AND BREAK SHARP EDGES

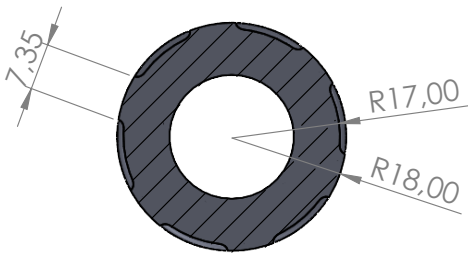
DO NOT SCALE DRAWING

REVISION

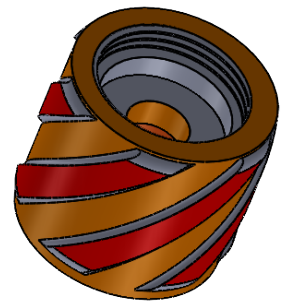
NAME	SIGNATURE	DATE	TITLE:
DRAWN			
CHK'D			
APP'V'D			
MFG			
Q.A.			
MATERIAL:			DWG NO.
WEIGHT:			Sensor housing
			SCALE:1:1
			SHEET 1 OF 1



DETAIL B
SCALE 2 : 1



SECTION C-C



UNLESS OTHERWISE SPECIFIED:
DIMENSIONS ARE IN MILLIMETERS
SURFACE FINISH:
TOLERANCES:
LINEAR:
ANGULAR:

FINISH:

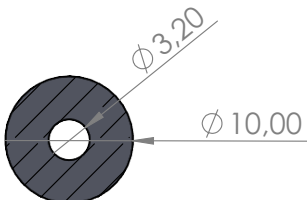
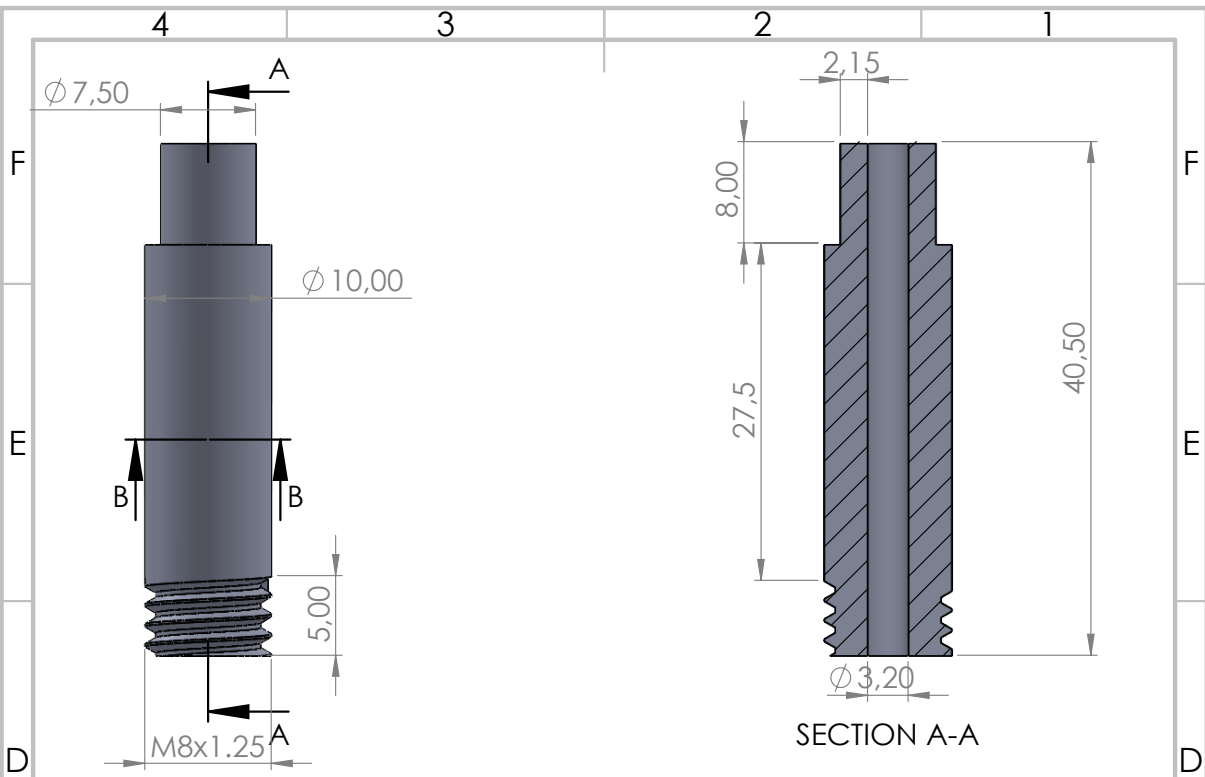
DEBURR AND
BREAK SHARP
EDGES

DO NOT SCALE DRAWING

REVISION

	NAME	SIGNATURE	DATE		
DRAWN					
CHK'D					
APPV'D					
MFG					
Q.A.					
				MATERIAL:	
				STÅL	
				WEIGHT:	

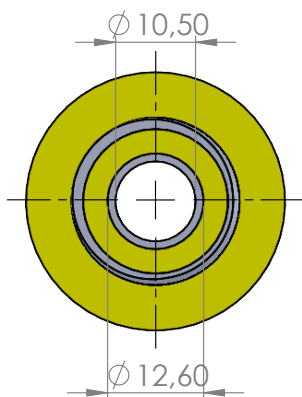
TITLE:	
DWG NO.	
Bearing housing	A4
SCALE:1:1	SHEET 1 OF 1



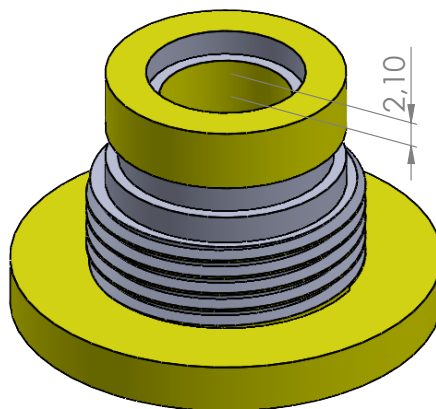
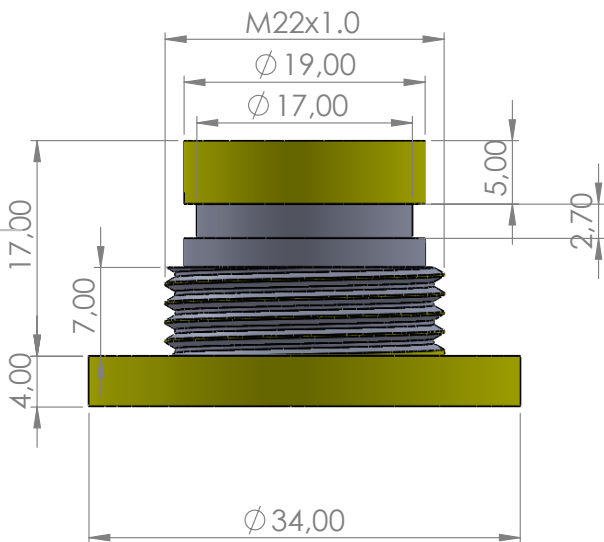
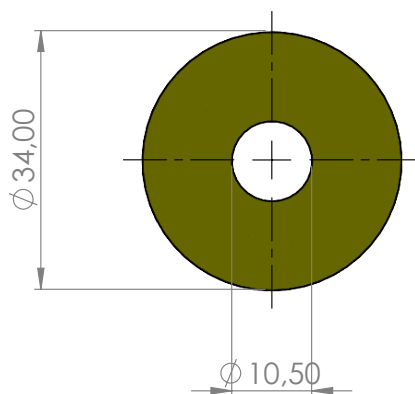
SECTION B-B

UNLESS OTHERWISE SPECIFIED: DIMENSIONS ARE IN MILLIMETERS SURFACE FINISH: TOLERANCES: LINEAR: ANGULAR:				FINISH:		DEBURR AND BREAK SHARP EDGES		DO NOT SCALE DRAWING		REVISION	
DRAWN				SIGNATURE		DATE		TITLE:			
CHK'D											
APP'VD											
MFG											
Q.A				MATERIAL: STÅL		DWG NO.		Drive shaft		A4	
				WEIGHT:		SCALE:2:1		SHEET 1 OF 1			

From the top



From the bottom



UNLESS OTHERWISE SPECIFIED:
DIMENSIONS ARE IN MILLIMETERS
SURFACE FINISH:
TOLERANCES:
LINEAR:
ANGULAR:

FINISH:

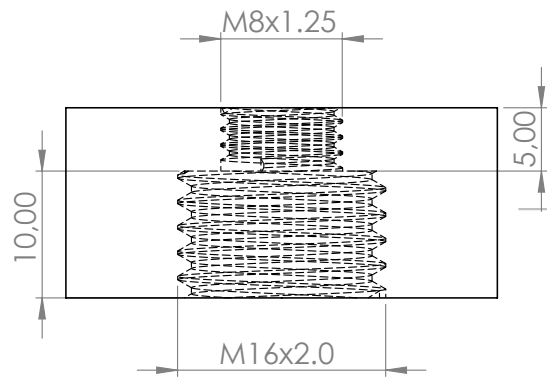
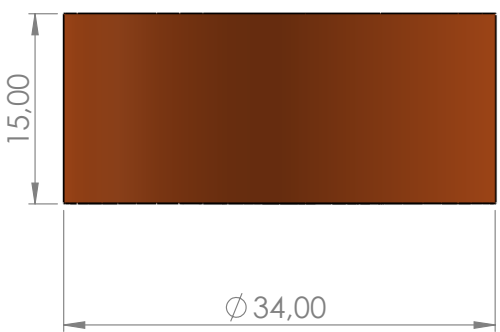
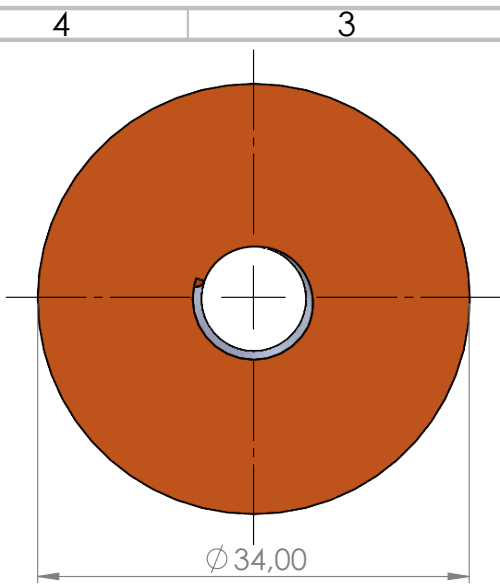
DEBURR AND
BREAK SHARP
EDGES

DO NOT SCALE DRAWING

REVISION

	NAME	SIGNATURE	DATE		
DRAWN					
CHK'D					
APP'VD					
MFG					
Q.A.					
			MATERIAL:	Teflon	
			WEIGHT:		

TITLE:	
DWG NO.	
Bearing packer	A4
SCALE:1:1	SHEET 1 OF 1



UNLESS OTHERWISE SPECIFIED:
 DIMENSIONS ARE IN MILLIMETERS
 SURFACE FINISH:
 TOLERANCES:
 LINEAR:
 ANGULAR:

FINISH:

DEBURR AND
 BREAK SHARP
 EDGES

DO NOT SCALE DRAWING

REVISION

	NAME	SIGNATURE	DATE		
DRAWN					
CHKD					
APPV'D					
MFG					
Q.A					
				MATERIAL:	
				STÅL	
				WEIGHT:	

TITLE:

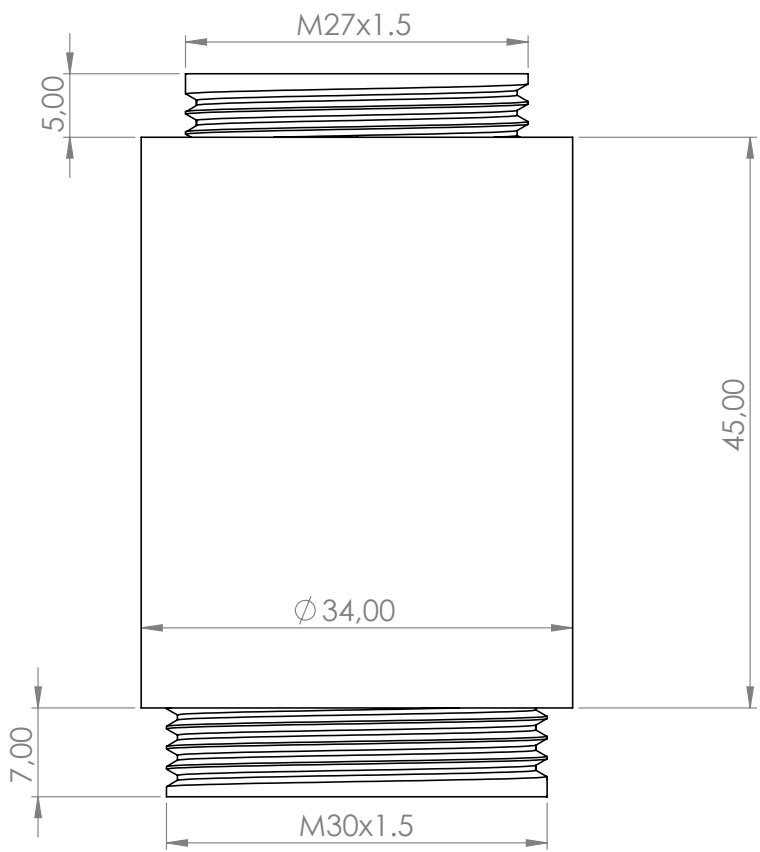
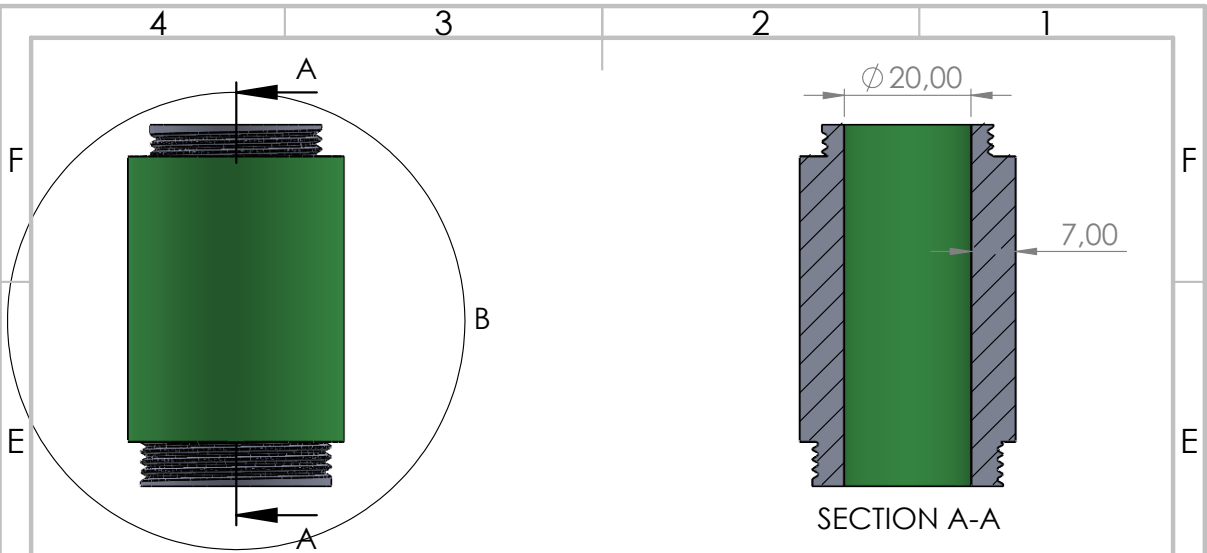
DWG NO.

Bit sub

A4

SCALE:1:1

SHEET 1 OF 1



UNLESS OTHERWISE SPECIFIED:
 DIMENSIONS ARE IN MILLIMETERS
 SURFACE FINISH:
 TOLERANCES:
 LINEAR:
 ANGULAR:

FINISH:

DEBURR AND
 BREAK SHARP
 EDGES

DO NOT SCALE DRAWING

REVISION

NAME	SIGNATURE	DATE	TITLE:
DRAWN			Straight Sub
CHK'D			
APP'VD			
MFG			
Q.A			
MATERIAL: STÅL			DWG NO.
WEIGHT:			SCALE:1:1
			SHEET 1 OF 1

(This page is intentionally left blank)

Appendix **P**

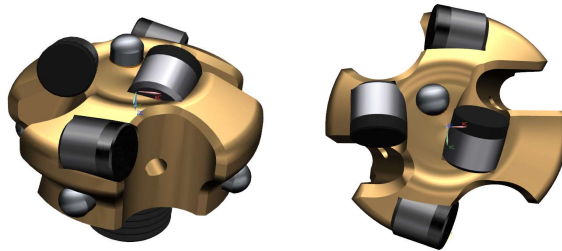
DSATS Drill bit

Contact: Kenneth Evans
 Baker Hughes
 9110 Grogan's Mill Road,
 The Woodlands, Texas, 77380, USA
Kenneth.Evans@bakerhughes.com



PDC Micro-Bit for the 2020 SPE Drillbotics Competition

For the 2020 Drillbotics directional drilling challenge, a generic directional PDC micro-bit has been designed. The changes from last year's design include increase of bit diameter from 1.25" to 1.5" and additional of fluid ports to a total of four. The bit features short bit length and high bit anisotropy. Most importantly, the bit has provision to let participants adjust the axial and side aggressiveness of the bit before a run by changing the exposure of the blunt tungsten carbide elements on the gage pads and on the bit face.



Bit Specifications

Overview	Steel body bit with 4 PDC cutters
Bit Diameter	1.5"
Bit Length	1.35"
Cutter Diameter	0.323"
Chamfer	0.010" x 45° (No ground flats)
Back Rake Angle	Cone Cutters (1-2): 25° Shoulder Cutters (3-4): 20°
Clearance at Gage Pads	Configurable+ 0"- 0.150"
Depth-of-cut Control	Configurable** (No bit body rubbing)
Hydraulics	Four ports 0.125" Diameter each
Connection	1/4" NPT Threads (Not to be modified)

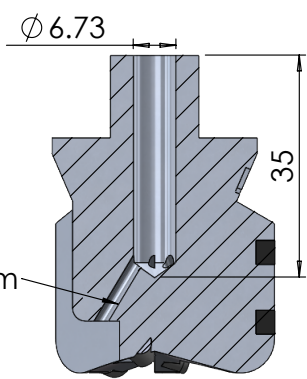
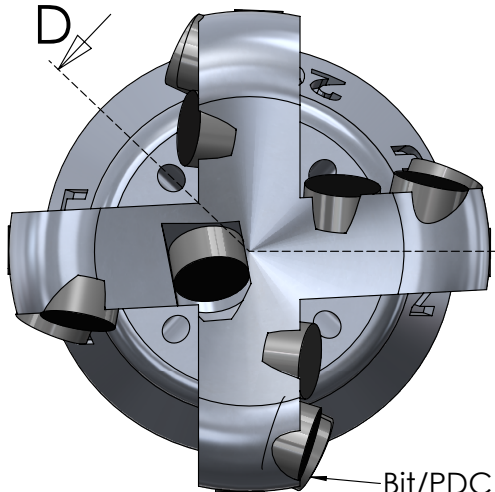
*Four tungsten carbide ovoid elements will be provided to adjust the gage configuration. The elements can be installed at a designed exposure using brazing or a special adhesive to adjust the clearance at the gage between 0" and 0.150"

**A tungsten carbide ovoid element will be provided to adjust the depth-of-cut control configuration. The element can be installed on the bit face at a designed exposure using brazing or a special adhesive.

Figure P.1: DSATS drill bit.

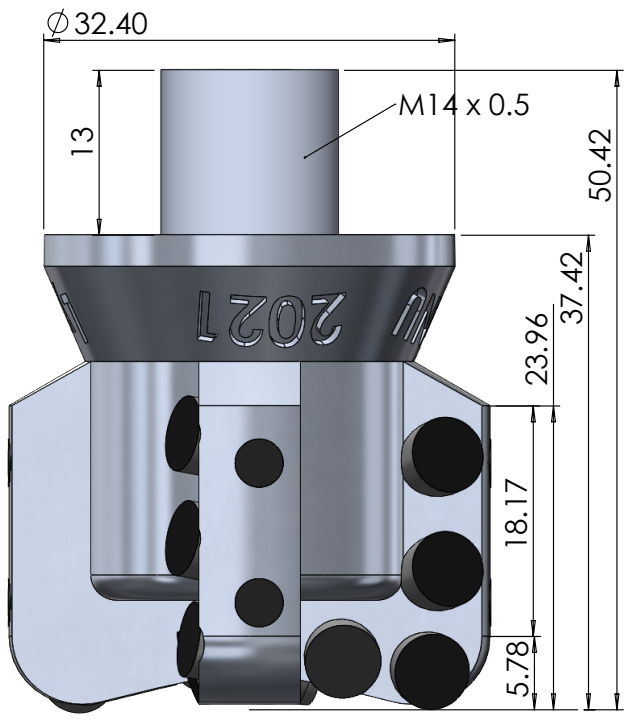
Appendix **Q**

Bit Design



SECTION D-D
SCALE 1 : 1

Bit/PDC dia : 38.1mm(1.5in)
Gagepad dia : 37.9mm(TURNED)
Insert pos: Ø38.1



ITEM NO.	PART NUMBER	QTY.
1	20210326-1-NTNUlyng	1
2	PDC0603	16
3	TSP Dia3.8x3	8

NOTES

- 1 MARK PART PER S-248807 METHOD 3, CONTENT 1
- 2 VENDOR MUST ADHERE TO SUPPLIER PART MARKING AND HANDLING SPECIFICATION T1000037

WEIGHT: 0.19 kg

REVISED	NAME	20YY-MM-DD
CHECKER	NAME	20YY-MM-DD
ENGINEER	ARE FUNDERUD	2021-04-02
DESIGNER	TRYGVE MIKAL VIGA SKRETING	2021-04-02



F DESCRIPTION Drillbotics bit NTNU 2021-1 F

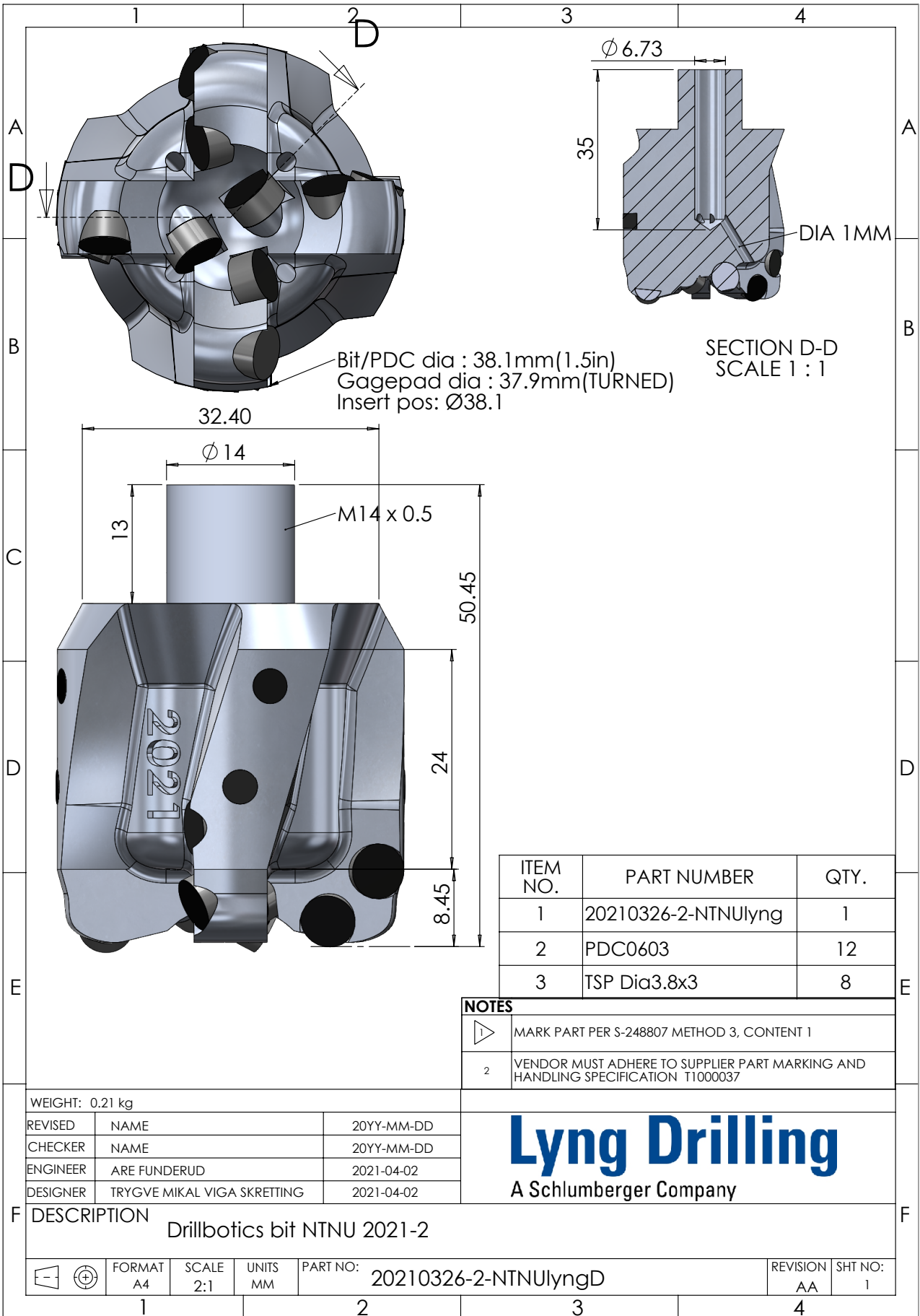
		FORMAT A4	SCALE 2:1	UNITS MM	PART NO: 20210326-1-NTNUlyngD	REVISION AA	SHT NO: 1
--	--	--------------	--------------	-------------	----------------------------------	----------------	--------------

1

2

3

4



Bit/PDC dia : 38.1mm(1.5in)
 Gagepad dia : 37.9mm(TURNED)
 Insert pos: Ø38.1

SECTION D-D
 SCALE 1 : 1

ITEM NO.	PART NUMBER	QTY.
1	20210326-2-NTNUlyng	1
2	PDC0603	12
3	TSP Dia3.8x3	8

NOTES	
1	MARK PART PER S-248807 METHOD 3, CONTENT 1
2	VENDOR MUST ADHERE TO SUPPLIER PART MARKING AND HANDLING SPECIFICATION T1000037

WEIGHT: 0.21 kg

REVISED	NAME	20YY-MM-DD
CHECKER	NAME	20YY-MM-DD
ENGINEER	ARE FUNDERUD	2021-04-02
DESIGNER	TRYGVE MIKAL VIGA SKRETING	2021-04-02

Lyng Drilling
 A Schlumberger Company

DESCRIPTION
 Drillbotics bit NTNU 2021-2

FORMAT A4	SCALE 2:1	UNITS MM	PART NO: 20210326-2-NTNUlyngD	REVISION AA	SHT NO: 1
--------------	--------------	-------------	----------------------------------	----------------	--------------

(This page is intentionally left blank)

Appendix R

Cuttings Transportation Derivation

To get sufficient hole cleaning, the buoyant force and viscous drag force caused by drilling fluid has to overcome gravitational force and slip velocity acting on the cutting particle. Slip velocity is caused by the weight of the solid particle given by Equation R.1.

$$W = -\rho_s \frac{\pi}{6} d_s^3 g \quad (\text{R.1})$$

where $W[N]$ is the weight force, $\rho_s[kg/m^3]$ is the density of the solid particle and d_s is the solid particle diameter. The buoyant force acting on the particle is estimated with Equation R.2 where $F_b[N]$ is the buoyant force and $\rho_f[kg/m^3]$ is the density of the drilling fluid.

$$F_b = \rho_f \frac{\pi}{6} d_s^3 g \quad (\text{R.2})$$

The viscous drag force is given by [33]:

$$F_d = 3\pi\mu_f d_s v_{sl} \quad (\text{R.3})$$

where $\mu_f[Pa\cdot s]$ is the fluid viscosity and $v_{sl}[m/s]$ is the slip velocity. By applying Newton's first law of motion given in Equation R.4 to Equation R.1 R.2 and R.3, it can be solved for v_{sl} .

$$\sum F = W + F_b + F_d = 0 \quad (\text{R.4})$$

$$v_{sl} = \frac{d_s^2 g (\rho_s - \rho_f)}{18\mu_f} \quad (\text{R.5})$$

Equation R.5 is also known as Stokes' law and is only valid for Newtonian fluids in laminar flow and Reynolds numbers below 0.1[7]. If $Re > 0.1$ the low regime has shear force given as [8]:

$$F_d = f \frac{\pi}{8} d_s \rho_f v_{sl}^2 \tag{R.6}$$

where f is an empirical friction factor found from Figure R.1. Here sphericity, Ψ , is set to be equal to 1 under the assumption of spherical cuttings. Reynolds number is calculated with Equation R.7, using estimated slip velocity from Equation R.5.

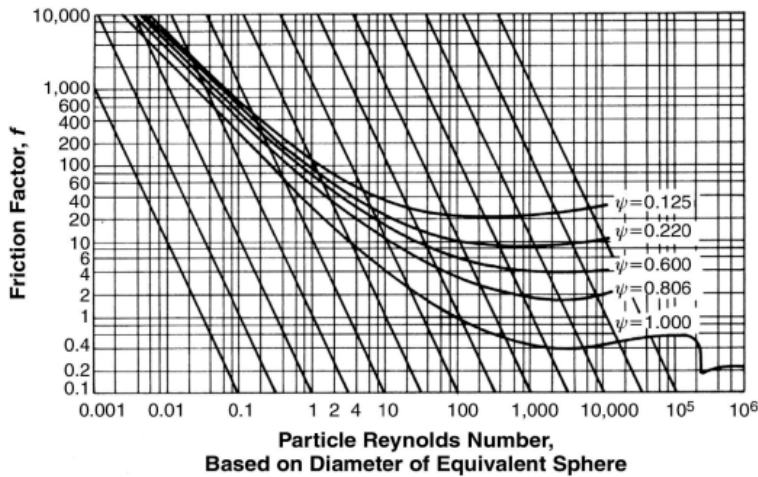


Figure R.1: Relationship between Re and f for settling particles in Newtonian fluids [7].

$$Re = \frac{\rho_f v_{sl} d_h}{\mu_f} \quad (R.7)$$

where d_h is the hydraulic diameter. For flow in annulus, area is given as:

$$d_h = OD_{hole} - OD_{DP/BHA} \quad (R.8)$$

and for flow inside pipe:

$$d_h = ID_{DP/BHA} \quad (R.9)$$

By using Equation R.4 with Equation R.6 as F_d , slip velocity of a particle in all flow regimes can be estimated as:

$$v_{sl} = \sqrt{\frac{4(\rho_s - \rho_f)gd_s^2}{3f\rho_f}} \quad (R.10)$$

